GLASS MELT CHEMISTRY AND PRODUCT QUALIFICATION

Prepared for

Nuclear Regulatory Commission
Contract NRC–02–97–009

Prepared by

Center for Nuclear Waste Regulatory Analyses
San Antonio, Texas

September 2000

GLASS MELT CHEMISTRY AND PRODUCT QUALIFICATION

Prepared for

Nuclear Regulatory Commission
Contract No. NRC–02–97–009

Prepared by

Vijay Jain
Yi-Ming Pan

Center for Nuclear Waste Regulatory Analyses
San Antonio, Texas

September 2000

PREVIOUS REPORTS IN SERIES

Number	Name	Date Issued
NUREG/CR–6666	Survey of Waste Solidification Process Technologies	In press
NUREG/CR–5751	Hanford Tank Waste Remediation System High-Level Waste Chemistry Manual	May 1999
CNWRA 97-0001	Hanford Tank Waste Remediation System Familiarization Report	July 1997

ABSTRACT

Vitrified waste forms produced by melting high-level waste (HLW) with glass forming oxides, are being used in the United States, France, England, Germany, Belgium, Japan, the Former Union of Soviet Socialists Republic, and India as the preferred technology for the disposal of HLW. Both the vitrification technology and the guidelines for disposal at a proposed geological repository impose stringent requirements for producing an acceptable product. The glass composition designed for vitrification should meet (i) processing constraints, such as viscosity, melting and liquidus temperatures, electrical conductivity, redox condition into the melt, solubility of noble metals, and sulfur concentration; and (ii) product constraints, such as durability, crystallinity, and glass transition temperature. This report provides a review of glass-melt properties and characteristics, the basis and importance of the imposed constraints on the design of glass composition, and aspects of the glass melting process that potentially can compromise worker safety. The review was conducted to assist the U.S. Nuclear Regulatory Commission in the development of the technical and regulatory tools for conducting radiological safety assessments of the privatized vitrification facilities.

The review of the history of waste form development, and the information (data and models) on glass-melt properties for various types of commercial and waste-glass compositions indicate that the behavior of glasses is complex and cannot be expressed in simple terms for all wastes. The glass composition needs to be designed uniquely for each waste type. The lessons learned, or the existing database of HLW glasses, can be used as a guideline to narrow the scope of R&D needed to meet the requirements.

CONTENTS

CONTENTS (cont'd)

CONTENTS (cont'd)

CONTENTS (cont'd)

FIGURES

FIGURES (cont'd)

FIGURES (cont'd)

FIGURES (cont'd)

TABLES

TABLES (cont'd)

ACRONYMS/ABBREVIATIONS

2D	Two-dimensional
3D	Three-dimensional
ASTM	American Society for Testing and Materials
BDAT	Best demonstrated available technology
BO	Bridging oxygen
CNWRA	Center for Nuclear Waste Regulatory Analyses
CVS	Compositional variability study
DOE	U.S. Department of Energy
DSC	Differential scanning calorimetry
DWPF	Defense Waste Processing Facility
EA	Environmental Assessment
EPA	U.S. Environmental Protection Agency
ESM	Engineering-scale melter
FEH	Free energy of hydration
HLW	High-level waste
HWVP	Hanford Waste Vitrification Plant
IDMS	Integrated [Defense Waste Processing Facility (DWPF)] melter system
IFO	Index of feed oxidation
KfK	Kernforschungszentrum Karlsruhe
LAW	Low-activity waste
MCC	Materials Characterization Center
NBO	Nonbridging oxygen
NCAW	Neutralized current acid waste
NRC	U.S. Nuclear Regulatory Commission
PCT	Product consistency test
PFA	Perfluoroalkoxy
PHA	Precipitate hydrolysis aqueous
PNNL	Pacific Northwest National Laboratory
PUREX	Plutonium Uranium Extraction Process
R&D	Research and development
RSM	Research scale melter
SA/V	Surface area/volume
SBS	Structural bond strength
SGM	Scale glass melter
SNF	Spent nuclear fuel
SPFT	Single-pass, flow-through
SRL	Savannah River Laboratory
SRS	Savannah River Site
SVS	Scaled Vitrification System
THOREX	Thorium Extraction Process
TOC	Total Organic Carbon
TTT	Temperature-time-transformation
TWRS	Tank Waste Remediation System

ACRONYMS/ABBREVIATIONS (cont'd)

TWRS-P	Tanks Waste Remediation System-Privatization
VFT	Vogel-Fulcher-Tammann
WAPS	Waste acceptance product specifications
WP	Waste package
WVDP	West Valley Demonstration Project

ACKNOWLEDGMENTS

This report was prepared to document work performed by the Center for Nuclear Waste Regulatory Analyses (CNWRA) for the U.S. Nuclear Regulatory Commission (NRC) under Contract No. NRC–02–97–009. The activities reported here were performed on behalf of the NRC Office of Nuclear Material Safety and Safeguards, Division of Fuel Cycle Safety and Safeguards. The report is an independent product of the CNWRA and does not necessarily reflect the views or regulatory position of the NRC.

The authors wish to acknowledge L. Yang, R. Pabalan, and N. Sridhar for technical reviews; W. Patrick for programmatic review; B. Long, J. Pryor, C. Cudd, C. Gray, and A. Woods for editorial reviews; and the assistance of J. Gonzalez, L. Selvey, A. Ramos, and J. Wike for preparation of the document.

QUALITY OF DATA, ANALYSES, AND CODE DEVELOPMENT

DATA: No CNWRA-generated original data are used in this report.

ANALYSES AND CODES: No computer codes were used for analyses contained in this report.

EXECUTIVE SUMMARY

This report provides a review of the glass melt properties and characteristics, the basis and importance of imposed constraints on the design of glass composition, and the potential safety and processing aspects of glass melting that can compromise radiological safety. This report has been written to assist the U.S. Nuclear Regulatory Commission (NRC) in

- Determining if sufficient information exists to assess safety considerations regarding vitrification of the waste stored at the Hanford site near Richland, Washington
- Determining whether current regulatory guidelines are adequate to control implementation of the vitrification process to immobilize high-level waste (HLW) at Hanford
- Identifying technical uncertainties
- Assessing where future guidance may be warranted

Research and development (R&D) of waste forms for immobilization of liquid radioactive wastes began in the mid-1950s. Initial investigations included evaluation of waste forms such as borosilicate glass, phosphate glass, nepheline-syenite glass, a variety of polyphase ceramics, and bituminous and concrete materials. The R&D continued through the 1970s with no coherent approach. Most of the programs did not even contemplate scaling up from laboratory studies to remote operations capable of handling millions of gallons of waste. A systematic evaluation using standardized tests was initiated by the U.S. Department of Energy in 1977 to select a waste form for HLW in the United States. This evaluation resulted in the selection of a borosilicate glass-based waste form as a reference waste form for immobilization of HLW in the United States. Currently, a vitrified waste form produced by melting HLW with glass forming oxides is being used in the United States, France, England, Germany, Belgium, Japan, the Former Union of Soviet Socialists Republic, and India as the preferred technology for the disposal of HLW. In the United States, HLW vitrification is ongoing at the West Valley Demonstration Project (WVDP), West Valley, New York and the Defense Waste Processing Facility (DWPF), Aiken, South Carolina, while vitrification is currently planned for the HLW contained in 177 aging underground storage tanks at the Hanford site in the state of Washington. The current plans for Hanford wastes call for pretreatment of wastes, prior to vitrification, that will separate the waste into HLW and low-activity waste (LAW) fractions. The separated HLW and LAW fractions will be vitrified into borosilicate glass.

The vitrification technology, as well as guidelines for the disposal at a proposed geologic repository, imposes stringent requirements for producing an acceptable waste-form product. The glass composition designed for vitrification should meet processing constraints, such as electrical conductivity (chapter 5), viscosity (chapter 6), liquidus temperature (chapter 8), redox condition of the melt (chapter 9), solubility of noble metals (chapter 10), and sulfur solubility limits (chapter 11); and product constraints such as glass transition temperature (chapter7), chemical durability (chapter 12), and phase stability (chapter 13). Waste acceptance criteria for the producers of the vitrified waste form are outlined in Waste Acceptance Product Specifications

(WAPS) by the U.S. Department of Energy (1996). The WAPS specify technical requirements that the waste form must meet and the documentation the producers must provide to assure the product complies with the NRC requirements in 10 CFR Part 60.[1]

The electrical conductivity in most oxide glasses is attributed to migration of positively charged alkali ions in the presence of an applied electric field. Joule-heated melters for nuclear waste vitrification require electrical conductivity of the glass melts between 10 and 100 S/m at melting temperature. The lower limit of 10 S/m for electrical conductivity is imposed on the glass melts at melting temperature to ensure the electrical conductivity of the glass melt is significantly higher than the electrical conductivity of the refractories surrounding the glass melt, which ensures the current does not flow through the refractories. The upper limit of 100 S/m for electrical conductivity is imposed on the glass melt at melting temperature to ensure the glass melt provides enough joule heating for melting without exceeding the maximum operating current density for Alloy 690 electrodes. The glass components, Li_2O and Na_2O, have the strongest tendencies to increase electrical conductivity, while SiO_2 has the strongest tendency to decrease electrical conductivity. Chapter 5 provides a review of published studies on electrical conductivity and its effect on the nuclear waste vitrification process.

Viscosity is a property of a liquid state and a measure of the resistance to shear deformation. Joule-heated melters for nuclear waste vitrification require the viscosity of glass melts to be between 2 and 10 Pa-s (20 and 100 P) at melting temperature. The limits are imposed on glass melts at melting temperature to ensure the glass melt is fluid enough to homogenize and pour. If the viscosity of the melt is below 2 Pa-s (20 P), the glass melt could increase erosion of the refractory; volatilization of alkalis, boron, and radionuclides; penetration of melt along the refractory joints; or settling of noble metals. If the viscosity is greater than 10 Pa-s (100 P), glass melt could plug the pour spout during pour, have undissolved components in the melt, or crystallize at cold spots in the melter. The glass components SiO_2, Al_2O_3, and ZrO_2 (in order) have the strongest effects for increasing the melt viscosity, while Li_2O, Na_2O, CaO, and B_2O_3 have the strongest effect for decreasing the melt viscosity. Chapter 6.0 provides a review of published studies on viscosity and its effect on the nuclear waste vitrification process.

At the time of shipment to a federal repository, the WAPS requires the producer certify that, after the initial cool-down, the waste form temperature has not exceeded 400 °C. This product specification was established to ensure the waste form is in a solid form at the time of shipment. The glass transition temperature (T_g) range marks the temperature interval over which a given system gradually transforms while cooling from a supercooled liquid state into the glass state. There is no absolute measure of T_g because its value is influenced by the thermal history and rate of cooling. Minor variations in composition, redox, or cooling rate do not show significant change in T_g. Chapter 7 provides a review of published studies on glass transition.

Liquidus temperature (T_L) is the highest temperature at which melt and primary crystalline phases can coexist at equilibrium. At temperatures higher than T_L, no crystalline phases are present in the melt. If the lowest temperature in the melter is lower than the T_L of the melt, crystalline phases can precipitate and cause processing problems. If the crystalline phases are electrically conductive, electrical shorting could occur in

[1]The current regulation governing deep geologic disposal of high-level waste is 10 CFR Part 60. At the direction of Congress, the U.S. Nuclear Regulatory Commission has proposed a regulation at 10 CFR Part 63 that would govern disposal at the proposed repository site at Yucca Mountain, Nevada.

the melter. In joule-heated melters operating at an average temperature of 1,150 °C, the T_L limit is set at 1,050 °C. Chapter 8 provides a review of published studies on T_L and its effect on the nuclear waste vitrification process.

Redox (reduction-oxidation) reactions involve a transfer of one or more electrons within the different oxidation states of a single multivalent element or from one multivalent element to another within a chemical system. Multivalent elements that can coexist in multiple valance states are redox couples (e.g., Fe redox couple can exist as either Fe^{2+}/Fe^{3+} or Fe^{0}/Fe^{2+}, depending on the available oxygen in the system). A glass melt is defined as extremely reducing if the Fe^{2+}/Fe^{3+} ratio is greater than one. Under such conditions, sufficient accumulation of conductive metals and metal sulfides could occur and short-circuit the melter. If the Fe^{2+}/Fe^{3+} ratio is less than 0.01, a glass melt is defined as extremely oxidizing. Under extremely oxidizing conditions, foaming is observed in the melter. Foam creates an insulating layer of gas bubbles between the cold cap and the melt, disrupting the thermal gradients in the melter. Knowledge of participating redox couples in redox reactions in glass melts and its temperature and compositional dependence is of great importance during vitrification of HLW in joule-heated melters as discussed in chapter 9.

Noble metals such as Ru, Rd, and Pd in the HLW originate from the fission of U-235. Noble metals in the borosilicate glass melts have been a major concern in the HLW vitrification process because of their low solubility, high volatilization rate, and high electrical conductivity. In 1985, the accumulation of the noble metals on the floor of the Pamela melter, in Mol, Belgium, resulted in electrical shorting of a joule-heated melter. Chapter 10 provides a review of published studies on effects of the noble metals on the nuclear waste vitrification process.

Borosilicate glass-based waste forms have limited sulfur solubility. In the WVDP and DWPF waste forms, SO_3 levels are maintained below 0.25 wt% to avoid formation of immiscible sodium sulfate phase in the melt. Traditionally, wastes containing high concentrations of sulfur are washed with water to remove soluble sulfate salts. If the concentration of SO_3 is in excess of 0.25 wt%, the SO_3 concentration limits the waste loading in the glass. The SO_3 solubility limit is established based on the operating redox range of 0.01 to 0.5. In chapter 11, a discussion on the sulfur solubility limit imposed on the glass composition is followed by a review of various studies on sulfur solubility and its implication on the LAW vitrification at the Hanford site.

When glass comes in contact with the repository environment, such as flowing or stagnant groundwater, acid rain, corrosive gases and vapors, or aqueous solutions, chemical reactions occur at the surface and spread to the whole of the glass, depending on its composition, pH of the solution, and the temperature of the environment. In chapter 12, a review of recent advances in understanding the dissolution behavior of glasses as a function of composition, pH, and temperature is provided.

Phase stability in glass can be affected by either liquid-liquid phase separation or crystallization on cooling from the melt. For the glass waste form, both the phase separation and crystallization processes can result in the development of an inhomogeneous microstructure that may affect the reliability of the waste glass process and product performance. The phase stability requirements, which include development of a temperature-time-transformation (TTT) diagram for each projected waste type, have been outlined in the WAPS. Crystallization can occur in nuclear waste glasses during continuous cooling of pour canisters and annealing of quenched glasses. A TTT diagram is a useful tool for scoping the heat treatment conditions for crystallization. Experimental results indicate that both liquid-liquid phase separation and crystallization have a detrimental effect on the durability of nuclear waste glasses. Controlling the glass compositions and defining

the heat treatment conditions that avoid phase separation and crystallization are keys to achieving waste glass durability control during processing, as discussed in chapter 13.

In summary, the review of the history of waste form development, and the information (data and models) on glass-melt properties for various types of commercial and waste-glass compositions indicates that the behavior of glasses is complex and cannot be expressed in simple terms for all wastes. The glass composition needs to be designed uniquely for each waste type. The lessons learned, or the existing database of HLW glasses, can be used as a guideline to narrow the scope of R&D needed to meet the requirements.

REFERENCE

U.S. Department of Energy. *Waste Acceptance Product Specifications for Vitrified High-Level Waste Forms*. EM-WAPS. Revision 2. Washington, DC: U.S. Department of Energy. 1996.

1 INTRODUCTION

1.1 BACKGROUND

The tank waste remediation system (TWRS) program at the Hanford, Washington, site was established in 1991 by the U.S. Department of Energy (DOE) to manage the cleanup of the nearly 54 million gal. (204,000 m^3) of radioactive waste currently in underground storage tanks. In addition, the DOE chose to use a privatization-type contract for the construction and operation of the TWRS facility.

The tank waste remediation systems privatization (TWRS-P) program was divided into two phases; Phase I was the proof-of-concept or demonstration phase and Phase II was the full-scale operations phase. Phase I was further divided into two phases, Part A and Part B (U.S. Department of Energy, 1998). After completion of Part A of Phase I in fiscal year (FY) 1998, the DOE decided to further subdivide Part B into two parts, Phase I Part B-1 and Phase I Part B-2. With this newly revised contract, DOE awarded a contractor team led by BNFL Inc. to proceed to the next phase (Phase I/Part B-1) of the TWRS-P project. This phase was a 24-mo design period during which BNFL Inc. would address technology scaleup; regulatory, financial, and permitting issues; and the safety basis for operations. As Part B-1 of Phase I neared completion, the contractor team led by BNFL Inc. presented a new estimate in April 2000 for Part B-2 of Phase I, which would include the construction and operation of a facility to process approximately 10 percent of the Hanford tank waste by mass and 20–25 percent by radioactivity. This new estimate was significantly higher than a prior estimate provided by the BNFL Inc. team approximately 18 mo earlier and resulted in the DOE decision to hold a new competition to seek other contractors for the project. In addition, it is not likely DOE will continue with a privatization-type contract, and, as a result, the U.S. Nuclear Regulatory Commission (NRC) may no longer be involved in the licensing and regulation of Phase II of the project as originally planned in the Memorandum of Understanding between DOE and NRC.[1] Consequently, the Center for Nuclear Waste Regulatory Analyses, which has been engaged by the NRC to assist in development of regulatory and technical guidance for TWRS-P project facilities, is now planning to close all current work and cease involvement in the project at the end of FY 2000.

1.2 SCOPE OF REPORT

This report provides a review of glass-melt properties and characteristics, basis and importance of imposed constraints on the design of glass composition, and potential safety and processing aspects of glass melting that can compromise radiological safety. This report was written to assist the NRC in

- Determining if sufficient information exists to assess safety considerations regarding vitrification of the waste stored at the Hanford site near Richland, Washington
- Determining if current regulatory guidelines are adequate to control implementation of the vitrification process to immobilize high-level wastes (HLW) at Hanford

---

[1]Memorandum of Understanding between the U.S. Nuclear Regulatory Commission and the U.S. Department of Energy, January 29, 1997, Federal Register, V. 62, No. 52, 12861, March 18, 1997.

- Identifying technical uncertainties
- Assessing where future guidance may be warranted

In chapter 2 of this report, a brief history of waste form development is provided, which is followed in chapter 3 by the Waste Acceptance Product Specifications (WAPS) imposed on the HLW vitrified waste form in the United States. In chapter 4, glass formation theories are discussed. These theories provide the backbone of many models used to predict glass properties.

The importance of electrical conductivity of glass melts, its temperature and compositional dependence, and its impact on the operations of electrically (joule) heated melters are discussed in chapter 5. The joule-heated melters for nuclear waste vitrification require electrical conductivity of the glass melts between 10 and 100 S/m at the melting temperature.

In chapter 6, the role of melt viscosity in the processing of glass is discussed. The joule-heated melters for nuclear waste vitrification require viscosity of glass melts between 2 and 10 Pa-s (20 and 100 P) at melting temperature. The limits are imposed on glass melts at melting temperature to ensure the glass melt is fluid enough to homogenize and pour. The models used for predicting melt viscosity from glass composition are also presented.

The WAPS require, at the time of shipment to a federal repository, the producer to certify that after the initial cool-down, the waste form temperature has not exceeded 400 °C. This product specification was established to ensure the waste form is in a solid form at the time of shipment. The glass transition temperature (T_g) range marks the temperature interval over which a given system gradually transforms on cooling from a supercooled liquid state into the glass state. There is no absolute measure of T_g because its value is influenced by the thermal history and rate of cooling. The importance of T_g is discussed in chapter 7.

Liquidus temperature (T_L) is the highest temperature at which the melt and primary crystalline phases can coexist at equilibrium. If the lowest temperature in the melter is lower than the T_L of the melt crystalline phases can precipitate and cause processing problems. In joule-heated melters operating at an average temperature of 1,150 °C, the T_L limit is set at 1,050 °C. Therefore, the understanding of T_L and its compositional dependence is important for the operations of joule-heated melters, and T_L is discussed in chapter 8.

Redox (reduction-oxidation) reactions involve a transfer of one or more electrons within the different oxidation states of a single multivalent element or from one multivalent element to another within a chemical system. An example of a multivalent element that can coexist in multiple valance states is Fe, which can exist as either Fe^{2+}/Fe^{3+} or Fe^{0}/Fe^{2+} depending on the available oxygen in the system. Knowledge of redox reactions in glass melts and their temperature and compositional dependence during vitrification of HLW in joule-heated melters is important. In chapter 9, a brief discussion of redox limits is followed by a discussion on the thermodynamic basis for redox reactions and the variables that impact redox reactions in glass melts. A redox response within a specified redox range is necessary to avoid process upsets that eventually could lead to permanent melter damage. A glass melt is defined as extremely reducing if the Fe^{2+}/Fe^{3+} ratio is greater than 1. Under such conditions, sufficient accumulation of conductive metals and metal sulfides could occur and short-circuit the melter. If the Fe^{2+}/Fe^{3+} ratio is less than 0.01, a glass melt is defined as extremely

oxidizing. Under extremely oxidizing conditions, foaming is observed in the melter. Foam creates an insulating layer of gas bubbles between the cold cap and the melt, disrupting the thermal gradients in the melter.

Noble metals such as Ru, Rh, and Pd in the HLW originate from the fission of U-235. Noble metals in the borosilicate glass melts have been a major concern in the HLW vitrification process because of their low solubility, high volatilization rate and high electrical conductivity. In silicate glasses, solubilities of Rh, Pd, and Ru are approximately 0.05, 0.03, and 0.01 wt%, respectively. In 1985, the accumulation of the noble metals on the floor of the Pamela melter, in Mol, Belgium, resulted in electrical shorting of the joule-heated melter. Potential issues related to noble metals in melts are discussed in chapter 10.

Borosilicate glass-based waste forms have limited sulfur solubility. In the West Valley Demonstration Project (WVDP) and the Defense Waste Processing Facility (DWPF) waste forms, SO_3 levels are maintained below 0.25 wt% to avoid formation of immiscible sodium sulfate phase in the melt. Traditionally, wastes containing high concentrations of sulfur are washed to remove soluble sulfate salts. If the concentration of SO_3 is in excess of 0.25 wt%, the SO_3 concentration limits the waste loading in the glass. The SO_3 solubility limit is established based on the operating redox range of 0.01 to 0.5. In chapter 11, a discussion of sulfur solubility limits imposed on the glass composition is followed by a review of various studies on sulfur solubility and the implication on the low-activity waste (LAW) vitrification at the Hanford site.

When glass comes in contact with the repository environment, such as flowing or stagnant groundwater, corrosive gases and vapors, or aqueous solutions, chemical reactions occur at the surface that spread to the whole of the glass depending on its composition, the pH of the solution, and the temperature of the environment. In chapter 12, a review of recent advances in the understanding of the dissolution behavior of glass as a function of glass composition, pH, and temperature is provided.

Crystallization of glass during cooling results in the formation of several phases in the glassy matrix. These phases can affect glass durability or even the glass melting behavior. In chapter 13, a review of the crystallization behavior of various waste forms is provided.

2 HISTORY OF WASTE FORM RESEARCH, EVALUATION, AND SELECTION

Research and development (R&D) of waste forms to immobilize liquid radioactive wastes began in the mid-1950s. Initial investigations included evaluating waste forms, such as borosilicate glass, phosphate glass, nepheline-syenite glass, a variety of polyphase ceramics, and bituminous and concrete materials (Hench et al., 1984). The R&D continued through the 1970s with no coherent approach. Most of the programs did not even consider scaling up from laboratory studies to remote operations capable of handling millions of gallons of waste. According to Hench (1995), efforts to compare various waste forms uncovered a potential problem—lack of standardized test methods to evaluate waste form materials. In 1977, the DOE initiated a comprehensive program to select a waste form for HLW in the United States based on standardized tests. The waste forms were reviewed again in 1994 for the Pu immobilization program. In addition, several review papers were published to summarize and compare various waste forms [e.g., Donald et al. (1997) provides the most current status of waste form for immobilization].

2.1 HIGH-LEVEL WASTE TECHNOLOGY PROGRAM

In 1979, the DOE initiated the National High-Level Waste Technology Program, which sponsored R&D at 14 laboratories, 3 universities, 3 industrial laboratories, and several DOE sites. The study evaluated 17 different waste forms as shown in table 2-1. In 1980, R&D activities for 10 waste forms were terminated based on reviews that indicated significant technical concerns about their viability as candidates for disposal (Hench et al, 1984). The remaining seven waste forms underwent the following assessments by the DOE teams:

- Evaluations at the DOE defense waste sites
- Peer-review evaluation
- Product performance evaluation
- Processability analysis

Based on the combined results, borosilicate glass was selected as the reference, and Synroc was selected as an alternative waste form for the U.S. HLW program. Important attributes supporting the selection of borosilicate glass as the reference waste form were

- Ability to incorporate a wide range of waste compositions
- Good durability in potential repository environments
- Low processing temperature
- Remote processing
- Relative insensitivity to radiation damage

Processability of borosilicate glass had an advantage factor of 2 to 4 times over Synroc. This advantage was attributed to the successful operation of calcine-fed and slurry-fed melters at Savannah River Laboratory (SRL) and proven operations at the Atelier de Vitrification de Marcoule facility in France. However, the relative economics of glass compared to Synroc was under debate because Synroc offered three times higher waste loading compared to borosilicate glass, which offered potential economic advantage.

Table 2-1. Candidate waste forms considered for geologic disposal of high-level waste (Hench et al., 1984)

Waste form	Comments
Borosilicate glass	Reference waste form
Synroc-C, -D*	Alternative waste form
Tailored ceramic	Semifinalist alternative waste form
High-silica glass	Semifinalist alternative waste form
Formed under elevated temperature and pressure concrete	Semifinalist alternative waste form
Coated sol-gel particles	Semifinalist alternative waste form
Glass marbles in Pb matrix	Semifinalist alternative waste form
Phosphate glass	Eliminated in 1979–1980
Clay ceramic	Eliminated in 1979–1980
Titanate ion-exchanger	Eliminated in 1979–1980
Stabilized calcine	Eliminated in 1979–1980
Pelletized calcine	Eliminated in 1979–1980
Normal concrete	Eliminated in 1979–1980
Hot-pressed concrete	Eliminated in 1979–1980
Cermet†	Eliminated in 1979–1980
Disc-pelletized coated particles	Eliminated in 1979–1980

*Synroc-C composition was originally proposed for immobilization of commercial reactor wastes, while Synroc-D was a modification of Synroc-C developed for immobilization of defense wastes.
†Cermet fixes high-level waste in a continuous, corrosion-resistant, thermally conductive, metal-alloy matrix.

Vitrification, using borosilicate glass waste forms, is successfully used in the United States, United Kingdom, France, Germany, Belgium, the Former Union of Soviet Socialists Republic, India, and Japan for immobilizing HLWs, while DOE-sponsored work on Synroc was discontinued effective January 1983. A review by Jain (2000) on vitrification facilities worldwide provides the current status, process description, lessons learned, and potential safety issues at various vitrification facilities.

2.2 PLUTONIUM IMMOBILIZATION PROGRAM

The waste forms for immobilization were revisited under the DOE Office of Fissile Materials Disposition program created in 1994 to manage DOE activities relating to the management, storage, and disposition of surplus fissile materials. The goal was to make Pu as unattractive and inaccessible for retrieval and use in weapons as the residual Pu in spent fuel from commercial reactors (Bronson et al., 1998). Under this program, based on the literature review, 70 waste forms were identified for immobilizing radioactive wastes. Initial screening was conducted based on pass/fail criteria shown in table 2-2. Failure of any one

Table 2-2. Initial screening criteria for Pu immobilization waste forms (Lawrence Livermore National Laboratory, 1996)

Criteria	Requirement	Basis
No free water	"Shall not contain free liquids in amount that could compromise the waste package."	10 CFR 60.135(b)(2)
Solidification and consolidation	"Shall be ... in solid form ... [and] ... consolidated ... to limit the availability and generation of particulate."	10 CFR 60.135(c)(1&2)
Stability	"Shall not contain explosive or pyrophoric or chemically reactive materials in an amount that could compromise the waste package..." and "...shall be noncombustible ..."	10 CFR 60.135(b)(1)&(c)(3)
Criticality control	"K_{eff} must ... show at least 5 % margin"	10 CFR 60.131(b)(7)
Resource Conservation Recovery Act metal content	Cannot contain significant quantities of the following free metals: arsenic, barium, cadmium, lead, mercury, selenium, and silver.	40 CFR 261.24
Readiness	Must be technically viable for use 20 yr after the record of decision (subsequently, 10 yr).	U.S. Department of Energy prescribed requirement.
Loading	Must maintain a feasible volume of waste for storage	Reasonable limit, factoring in increased resources required to handle excess volumes of immobilized material and limited storage sites/volumes.

criterion or "probable" failure of two criteria resulted in elimination of the waste form. Based on this evaluation, 16 waste forms shown in table 2-3 were selected for stage 2 evaluation.

The following attributes were used for the second stage of the screening process.

- Resistance to Pu theft, diversion, and recovery by a terrorist organization or rogue nation
- Technical viability, including technical maturity, development risk, and acceptability for repository disposal
- Environmental safety, and health factors
- Cost effectiveness
- Timeliness

Table 2-3. Final ranking of waste forms for Pu immobilization (Lawrence Livermore National Laboratory, 1996)

Waste form	Utility
Borosilicate glass	0.89
Synroc	0.66
Phosphate glass	0.55
Monazite	0.49
Metallic alloy	0.47
High-silica glass	0.44
Formed under elevated temperature and pressure concrete	0.40
Hot-pressed concrete	0.24
Phosphate-bonded ceramic	0.17
Silica-zirc phosphate	0.17
Ceramics in concrete	0.14
Iron-enriched basalt	0.13
Ceramic pellets in metal matrix	0.13
Supercalcine	0.08
Glass-ceramic monoliths	0.03
Cermet*	0.00

*Cermet fixes high-level waste in a continuous, corrosion-resistant, thermally conductive, metal-alloy matrix.

Based on the second stage screening, a well-balanced portfolio of waste forms consisting of borosilicate glass, ceramic (Synroc), and metallic alloy was selected for further evaluation, while glass-bonded zeolite was retained as a reasonable alternative. Borosilicate glass was chosen because it is consistently the highest performing waste form over all other glasses. Ceramic waste form was selected because it performed better than all other glasses except borosilicate glass. Metallic alloy was selected over concrete formed under elevated temperature and pressure. However, for the disposal of Al-based spent nuclear fuel, in 2000 DOE selected melt dilute technology as a preferred alternative. The melt-dilute technology produces a metallic-alloy waste form (Adams et al., 2000).

In September 1997, based on the technical evaluation and assessments, Synroc was recommended for deployment in the planned Pu immobilization plant based on the following advantages over borosilicate glass.

- Ceramic waste form is expected to be much more durable in the repository environment and should retain Pu and its decay products for longer periods than the glass waste form.
- Ceramic waste form process has a significantly lower source term and potential for worker exposure, which enhances its preference by reason of the as-low-as-is-reasonably-achievable standard.
- Ceramic waste form and process offer significant cost savings compared to the glass technology.
- Ceramic waste form is somewhat more robust to the threat of theft and diversion by terrorists or rogue states.
- Maturity of the ceramic waste form technology was found to be comparable to glass.

2.3 SELECTION OF A WASTE FORM FOR HANFORD HIGH-LEVEL WASTE

Westinghouse Hanford Company (1990) wrote a white paper to justify its selection of borosilicate glass as a suitable waste form for the HLW stored at the Hanford site. The paper cites the following strengths of the borosilicate glass waste form.

- Based on independent investigation conducted in many countries, borosilicate glass waste form is the dominant choice for immobilization.
- Thirteen borosilicate glass-based vitrification facilities are in operation or under construction around the world.
- Decisions to convert HLW into borosilicate glass were made at WVDP and DWPF in 1982, and for Hanford wastes in 1988 but only after an in-depth examination of the alternatives.
- Borosilicate glass waste form is capable of meeting all waste form specifications, including NRC and U.S. Environmental Protection Agency (EPA) regulations for geologic disposal of HLW.

- Because of the wide acceptance of borosilicate glass as a waste form, there has been relatively little investigation of alternative waste forms.

- In 1990, EPA promulgated vitrification as the treatment standard [i.e., best demonstrated available technology (BDAT)] for the high-level fraction of the mixed waste generated during reprocessing of nuclear fuel. In the ruling, EPA concluded that vitrification will provide effective immobilization of the inorganic Resource Conservation and Recovery Act hazardous constituents in the high-level mixed waste generated during the reprocessing of fuel rods.

Vitrification is currently planned for the HLW contained in 177 aging underground storage tanks at the Hanford site. The current plans for Hanford wastes call for pretreatment of the wastes prior to vitrification that will separate the waste into HLW and LAW fractions. The HLW and LAW will be separately vitrified into borosilicate glass. The status of the wastes stored at the Hanford site and its chemistry have been reviewed by Cragnolino et al. (1997) and Pabalan et al. (1999).

2.4 CURRENT STATUS OF VARIOUS WASTE FORMS

Review of the various waste forms indicates that borosilicate glass is the generally accepted waste form for the immobilization of HLW and low-level waste. The borosilicate glass waste form-based vitrification technology is mature, proven, and safe, but with the emergence of new sources of radioactive materials, such as surplus Pu, requiring immobilization, there is renewed interest in the ceramic (Synroc) waste form. Donald et al. (1997) provided a comprehensive review of various waste forms for radioactive wastes. This reference provides the most current status of suitability of various waste forms for immobilization. Donald et al. (1997) state that although, at the present time, borosilicate glass is the generally accepted first generation waste form for the immobilization of HLW, the emergence of additional sources of highly radioactive materials requiring immobilization has renewed the interest in a reexamination of many of the alternative candidates such as Synroc-based titanate, zirconate, and phosphate ceramics, iron phosphate glasses, and basaltic glass-ceramics. Except for Synroc, the majority of alternate waste forms have been studied only marginally.

2.5 REFERENCES

Adams, T.M., H.B. Peacock, N.C. Iyer, M.W. Barlow, H.M. Brooks, W.F. Swift, and F.C. Rhode. *Melt-Dilute Treatment Technology for Aluminum-Based Research Reactor Fuel.* WSRC–MS–2000–00206. Aiken, SC: Westinghouse Savannah River Company. 2000.

Bronson, M., J. Diaz, T.A. Edmunds, L.W. Gray, D.C. Riley, and T.L. Rising. Plutonium immobilization form evaluation. *Proceedings of the Waste Management '98 Symposium.* CD Rom version: Paper No. 65-02. Tucson, AZ: WM Symposia Inc. 1998.

Cragnolino, G.A., M.S. Jarzemba, J. Ledbetter-Ferrill, W.M. Murphy, R.T. Pabalan, D.A. Pickett, J.D. Prikryl, and N. Sridhar. *Hanford Tank Waste Remediation System Familiarization Report.* CNWRA 97-001. San Antonio, TX: Center for Nuclear Waste Regulatory Analyses. 1997.

Donald, I.W., B. L. Metcalfe, and R.N.J. Taylor. Review the immobilization of high-level radioactive wastes using ceramics and glasses. *Journal of Materials Science* 32: 5,851–5,887. 1997.

Hench, L.L., D.E. Clark, and J. Campbell. High-level waste immobilization forms. *Nuclear and Chemical Waste Management* 5: 149–173. 1984.

Hench, L.L. The '70's: From selection of alternative waste forms to evaluation of storage system variables. *Proceedings of the International Symposium on Environmental Issues and Waste Management Technologies in the Ceramic and Nuclear Industries. 97th Annual Meeting of the American Ceramic Society, Cincinnati, Ohio, May 1–5, 1995.* Ceramic Transactions Volume 61. Westerville, OH: American Ceramic Society: 129–137. 1995.

Jain, V. *Survey of Waste Solidification Process Technologies.* NUREG/CR–6666. Washington, DC: U.S. Nuclear Regulatory Commission. 2000.

Lawrence Livermore National Laboratory. *Fissile Material Disposition Program Screening of Alternate Immobilization Candidates for Disposition of Surplus Fissile Materials.* UCRL–ID–118819, L–207790–1. Livermore, CA: Lawrence Livermore National Laboratory. 1996.

Pabalan, R.T., M.S. Jarzemba, D.A. Pickett, N. Sridhar, J. Weldy, C.S. Brazel, J.T. Persyn, D.S. Moulton, J.P. Hsu, J. Erwin, T.A. Abrajano, Jr., and B. Li. *Hanford Tank Waste Remediation System High-Level Waste Chemistry Manual.* NUREG/CR–5751. Washington, DC: U.S. Nuclear Regulatory Commission. 1999.

Westinghouse Hanford Company. *Evaluation and Selection of Borosilicate Glass as the Waste form for Hanford High-Level Radioactive Waste.* DOE/RL–90–27. Richland, WA: Westinghouse Hanford Company. 1990.

3 WASTE ACCEPTANCE CRITERIA FOR GEOLOGIC DISPOSAL

Waste acceptance criteria for the producers of the vitrified waste form are outlined in the WAPS document by the DOE (1996). WAPS define the characteristics of the vitrified product and the canistered waste form that will be produced at the vitrification plants and are the first step in the waste acceptance process. WAPS specify technical requirements that the waste form must meet and the documentation the producers must provide to assure that products comply with the NRC requirements in 10 CFR Part 60[1] (Stahl and Cloninger, 1991). The WAPS are shown in table 3-1.

3.1 PRINCIPAL WASTE ACCEPTANCE CRITERIA

Since the intent of this report is to present the chemistry of the vitrification process and to focus on processing and safety issues that could result from inadequate control during processing, the discussion is limited to waste form properties and characteristics that are important in producing waste forms. To meet waste form specifications, the glass composition of the vitrified waste form must be designed to ensure it meets WAPS and is also safely processible using joule-heating melter technology. WAPS that are dictated by the glass composition and vitrification process are

- Chemical composition. The WAPS state that the "...producer shall project the chemical composition, identify crystalline phases expected to be present, and project the amount of each crystalline phase, for each waste type," and the "...producer shall report the oxide composition of the waste form. The reported composition shall include all elements, excluding oxygen, present in concentrations greater than 0.5 percent by weight of the glass, for each waste type."

- Product Consistency. The WAPS state that "the producer shall demonstrate control of waste form production by comparing, either directly or indirectly, production samples to the Environmental Assessment (EA) benchmark glass. The consistency of the waste form shall be demonstrated using the Product Consistency Test (PCT). For acceptance, the mean concentrations of lithium, sodium, and boron in the leachate, after normalizing for the concentrations in the glass, shall each be less than those of the benchmark glass... ." "One acceptable method of demonstrating that the acceptance criteria are met, would be to ensure that the mean PCT results for each waste type are at least two standard deviations below the mean PCT of the EA glass."

- Phase Stability. The WAPS state that, "the producer shall provide the following data for each projected waste type: (a) The glass transition temperature and (b) time-temperature-transformation diagram that identified the duration of exposure at any temperature that causes significant changes in either the phase structure or the phase compositions. ...Producer shall certify that after the initial cool-down, the waste form temperature has not exceeded 400 C."

---

[1]The current regulation governing deep geologic disposal of high-level waste is 10 CFR Part 60. At the direction of Congress, the U.S. Nuclear Regulatory Commission has proposed a regulation at 10 CFR Part 63 that would govern disposal at the proposed repository site at Yucca Mountain, Nevada.

Table 3-1. Waste acceptance preliminary specifications (U.S. Department of Energy, 1996)

Area	Specification
Waste form specification	1.1 Chemical specification
	1.2 Radionuclide inventory specification
	1.3 Specification for product consistency
	1.4 Specification for phase stability
	1.5 Hazardous waste specification
Canister specifications	2.1 Material specification
	2.2 Fabrication and closure specification
	2.3 Identification and labeling specification
	2.4 Specification for canister length and diameter
Canistered waste form specifications	3.1 Free-liquid specification
	3.2 Gas specification
	3.3 Specification for explosiveness, pyrophoricity, and combustibility
	3.4 Organic materials specification
	3.5 Chemical compatibility specification
	3.6 Fill height specification
	3.7 Specification for removal of radioactive
	3.8 Heat generation specification
	3.9 Specification for maximum dose rates
	3.10 Subcriticality specification
	3.11 Specification for weight, length, diameter, and overall dimensions
	3.12 Drop test specification
	3.13 Handling features specification
Quality assurance	4.0 Quality assurance specifications
Documentation and other requirements	5.1–5.14 (14 different specifications)

A vitrified waste form can meet waste form specifications if the glass melt properties such as viscosity, electrical conductivity, T_L, T_g, and melt characteristics such as redox, volatilization, phase separation, and precipitation are defined and controlled during processing. Both product specifications in the WAPS and process requirements determined based on technology have to be considered together in developing glass composition for vitrified waste form. In this report, the role of various glass properties and characteristics in optimizing the glass melt chemistry and chemical composition to safely produce a vitrified waste form is discussed.

3.2 REFERENCES

Stahl, D., and M.O. Cloninger. Waste acceptance for vitrified high-level waste forms. *Proceedings of the Fifth International Symposium on Nuclear Waste Management IV. 93rd Annual Meeting of the American Ceramic Society, Cincinnati, Ohio, April 29–May 3, 1991.* Ceramic Transactions Volume 23. G.C. Wicks, D.F. Bickford, and L.R. Bunnell, eds. Westerville, OH: American Ceramic Society: 433–441. 1991.

U.S. Department of Energy. *Waste Acceptance Product Specifications for Vitrified High-Level Waste Forms*. EM-WAPS. Revision 2. Washington, DC: U.S. Department of Energy. 1996.

4 GLASS FORMATION

The word glass is derived from a Latin term glaesum, which refers to a lustrous or transparent material. Glass is also referred to as vitreous, originating from the Latin word vitrum. The American Society for Testing and Materials (ASTM) defines glass as an inorganic product of fusion that has been cooled to a rigid condition without crystallizing. This ASTM definition is fairly restrictive, since several organic systems can make glass, and processes such as sol-gel and chemical vapor deposition do not require fusion to make glass. To avoid such restrictions, glass is defined here as solid with a liquid-like structure, a noncrystalline solid or an amorphous solid. A typical volume-temperature relationship for a glass-forming liquid is shown in figure 4-1. Glass-forming liquids when cooled from location a, skip the crystallization temperature at location b and continue to follow the path shown. The glass-transition range starts at a point where the cooling path begins to depart from the supercooled liquid path and ends when the cooling profile attains a constant slope as shown in figure 4-1. This constant slope after the transition range is referred to as glassy state. Also shown in figure 4-1 is the effect of the cooling rate. The faster the glass is cooled, the higher the specific volume of glass.

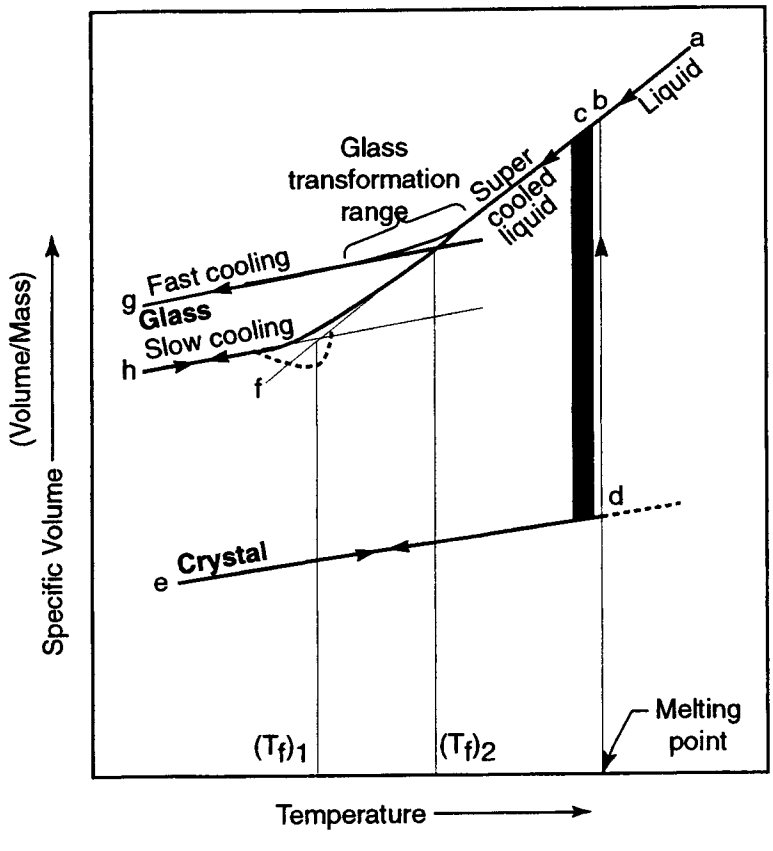

Figure 4-1. Specific volume-temperature diagram for a glass-forming liquid

4.1 GLASS FORMATION PRINCIPLES

Several structural theories—Goldschmidt's radius ratio criterion, Zachariasen's random network theory, Smekal's mixed bonding rule, Stanworth's electronegativity rule, Sun's single-bond strength criterion, Dietzel's field strength criterion, and Phillips' topological constraint model—and kinetic theory have been put forward to explain the formation of glass. These theories are discussed in detail in textbooks by Varshneya (1994), Paul (1982), and Rawson (1967). In this chapter, Zachariasen's random network theory and Sun's bond strength criterion, both of which had significant influences on our current understanding of glass formation principles and are used by several researchers to model nuclear waste glasses, are reviewed. The kinetic theory, which is important in analyzing phase separation and crystallization in glass, is presented in chapter 13.

4.1.1 Zachariasen's Random Network Theory

The random network theory was proposed by Zachariasen in 1932. Zachariasen argued that the interatomic forces in glass must be similar to those in the corresponding crystals, since the mechanical properties of the two forms are similar. Similar to crystals, the atoms in the glass must form extended three-dimensional (3D) networks but not in a symmetrical or periodic pattern. He defined glass as a "substance (that) can form extended 3D networks lacking periodicity with an energy content comparable with that of the corresponding crystal network" and laid the following four rules for glass formation in a compound A_mO_n:

(1) An oxygen atom is linked to no more than two atoms of A.
(2) The oxygen coordination around A is small, say three or four.
(3) The cation polyhedra shares corners, not edges or faces.
(4) At least three corners are shared.

Based on the theory, Group I and II (oxides of formula A_2O and AO) cations cannot satisfy rules 1 to 3, and, therefore, do not form glass. For Group III oxides (A_2O_3), rules 1, 3, and 4 are satisfied if the oxygens form triangles around A. B_2O_3 in this category is a glass former. Group IV oxides (AO_2) and Group V oxides (A_2O_5) would form glass if the oxygen formed tetrahedra around the cations. Glass formers in this category include SiO_2, GeO_2, P_2O_5, and As_2O_5. Oxides in Group VI, VII, and VIII can satisfy rules 1, 3, and 4 if cation octahedra are formed, but rule 2 is violated. Zachariasen's theory received wide support and acceptance with the following limitations (Paul, 1982).

- In most of the oxides, oxygen has a coordination number of two. However, in the binary Tl_2O-B_2O_3 system with low Tl_2O concentration, the coordination number for oxygen may be three.

- The coordination number for Si, P, and B in glass are four, and three or four. However, the coordination number of Te in the PbO-TeO_2 glass system is six.

- Alkali phosphate glasses containing more than 50 mol% alkali oxide contain two-dimensional (2D) chains of various sizes. Thus, a 3D network may not be necessary.

4.1.2 Sun's Single-Bond Strength Criterion

In 1947, Sun proposed a single-bond strength criterion for glass formation. According to Sun, the process of glass formation involves inability of the bonds in the liquid state to rearrange during crystallization and, hence, the higher the bond strength the better the glass former. Bond strengths associated with various oxides are shown in table 4-1. Based on the bond strengths, Sun classified the glass forming oxides as follows:

- Oxides exceeding bond strength 334 kJ/mol (80 kcal/mol) as glass network formers.
- Oxides with bond strengths lass than 251 kJ/mol (60 kcal/mol) as glass network modifiers.
- Oxides with bond strengths between 251 and 334 kJ/mol (60 and 80 kcal/mol) as intermediates.

The important contribution made by Sun was the introduction of an intermediate category. Sun's model is widely used in the development of glass property models based on a thermodynamic approach.

4.2 GLASS FORMING SYSTEMS

Tables 4-2 and 4-3 show the composition of several commercial glass-forming systems and nuclear waste glasses, respectively. Silica based glass forming systems are widely used in commercial industry and consist of silica as a major constituent along with alkalis, alkaline earths, boric oxide, and lead oxide. To help understand the behavior of nuclear-waste glasses and models used to relate glass properties to composition, a review of the basic glass-forming systems of nuclear waste glasses is provided in the following sections.

4.2.1 Vitreous Silica Glass

Silica glass is highly refractory and has high chemical resistance to corrosion, low electrical conductivity, near-zero thermal expansion, and good ultraviolet transparency. Silica glass is widely used in optical fibers and astronomical mirrors. The structure of silica glass consists of slightly distorted SiO_4 tetrahedra joined to each other at the corners as shown in figure 4-2. Each oxygen acts as a bridge between neighboring tetrahedra and is called bridging oxygen (BO). In borosilicate-based nuclear waste glasses, SiO_4 tetrahedras are the basic building blocks of the glass structure.

4.2.2 Alkali Silicate Glass

Alkalis, as shown by Sun's bond strength criterion, are classified as network modifiers. When an alkali (M) is added to silica glass, it enters the glass structure by breaking the -Si-O-Si- bond and attaching itself to the broken oxygen bond as shown by Eq. (4-1).

$$\equiv Si - O - Si \equiv + M_2O \rightarrow \equiv Si - O^-M^+ + M^+{}^-O - Si \equiv \qquad (4\text{-}1)$$

As shown by Eq. (4-1), each alkali ion results in the creation of one nonbridging oxygen (NBO). The addition of alkali ions results in the breakdown of the silica tetrahedra connectivity, and the glass properties are significantly affected. The effect of alkali ions on glass properties is presented in various chapters of this report.

Table 4-1. Single-bond strengths for oxides (Varshneya, 1994)

	M in MO_x	Valence	Dissociation Energy E_d, per MO_x kJ (kcal)	Coordination Number	Single-Bond Strength kJ (kcal)
Glass formers	B	3	1.49×10^3 (356)	3	498 (119)
	Si	4	1.77×10^3 (44)	4	444 (106)
	Ge	4	1.80×10^3 (431)	4	452 (108)
	Al	3	1.68×10^3–1.32×10^3 (402–317)	4	423–331 (101–79)
	B	3	1.49×10^3 (356)	4	373 (89)
	P	5	1.85×10^3 (442)	4	465–368 (111–88)
	V	5	1.88×10^3 (449)	4	469–377 (112–90)
	As	5	1.46×10^3 (349)	4	364–293 (87–70)
	Sb	5	1.42×10^3 (339)	4	356–285 (85–68)
	Zr	4	2.03×10^3 (485)	6	339 (81)
Intermediates	Ti	4	1.78×10^3 (435)	6	306 (73)
	Zn	2	0.60×10^3 (144)	2	301 (72)
	Pb	2	0.61×10^3 (145)	2	306 (73)
	Al	3	1.32×10^3–1.68×10^3 (317–402)	6	222–281 (53–67)
	Th	4	2.16×10^3 (516)	8	268 (64)
	Be	2	1.05×10^3 (250)	4	264 (63)
	Zr	4	2.03×10^3 (485)	8	255 (61)
	Cd	2	0.50×10^3 (119)	2	251 (60)
Modifiers	Sc	3	1.52×10^3 (362)	6	251 (60)
	La	3	1.70×10^3 (406)	7	243 (58)
	Y	3	1.67×10^3 (399)	8	209 (50)
	Sn	4	1.16×10^3 (278)	6	193 (46)
	Ga	3	1.12×10^3 (267)	6	188 (45)
	In	3	1.08×10^3 (259)	6	180 (43)
	Th	4	2.16×10^3 (516)	12	180 (43)
	Pb	4	9.71×10^2 (232)	6	163 (39)
	Mg	2	9.30×10^2 (222)	6	155 (37)
	Li	1	6.03×10^2 (144)	4	151 (36)
	Pb	2	6.07×10^2 (145)	4	151 (36)
	Zn	2	6.03×10^2 (144)	4	151 (36)
	Ba	2	1.09×10^3 (260)	8	138 (33)
	Ca	2	1.07×10^3 (257)	8	134 (32)
	Sr	2	1.07×10^3 (256)	8	134 (32)
	Cd	2	4.98×10^2 (119)	4	126 (30)
	Na	1	5.02×10^2 (120)	6	83.7 (20)
	Cd	2	4.98×10^2 (119)	6	83.7 (20)
	K	1	4.82×10^2 (115)	9	54.4 (13)
	Rb	1	4.82×10^2 (115)	10	50.2 (12)
	Hg	2	2.85×10^2 (68)	6	46.1 (11)
	Cs	1	4.77×10^2 (114)	12	41.9 (10)

Table 4-2. Commercial glass compositions in oxides (wt%) (Varshneya, 1994)

	Vitreous Silica	Vycor	Plate	Window	Bottle or Container	Bulb	Tubing	Lime Table-ware	Pyrex Type	Thermo-meter	Borosi-licate Crown	Lead Table-Lamp	Glass Halogen Lamp	E Glass	S Glass	Optical Flint
SiO_2	100.00	94.0	72.7	72.0	74.0	73.6	72.1	74.0	81.0	72.9	69.6	67.0	60.0	52.9	65.0	49.8
Al_2O_3	—	—	0.5	0.6	1.0	1.0	1.6	0.5	2.0	6.2	—	0.4	14.3	14.5	25.0	0.1
B_2O_3	—	5.0	—	—	—	—	—	—	12.0	10.4	9.9	—	—	9.2	—	—
SO_3	—	—	0.5	0.7	Tr.	—	—	—	—	—	—	—	0.3	—	—	—
CaO	—	—	13.0	10.0	5.4	5.2	5.6	7.5	—	0.4	—	—	6.5	17.4	—	—
MgO	—	—	—	2.5	3.7	3.6	3.4	—	—	0.2	—	—	—	4.4	10.0	—
BaO	—	—	—	—	Tr.	—	—	—	—	—	2.5	—	18.3	—	—	13.4
PbO	—	—	—	—	—	—	—	—	—	—	—	17.0	—	—	—	18.7
Na_2O	—	1.0	13.2	14.2	15.3	16.0	16.3	18.0	4.5	9.8	8.4	6.0	0.01	—	—	1.2
K_2O	—	—	—	—	0.6	0.6	1.0	—	—	0.1	8.4	9.6	Tr.	1.0	—	8.2
ZnO	—	—	—	—	—	—	—	—	—	—	—	—	—	—	—	8.0
As_2O_3	—	—	Tr.	Tr.	Tr.	Tr.	—	Tr.	—	Tr.	0.3	Tr.	—	—	—	0.4

Table 4-3. Compositions of selected candidate waste glasses (mol%) (Ellison et al., 1994)

Glass	SiO_2	B_2O_3	Na_2O	Li_2O	Al_2O_3	Fe_2O_3	CaO	MgO	TiO_2	ZnO	ZrO_2	BaO	MnO_2	MoO_3
HW-39-1	56.74	9.16	11.15	8.45	2.80	4.62	3.44	1.32	—	—	0.32	0.04	0.15	0.14
SRL 131A	51.15	9.73	13.69	7.05	2.25	5.57	1.16	2.28	0.57	0.02	0.13	0.07	1.96	—
SRL 165A	58.09	6.41	11.56	9.24	2.64	4.85	1.91	1.15	0.12	0.03	0.35	0.03	2.60	—
SRL 202A	55.15	7.75	9.74	9.58	2.55	4.84	1.45	2.22	0.77	0.02	0.05	0.10	1.72	0.02
SRL 211	48.30	7.68	16.71	6.98	2.44	6.13	6.22	—	—	—	—	0.15	3.02	—
WVCM-47	51.30	12.56	10.83	4.92	5.71	5.53	0.77	2.39	0.90	—	0.17	0.02	1.09	0.01
WVCM-50	48.38	12.94	11.59	5.45	7.10	5.48	1.07	1.44	0.77	0.03	0.24	0.09	1.02	0.02
WVCM-70, Ref-6	48.62	13.20	9.20	8.85	4.19	5.37	0.61	1.57	0.71	0.02	0.76	0.07	0.83	0.02
WV205	51.75	9.84	12.20	7.13	2.23	5.08	0.75	2.22	0.86	—	1.73	0.27	1.34	—
PNL 76-68	52.59	9.03	17.87	—	0.33	4.99	2.83	—	2.82	4.32	0.99	0.25	0.03	0.97
GP 98/12	57.98	9.39	16.79	—	0.93	0.04	4.75	4.88	2.70	—	0.53	0.12	0.16	0.40
UK 209	53.95	10.18	8.53	8.51	3.19	1.09	—	10.02	—	0.31	0.74	0.16	—	0.78
UK 189	44.78	20.36	8.03	8.00	3.20	1.09	—	10.02	—	0.32	0.73	0.16	—	0.78
C 31/3	46.84	4.82	4.34	2.66	8.17	0.75	5.55	2.89	2.84	4.86	2.71	7.82	0.32	1.33
B 1/3	37.80	7.46	4.97	6.51	10.18	0.77	5.79	2.41	4.63	3.59	2.14	8.20	0.32	1.33
VG 98/3	49.10	10.61	25.31	—	0.83	0.31	2.92	0.70	3.11	—	1.34	0.29	0.32	1.06
SON 58	55.86	21.01	11.68	—	0.76	0.29	—	—	—	—	1.96	0.50	—	0.16
SON 64	56.76	19.13	14.62	—	1.20	2.46	—	—	—	—	1.15	0.29	—	0.95

Table 4-3. Compositions of selected candidate waste glasses (mol%) (Ellison et al., 1994) (cont'd)

Glass	SiO_2	B_2O_3	Na_2O	Li_2O	Al_2O_3	Fe_2O_3	CaO	MgO	TiO_2	ZnO	ZrO_2	BaO	MnO_2	MoO_3
SON 64/G3	56.35	19.03	14.21	—	0.15	2.83	—	—	—	—	1.22	0.31	—	1.06
SON 68 18 17 L1C2A2Z1	5.47	13.96	11.03	4.59	3.34	1.26	4.99	—	—	2.13	1.49	0.28	0.59	0.82
SAN 60	46.49	15.71	11.08	10.77	11.42	0.13	4.02	—	—	—	0.08	0.02	—	0.07
SM 58 LW 11	58.70	10.94	8.31	7.76	0.71	0.45	4.24	3.15	3.45	—	0.57	0.26	0.13	0.51
ABS 29	57.47	15.16	10.07	6.67	1.63	0.25	—	—	—	4.90	0.69	0.20	0.59	0.75
ABS 41	58.31	15.39	10.22	6.76	1.65	1.27	—	—	—	2.48	0.70	0.20	0.60	0.76
ABS 39	57.09	19.40	14.72	—	2.15	2.52	—	—	—	—	0.73	0.21	0.63	0.80
ABS 118	52.45	13.93	11.06	4.64	3.33	1.26	4.94	—	—	2.13	1.47	0.26	0.77	0.98
JSS-A	52.19	14.37	10.97	4.58	3.32	1.26	4.97	—	—	2.15	1.48	0.27	0.57	0.82
JW-D	54.86	18.14	12.39	4.25	1.33	1.51	2.27	—	—	—	1.58	0.28	0.20	0.82
GC–12/9B	52.35	13.10	9.96	7.75	2.80	2.23	3.04	2.53	4.36	—	1.11	—	0.03	—
Average (when present)	52.55	12.77	11.82	6.87	3.19	2.56	3.22	3.20	2.04	1.82	0.97	0.75	0.83	0.64
Average (all glasses)	52.55	12.77	11.82	5.21	3.19	2.56	2.33	1.77	0.99	0.94	0.94	0.72	0.66	0.53
Median	52.47	12.94	11.08	7.01	2.55	1.51	3.04	2.34	1.80	2.13	0.75	0.21	0.59	0.78
Minimum	37.80	4.82	4.34	2.66	0.15	0.04	0.61	0.70	0.12	0.02	0.05	0.02	0.03	0.01
Maximum	58.70	21.01	25.31	10.77	11.42	6.13	6.22	10.02	4.63	4.90	2.71	8.20	3.02	1.33
Occurrence (%)	100	100	100	76	100	100	72	55	48	52	97	97	79	83

Table 4-3. Compositions of selected candidate waste glasses (mol%) (Ellison et al., 1994) (cont'd)

Glass	K_2O	NiO	CeO_2	Nd_2O_3	P_2O_5	Cs_2O	RuO_2	SrO	Cr_2O_3	ThO_2	La_2O_3	U_3O_8	PdO	Pr_2O_3
HW-39-1	—	0.53	0.08	0.10	—	0.05	0.05	0.06	0.57	—	0.10	—	—	0.02
SRL 131A	2.88	1.17	—	—	—	—	—	0.01	0.06	—	0.00	0.23	—	—
SRL 165A	0.13	0.75	—	—	—	—	—	0.07	—	—	—	0.07	—	—
SRL 202A	2.67	0.74	—	—	—	—	—	0.02	0.04	0.07	—	0.16	—	—
SRL 211	0.04	1.53	0.35	0.19	—	—	—	0.24	0.00	—	—	—	—	—
WVCM-47	0.99	0.27	0.03	0.03	1.28	0.02	—	0.02	0.10	0.99	0.01	0.05	—	0.01
WVCM-50	1.25	0.30	0.31	0.03	1.28	0.02	—	0.01	0.07	0.98	0.01	0.05	—	0.01
WVCM-70, Ref-6	3.78	0.24	0.07	0.03	0.60	0.02	0.04	0.01	0.07	0.96	0.01	0.05	0.02	0.01
WV 205	2.55	0.64	0.06	—	1.21	0.02	—	—	0.10	—	—	—	—	—
PNL 76-68	—	0.25	0.44	0.90	0.36	0.22	0.43	—	0.24	—	0.11	—	—	—
GP98/12	—	0.08	0.16	0.07	0.20	0.05	0.25	—	0.02	—	0.02	0.02	0.17	0.02
UK 209	—	0.31	0.37	0.34	0.10	0.17	0.33	0.20	0.23	—	0.09	—	0.23	0.08
UK 189	—	0.31	0.37	0.34	0.11	0.17	0.32	0.20	0.23	—	0.09	—	0.22	0.08
C 31/3	—	0.25	0.62	0.58	—	0.49	0.56	0.46	0.22	—	0.16	0.04	0.07	0.15
B 1/3	—	0.26	0.62	0.58	—	0.49	0.32	0.46	0.23	—	0.16	0.05	0.05	0.15
VG 98/3	—	0.20	0.64	0.45	0.30	0.34	0.56	0.34	0.11	—	0.13	0.10	0.36	0.12
SON 58	—	1.13	0.93	0.68	0.33	0.49	1.08	0.49	0.10	—	0.46	0.33	0.61	0.21
SON 64	—	0.23	0.54	0.40	—	0.29	0.34	0.29	0.20	0.12	0.13	0.04	0.20	0.12

Table 4-3. Compositions of selected candidate waste glasses (mol%) (Ellison et al., 1994) (cont'd)

Glass	K_2O	NiO	CeO_2	Nd_2O_3	P_2O_5	Cs_2O	RuO_2	SrO	Cr_2O_3	ThO_2	La_2O_3	U_3O_8	PdO	Pr_2O_3
SON 64/G3	—	0.21	0.58	0.42	0.22	0.31	0.37	0.10	0.25	—	0.14	0.08	0.21	0.13
SON 68 18 17 L1C2A2Z1	—	0.69	0.37	0.33	0.14	0.32	—	0.23	0.23	0.09	0.19	0.04	—	0.09
SAN 60	—	—	0.04	0.01	—	—	—	0.03	—	—	0.04	—	—	0.02
SM 58 LW 11	—	0.09	0.23	0.39	—	—	—	—	—	—	—	—	—	—
ABS 29	—	0.33	0.29	0.24	—	0.21	—	0.17	—	—	0.14	0.13	—	0.08
ABS 41	—	0.33	0.29	0.24	—	0.21	—	0.17	—	—	0.15	0.13	—	0.08
ABS 39	—	0.35	0.31	0.25	—	0.22	—	0.18	—	—	0.15	0.14	—	0.08
ABS 118	—	0.80	0.38	0.31	0.15	0.27	—	0.22	0.23	—	0.19	0.07	—	0.10
JSS-A	—	0.69	0.37	0.33	0.23	0.35	—	0.22	0.23	0.04	0.19	0.04	—	0.09
JW-D	—	0.30	0.56	0.33	—	0.24	—	0.22	—	—	0.11	—	—	0.10
GC–12/9B	0.01	0.07	—	0.15	—	—	—	0.06	0.05	—	—	0.38	—	—
Average (when present)	1.59	0.47	0.36	0.31	0.46	0.23	0.39	0.18	0.16	0.46	0.12	0.11	0.21	0.08
Average (all glasses)	0.49	0.45	0.31	0.27	0.22	0.17	0.16	0.16	0.12	0.11	0.10	0.08	0.07	0.06
Median	1.25	0.31	0.37	0.33	0.27	0.22	0.33	0.17	0.16	0.12	0.13	0.07	0.21	0.08
Minimum	0.01	0.07	0.03	0.01	0.10	0.02	0.04	0.01	0.00	0.04	0.00	0.02	0.02	0.01
Maximum	3.78	1.53	0.93	0.90	1.28	0.49	1.08	0.49	0.57	0.99	0.46	0.38	0.61	0.21
Occurrence (%)	31	97	86	86	48	76	41	90	76	24	79	69	3	72

Table 4-3. Compositions of selected candidate waste glasses (mol%) (Ellison et al., 1994) (cont'd)

Glass	Gd_2O_3	TeO_2	Y_2O_3	Te_2O_3	CuO	Sm_2O_3	CoO	As_2O_3	Ag_2O
HW-39-1	—	—	0.01	—	0.08	0.01	—	—	—
SRL 131A	—	—	—	0.01	0.02	—	—	—	—
SRL 165A	—	—	—	—	—	—	—	—	—
SRL 202A	—	—	—	0.01	0.34	—	—	—	—
SRL 211	—	—	—	—	0.00	—	—	—	—
WVCM-47	—	—	0.01	—	—	0.01	—	—	—
WVCM-50	—	—	0.01	—	0.04	—	—	—	—
WVCM-70, Ref-6	—	—	0.01	—	0.03	0.01	0.02	—	—
WV205	—	—	—	—	—	—	—	—	—
PNL 76-68	0.01	—	—	—	—	—	—	—	—
GP 98/12	—	0.04	0.02	—	—	0.01	—	—	—
UK 209	—	—	0.05	—	—	—	—	—	—
UK 189	—	—	0.05	—	—	—	—	—	—
C31/3	—	0.13	0.12	—	—	—	—	0.20	—
B 1/3	—	0.13	0.12	—	—	—	—	0.16	—
VG 98/3	0.01	0.11	0.10	—	—	—	—	—	—
SON 58	0.02	0.24	0.13	0.21	—	—	—	—	0.01
SON 64	0.01	0.14	0.07	0.12	—	—	—	—	0.01

Table 4-3. Compositions of selected candidate waste glasses (mol%) (Ellison et al., 1994) (cont'd)

Glass	Gd_2O_3	TeO_2	Y_2O_3	Tc_2O_3	CuO	Sm_2O_3	CoO	As_2O_3	Ag_2O
SON 64/G3	1.25	0.15	0.08	0.13	—	—	—	—	0.01
SON 68 18 17 L1C2A2Z1	—	0.10	0.06	—	—	—	0.11	—	0.01
SAN 60	—	—	—	0.04	—	—	—	—	—
SM 58 LW 11	—	—	—	—	—	—	0.09	—	—
ABS 29	—	—	0.04	—	—	—	—	—	—
ABS 39	—	—	0.05	—	—	—	—	—	—
ABS 118	—	—	0.06	—	—	—	—	—	—
JSS-A	—	0.10	0.06	—	—	—	0.11	—	0.01
JW-D	0.01	0.10	0.06	—	—	0.06	0.11	—	0.10
GC12/9B	—	—	—	—	—	—	—	—	—
Average (when present)	0.22	0.12	0.06	0.09	0.08	0.05	0.09	0.18	0.02
Average	0.05	0.04	0.04	0.02	0.02	0.02	0.02	0.01	0.00
Median	0.01	0.12	0.05	0.08	0.03	0.06	0.11	0.18	0.01
Minimum	0.01	0.04	0.01	0.01	0.00	0.01	0.02	0.16	0.01
Maximum	1.25	0.24	0.13	0.21	0.34	0.13	0.11	0.20	0.10
Occurrence (%)	21	34	69	21	21	31	17	7	21

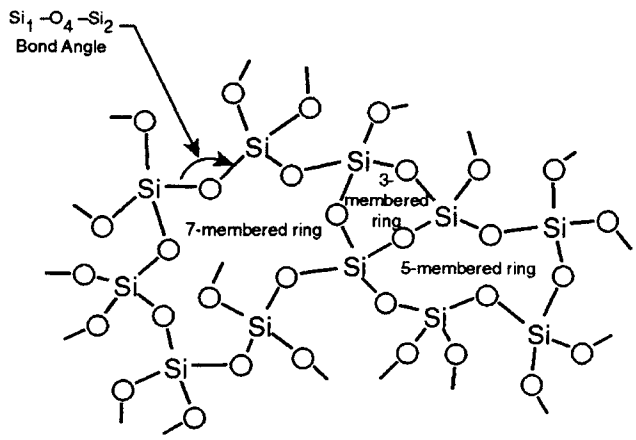

Figure 4-2. Schematics of the silica glass network (Varshneya, 1994)

4.2.3 Alkali-Alkaline Earth-Silicate Glasses

Alkaline earth cations (N) are bivalent, similar to alkali ions, behave like network modifiers, and occupy interstitial sites in the glass network. The addition of one alkaline earth ion creates two NBO sites as shown by Eq. (4-2).

$$\equiv Si - O - Si \equiv + NO \rightarrow \equiv Si - O^{-+}N^{+-}O - Si \equiv \qquad (4\text{-}2)$$

Compared to alkalis, which have a significant effect on glass properties, the alkaline earth ions tend to provide stability to the glass structure.

4.2.4 Alkali Borate Glasses

B_2O_3 is a glass former oxide, and its basic structural unit is the BO_3 triangle. The addition of an alkali oxide could result in (a) creation of an NBO as shown by Eq. (4-3) or (b) conversion of a 3-coordinated boron (B_3) state to a 4-coordinated boron (B_4) state as shown by Eq. (4-4).

$$= B - O - B = + M_2O \rightarrow \equiv B - O^{-+}M + M^{+-}O - B \equiv \qquad (4\text{-}3)$$

$$= B - O - B = + M_2O \rightarrow [\equiv B - O]^{-+}M + M^{+-}[O - B \equiv] \qquad (4\text{-}4)$$

As alkali ions are added, B_3 states are converted to B_4 states. The extra negative charge is satisfied by the alkali ion while increasing the connectivity of the system (increase in coordination number). Increased connectivity results in an increase in the viscosity and decrease in thermal expansion. Since the negative charge is distributed over a large $[BO_4]^-$ group (not localized as in the case of NBO where an alkali ion is attached only to oxygen), the alkali ion is expected to be more mobile than when in the B_3 state.

Figure 4-3 shows the effect of adding Na_2O to B_2O_3. Curve "c" shows the thermal expansion behavior, which indicates a minimum at 16 wt% Na_2O. Biscoe and Warren (Varshneya, 1994) suggested that the addition of each alkali ion (up to 16 wt%) to boron oxide causes one boron to change from the B_3 state to the B_4 state with no creation of NBOs causing thermal expansion to decrease. An alkali oxide greater than 16 wt% causes production of NBOs, which increases thermal expansion. In 1963, Bray and O'Keefe (Varshneya, 1994) experimentally determined the fraction N_4 of B_4 in alkali borates. Figure 4-4 shows their results. For alkali borate composition $xNa_2O\bullet(1-x)B_2O_3$, a fraction of N_4 is given by $x/(1-x)$. This behavior is shown by the solid line in figure 4-4. N_4 increases with the increase in alkali content but, instead of stopping at 16 mol% alkali, it continues up to 45 mol% and decreases thereafter. The N_4 concentration does drop go to zero until 70 mol% alkali. Bray and O'Keefe confirmed Biscoe and Warren's argument of change in coordination number; however, the B anomaly occurring at 16 wt% alkali oxide cannot be explained merely by the change in coordination number. (This behavior is known as a boron anomaly). Kuppinger and Shelby (1985) showed an anomaly to occur over a much wider range (up to

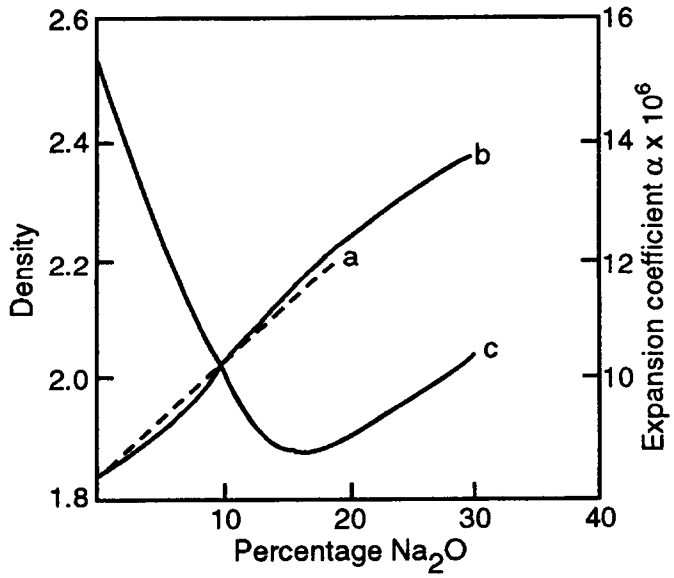

Figure 4-3. Thermal expansion coefficient and density of $Na_2O-B_2O_3$ glasses. Curve a: calculated density, curve b: measured density, and curve c: measured thermal expansion coefficient (Varshneya, 1994)

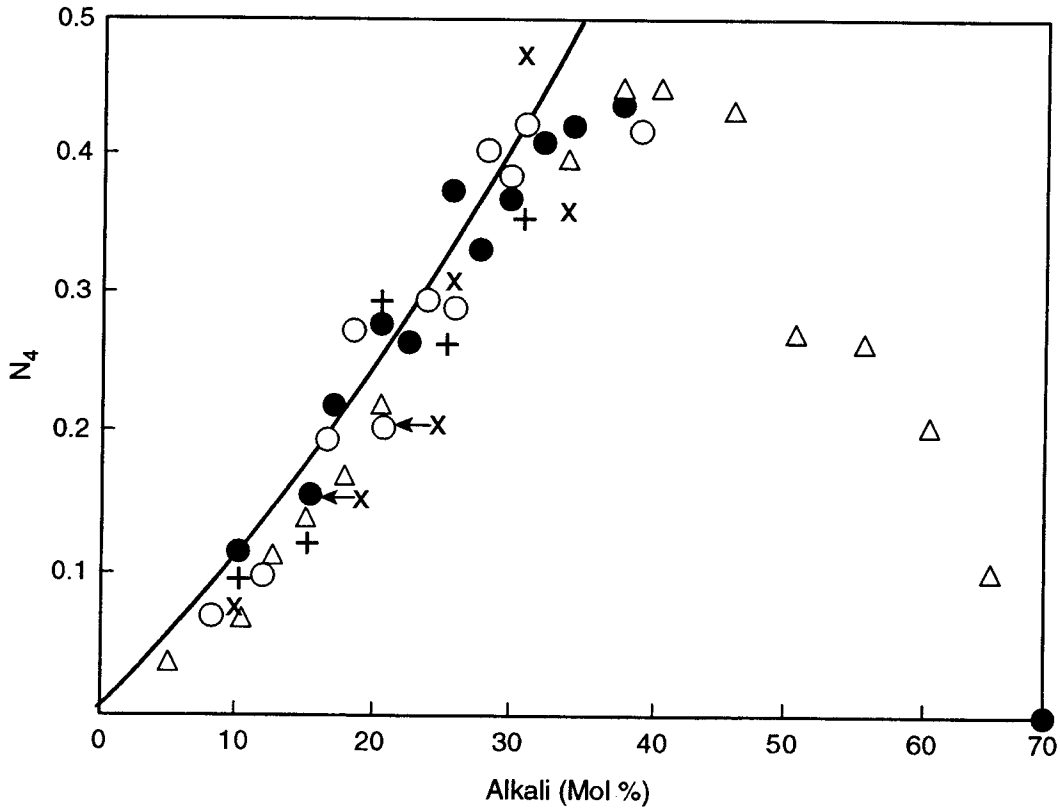

Figure 4-4. The fraction N_4 of 4-coordinated boron atoms in alkali borate glasses as a function of mol% alkali. Na_2O (•); K_2O (O); Li_2O (Δ); Rb_2O (+); Cs_2O (×). (Varshneya, 1994)

30 wt%). Currently, a boron anomaly is regarded as a manifestation of the various boron oxide groups, such as boroxol, pentaborate, triborate, or diborate, present in the system.

The number of NBOs in the alkali borate system can be calculated using Gupta's rule (Varshneya, 1994). If the alkali borate composition is expressed as $T Na_2O \cdot B_2O_3$ then $N_4 = T$, and $f_{NBO} = 0$ up to $T = 0.5$. When $T > 0.5$, then N_4 is given by $(3-T)/5$ and f_{NBO} is calculated by alkali ions not used by N_4.

4.2.5 Alkali Borosilicate Glasses

Alkali borosilicate glasses have two network formers—B and Si—and glasses are represented by a general formula of $T Na_2O \cdot K SiO_2 \cdot B_2O_3$. The addition of an alkali ion either creates an NBO with Si or B. Nuclear magnetic resonance studies have indicated that alkali ions tend to associate with the boron as long as $T < 0.5$. Beyond $T = 0.5$, alkali distribution is partitioned depending on the ratio of K, which is defined as $[SiO_2]/[B_2O_3]$ and shown in figure 4-5.

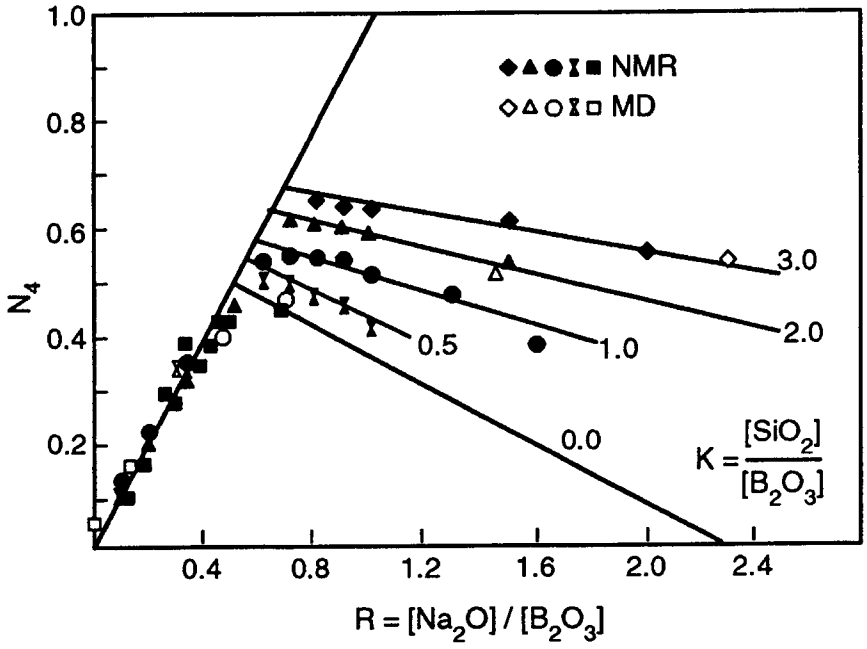

Figure 4-5. Fraction of tetrahedrally coordinated borons (N_4) as a function of mol Na_2O/B_2O_3 and SiO_2 ratios determined using nuclear magnetic resonance and molecular dynamics simulation (Varshneya, 1994)

4.2.6 Alkali Aluminosilicate Glasses

The structural configuration of Al^{3+} in alkali aluminosilicate glass depends on the ratio of Al_2O_3/M_2O. When the Al_2O_3/M_2O ratio is <1, the Al^{3+} ion goes in the glass as a tetrahedrally coordinated network former similar to the boron B_4 coordination discussed earlier. The excess negative charge on the $[AlO_4]^-$ group is satisfied by the alkali ion in the system. Thus, the addition of one Al^{3+} ion to alkali silicate glass removes one NBO. For $Al_2O_3/M_2O > 1$, the Al^{3+} ion goes in the network as a modifier in an octahedral coordination. The number of NBOs are calculated by associating each alkali ion with Al^{3+} ion. If the number of alkali ions is greater than Al^{3+} ions, the alkali ions create NBOs with Si. If the Al^{3+} ions are greater than alkali ions, alkali ions are associated with Al^{3+} and the remaining Al^{3+} ions create three NBOs.

4.2.7 Alkali Aluminoborosilicate Glasses

In alkali aluminoborosilicate glasses, there are three glass formers: Al, B, and Si. Darab et al. (1996) showed, using magic-angle spinning nuclear-magnetic resonance, that for $Al_2O_3/M_2O < 1$, the preferred sequence of alkali ions attaching to various glass formers is Al, B, and Si.

4.2.8 Fe^{3+} in Alkali Silicate, Aluminosilicate, and Borosilicate Glasses

Fe^{3+} ions, similar to Al^{3+} ions, exist in four-fold coordination and behave like a glass former. But under reducing conditions, Fe^{3+} reduces to Fe^{2+} ion and enters the structure as a network modifier. Figure 4-6 shows the dependence of $Fe^{2+}/Fe(tot)$ on $K_2O/(Al_2O_3+K_2O)$ in alkali alumino silicate glasses (Dickenson and Hess, 1986). For $K_2O/(Al_2O_3+K_2O) < 0.5$, there are not enough K^+ ions to charge balance all Al^{3+} ions. Therefore, Fe as Fe^{2+} ions compete for charge balancing. Therefore, $Fe^{2+}/Fe(tot)$ increases sharply with the decrease in $K_2O/(Al_2O_3+K_2O)$ ratio. For $K_2O/(Al_2O_3+K_2O) > 0.5$, there are sufficient K^+ ions to charge balance all Al^{3+} ions and some Fe^{2+} ions depending on the K^+ ion concentration. This study indicates that, in alkali aluminosilicate glasses with Fe, the preferred sequence of alkali ions attaching to various glass formers is Al, Fe, and Si.

The role of Fe^{3+} ions in sodium borosilicate glasses containing up to 12 wt% Fe_2O_3 has been studied by Magini et al. (1984), Licheri et al. (1985) and Agostinelli et al. (1987). The studies showed the presence of Fe^{3+} ions in four-fold coordination suggesting that Na^+ ions balance the charge with Fe^{3+} ions before B^{3+} ions.

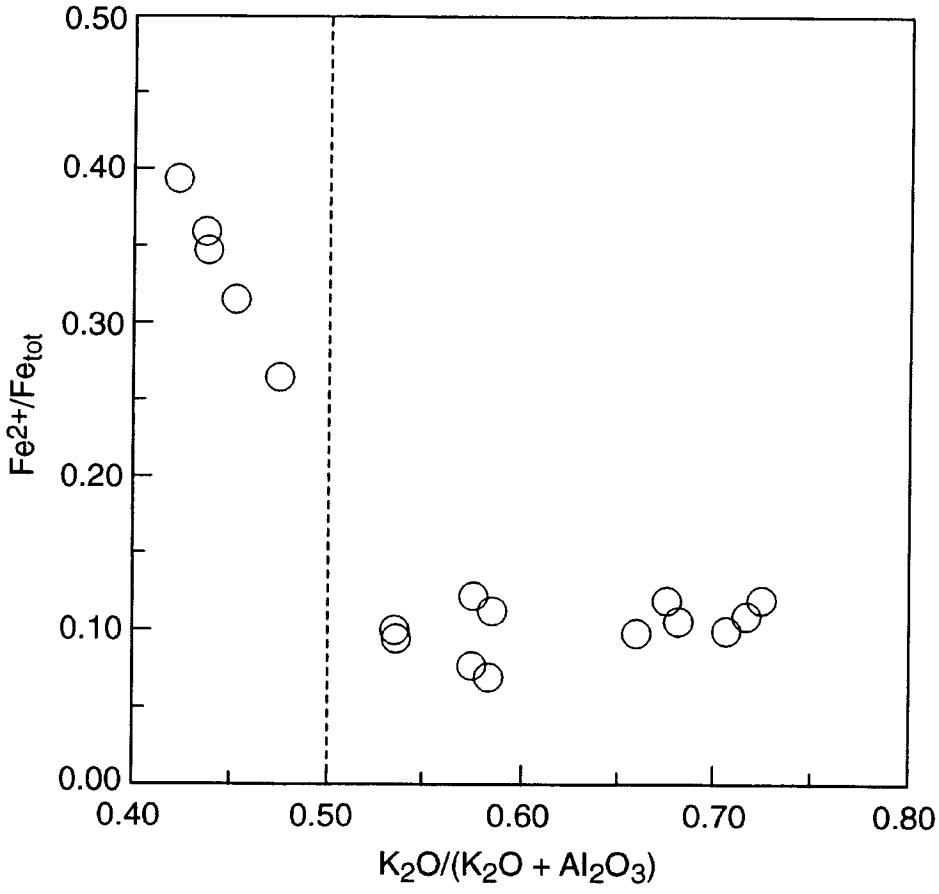

Figure 4-6. The ratio of Fe^{2+}/Fe_{tot} in $(20-x)\ K_2O{\cdot}xAl_2O_3{\cdot}80SiO_2$ containing approximately 1 mol% Fe_2O_3 (Dickenson and Hess, 1986)

DeYoreo et al. (1990) determined stabilization enthalpies for various trivalent cations and showed that Al^{3+} ions are most effective followed by Fe^{3+} ions and B^{3+} ions in the structure for charge balancing.

4.3 USE OF NONBRIDGING OXYGEN IN DEVELOPING NUCLEAR WASTE GLASS PROPERTY MODELS

Glass properties, such as viscosity, electrical conductivity, thermal expansion, T_g, and T_L, are influenced by the connectivity of the glass structure, which is determined by the number of NBOs. The lower the number of NBOs, the higher the glass structure connectivity. Determining the number of NBOs in a multicomponent system having four or five glass-forming oxides requires experimental studies to determine preferred sequencing or partitioning of alkali and alkaline earth oxides among various glass-forming oxides. Jantzen (1991) developed electrical conductivity, viscosity, and liquidus models based on the number of NBOs in the glass structure. In a multiple-component system, each component could either add or reduce NBO. Jantzen (1991) assumed the following rules to determine the total NBOs in a glass melt:

- Al_2O_3 forms AlO_4 tetrahedral linkages and two BO bonds for each Al_2O_3 present.
- Fe_2O_3 can form BO and NBO bonds depending on the amount of M_2O and Al_2O_3.
- For glasses with $Al_2O_3/M_2O < 3/4$, low concentrations of B_2O_3 enter the glass structure as $(BO_4)^-$ tetrahedra, while at higher B_2O_3 concentrations these tetrahedra are converted into planer $(BO_3)^-$ groups containing one NBO.

The total number of NBO in a given melt composition, is calculated by Eq. (4-5)

$$NBO = \frac{2(M_2O + Fe_2O_3 - Al_2O_3) + B_2O_3}{SiO_2} \qquad (4\text{-}5)$$

where $M_2O = Na_2O + K_2O + Li_2O + Cs_2O$

Based on recent studies noted in section 4.2.8, the association of Fe_2O_3 in the glass structure depends on various other components. Therefore, the assumption that each mol of Fe_2O_3 creates 2NBO may only be partially valid. It is advised to evaluate the number of NBOs to glass composition using rules discussed below.

Combining NBO formation rules provided in the standard glass science textbook (Varshneya, 1994), and in papers previously discussed, the following rules can be used for estimating NBOs in multicomponent glasses:

- All calculations are made on a molar basis.
- Each alkali ion creates one NBO.
- Each alkaline-earth ion creates two NBOs.

- A boron ion can exist either in a 3-coordination state (B_3) or 4-coordination state (B_4). For each alkali (M^+) ion added, one B from a B_3 state converts to a B_4 state without creating any NBO provided T, which is defined as the ratio of $M_2O/B_2O_3 < 0.5$. If $T > 0.5$, the number of B_4 states can be estimated using Gupta's approximation $N_4 = (3-T)/5$ (Varshneya, 1994).

- In alkali borosilicate glasses, there are two glass formers: Si and B. The alkali could either associate with Si creating an NBO or with B converting a B_3 state to a B_4 state and creating no NBOs. Studies indicate that alkalis prefer to associate with B as long as $T < 0.5$. The remaining alkali are attached to silicon.

- In alkali aluminosilicate glasses, $Al_2O_3/M_2O < 1$, Al^{3+} ions go in as a network former and remove one NBO. If $Al_2O_3/M_2O > 1$, Al^{3+} enters the network as a modifier in octahedral coordination with three oxygen as NBO and three BO. Remaining alkali ions are attached to Si.

- In alkali aluminoborosilicate glasses, there are three glass formers: Al, B, and Si. Darab et al. (1996) showed that for $Al_2O_3/M_2O < 1$, the preferred sequence of alkali ions attaching to various glass formers is Al, B, and Si.

- In alkali aluminoborosilicate glasses containing iron, the preferred sequence of alkali ions attaching to various glass formers is Al, Fe, B, and Si.

- The coexistence of Fe as Fe^{2+} and Fe^{3+} requires that Fe^{2+} should be considered along with an alkaline earth ion, and Fe^{3+} should be considered along with trivalent ions.

4.4 SUMMARY

This chapter provided a brief review of glass structure and glass forming principles and systems. While the discussion was focused on simple systems, complex systems such as nuclear waste glasses follow similar glass formation rules. The information provided in this chapter is used in the following chapters to explain various properties of the nuclear waste glasses.

4.5 REFERENCES

Agostinelli, E., D. Fiorani, and E. Paparazzo. XPS Studies of iron sodium borosilicate glasses. *Journal of Non-Crystalline Solids* 95 and 96: 373–380. 1987.

Darab, J.G., X. Feng, J.C. Linehan, and P.A. Smith. Composition-structure relationships in model Hanford low-level waste glasses. *Proceedings of the Environmental Issues and Waste Management Technologies for the Ceramic and Nuclear Industries II Symposium. 98th Annual Meeting of the American Ceramic Society, Indianapolis, Indiana, April 14–17, 1996.* Ceramic Transactions Volume 72. V. Jain and D. Peeler, eds. Westerville, OH: American Ceramic Society: 103–110. 1996.

DeYoreo, J.J., A. Navrotsky, and D.B. Dingwell. Energetics of the charge-coupled substitution Si4+ -> Na+ + T3+ in the glasses NaTO2-SiO2 (T=/Al,Fe,Ga,B). *Journal of the American Ceramic Society* 73(7): 2,068–2,072. 1990.

Dickenson, M.P., and P.C. Hess. The structural role and homogeneous redox equilibria of iron in peraluminous, metaluminous and peralkaline silicate melts. *Contrib. Mineral Petrol.* 92: 207–217. 1986.

Ellison, A.J., J.J. Mazar, and W.L. Ebert. *Effect of Glass Composition on Waste Form Durability: A Critical Review.* ANL–94/28. Argonne, IL: Argonne National Laboratory. 1994.

Jantzen, C.M. First principles process-product models for vitrification of nuclear waste: Relationship of glass composition to glass viscosity, resistivity, liquidus temperature, and durability. *Proceedings of the Fifth International Symposium on Nuclear Waste Management IV. 93rd Annual Meeting of the American Ceramic Society, Cincinnati, Ohio, April 29–May 3, 1991.* Ceramic Transactions Volume 23. G.C. Wicks, D.F. Bickford, and L.R. Bunnell, eds. Westerville, OH: American Ceramic Society: 37–51. 1991.

Kuppinger, C.M., and J.E. Shelby. Viscosity and thermal expansion of mixed-alkali sodium-potassium borate glasses. *Journal of American Ceramic Society* 68(9): 463–467. 1985.

Licheri, G., G. Paschina, G. Piccaluga, G. Pinna, M. Magini, and G. Cocco. On the coordination of iron ions in sodium borosilicate glasses. EXAFS Investigation. *Journal of Non-Crystalline Solids* 72: 211–220. 1985.

Magini, M., A.F. Sedda, G. Licheri, G. Paschina, G. Piccaluga, G. Pinna, and G. Cocco. On the coordination of iron ions in sodium borosilicate glasses. Wide Angle X-Ray Diffraction Investigation. *Journal of Non-Crystalline Solids* 65: 211–220. 1984.

Paul, A. *Chemistry of Glasses.* New York: Chapman & Hall. 1982.

Rawson, H. *Inorganic Glass-Forming Systems.* New York: Academic Press, Inc. 1967.

Varshneya, A.K. *Fundamentals of Inorganic Glasses.* New York: Academic Press, Inc. 1994.

5 ELECTRICAL CONDUCTIVITY

The electrical conductivity in most oxide glasses is attributed to migration of positively charged alkali ions in the presence of an applied electric field. Because alkali ions are weakly linked with the glass structure, they are relatively more mobile than other ions and become carriers of the electrical current. Electrical conductivity is influenced by the size of the ions and the strength of their bonds in the glass structure. An understanding of the electrical conductivity of glass melts and its temperature and compositional dependence is important for the operation of joule-heated melters. Glass compositions are designed to provide specific electrical conductivity at melting temperatures. In addition, electrical conductivity data are used to estimate power requirements for a joule-heated melter. Even though electrical conductivity is a process parameter that is defined by the glass composition, processing conditions could lower electrical conductivity by the formation of metallic or highly conductive species in the melt. In this chapter, a brief discussion on electrical conductivity limits imposed on the glass composition is followed by a review of various compositional studies on electrical conductivity and models correlating composition to electrical conductivity and the impact of melter conditions on electrical conductivity.

5.1 ELECTRICAL CONDUCTIVITY LIMITS

The joule-heated melters for nuclear waste vitrification require electrical conductivity of the glass melts to be between 10 and 100 S/m at the melting temperature (Hrma et al., 1994).

The lower limit of 10 S/m for electrical conductivity is imposed on the glass melts at melting temperature to ensure the electrical conductivity of the glass melt is significantly higher than the electrical conductivity of the refractories surrounding the glass melt. The electrical conductivity of the high-chrome refractory at 1,150 °C is 0.5 S/m, which is a factor of 20 lower than the glass melt electrical conductivity. If the electrical conductivity of the melt is below 10 S/m, it could require higher voltage to maintain desired operating conditions in the melter. This higher voltage could cause the current to flow through the refractory.

The upper limit of 100 S/m for electrical conductivity is imposed on the glass melt at melting temperature to ensure the glass melt provides enough joule heating for melting. Highly conductive glass melts will require high current density for melting and could exceed the maximum operating current density of 3×10^4 A/m^2 specified for Alloy 690 electrodes (Wang et al., 1996).

For the joule heating of glass, alternating current is used because the electrolytic properties of glass are such that the use of direct current causes polarization in the melt with alkali ions moving to cathode and oxygen being liberated at the anode. In addition, direct current causes formation of deposits and blisters on the electrode surfaces.

5.2 ELECTRICAL CONDUCTIVITY IN GLASS MELTS

The electrical conductivity in most of the borosilicate-based waste glasses is attributed to positively charged alkali ions. Because alkali ions are weakly linked with the glass structure, they are relatively more mobile than other ions and become carriers of the electrical current. The electrical conductivity is influenced by the size of the ions and the strength of their bonds in the glass structure. Between Na^+ and K^+ ions, K^+ ions are bound less strongly, but because of their larger size face a higher resistance during migration. The Li^+ ions,

on the other hand, are smaller in size than Na^+ ions but are more strongly bound to the glass structure, and face more resistance than Na^+ ions. Therefore, Na^+ ions are the principal contributor to electrical conductivity and are the most mobile ions in the glass melts. Glasses containing a mixture of alkali ions exhibit a nonlinear behavior in which the conductivity passes through a pronounced minimum as one alkali ion is substituted for the other in the glass composition. This behavior is referred to as the mixed-alkali effect. Figure 5-1 shows the mixed-alkali effect in a mixed Na_2O and K_2O aluminosilicate glass melt (Kim, 1996). The minimum in electrical conductivity becomes less pronounced at higher temperatures.

The electrical conductivity increases as temperature increases. The temperature dependence of the electrical conductivity of a glass melt is Arrhenius in nature and can be expressed as

$$\varepsilon = \varepsilon_o e^{-\frac{E_a}{RT}} \tag{5-1}$$

where, ε_o is a constant, E_a is activation energy, R is a gas constant, and T is the temperature in K. Equation (5-2) can be rewritten as

$$\log(\varepsilon) = a + \frac{b}{T} \tag{5-2}$$

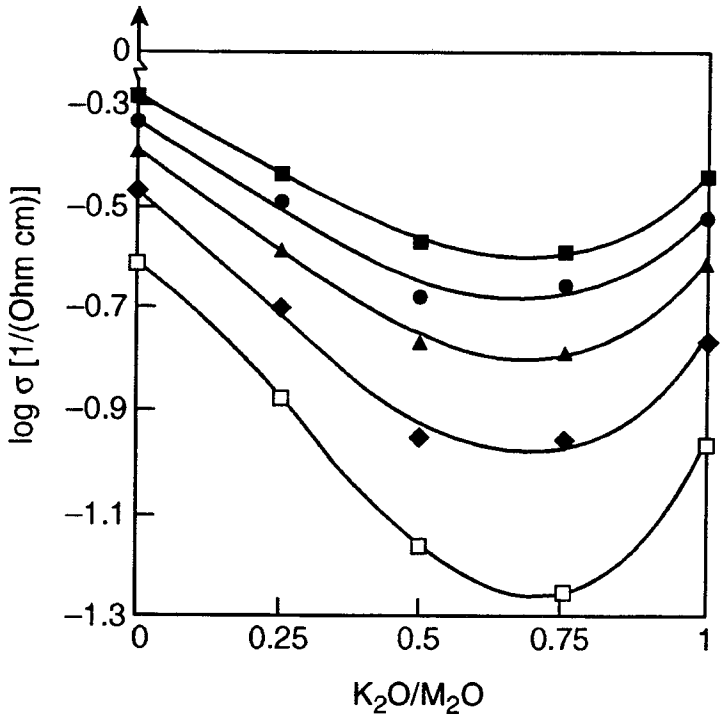

Figure 5-1. Conductivity (σ) isotherms for $25R_2O–10Al_2O_3$ mixed-alkali melts against K_2O/M_2O at five temperatures (□) 1,000 °C; (♦) 1,100 °C; (▲) 1,200 °C; (•) 1,300 °C; and (■) 1,400 °C ($M_2O = Na_2O + K_2O$ mol%) (Kim, 1996)

where

$$a = \log \varepsilon_o \tag{5-2a}$$

and

$$b = \frac{E_a}{2.303R} \tag{5-2b}$$

Electrical conductivity of glass melts is measured using an experimental configuration as shown in figure 5-2 (Eaton et al., 1991). The apparatus consists of a furnace, in which a platinum or alumina crucible filled with a test sample is placed, and a probe head, which consist of two electrodes and a thermocouple. The probehead is lowered into a glass melt to a predetermined height. The electrodes are either rods or plates made of Pt-Rh alloy. Electrodes are connected to an impedance analyzer. Electrical conductivity is measured by applying current frequency ranging from 0.1 to 100 kHz and measuring electrical resistance between the electrodes. In glass melts, no frequency dependence is observed at frequencies >1 kHz. Since the cell geometry is not specifically defined, a cell constant is obtained by measuring electrical conductivity of standard KCl solution and verified by measuring electrical conductivity of a standard glass. Electrical conductivity is determined by Eq. (5-3).

$$\varepsilon = \frac{L/A}{R} \tag{5-3}$$

where L/A is a cell constant, and R is a measured resistance at a given frequency.

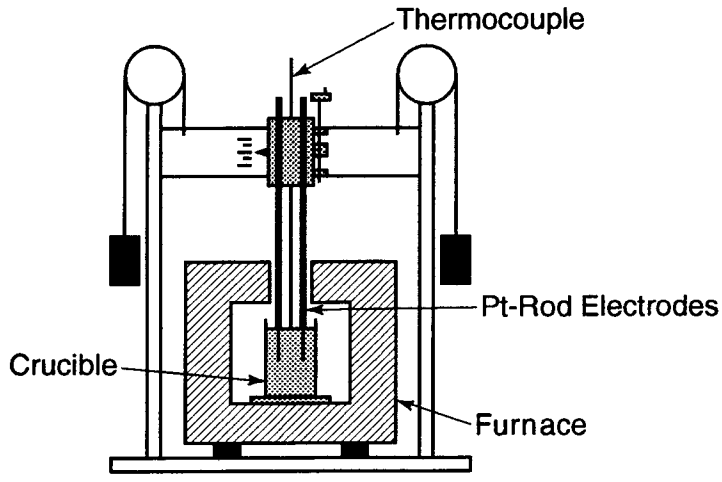

Figure 5-2. Schematic of an electrical resistivity apparatus (Eaton et al., 1991)

5.3 ELECTRICAL CONDUCTIVITY DATA AND MODELS

Hrma et al. (1994) conducted a multiyear, statistically designed compositional variability study (CVS) to characterize the relationship between composition and properties. Table 5-1 shows target composition, and the upper and lower limits for various components in the study. The target composition, HW–39–4, is based on the proposed Hanford HLW glass composition for the neutralized current acid waste (NCAW) (now known as Envelope B/D waste) (Calloway et al., 1999). Electrical conductivity was measured on 120 glasses at three to five different temperatures between 950 °C and 1,250 °C. The electrical conductivity at 1,150 °C was determined by Arrhenius fit.

Compositional dependence on electrical conductivity in S/m, at 1,150 °C was determined by the first-order mixture models as shown by Eq. (5-4).

$$\ln \varepsilon_{1150} = \sum_{1}^{10} b_i x_i \qquad (5\text{-}4)$$

where ε_{1150} is electrical conductivity at 1,150 °C, x_i and b_i are mass fraction and regression coefficients for component, respectively, i. The estimated regression coefficients are shown in table 5-2. Hrma et al. (1994) also used second-order mixture model with first-order mixture model terms and several second-order terms, which were selected by using statistical variable selection techniques to improve the relationship between electrical conductivity and temperature and composition. The second-order mixture model did not fit the electrical conductivity data substantially better than the first-order mixture model.

Based on the regression coefficients provided in the table 5-2, a component effects plot was developed centered around the composition HW–39–4 (figure 5-3). The analysis predicts Li_2O and Na_2O have the strongest effects in increasing the electrical conductivity while SiO_2 has the strongest effect in decreasing the electrical conductivity.

Table 5-1. Composition region (mass fraction) studied by Hrma et al. (1994)

	HW–39–4	Lower Limit	Upper Limit
SiO_2	0.5353	0.42	0.57
B_2O_3	0.1053	0.05	0.20
Na_2O	0.1125	0.05	0.20
Li_2O	0.0375	0.01	0.07
CaO	0.0083	0.00	0.10
MgO	0.0084	0.00	0.08
Fe_2O_3	0.0719	0.02	0.15
Al_2O_3	0.0231	0.00	0.15
ZrO_2	0.0385	0.00	0.13
Others	0.0592	0.01	0.10

Table 5-2. Regression coefficients for ln ε_{1150} (Hrma et al., 1994)

x_i	b_i
SiO_2	0.8471
B_2O_3	2.2581
Na_2O	11.0396
Li_2O	23.5355
CaO	1.4129
MgO	1.0565
Fe_2O_3	2.5863
Al_2O_3	1.3108
ZrO_2	1.1224
Others	3.4531

Fu (1998) analyzed electrical conductivity data on 43 simulated and actual waste glasses from six different projects. The selected glasses were required to (i) contain a minimum of five cations from several projects, (ii) contain <1 mol% anions other than O^{2-}, (iii) have the analyzed and calculated composition to agree within 10 relative percent, and (iv) contain only one phase. The conductivity of these glasses ranged from 0.6 to 130 S/cm. The composition range is shown in table 5-3. In figure 5-4, electrical conductivity is plotted as a function of total mols of alkali oxide disregarding the concentration of individual alkali oxide. The following empirical equation was obtained using a quadratic fit with r^2 of 0.94.

$$\ln\varepsilon_{1150} = 0.282 \times (M_2O) - 0.00373 \times (M_2O)^2 - 5.34 \qquad (5\text{-}5)$$

where M_2O is mol% total alkali oxide, and ε is electrical conductivity in S/cm. For 25 new compositions, this model predicted electrical conductivity within 25 relative percent error, but the model failed to predict electrical conductivity in glasses containing a sodium sulfate phase. In contrast to the conclusion reached by Hrma et al. (1994) that Li_2O affects the electrical conductivity more strongly than Na_2O, this model assumes that all alkali contribute equally and that the mixed alkali effect plays a minor role in the determination of melt conductivity for multicomponent oxide glasses.

Jantzen (1991) developed an electrical-resistivity model based on the number of NBO in the glass structure. The total number of NBO is a given melt composition, is calculated by Eq. (4-5). Based on the NBO calculations, an empirical relationship, shown in Eq. (5-6), was developed. The relationship provided an $r^2 = 0.57$ indicating significant scatter in the data.

$$\log\rho_{1150} = -0.48\text{NBO} + 0.648 \qquad (5\text{-}6)$$

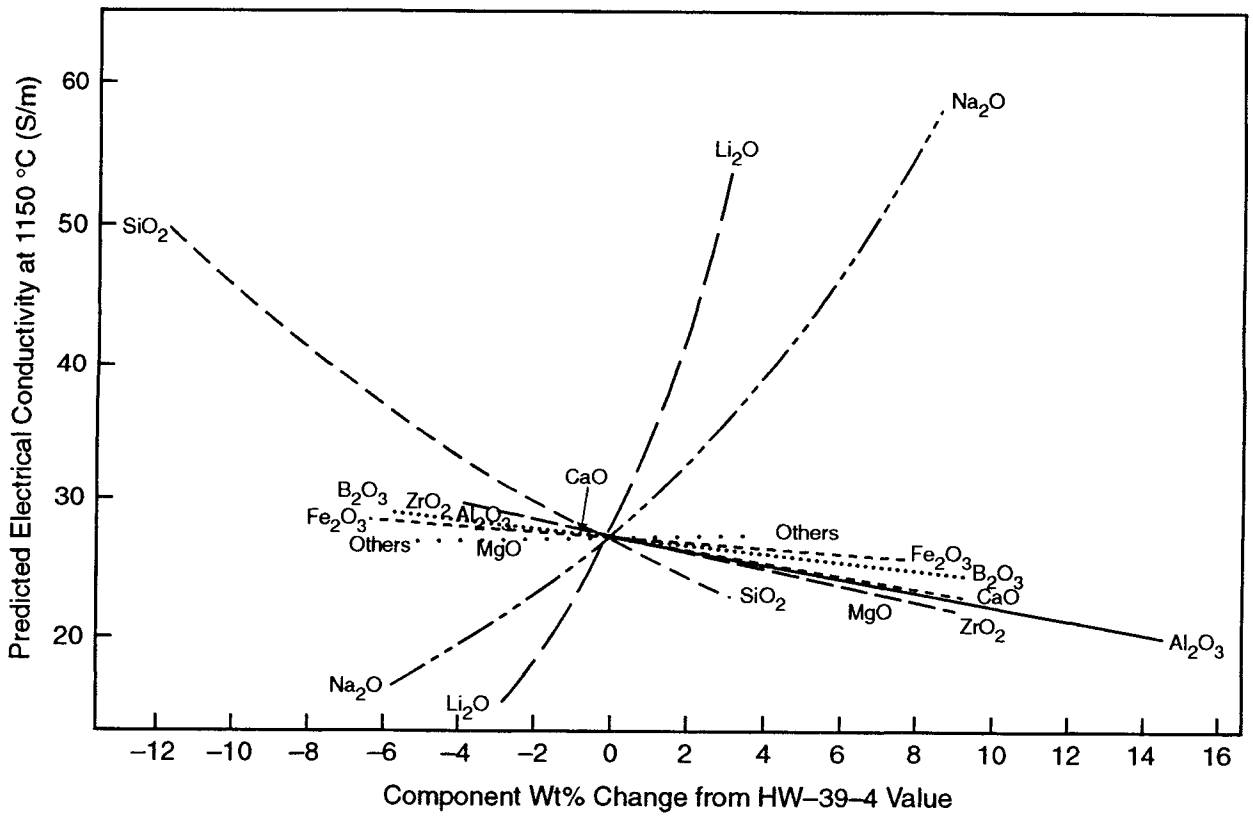

Figure 5-3. Predicted component effects on electrical conductivity at 1,150 °C relative to the HW–39–4 composition, based on the first-order mixture model using mass fractions (Hrma et al., 1994)

Table 5-3. Compositional ranges of six multicomponent systems and their viscosity and conductivity ranges at 1,150 °C (Fu, 1998)

Components	Composition (mol%)					
	Series I	Series II	Series III	Series IV	Series V	Series VI
Al_2O_3	7.0	5.0–6.8	6.2–10.6	0–10.7	4.3–6.8	7.0–12.4
B_2O_3	9.7	9.6–14.9	9–15/2	9.58	6.1–9.6	11.2–12.7
BaO	0.0	0.0	1.12–1.3	0.0	0.0	0.01
CaO	35–0	9.2–12.1	8.1–17.3	25.35	16.2–25.4	0.2–0.4
Fe_2O_3	0.0	0.0	1.7–4.6	0.0	0–10.1	1.4–5.8
K_2O	0.0	0.0	0.5–0.9	0.0	0.0	0.6–1.1
Li_2O	0.0	0.0	0.4–4.5	0.0	0.0	0.1–7.7
MgO	35–0	0.0	4.8–8.9	0.0	0.0	0.2–6.4
Na_2O	0.0	19.6–23.0	7.1–8.1	17.45–6.75	10.7–32.8	15–28
NiO	0.0	0.0	0.1–0.4	0.0	0.0	0.7–2.0
P_2O_5	0.0	0.0	1.1–3.3	0.0	0.0	1.2–2.1
PbO	0.0	0.0	0.7–1.8	0.0	0.0	NA
SO_3	0.0	0.0	0–1.3	0.0	0.0	NA
SiO_2	48.9	46.3–48.4	39.3–43.5	47.62	30.4–47.6	39.9–51.1
U_3O_8	0.0	0.0	0.0	0.0	0.0	0.2–0.5
ZrO_2	0.0	1.6–2.1	0–0.3	0.0	0.0	0.01–3.7
Total	100.0	100.0	100.0	100.0	100.0	100.0
Viscosity range (poise) at 1,150 °C	30–72	30–73	53–300	15–135	9–58	45–1,550
Conductivity range (S/cm) at 1,150 °C	0.006–1.3	0.24–0.76	0.02–0.08	0.08–1.09	0.08–1.1	0.17–0.62

NA = Not analyzed

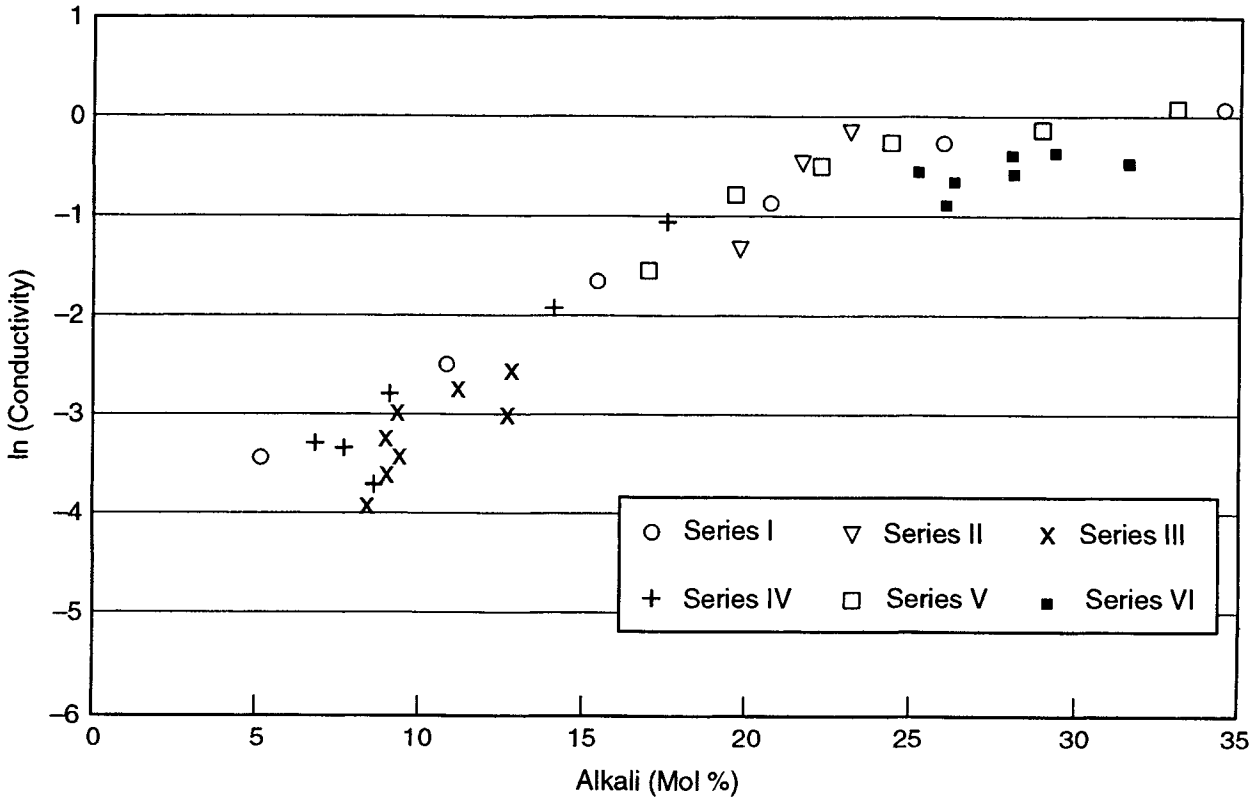

Figure 5-4. Conductivity as a function of alkali content at 1,150 °C (Fu, 1998)

where ρ is defined as electrical resistivity in Ω-cm. Combination of compositional dependence and temperature yielded the relationship shown in Eq. (5-7) with $r^2 = 0.92$.

$$\log\rho = -2.48 + \frac{4399.57}{T(^{\circ}\mathrm{K})} - 0.45\mathrm{NBO} \qquad (5\text{-}7)$$

DWPF uses Eqs. (5-6) and (5-7) to estimate electrical resistivity (reciprocal of electrical conductivity) of glass melts. Jantzen's model, similar to Fu's model, assumes all alkalis contribute equally to electrical conductivity. Based on Hrma's experimental work, this assumption is not supported. The models reviewed in this section were developed for a specific range of glass compositions and glass components. The applicability of these models to other wastes, however, is limited. The user, however, is cautioned to perform a careful and rigorous evaluation prior to using any model for predicting electrical conductivity of glass melts.

5.4 EFFECT OF MELTER CONDITIONS ON ELECTRICAL CONDUCTIVITY

Even though electrical conductivity is a process parameter that is defined by the glass composition, the processing conditions in the melter could lead to the lowering of electrical conductivity through the formation of a species causing electronic conduction in the melt. A species causing electronic conduction could form either through the accumulation of noble metals or the formation of highly conductive species such as NiS, CuS, or FeS. The formation of such species results in electronic conduction in the melt, which is several orders of magnitude higher than ionic conduction; thus leading to electrical shorting in the melter.

5.4.1 Noble Metal Accumulation

Noble metals are present in the HLW as a result of radioactive decay, and they have a very limited solubility in the glass melt. Depending on the residence time of glass melt in the melter, noble metals either flush out with the molten glass during pour or settle on the melter floor. Since the failure of the Pamela Melter in Mol, Belgium, melters are designed to accommodate the accumulation of noble metals or are provided with drains to flush noble metals. A detailed discussion on the subject is provided in Jain (2000). Monitoring the power supply in the melter is a key to monitoring the accumulation of noble metals in the melter. An increase in the current between electrodes could signal an accumulation of conductive species in the melter.

5.4.2 Formation of Conductive Species

Extremely reducing conditions ($Fe^{2+}/Fe^{3+} > 1$) in the melter could lead to the formation of highly conductive species in the melter. In the presence of sulfur, conductive species such as FeS, CuS, and NiS could form at a much lower Fe^{2+}/Fe^{3+} ratio. Since the waste compositions contain a significant amount of transition elements, an effective redox control strategy, as discussed in chapter 9 of this report, is required for maintaining redox within a specified range. An increase in current between electrodes could signal formation of conductive species in the melter.

Even though the electrical conductivity of the target glass composition does not pose any safety issue, the processing conditions in the melter could lead to a lowering of electrical conductivity that could result in a short-circuit in the melter. A melter designed to accommodate noble metals, an effective redox control strategy, and administrative controls on monitoring the power supply to the melter could reduce the risk and consequences of a melter failure caused by a short circuit.

5.5 TANK WASTE REMEDIATION SYSTEM CONCERNS

The LAW glass composition contains a significantly higher concentration of Na ions than HLW glass composition based on the proposed process flowsheet. The LAW glass composition could have higher electrical conductivity than HLW glass composition, but as long as both compositions fall within the prescribed electrical conductivity range, there is little risk of processing problems in the melter. The risk caused by the formation of a conductive species or noble metal accumulation in the melter for LAW glass composition is much less glass composition compared to HLW. Compared to HLW, LAW composition contains a smaller amount of transition metal elements that could form species that can cause electronic conduction in the melter and have not noble metals.

5.6 SUMMARY

The electrical conductivity in most oxide glasses is attributed to migration of positively charged alkali ions in the presence of an applied electrical field. Because alkali ions are weakly linked with the glass structure, they are relatively more mobile than other ions and become carriers of the electrical current. The electrical conductivity is influenced by the size of the ions and the strength of their bonds in the glass structure.

The joule-heated melters for nuclear waste vitrification require electrical conductivity of the glass melts between 10 and 100 S/m at melting temperature (Hrma et al., 1994). The lower limit of 10 S/m for electrical conductivity is imposed on the glass melts at melting temperature to ensure that the electrical conductivity of the glass melt is significantly higher than the electrical conductivity of the refractories surrounding the glass melt, which ensures the current does not flow through refractories. The upper limit of 100 S/m for electrical conductivity is imposed on the glass melt at melting temperature to ensure the glass melt provides enough joule heating for melting without exceeding the maximum operating current density for Inconel 690 electrodes.

The electrical conductivity increases as temperature increases and is Arrhenius in nature. The first-order mixture model, based on statistically designed experiments (Hrma et al., 1994), predicts Li_2O and Na_2O have the strongest effects on increasing the electrical conductivity, while SiO_2 has the strongest effect on decreasing the electrical conductivity. In contrast to the conclusion reached by Hrma et al. (1994) that Li_2O affects the electrical conductivity more strongly than Na_2O, Jantzen (1991) and Fu (1998) concluded that all alkalis contribute equally and that the mixed alkali effect plays a minor role in determining melt conductivity for multicomponent oxide glasses. The models reviewed in this section were developed for a specific range of glass compositions and glass components. The applicability of these models to other wastes, however, is limited.

Even though electrical conductivity is a process parameter defined by the glass composition, the processing conditions in the melter could lower electrical conductivity by forming metallic species in the melt. The formation of species causing electronic conduction could occur either through the accumulation of noble metals or formation of highly conductive species, such as NiS, CuS, or FeS. The formation of such species results in metallic conduction in the melt, which is several orders of magnitude higher than ionic conduction; thus leading to electrical shorting in the melter. A melter designed to accommodate noble metals, an effective redox control strategy, with administrative controls for monitoring the power supply to the melter, could reduce the risks and consequences of a melter failure caused by a short-circuit.

5.7 REFERENCES

Calloway, T.B., Jr., C.A. Nash, D.J. McCabe, C.T. Randall, S.T. Wach, D.P. Lambert, C.L. Crawford, S.F. Peterson, and R.E. Eibling. Research and development activities in support of Hanford privatization—SRTC program (U). *Proceedings of the Waste Management '99 Conference, Tucson, Arizona, February 28–March 4, 1999.* CD-ROM Version. Tucson, AZ: WM Symposia, Inc. 1999.

Eaton, W.C., I. Joseph, and L.D. Pye. Some high-temperature properties of simulated West Valley nuclear waste glass. *Proceedings of the Fifth International Symposium on Nuclear Waste Management IV. 93rd Annual Meeting of the American Ceramic Society, Cincinnati, Ohio, April 29–May 3, 1991.* Ceramic Transactions Volume 23. G.C. Wicks, D.F. Bickford, and L.R. Bunnell, eds. Westerville, OH: American Ceramic Society: 509–518. 1991.

Fu, S. Predicting melt conductivities of waste glasses. *Proceedings of the International Symposium on Environmental Issues and Waste Management Technologies in the Ceramic and Nuclear Industries III, Cincinnati, Ohio, May 4–7, 1998.* Ceramic Transactions Volume 87. D.K. Peeler and J.C. Marra, eds. Westerville, OH: American Ceramic Society: 253–260. 1998.

Hrma, P.R., G.F. Piepel, M.J. Schweiger, D.E. Smith, D.-S. Kim, P.E. Redgate, J.D. Vienna, C.A. LoPresti, D.B. Simpson, D.K. Peeler, and M.H. Langowski. *Property/Composition Relationships for Hanford High-Level Waste Glasses Melting at 1,150 °C*. Volume 1 Chapters 1–11. PNL–10359. Richland, WA: Pacific Northwest National Laboratory. 1994.

Jain, V. *Survey of Waste Solidification Process Technologies*. NUREG/CR–6666. Washington, DC: Nuclear Regulatory Commission. 2000.

Jantzen, C.M. First principles process-product models for vitrification of nuclear waste: Relationship of glass composition to glass viscosity, resistivity, liquids temperature, and durability. *Proceedings of the Fifth International Symposium on Nuclear Waste Management IV. 93rd Annual Meeting of the American Ceramic Society, Cincinnati, Ohio, April 29–May 3, 1991*. Ceramic Transactions Volume 23. G.C. Wicks, D.F. Bickford, and L.R. Bunnell, eds. Westerville, OH: American Ceramic Society: 37–51. 1991.

Kim, K.-D. Electrical conductivity in mixed-alkali aluminosilicate melts. *Journal of the American Ceramic Society* 79(9): 2,422–2,428. 1996.

Wang, E., R.K. Mohr, A.C. Buechele, and I.L. Pegg. Current density effects on the corrosion of ceramic and metallic electrode materials in waste glasses. *Proceedings of the Materials Research Society Conference*. Symposium Proceedings 412. Pittsburgh, PA: Materials Research Society: 173–188. 1996.

6 GLASS MELT VISCOSITY

Viscosity is a property of a liquid state and a measure of the resistance to shear deformation. The application of a shear force causes the atoms and molecules to undergo displacement with respect to each other that continues with time as force continues to be applied. The viscosity of the glass forming melt and its temperature dependence is of paramount importance in manufacturing glass. Commercial glass manufacturing processes require specific viscosity at each processing step. A typical log viscosity temperature behavior of a commercial glass is shown in figure 6-1. Glass is melted at the melting point, which has a viscosity of approximately 10 Pa-s (100 P), shaped between the working point and softening point, which is called the working range, and annealed between annealing point and strain point. The glasses that have a wider temperature range between the working point and softening point viscosities are called long glasses, and the glasses that have a narrow temperature range between working point and softening point viscosities are called short glasses. In the nuclear waste vitrification process, glass compositions are designed to have a viscosity of less than 10 Pa-s (100 P) at 1,150 °C, which is the upper operating limit of a joule-heated melter. In this chapter, a brief discussion of glass-melt viscosity limits imposed on glass composition is followed by a review of studies on glass-melt viscosity, models for predicting melt viscosity using compositional information, and the impact of melter conditions on viscosity.

6.1 MELT VISCOSITY LIMITS

The joule-heated melters for nuclear waste vitrification require the viscosity of glass melts to be between 2 and 10 Pa-s (20 and 100 P) at melting temperature (Hrma et al., 1994). The limits are imposed on glass melts at melting temperature to ensure the glass melt is fluid enough to homogenize and pour.

If the viscosity of the melt is below 2 Pa-s (20 P), the glass melt could increase

- Erosion of the refractory through enhanced convective currents
- Volatilization of alkalis, boron, and radioactive elements such as Cs and Tc
- Penetration of melt along the refractory joints
- Settling of noble metals (potential for electrical shorting)

If the viscosity is greater than 10 Pa-s (100 P), the glass melt could

- Plug the pour spout during pour
- Leave undissolved components in the melt
- Crystallize at cold spots in the melter

6.2 VISCOSITY OF GLASS MELTS

In glasses, the addition of network modifiers, such as alkalis and alkaline earths, to glass forming oxides such as silica, tend to decrease the viscosity of the melt. Boron on the other hand, as discussed in section 4.2.5 (boron anomaly), results in an increase in viscosity with the addition of alkalis and alkaline earth ions. The viscosity is also influenced by the size of the ions and the strength of their bonds in the glass structure as shown in figure 6-2. Glasses containing a mixture of alkali ions exhibit mixed alkali effect, a

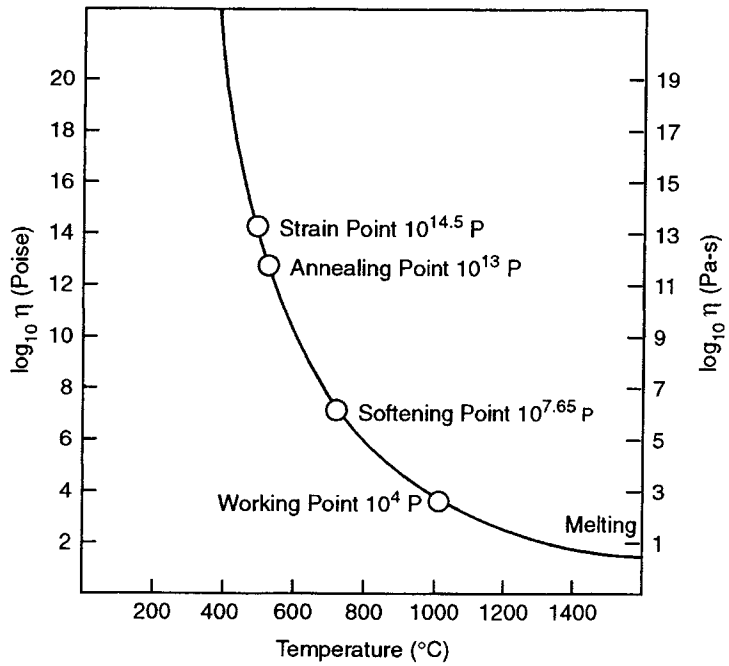

Figure 6-1. Variation of the viscosity of a common soda lime silica glass with temperature (Varshneya, 1994)

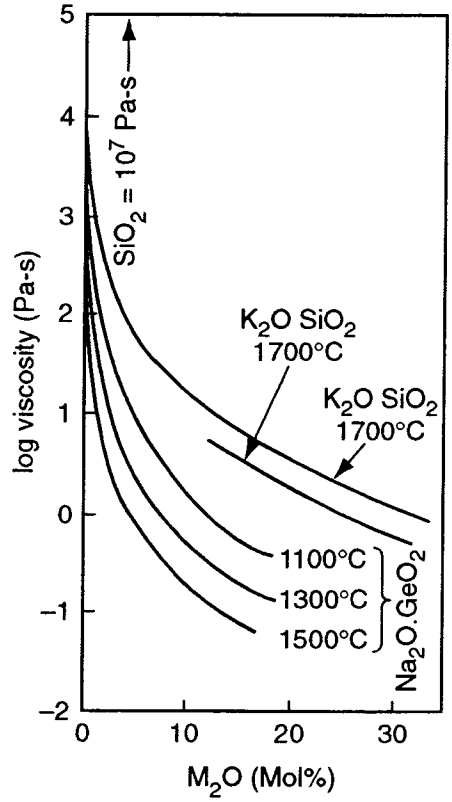

Figure 6-2. Viscosity of melts in binary silicate and germanate systems as a function of alkali oxide (M_2O) concentration (Varshneya, 1994)

nonlinear behavior, with varying composition, which passes through a minimum as one alkali ion is substituted for the other. Figure 6-3 shows the mixed alkali effect.

The viscosity decreases as temperature increases. The temperature dependence of the melt viscosity (η) of a glass is Arrhenius in nature and can be expressed as

$$\eta = \eta_o e^{\frac{E_a}{RT}} \tag{6-1}$$

where, η_o is a constant, E_a is activation energy for viscous flow, R is a gas constant, and T is the temperature in K. Equation (6-1) can be rewritten as

$$\log(\eta) = A + \frac{B}{T} \tag{6-2}$$

where

$$A = \log \eta_o$$

and

$$B = -\frac{E_a}{2.303R}$$

In addition to Eq. (6-1) or (6-2), several other expressions are used to describe viscosity-temperature behavior (Varshneya, 1994). The most widely used expression was described by Vogel-Fulcher-Tammann (VFT), which is usually referred to as the VFT equation [Eq. (6-3)].

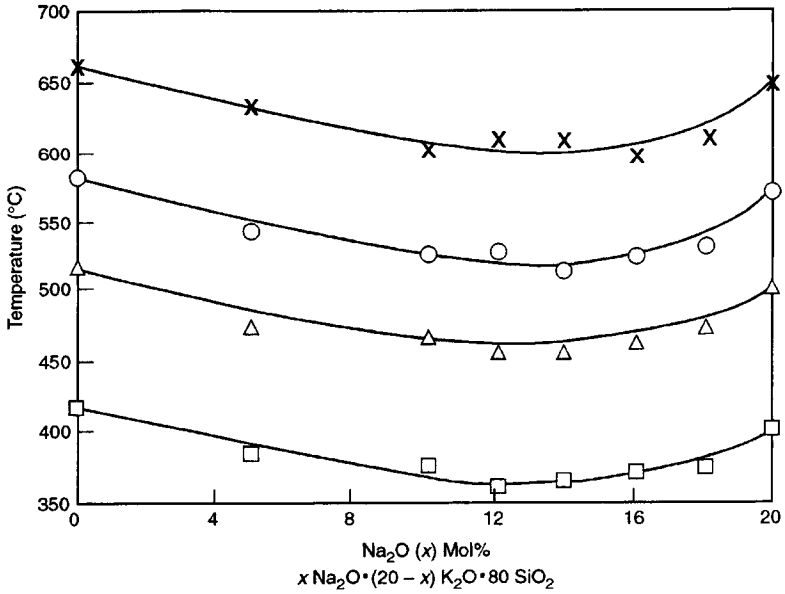

Figure 6-3. Isokom (equal viscosity) temperatures for xNa$_2$O (20−x) K$_2$O·80 SiO$_2$ glasses. Log η (poise)=8.0(×); 10.0 (O); 12.0 (Δ); 16.0 (□) (Varshneya, 1994)

$$\log(\eta) = -A + \frac{B}{(T - T_o)} \tag{6-3}$$

where A, B and T_o are constants. If T_o is equal to 0, the VFT equation reverts back to the Arrhenius equation.

Glass melt viscosities in the range between 0.05 Pa-s (0.5 P) and 5 $\times 10^3$ Pa-s (5 $\times$ 10^4 P) are measured using the rotating viscometer. A typical experiment configuration is shown in figure 6-4. The apparatus consists of a temperature-controlled furnace in which a platinum-rhodium alloy crucible filled with a test sample is placed, and a probe head consisting of a Pt-Rh alloy spindle lowered into a glass melt to a predetermined height. The probe head is connected to a measuring system that applies a constant speed to the spindle, and the resulting torque is measured. Since the cell geometry is not specifically defined, a geometric cell constant is obtained by developing torque-speed curves for standard viscosity oils and verified by a standard glass. Viscosity at a given temperature is determined by Eq. (6-4).

$$\eta = \frac{Gt}{N} \tag{6-4}$$

where G, N, and τ are geometric cell constant, spindle speed, and measured torque.

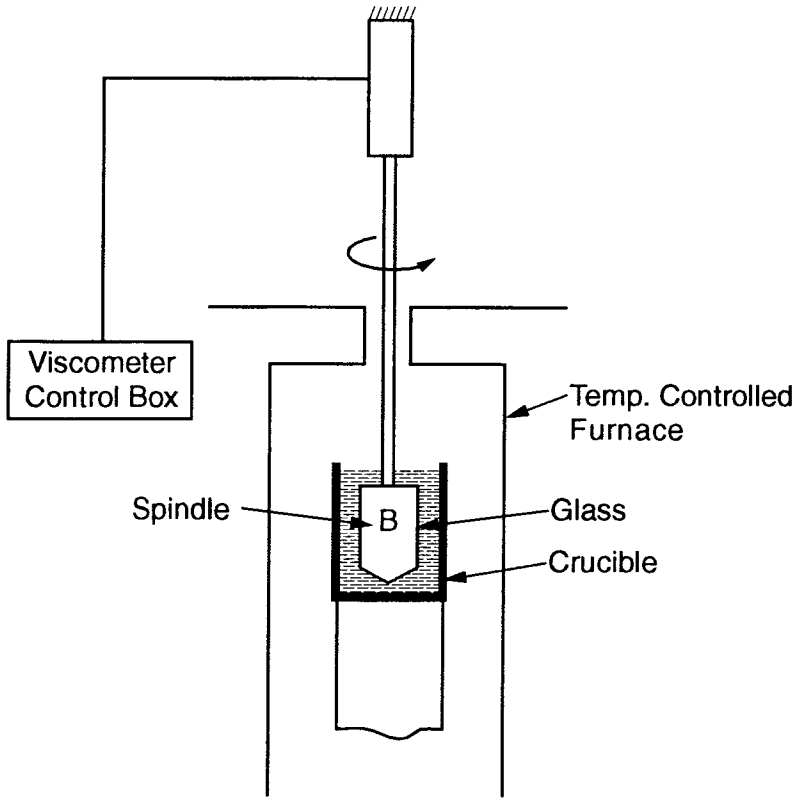

Figure 6-4. Schematic of a rotating viscometer

6.3 VISCOSITY DATA AND MODELS

Viscosity is one of the most widely studied melt properties because of its importance in the processing and manufacture of glass. While there is an enormous amount of data on commercial glasses, this review is restricted to viscosity data and models by Feng et al. (1990), Jantzen (1991), and Hrma et al. (1994) in use for predicting the viscosity of nuclear waste glasses.

Feng et al. (1990) developed a viscosity-composition-temperature model based on the heat of formation. The model is based on the assumption that the bond strength, developed by Sun (table 4-1) and given by Eq. (6-5), between atoms in the glass is a predominant factor in controlling the composition dependence on viscosity and other physical properties, such as durability. The bond strengths can be obtained from known heat of formation of the components. The role of various oxides in the glass can be categorized into network formers, such as SiO_2, Al_2O_3, ZrO_2, intermediates, and network modifiers (or breakers), such as alkali oxides.

$$D(X-O)=\frac{2\Delta H_f}{nZ} \tag{6-5}$$

where ΔH_f is the standard heat of formation of X_nO_n oxide and Z is the coordination number of X. Formation energies were estimated using the following four rules:

(1) For SiO_2, Al_2O_3, and ZrO_2, which form the network of the glass, formation energies, ΔH_i, were obtained by Eq. (6-6).

$$\Delta H_i = 2\Delta H_i^0 \tag{6-6}$$

where Δ_i^0 is the standard heat of formation of the pure oxide i. The factor of two is an average ratio of binding energy and heat of formation.

(2) For network modifiers, the formation energy, ΔH_i, was calculated from the standard heat of formation for the pure oxides less an energy term (E_{net}) that corresponds to mean binding energy created by network formers as shown by Eq. (6-7).

$$\Delta H_i = \Delta H_i^0 - E_{\text{net}} \tag{6-7}$$

where

$$E_{\text{net}} = \frac{\sum_i m_i \Delta H_i}{a_i m_i}$$

where m_i is the mol fraction of glass formers in rule 1, and a_i is the number of bonds formed from each mol of the network former i.

(3) For intermediates, the formation energy, ΔH_i, was assumed equal to their standard heat of formation given by

$$\Delta H_i = \Delta H_i^0 \tag{6-8}$$

(4) Special rule for B_2O_3. B_2O_3 is considered an excellent glass former. However, the addition of B_2O_3 to alkali silicate glasses decreases the viscosity of the glass. This anomaly was discussed in chapter 4. To account for this anomaly, the expression shown by Eq. (6-9) is used for calculating the contribution to the heat of formation from B_2O_3.

$$\Delta H_i = \Delta H_i^0 - 2E_{\text{net}} \tag{6-9}$$

The total glass formation energy is given by Eq. (6-10).

$$\Delta H = \sum_i x_i \Delta H_i \tag{6-10}$$

Feng et al. (1990) used Eq. (6-3) to represent the temperature dependence of viscosity (poise), and the following composition dependence was used for the constants represented in Eq. (6-3).

$$A = a_0 + a_1 DH$$
$$B = b_0 + b_1 DH$$
$$T_0 = t_0 + t_1 DH$$

Regression coefficients were determined by using 1664 data points from 372 glasses. Results showed no significant contributions from parameters t_0, t_1 and b_0. The following values of the regression coefficients were recommended for determining the viscosity of the glasses.

$$a_0 = -4.341(0.09)$$
$$a_1 = -0.00474(0.0003)$$
$$b_1 = -23.451(0.3)$$

The values in parentheses indicate the standard deviation. This model provides a reasonable representation of the viscosity behavior covering a significant composition range.

Hrma et al. (1994) conducted a multiyear statistically designed study to characterize the relationship between composition and properties. Table 5-1 shows target composition and upper and lower limits for various components in the study. Viscosity was measured on 120 glasses at three to five different temperatures between 950 and 1,250 °C. The melt viscosity at 1,150 °C was determined by the VFT equation. Compositional dependence of viscosity at 1,150 °C was determined by the first-order mixture models as shown by Eq. (6-11).

$$\ln \eta_{1150} = \sum_{1}^{10} b_i x_i \qquad (6\text{-}11)$$

where η_{1150} is viscosity at 1,150 °C in Pa-s, x_i and b_i are mass fraction and regression coefficients for component *i*. The estimated regression coefficients are shown in table 6-1. Hrma et al. (1994) also used a second-order mixture model using first-order mixture model terms and several second-order terms that were selected by using statistical variable selection techniques to improve the relationship between melt viscosity, temperature and composition. The second-order mixture model showed some improvement in predicting the melt viscosity compared to the first-order mixture model.

Based on the regression coefficients provided in the table 6-1, a component effects plot was developed centered around composition HW–39–4 (figure 6-5). The analysis predicts SiO_2, Al_2O_3, and ZrO_2 (in order) have the strongest effects in increasing the melt viscosity while Li_2O, Na_2O, CaO, and B_2O_3 (in order) have the strongest effect in decreasing the melt viscosity. In addition, Hrma et al. (1994) reviewed the historical database of 680 glasses and 160 selected glasses whose viscosity at 1,150 °C was available. The viscosity of 160 glasses ranged from 1 to 400 Pa-s. First-order mixture models predicted $r^2 = 0.8998$.

Jantzen (1991), developed a viscosity model based on the number of NBO in the glass structure. The total number of NBO is a given melt composition, as calculated by Eq. (4-5). Based on the NBO calculations, an empirical relationship shown in Eq. (6-12) was developed. The relationship provided an $r^2 = 0.95$.

$$\log \eta_{1150} = -1.562\text{NBO} + 3.306 \qquad (6\text{-}12)$$

Table 6-1. Regression coefficients for ln η_{1150} (Hrma et al., 1994)

x_i	b_i
SiO_2	8.967982
B_2O_3	-6.204318
Na_2O	-11.016616
Li_2O	-34.239274
CaO	-7.466158
MgO	-2.776217
Fe_2O_3	-0.036918
Al_2O_3	11.306471
ZrO_2	7.433982
Others	0.9260

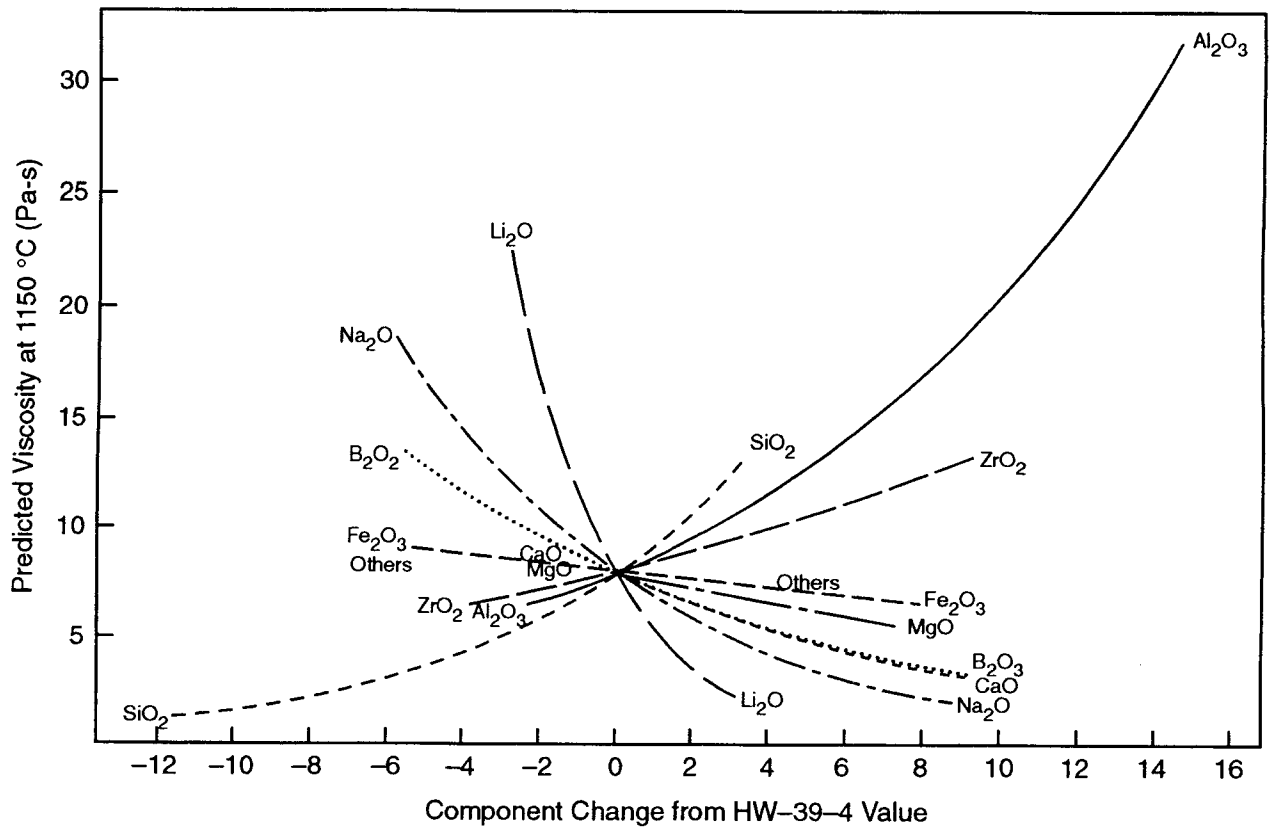

Figure 6-5. Predicted component effects on viscosity at 1,150 °C compared to the HW–39–4 composition, based on the first-order mixture model using mass fractions (Hrma et al., 1994)

where η is in poise. The combination of compositional dependence and temperature yielded the relationship shown in Eq. (6-13) with $r^2 = 0.976$.

$$\log \eta = -0.61 + \frac{4472.45}{T(^\circ C)} - 1.534 NBO \qquad (6\text{-}13)$$

DWPF uses Eq. (6-13) to estimate melt viscosity. Jantzen's model assumes all alkalis contributes equally to the melt viscosity. Based on Hrma's experimental work, this assumption is not supported. Hrma et al. (1994) used viscosity data from 124 glasses and Jantzen's model to predict the melt viscosity. Results indicated that 84 out of 126 glasses over-predicted the viscosity of the composition. The r^2 value was 0.697.

The models reviewed in this section were developed for a specific range of glass compositions and glass components. The applicability of these models to other wastes as indicated by inputting Hanford Waste Vitrification Waste (HWVP) glass data in the DWPF model, however, is limited. The user, however, is cautioned to perform a careful and rigorous evaluation prior to using any model for predicting melt viscosity. In addition, the reader should ensure correct units of viscosity are used during analysis because models are either developed using poise or Pa-s. Lower temperatures (< 1,050 °C) could lead to higher viscosities that could result in homogenities in the glass (incomplete melting) or plug the melter drain. If the temperature is higher than 1,150 °C, alkalis, boron, and radionuclides, such as Cs and Tc, could volatilize.

6.4 EFFECT OF MELTER CONDITIONS ON VISCOSITY

Melter conditions have no significant effect on viscosity provided the temperature of the melter is maintained within the operating range to ensure that the glass melt is maintained within the prescribed viscosity range of 2 to 10 Pa-s (20 to 100 P).

6.5 TANK WASTE REMEDIATION SYSTEM CONCERNS

The LAW glass composition contains a significantly higher concentration of Na ions than HLW glass composition based on the proposed process flowsheet. The LAW glass composition could have lower viscosity than HLW glass composition, but as long as both compositions fall within the prescribed viscosity range, there is little risk of processing problems in the melter.

6.6 SUMMARY

Viscosity is a property of a liquid state and a measure of the resistance to shear deformation. The application of a shear force causes the atoms and molecules to undergo displacement with respect to each other that continues with time as the application of force continues. The viscosity of the glass forming melt and its temperature dependence is of paramount importance in manufacturing glass. The joule-heated melters for nuclear waste vitrification require viscosity of glass melts between 2 and 10 Pa-s (20 and 100 P) at melting temperature (Hrma et al., 1994). The limits are imposed on glass melts at melting temperature to ensure the glass melt is fluid enough to homogenize and pour. If the viscosity of the melt is below 2 Pa-s (20 P), glass melt could increase erosion of refractory; volatilization of alkalis, boron, and radionuclides; penetration of melt along the refractory joints; or settling of noble metals. If the viscosity is greater than 10 Pa-s (100 P), glass melt could plug the pour spout during pour, have undissolved components in the melt,

or crystallize at cold spots in the melter. The first-order mixture model predicts SiO_2, Al_2O_3, and ZrO_2 (in order) have the strongest effects in increasing the melt viscosity, while Li_2O, Na_2O, CaO, and B_2O_3 (in order) have the strongest effect in decreasing the melt viscosity. The temperature dependence of the melt viscosity (η) of a glass is Arrhenius in nature. The models reviewed in this section were developed for a specific range of glass compositions and glass components. The applicability of these models to other wastes as indicated by inputting Hrma's data on HWVP glasses in Jantzen's DWPF model, however, is limited. Consequently, the user is cautioned to perform a careful and rigorous evaluation prior to using any model for predicting melt viscosity.

6.7 REFERENCES

Feng, X., E. Saad, and I.L. Pegg. A model for the viscosity of multicomponent glass melts. *Proceedings of the Nuclear Waste Management III. Annual Meeting of the American Ceramic Society.* Ceramic Transactions Volume 9. G.B. Mellinger, ed. Westerville, OH: American Ceramic Society: 457–468. 1990.

Hrma, P.R., G.F. Piepel, M.J. Schweiger, D.E. Smith, D.-S. Kim, P.E. Redgate, J.D. Vienna, C.A. LoPresti, D.B. Simpson, D.K. Peeler, and M.H. Langowski. *Property/Composition Relationships for Hanford High-Level Waste Glasses Melting at 1,150 °C.* Volume 1. Chapters 1–11. PNL–10359. Richland, WA: Pacific Northwest National Laboratory. 1994.

Jantzen, C.M. first principles process-product models for vitrification of nuclear waste: relationship of glass composition to glass viscosity, resistivity, liquidus temperature, and durability. *Proceedings of the Fifth International Symposium on Nuclear Waste Management IV. 93rd Annual Meeting of the American Ceramic Society, Cincinnati, Ohio, April 29–May 3, 1991.* Ceramic Transactions Volume 23. G.C. Wicks, D.F. Bickford, and L.R. Bunnell, eds. Westerville, OH: American Ceramic Society: 37–51. 1991.

Varshneya, A.K. *Fundamentals of Inorganic Glasses.* San Diego, CA: Academic Press, Inc. 1994.

7 GLASS TRANSITION TEMPERATURE

The glass transition (or transformation) range (T_g range) designates the temperature interval at which a given system gradually transforms as it cools from a supercooled liquid state into the glass state (Varshneya, 1994). Figure 4-1 shows a volume temperature diagram for a glass-forming melt. Glass-forming liquids, when cooled from location a, skip the crystallization temperature at location b and continues to follow the path shown. The glass transition range begins at a point at which the cooling path starts, departs from the supercooled liquid path, and ends when the cooling profile attains a constant slope. Also shown in the figure is the effect of cooling. The faster the glass is cooled, the higher the glass transition temperature. There is no absolute measure of T_g because its value is influenced by the thermal history and rate of cooling. For most purposes, T_g is defined as the intersection of the extrapolated liquid and glassy state lines. This temperature is also referred to as the fictive temperature. On a viscosity curve (figure 6-1), T_g range is bounded between the strain and annealing points (Marra et al., 1991). The annealing point has a viscosity of 10^{12} Pa-s (10^{13} P), while the strain point has a viscosity of $10^{13.5}$ Pa-s ($10^{14.5}$ P). Understanding of T_g of glass and its compositional dependence is of great importance in commercial glass-forming processes. In the disposal of the vitrified HLW, T_g provides an upper bound above which the mechanical integrity and chemical durability are compromised. In this chapter, a brief discussion on T_g limit imposed on the glass composition is followed by a review of various compositional studies on T_g and models correlating composition to T_g.

7.1 GLASS TRANSITION TEMPERATURE LIMIT

The WAPS require, at the time of shipment, the producer to certify that, after the initial cool-down, the waste form temperature has not exceeded 400 °C (West Valley Nuclear Services, 1996). This product specification was established to ensure that the waste is in solid form at the time of shipment. At temperatures above T_g, glass is considered to be in a liquid state, and the stability of the glass could be compromised due to nucleation and crystallization of new phases. These changes can affect chemical durability and mechanical integrity.

7.2 GLASS TRANSITION TEMPERATURE MEASUREMENTS

The commonly used methods for measuring T_g are differential scanning calorimetry (DSC), dilatometry, and fiber elongation (ASTM C336–71). DSC measures the heat-generation rate as a function of temperature. The change in the slope of the heat-generation rate profile as shown in figure 7-1 represents the onset of the T_g range. The T_g is defined at the intersection of the extrapolated lines as shown in the figure. Dilatometry measures the thermal expansion in a sample as a function of temperature. The change in the slope of the thermal expansion profile (figure 7-2) represents the onset of the T_g range. The T_g is defined as the intersection of the extrapolated lines as shown in the figure. The reproducibility of data is ±5 °C between DSC and dilatometry methods as discussed in section 7.3. The fiber elongation method is based on measuring viscosity of 10^{12} Pa-s (10^{13} P) at the annealing point and a viscosity of $10^{13.5}$ Pa-s ($10^{14.5}$ P) at the strain points. The fiber elongation method is an ASTM method widely used in the commercial glass industry to determine annealing and strain point of glass compositions (American Society for Testing and Materials, 1991). DSC and dilatometry methods were used by WVDP to determine T_g, while the fiber elongation method was used by DWPF to determine T_g.

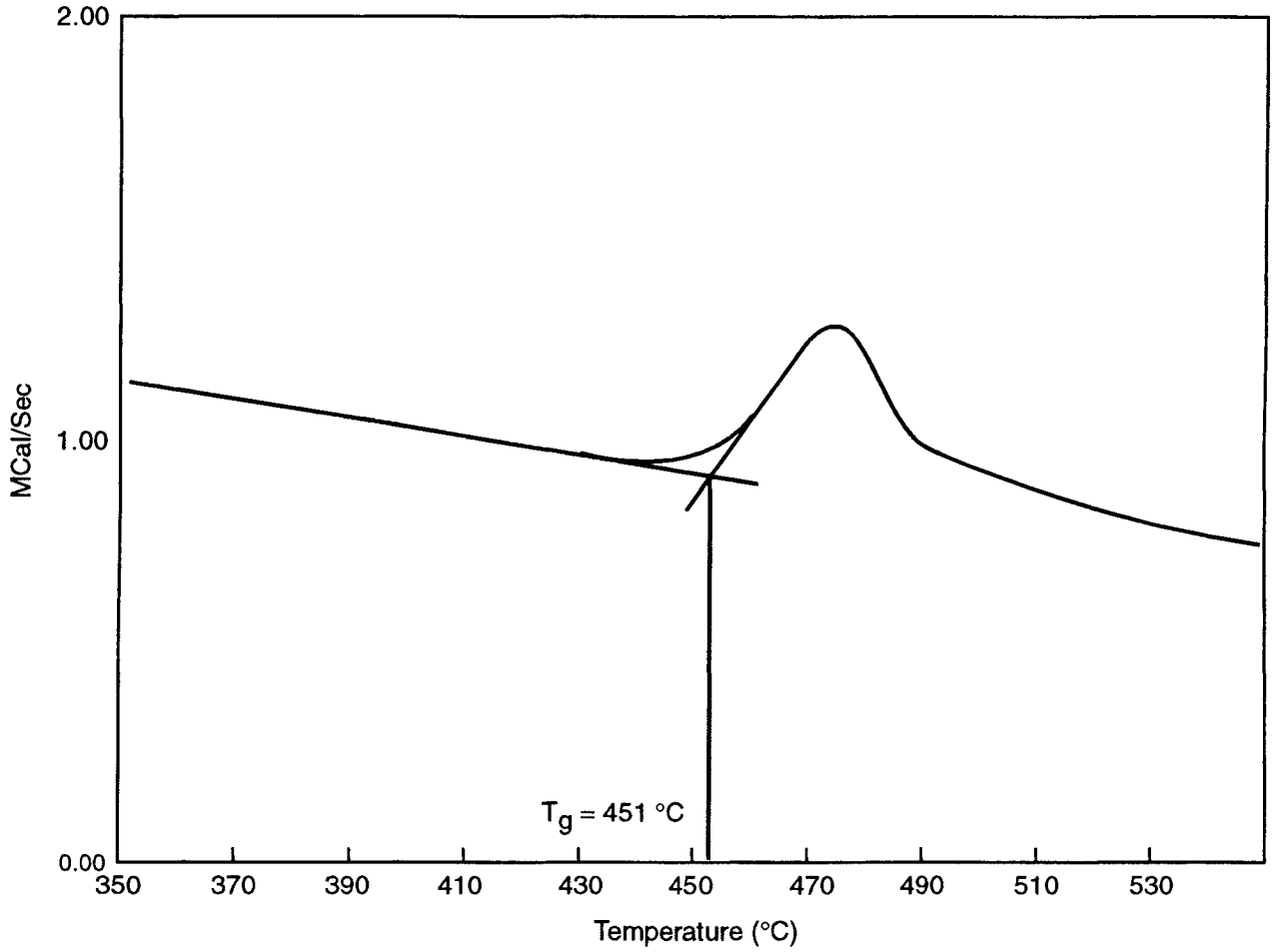

Figure 7-1. Determination of transition temperature using differential scanning calorimetry (West Valley Nuclear Services, 1996)

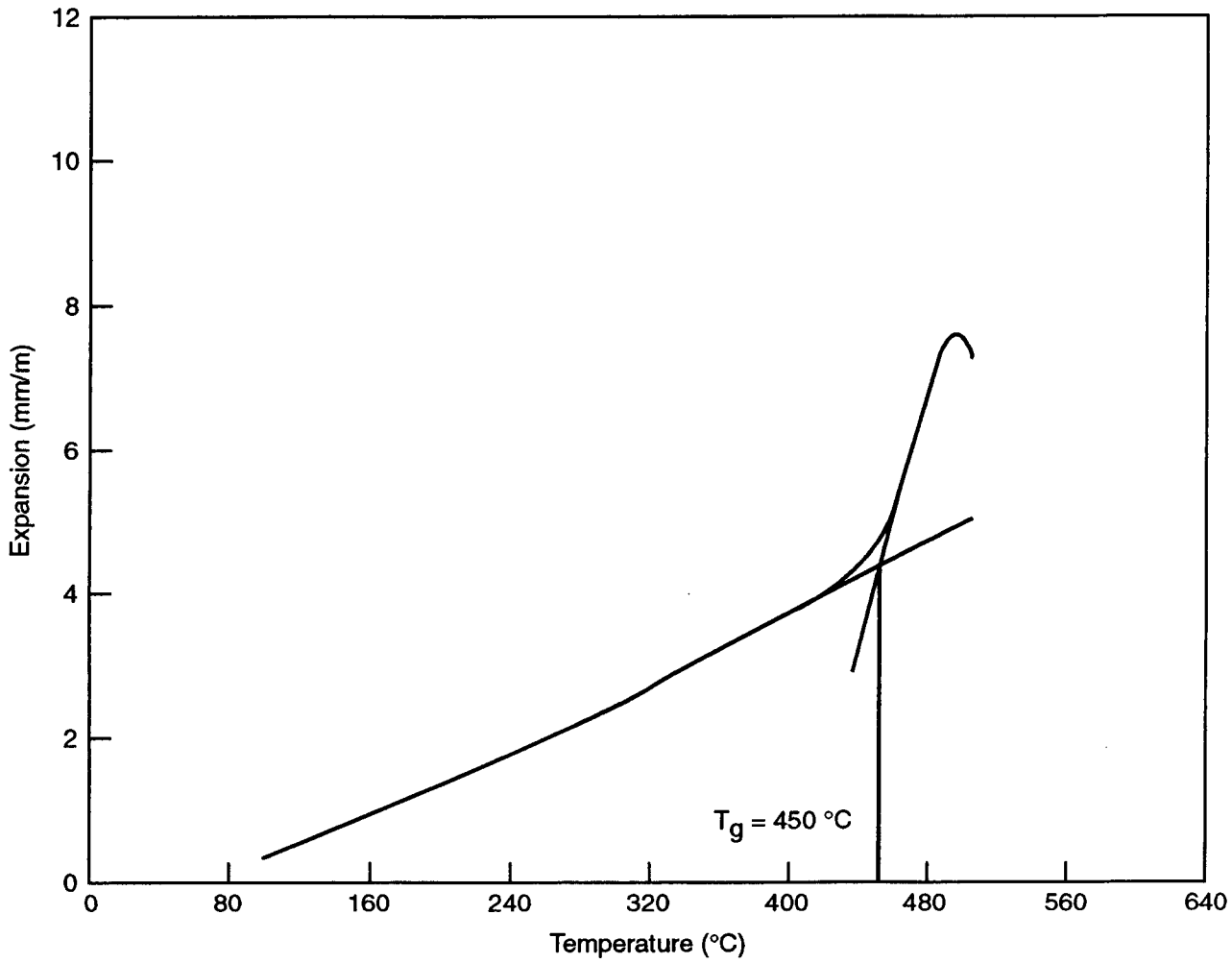

Figure 7-2. Determination of transition temperature using dilatometry (West Valley Nuclear Services, 1996)

7.3 GLASS TRANSITION TEMPERATURE DATA AND MODELS

There is no absolute measure of T_g because its value is influenced by the thermal history and rate of cooling. T_g is a required product specification for the disposal of the vitrified HLW, and is strongly dependent on chemical composition (e.g., T_g of fused silica glass can be lowered from 1,200 to below 400 °C by the addition of alkali oxides). As alkali oxides are added to the silica structure, the network connectivity is broken, which reduces the structure rigidity, and, hence, the T_g. For most vitrified HLW, T_g is above 400 °C (required by the specification) but below 500 °C. To obtain T_g above 500 °C requires melting at temperatures higher than 1,150 °C, which exceeds the maximum operating temperature for joule-heated Alloy 690 melters. The T_g ranges for the various HLW target compositions at DWPF are shown in table 7-1. Measurements indicate no significant changes in T_g despite differences in the chemical composition. This lack of change could be attributed to the fact that for the given variability in compositions, the net effects of various components on T_g cancel each other. The differences in the chemical composition (major components only) are shown in table 7-2.

Even though T_g is a widely measured property in the glass industry, no systematic attempts have been made to establish correlation of T_g to chemical composition. For the vitrified HLW, Hrma et al. (1994) conducted a multiyear statistically designed study to characterize the relationships between composition and properties. Table 5-1 shows target composition and upper and the lower limits for various components in the study. The target composition, HW–39–4, is based on the proposed Hanford HLW glass composition for the NCAW (now known as envelope B/D waste). T_g was measured on 120 glasses using dilatometry. Compositional dependence on T_g was determined by the first-order mixture models as shown by Eq. (7-1).

$$T_g = \sum_{1}^{10} b_i x_i \qquad (7\text{-}1)$$

where T_g is glass transition temperature in °C, x_i and b_i are mass fraction and regression coefficients for component i, respectively. The estimated regression coefficients are shown in table 7-3. Even though r^2 was

Table 7-1. Transition temperature for Defense Waste Processing Facility high-level waste compositions using fiber elongation method (Marra et al., 1991)

Glass Composition*	Annealing Point (°C)	Strain Point (°C)
Blend	446	421
Batch 1	442	418
Batch 2	446	421
Batch 3	446	420
Batch 4	446	420
HM	460	432
PUREX†	445	421

*See table 7-2 for the composition
†Plutonium uranium extraction process

Table 7-2. Defense Waste Processing Facility projected compositions (Marra et al., 1991)

Glass Components wt%	Blend	HM	PUREX*	Batch 1	Batch 2	Batch 3	Batch 4
Al_2O_3	4.16	7.15	2.99	4.88	4.63	3.44	3.43
B_2O_3	8.05	7.03	10.33	7.78	7.88	7.69	8.14
CaO	1.03	1.01	1.09	1.22	1.08	0.99	0.84
CuO	0.44	0.25	0.42	0.40	0.42	0.40	0.45
Fe_2O_3	10.91	7.78	13.25	12.84	11.12	11.71	11.71
K_2O	3.68	2.21	3.41	3.4	3.38	3.40	3.86
Li_2O	4.44	4.62	3.22	4.43	4.50	4.51	4.29
MgO	1.41	1.49	1.14	1.42	1.42	1.42	1.43
MnO_2	2.05	2.15	2.07	2.11	1.73	1.87	3.11
Na_2O	9.13	8.56	12.62	9.00	9.21	9.01	9.16
NiO	0.89	0.41	1.19	0.75	0.90	1.05	1.06
SiO_2	51.9	55.8	46.5	50.2	52.1	52.6	50.1
TiO_2	0.89	0.56	0.68	0.68	0.69	0.68	1.03
ZrO_2	0.14	0.33	0.05	0.10	0.17	0.12	0.22

*Plutonium uranium extraction process

Table 7-3. Regression coefficients for transition temperature (Hrma et al., 1994)

x_i	b_i
SiO_2	622.973
B_2O_3	584.939
Na_2O	128.504
Li_2O	-571.109
CaO	621.517
MgO	494.391
Fe_2O_3	427.129
Al_2O_3	544.451
ZrO_2	730.071
Others	363.637

0.8822, the data showed that the first-order mixture model over-predicted lower T_g and under-predicted higher T_g. Hrma et al. (1994) also used second-order mixture model using first-order mixture model terms and several second-order terms that were selected by using statistical variable selection techniques to improve relationship between T_g and composition. The second-order mixture model did not fit the T_g data substantially better than the first-order mixture model.

Based on the regression coefficients provided in table 7-3, a component effects plot was developed centered around the composition HW–39–4 (figure 7-3). The analysis predicts that Li_2O would have a much stronger effect in decreasing the T_g as compared to Na_2O. SiO_2 and ZrO_2 increase the T_g, although not as strongly as Li_2O and Na_2O decrease it. CaO and B_2O_3 also increase the T_g, but not as much as SiO_2 and ZrO_2. In addition, Hrma et al. (1994) reviewed historical database of 680 glasses and selected 143 of these glasses whose T_g values were available. The T_g of 143 glasses ranged from 280–690 °C. A first-order mixture model predicted $r^2 = 0.3871$, which indicated that historical data were not representative of the composition range studied. The model reviewed in this section was developed for a specific range of glass compositions and glass components. The applicability of these models to other wastes, however, is limited.

Table 7-4 shows the effect of redox conditions on T_g for the WVDP reference glass. The Fe^{2+}/Fe^{3+} ratio was changed from 0 to 1.04, and the T_g was measured using DSC and dilatometry. Results indicate that the T_g decreases by 21 °C from 468 °C to 447 °C as the Fe^{2+}/Fe^{3+} changes from a fully oxidized condition to 1.04. This slight reduction in T_g is attributed to the increase in Fe^{2+} ions, which act as network modifiers and the decrease in the Fe^{3+} ions, which act as network formers. Because network modifiers tend to increase the number of NBO sites or reduce the network connectivity, the T_g decreases. Within the normal operating range of Fe^{2+}/Fe^{3+} of 0.10 and 0.50, no significant change in T_g was observed.

To simulate the effect of thermal history and the cooling rate of glass in a canister, WVDP reference glass was subjected to various isothermal heat treatments at different temperatures and durations. In addition, glass-cooling profiles from various locations within a canister were simulated in a furnace, and the samples were non-isothermally heat treated to determine the effect of cooling rates on T_g. The T_g data on isothermal and nonisothermal heat treated glasses are shown in table 7-5. The sample ID WVCM70–OX–600–96 refers to WVCM70 oxidized glass heat treated at 600 °C for 96 hr. The channel number in the table refers to nonisothermal temperature profiles in the canister during cool-down. A typical cooling profile inside a WVDP canister, is shown in figure 7-4. The solid line refers to cooling at the surface of the canister while the dashed line refers to cooling at the center of the canister at a specific height in the canister. The isothermally heated samples indicate a slight increase in T_g. The samples cooled along the canister cooling curves did not show any significant change in T_g.

Literature review indicates that minor changes in composition, redox, or cooling rate do not result in significant changes in T_g. If the T_g is close to WAPS (400 °C), the effects of redox and glass-cooling history could become important.

7.4 EFFECT OF MELTER CONDITIONS ON GLASS TRANSITION TEMPERATURE

Melter conditions such as redox show a slight decrease in T_g as the redox ratio increases as shown in tables 7-4 and 7-5 for the West Valley glasses (West Valley Nuclear Services, Inc., 1996).

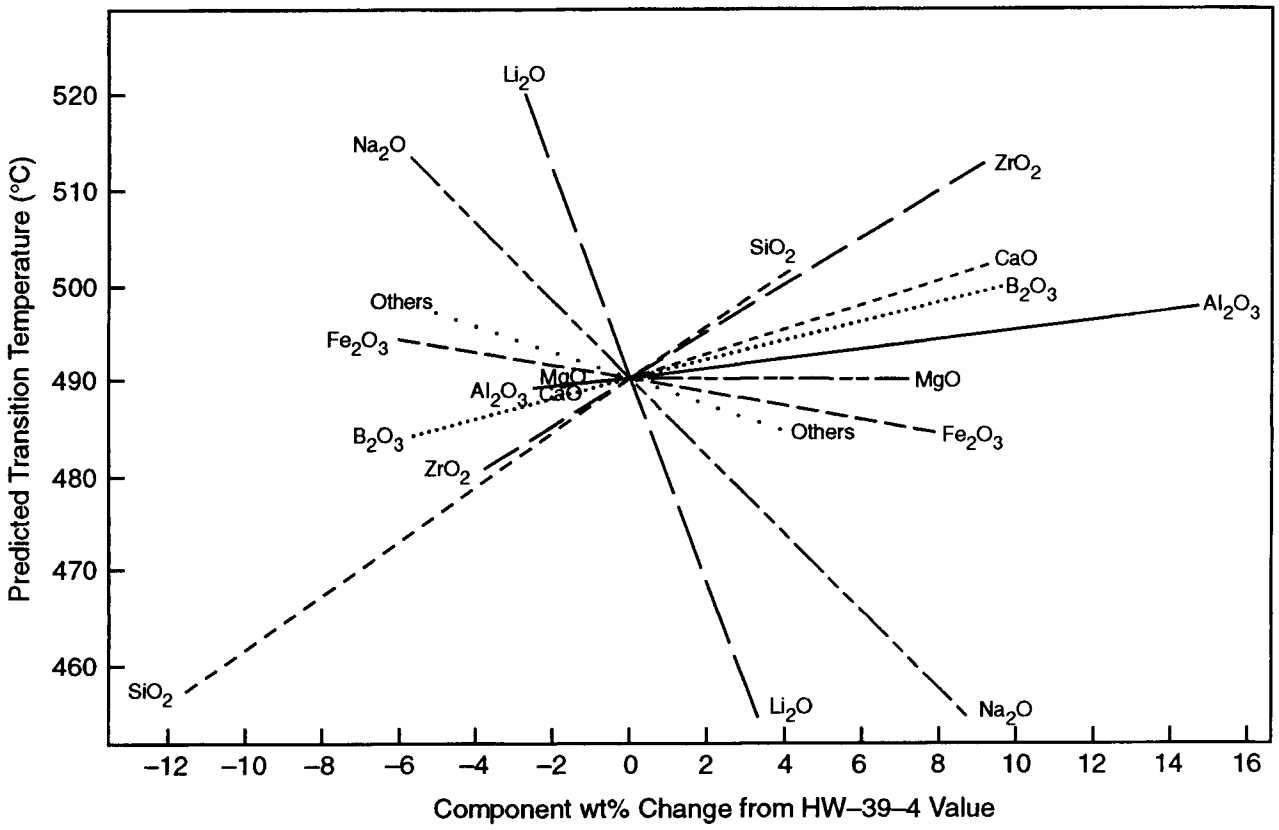

Figure 7-3. Predicted component effects on transition temperature relative to the HW–39–4 composition, based on the first-order mixture model using mass fractions (Hrma et al., 1994)

Table 7-4. Effect of Fe^{2+}/Fe^{3+} on transition temperature (°C) (West Valley Nuclear Services, 1996)

Sample Identification	Fe^{2+}/Fe^{3+}	Transition Temperature (°C) using Differential Scanning Calorimetry	Transition Temperature (°C) using Dilatometry	Average Transition Temperature (°C)
WVCM70–0	0.00	468	467	468
WVCM70–13	0.15	454	455	455
WVCM70–28	0.39	452	452	452
WVCM70–51	1.04	447	446	447

Table 7-5. Effect of isothermal and nonisothermal heat treatment on transition temperature (°C) (West Valley Nuclear Services, 1996)

Sample Identification	Transition Temperature (°C) using Differential Scanning Calorimetry	Transition Temperature (°C) using Dilatometry	Average Transition Temperature (°C)
WVCM70–OX–600–96	456	453	468
WVCM70–OX–700–96	462	462	455
WVCM70–OX–800–24	455	453	454
WVCM70R–600–96	466	465	465
WVCM70R–700–96	465	464	464
WVCM70R–800–24	456	452	454
WVCM70–OX–Channel–1	455	452	454
WVCM70–OX–Channel–5	454	453	454
WVCM70–OX–Channel–6	455	453	454
WVCM70–OX–Channel–53	453	451	452
WVCM70–OX–Channel–57	452	456	454
WVCM70–OX–Channel–58	451	450	451

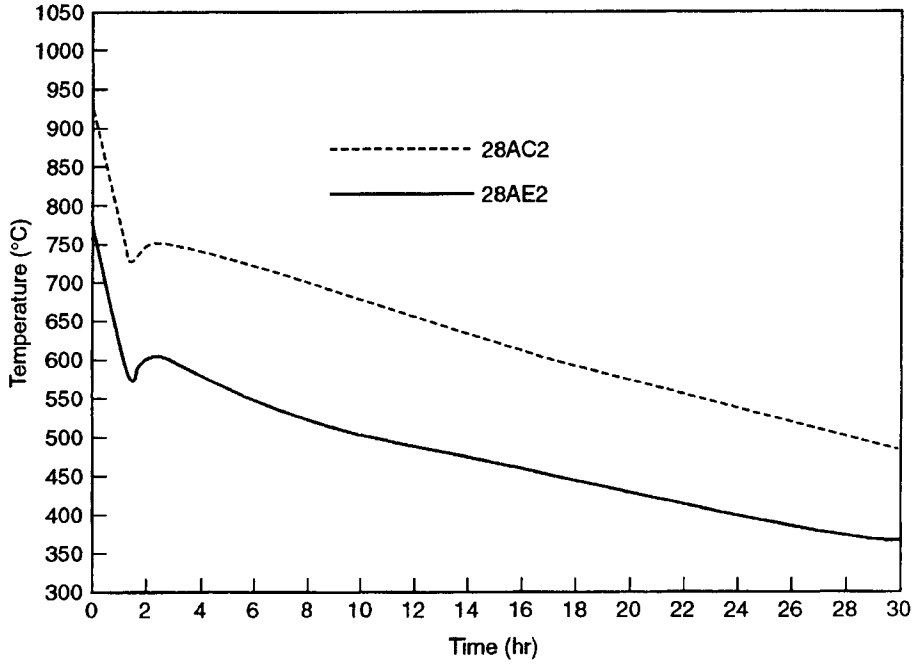

Figure 7-4. Typical canister profiles in the West Valley Demonstration Project (Jain and Barnes, 1991)

7.5 TANK WASTE REMEDIATION SYSTEM CONCERNS

T_g is an important specification for the vitrified HLW. The target glass composition should be designed to meet the specification and to accommodate variability in T_g due to composition variability, redox, or thermal-cooling history.

7.6 SUMMARY

The WAPS require, at the time of shipment, the producer to certify that after the initial cool-down, the waste form temperature has not exceeded 400 °C. This product specification was established to ensure that the waste is in a solid form at the time of shipment. T_g range marks the temperature interval at which a given system gradually transforms on cooling from a supercooled liquid state into the glass state. There is no absolute measure of T_g because its value is influenced by the thermal history and rate of cooling. For most purposes, T_g is defined as the intersection of the extrapolated liquid and glassy state lines. The commonly used methods for measuring T_g are DSC, dilatometry, and fiber elongation. A CVS by Hrma et al. (1994) showed that Li_2O has a much stronger effect compared to Na_2O in decreasing the T_g. SiO_2 and ZrO_2 increase the T_g, although not as strongly as Li_2O and Na_2O decrease it. CaO and B_2O_3 also increase the T_g, but not as much as SiO_2 and ZrO_2. Literature review indicates that minor changes in composition, redox, or cooling rate do not show significant change in T_g. If the T_g is close to 400 °C, the effect of redox and glass-cooling history could become important. T_g is an important specification for the vitrified HLW. The target glass composition should be designed to meet the specification and to accommodate variability in T_g due to composition variability, redox, or thermal-cooling history.

7.7 REFERENCES

American Society for Testing and Materials. Standard test method for annealing point and strain point of glass by fiber elongation. *C336–71: Annual Book of ASTM Standards. Volume 15.02: General Products, Chemical Specialities, and End Use Products*. Philadelphia, PA: American Society for Testing and Materials. 1991.

Hrma, P.R., G.F. Piepel, M.J. Schweiger, D.E. Smith, D.-S. Kim, P.E. Redgate, J.D. Vienna, C.A. LoPresti, D.B. Simpson, D.K. Peeler, and M.H. Langowski. *Property/Composition Relationships for Hanford High-Level Waste Glasses Melting at 1,150 °C*. Volume 1. Chapters 1–11. PNL–10359. Richland, WA: Pacific Northwest National Laboratory. 1994.

Jain, V., and S.M. Barnes. Effect of glass pour cycle on the crystallization behavior in the canistered product at the West Valley Demonstration Project. *Proceedings of the Fifth International Symposium on Nuclear Waste Management IV. 93rd Annual Meeting of the American Ceramic Society, Cincinnati, Ohio, April 29–May 3, 1991*. Ceramic Transactions Volume 23. G.C. Wicks, D.F. Bickford, and L.R. Bunnell, eds. Westerville, OH: American Ceramic Society: 239–250. 1991.

Marra, S.L., C.M. Jantzen, and A.A. Ramsey. DWPF glass transition temperatures—What they are and why they are important. *Proceedings of the Fifth International Symposium on Nuclear Waste Management IV. 93rd Annual Meeting of the American Ceramic Society, Cincinnati, Ohio, April 29–May 3, 1991*. Ceramic Transactions Volume 23. G.C. Wicks, D.F. Bickford, and L.R. Bunnell, eds. Westerville, OH: American Ceramic Society: 465–473. 1991.

Varshneya, A.K. *Fundamentals of Inorganic Glasses*. San Diego, CA: Academic Press, Inc. 1994.

West Valley Nuclear Services. *Waste Qualification Report*. WVNS–186. Revision 1. West Valley, NY : West Valley Nuclear Services. 1996.

8 LIQUIDUS TEMPERATURE

Liquidus temperature (T_L) is the highest temperature at which melt and primary crystalline phases can co-exist at equilibrium. At temperatures higher than the T_L, no crystalline phases are present in the melt. If the lowest temperature in the melter is lower than the T_L, crystalline phases can precipitate and cause processing problems. If the crystalline phases are electronically conductive, electrical shorting could occur in the melter. Experimental vitrification studies using joule-heated melters in the late 1970s at the Pacific Northwest National Laboratory (PNNL) and at the SRL produced large amounts of insoluble crystalline phases in the melter (Jantzen, 1991). The dominant crystalline species formed at the PNNL melter was cerium oxide, while nickel-iron spinel was most dominant in the SRL melter. These observations led to the development of more robust melters and glass compositions to handle crystal formation in the melter. Therefore, the understanding of T_L and its compositional dependence is of great importance for the operation of electrically (joule) heated melters. In addition, the data from the first year of DWPF operation show that waste loading is limited by T_L with spinel as a primary phase. Any improvement in increasing the waste loading through better understanding of the T_L could result in significant cost savings. A 1 wt% increase in DWPF glass waste loading could reduce cleanup cost by $200 million (Hrma et al., 1998). Glass compositions are designed to provide specific T_L. In this chapter, a brief discussion on T_L limit imposed on the glass composition is followed by a review of various studies on T_L and models correlating T_L to composition.

8.1 LIQUIDUS TEMPERATURE LIMITS

Liquidus temperature is a process property and requires that the lowest temperature in the joule-heated melters be above the T_L of the melt. In joule-heated melters operating at an average temperature of 1,150 °C, the T_L limit is set at 1,050 °C.

8.2 LIQUIDUS TEMPERATURE MEASUREMENTS

T_L is measured by heating glass samples in a furnace and determining the highest temperature at which crystals can be formed in the melt. Each sample is placed in a Pt-Au or Pt-10 percent Rh container with lid and heat treated for 24 hr. The use of a temperature-gradient furnace offers a quick method to study the entire temperature range in a single test compared to a uniform temperature furnace, which requires each sample be heat-treated separately. In the temperature gradient furnace, however, T_L measurements could be compromised (i) due to excessive volatilization at the hot end of the furnace and condensation at the cold end of the furnace, (ii) drifting of crystalline phases from the cold end toward the hot end of the furnace, and (iii) convective flow of glass in the sample container, which is shaped like a boat.

The heat-treatment temperature could be reached by heating the sample to the heat-treatment temperature or cooling the glass melt to the heat treatment temperature. Heating the sample is preferred over cooling because (i) melting small samples at $T > T_L$ could cause volatilization; (ii) a portion of the melt, which could be significant due to small sample size, could be lost due to capillary action between crucible and lid; and (iii) melting could destroy nuclei and prevent the sample from crystallization. After heat treatment, samples are thin-sectioned and analyzed in an optical or scanning electron microscope to evaluate crystallization. Other than volatilization during heat treatment, T_L could be affected by the presence of insoluble species such as RuO_2, which could act as nucleating agents and redox conditions.

8.3 LIQUIDUS TEMPERATURE DATA AND MODELS

The importance of T_L in a joule-heated melter for vitrifying HLW is clearly evident from the test runs at PNNL and SRL, in which significant amounts of crystals precipitated in the melter. Since these test runs, several detailed studies have been conducted to design glass compositions to minimize crystal formation during melting. Crystal formation in glass melts cannot be completely eliminated, but glass compositions can be designed to provide minimum crystallization during melting. The T_L is the main property that is used in the glass composition design process for minimizing crystal formation during melting. Even though operating a melter at temperatures higher than T_L ensures minimum crystal formation in the melt, the settling of limited solubility species such as noble metals or formation of sulfides and metals due to uncontrolled reducing conditions in the melter could result in formation of secondary phases. The formation of these secondary phases resulting from uncontrolled melter conditions is discussed in chapter 11.

Jantzen (1991) developed the T_L model for spinels in the DWPF HLW glasses. The model is based on the free energy of formation of the liquidus phases—spinel and nepheline ($Na\,AlSiO_4$), which are the two main phases formed in the DWPF process. The model assumes that

- Amorphous SiO_2 is the predominant solvent in the borosilicate waste glass.
- Fe_2O_3 is considered as the limiting species for spinel precipitation.
- Al_2O_3 is considered as the limiting species for nepheline precipitation.

Based on the T_L measurements on 30 glasses, Jantzen (1991) developed the following relationship for calculating T_L.

$$T_L = 803.6 + 2277\kappa \qquad r^2 = 0.77 \tag{8-1}$$

where κ is defined as a pseudo-equilibrium constant and is expressed as

$$\kappa = \frac{m(Fe_2O_3) \times \Delta G_{fm}[NiFe_2O_4]}{m(SiO_2) \times \Delta G_{fm}[SiO_2] - m(Al_2O_3) \times \Delta G_{fm}[NaAlSiO_4]} \tag{8-2}$$

In Eq. (8-2), $m(Fe_2O_3)$, $m(SiO_2)$, and $m(Al_2O_3)$ are mole fractions of Fe_2O_3, SiO_2, and Al_2O_3 in the glass and Gibbs free energy of formation at 1,050 °C are

$$\Delta G_{fm}\,[NiFe2O4] = -134 \text{ kcal/mol}$$
$$\Delta G_{fm}\,[SiO2] = 156 \text{ kcal/mol}$$
$$\Delta G_{fm}\,[NaAlSiO4] = -360 \text{ kcal/mol}$$

DWPF routinely uses Eq. (8-1) to predict the T_L, but uncertainty is significant because the model is based on a limited number of samples. Currently, additional T_L data on 53 glasses have been collected and are being analyzed to improve the T_L model (Hrma et al., 1998).

Hrma et al. (1994) conducted a multiyear statistically designed study to characterize relationship between composition and properties. Table 5-1 shows target composition and upper and lower limits for

various components in the study. Liquidus temperature was measured on 110 glasses. Figure 8-1 summarizes the T_L of major crystalline phases identified in the study. The T_L for spinels, clinopyroxene, and Zr-containing crystals were modeled by the first-order mixture model as shown by Eq. (8-3).

$$T_L = \sum_{1}^{10} b_i x_i \tag{8-3}$$

where T_L is T_L, x_i and b_i are mass fraction and regression coefficients for component i, respectively. The estimated regression coefficients for various types of crystals are shown in table 8-1. The predicted versus measured T_L values for clinopyroxene, spinel, and Zr-containing crystals are shown in figures 8-2, 8-3, and 8-4, respectively. Overlaid on figures 8-3 and 8-4 are the measured T_L for several samples containing spinel and Zr-containing crystals that had T_L greater than the hot-end temperature (1,100 °C). These data were not included in the calculation for the first-order mixture model coefficients but were used to provide information on the extrapolative predictive capability of the model. The $r^2 = 0.906$ for clinopyroxene, as shown in table 8-1, shows a good correlation between T_L and glass composition. However, the fit for spinels was poor ($r^2 = 0.643$) and for Zr-containing crystals, the fit could be obtained only after including three different types of Zr-containing crystals (Zircon, sodium zirconium silicate, and ZrO_2), which provided a sufficiently large data set to perform regression analysis. The fit for Zr-containing crystals was acceptable with $r^2 = 0.79$.

For the six glasses with T_L greater than the hot-end temperature for Zr-containing crystals, the model predicted T_L to be higher than with the hot-end temperature for all six glasses. These data suggest that the model for Zr-containing crystals could be used for extrapolative estimation of T_L for glasses outside the experimentally tested range. For 15 spinel-containing glasses with T_L higher than the hot-end temperature, the

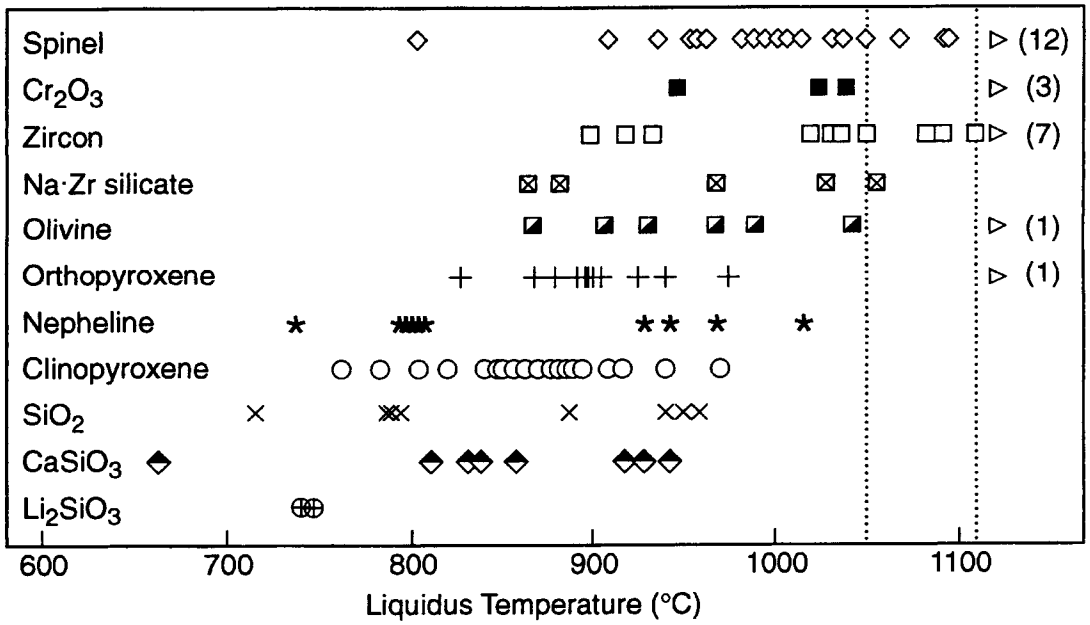

Figure 8-1. Liquidus temperatures of major crystalline phases in compositional variability study glasses. The quantities in parentheses at the right of the figure represent the number of samples with $T_L \geq$ 1,110 °C (Hrma et al., 1994)

Table 8-1. Regression coefficients for liquidus temperature (Hrma et al.,1994)

x_i	Clinopyroxene b_i, unit	Spinel b_i, unit	Zr-containing crystals b_i, unit
SiO_2	855.65	989.31	753.78
B_2O_3	314.72	666.42	1095.83
Na_2O	38.83	3.77	74.31
Li_2O	-207.05	-128.77	-956.39
CaO	1372.44	1366.21	886.76
MgO	2387.62	2830.58	2458.47
Fe_2O_3	1506.69	2256.00	1461.04
Al_2O_3	1319.48	1735.03	1138.06
ZrO_2	1844.50	928.11	4541.99
Others	1357.40	1005.56	657.99
Number of data points	29.00	28.00	22.00
r^2	0.91	0.64	0.79
Measured T_L Range (°C)	761–969	800–1129	856–1129

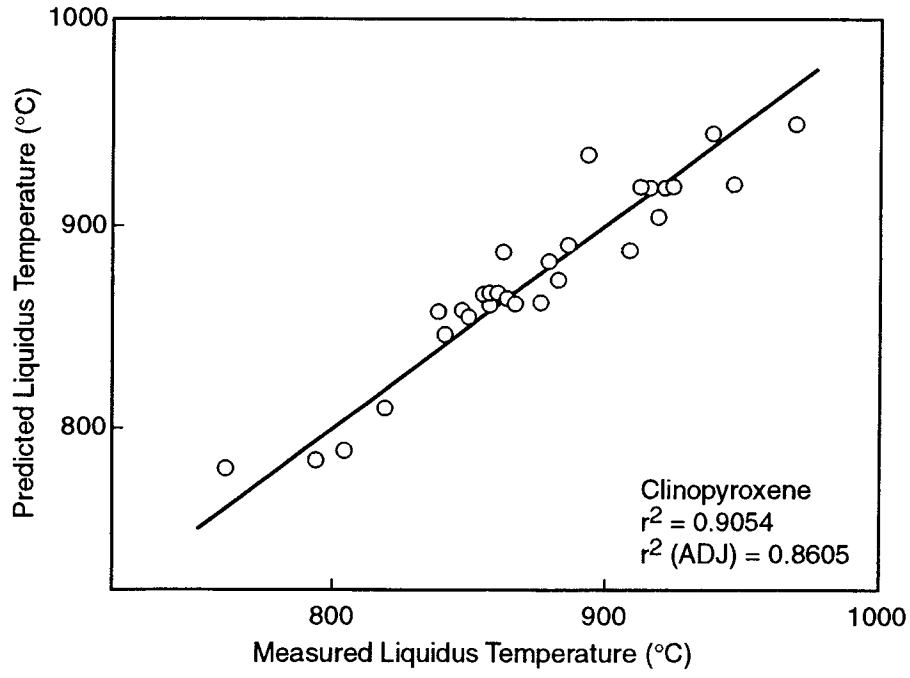

Figure 8-2. Predicted versus measured liquidus temperature of clinopyroxene for the first-order mixture model (Hrma et al., 1994)

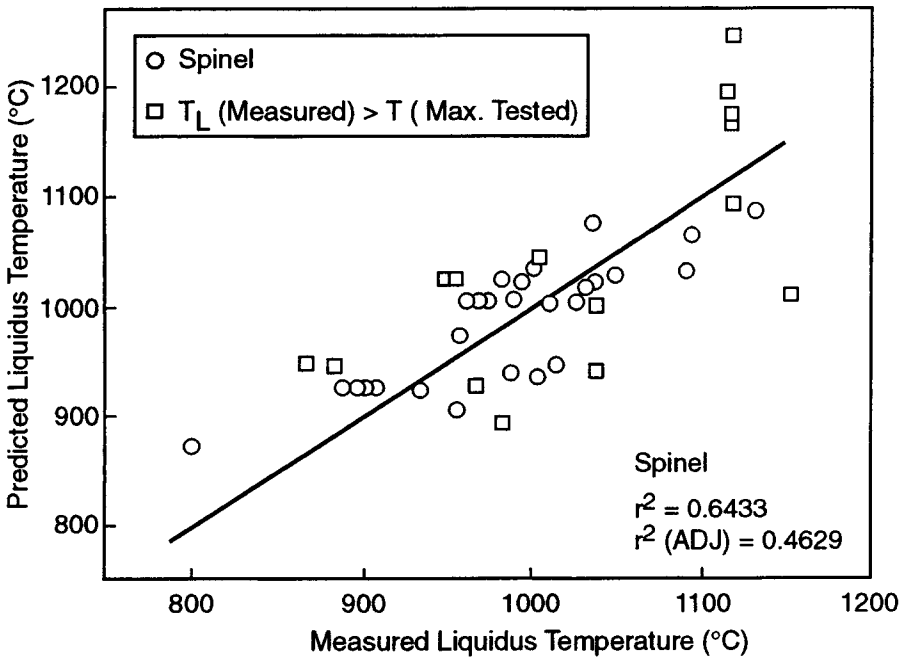

Figure 8-3. Predicted versus measured liquidus temperature of spinel for the first-order mixture model (Hrma et al., 1994)

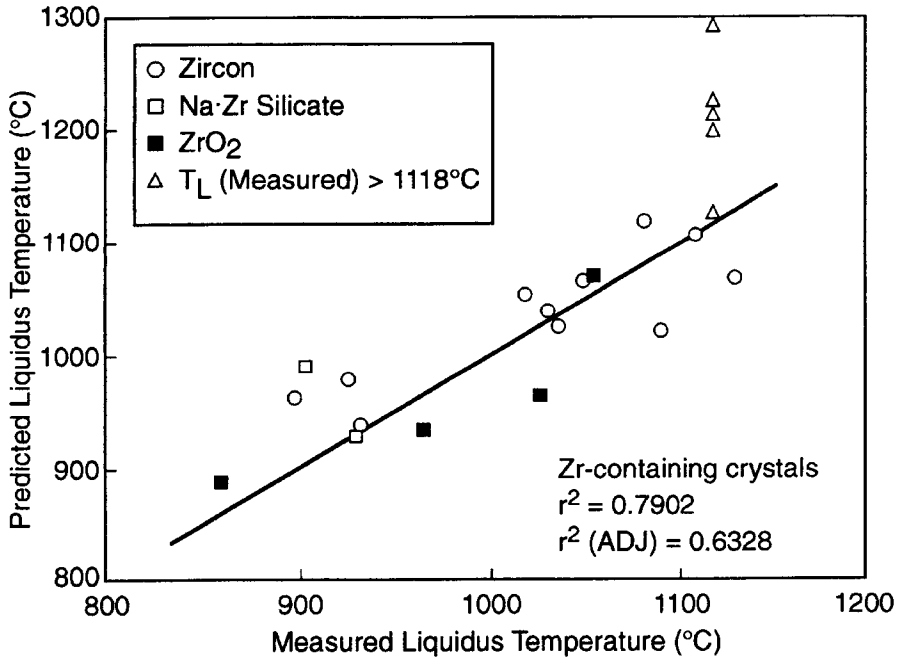

Figure 8-4. Predicted versus measured liquidus temperature of Zr-containing crystals for the first-order mixture model (Hrma et al., 1994)

model predicted T_L higher than hot-end temperature for nine glasses and lower than hot-end temperature for six glasses. The poor extrapolative prediction is attributed to the uncontrolled redox conditions during the test, which could result in varying concentrations of FeO in the sample. The presence of FeO is important in the formation of spinels.

Based on the regression coefficients provided in table 8-1, component effects plots were developed centered around the composition HW–39–4 (figures 8-5, 8-6, and 8-7). Alkali oxides (Li_2O and Na_2O) decrease the liquidus of all three crystalline phases with Li_2O having the strongest effect. B_2O_3 decreases the T_L of clinopyroxene and spinel, but has little effect on Zr-containing crystals. The addition of MgO, ZrO_2, and Fe_2O_3 is most effective in increasing the formation of clinopyroxene because both Mg and Fe are components of clinopyroxene. The T_L for spinel was strongly increased by MgO and Fe_2O_3. The effect of MgO influence is surprising because experimental results do not indicate the presence of MgO in spinel crystals. In Zr-containing crystals, ZrO_2 showed the strongest effect in increasing the T_L, closely followed by MgO. The effect of MgO was surprising. Because of low r^2 values for spinel and Zr-containing crystals, these models should be used with caution.

In developing a test matrix for studying glass properties, multiple-component constraints are usually imposed on the glass components to ensure that the selected test matrix meets the required properties. For the T_L, these constraints are shown in table 8-2. As shown in table 8-2, small r^2 values indicate that none of the multicomponent constraints shows any correlation with T_L. This lack of correlation clearly indicates that the T_L depends on the concentrations of components other than those selected as constraints. Hrma et al. (1994) also attempted to fit the T_L data collected on 110 samples using a phase-equilibria T_L model. This model, developed by Pelton et al. (1996), and it optimizes the thermodynamic properties of crystalline phases as functions of temperature and composition by analyzing all available phase diagrams and thermodynamic databases. The model lacks thermodynamic data for Fe, Ni, and Cr, which are major components of the spinel phase. Excluding spinels, the model predicts one or more possible primary phases with T_L. The model was tested using 89 glasses The primary phase agreed with the predicted first phase in 31 glasses, and with the predicted second or third phase in 20 glasses. The model failed to agree with any phase in 38 glasses. The overall fit of predicted versus measured T_L was poor with $r^2 = 0.431$. In addition, the phase equilibria model predicted a fairly narrow range for T_L between 825 °C and 950 °C for the majority of data points; the experimental range was between 650 °C and 1,025 °C. The phase equilibria model in the present form is not adequate to predict T_L. According to Kim and Hrma (1994), modifications are required to improve the predictive capability of phase-equilibria model.

The most recent T_L study was completed by Hrma et al. (1998) as part of Tank Focus Area activity. Hrma et al. (1998) measured T_L on 53 glasses that were within and outside the current DWPF processing region. The composition region, as shown in table 8-3, was selected using statistical experimental design methods, and experiments were performed using a uniform temperature furnace. The SG series, which bounds the DWPF series shown in table 8-3, is based on DWPF processing region and Hanford processing region for HLW glass. All glasses formed an iron-containing primary phase. Nine glasses formed acmite-augite clinopyroxene phase, while the others formed spinel as the primary phase. Occasionally, spinel crystals nucleated on the RuO_2 precipitated from the glass. Spinel contained Fe, Ni, and Cr as major components and Mn, Mg, and Al as minor components. The T_L span ranged from 865 °C to 1,316 °C for spinel and from 793 °C to 996 °C for the clinopyroexne phase. The study characterized the effect of glass components on T_L into four groups—(Cr_2O_3, NiO) >> (MgO, TiO_2, Al_2O_3, Fe_2O_3) > (U_3O_8, MnO, CaO,

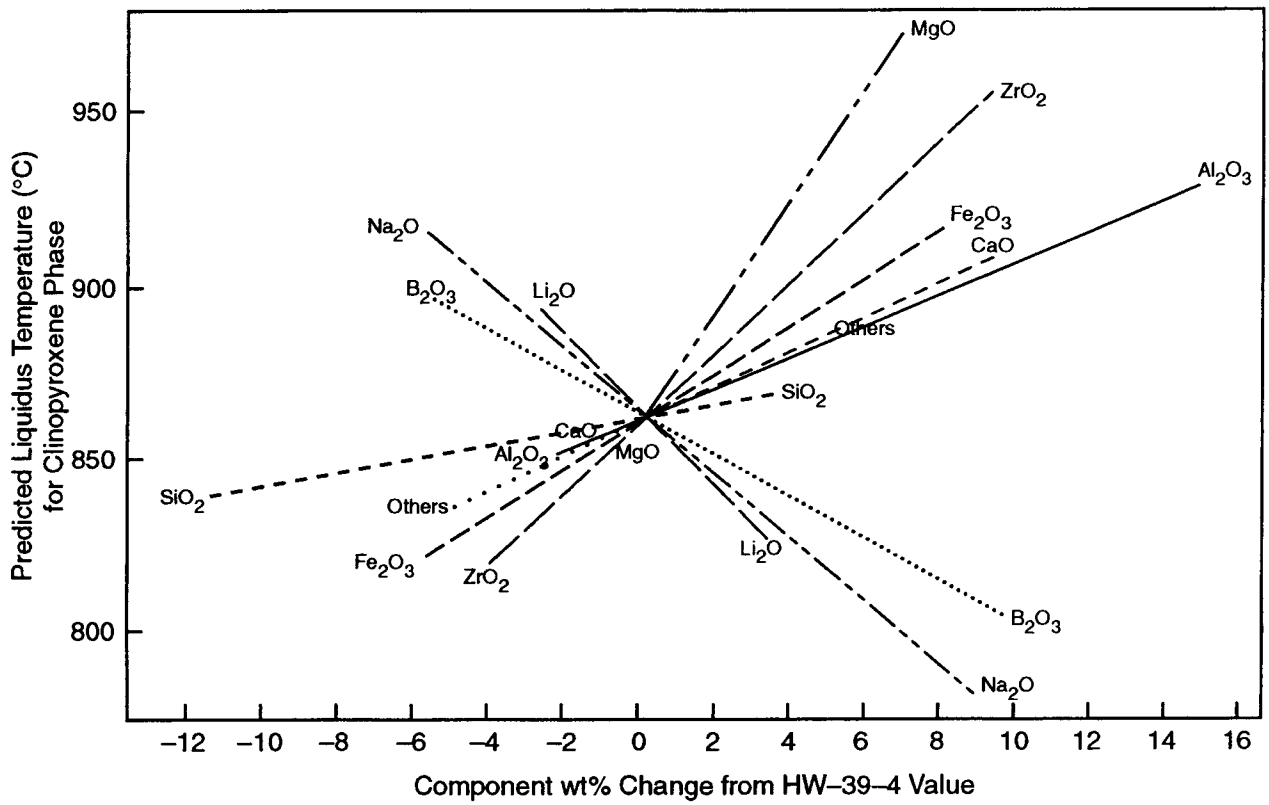

Figure 8-5. Predicted component effects on liquidus temperature of clinopyroxene relative to the HW–39–4 composition, based on the first-order mixture model using mass fraction (Hrma et al., 1994)

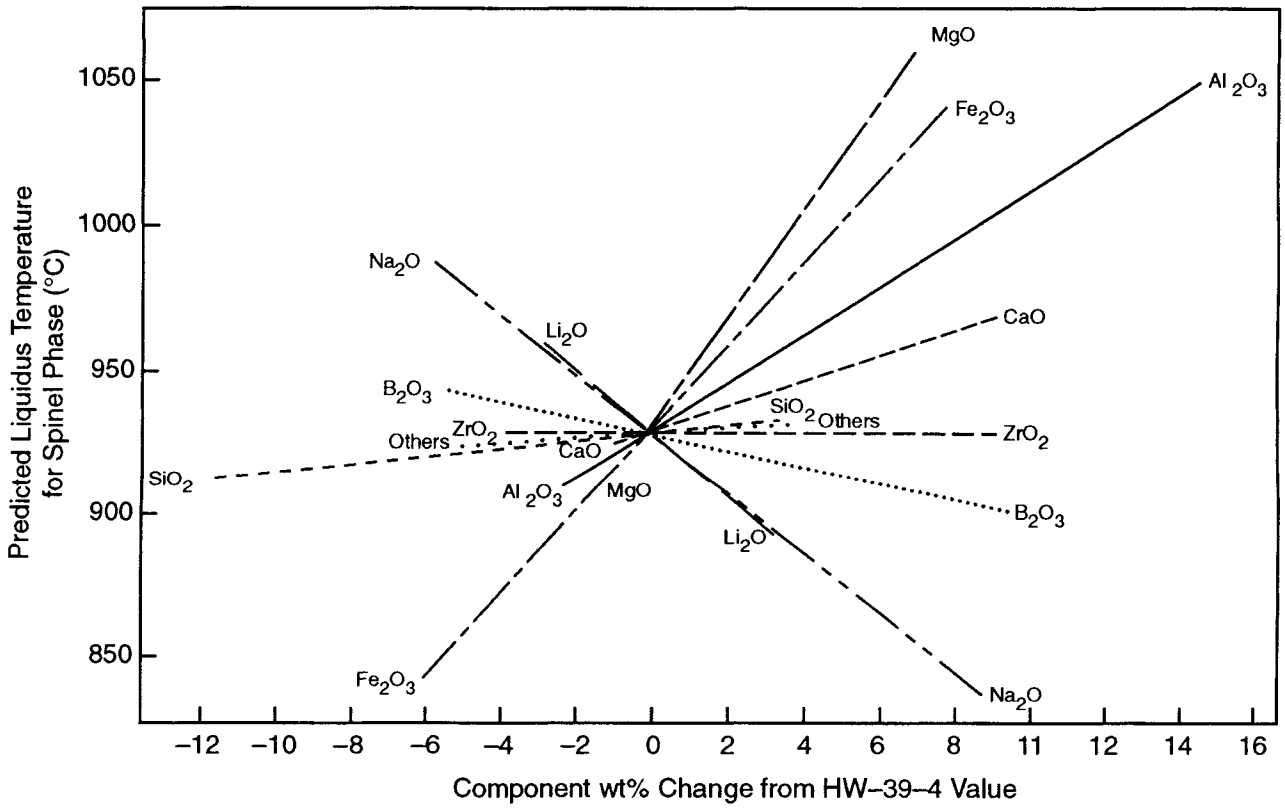

Figure 8-6. Predicted component effects on liquidus temperature of spinal relative to the HW–39–4 composition, based on the first-order mixture model using mass fraction (Hrma et al., 1994)

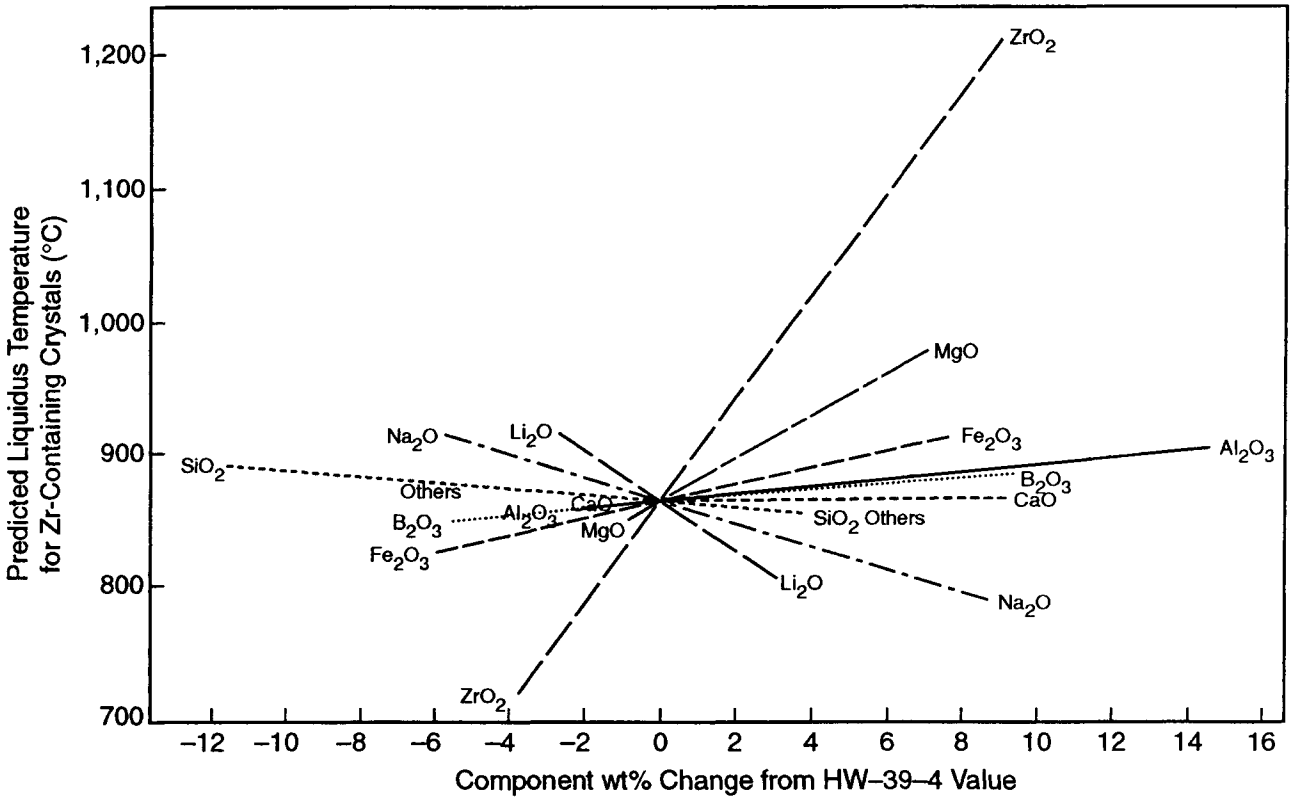

Figure 8-7. Predicted component effects on liquidus temperature of Zr-containing crystals relative to the HW–39–4 composition, based on the first-order mixture model using mass fraction (Hrma et al., 1994)

Table 8-2. Multicomponent crystallinity constraints and their correlation with liquidus temperature (Kim and Hrma, 1994)

Sum of Oxide (Mol fraction)	r^2
$CaO + MgO = 0.10$	0.036
$Al_2O_3 + ZrO_2 = 0.18$	0.000
$CaO + MgO + ZrO_2 = 0.18$	0.314
$Fe_2O_3 + Al_2O_3 + ZrO_2 + Others = 0.24$	0.058
$Al_2O_3/SiO_2 = 0.33$	0.078

Table 8-3. Composition regions (in mass fractions of components) for Defense Waste Processing Facility and SP and SG glasses (Hrma et al., 1998)

	Defense Waste Processing Facility Region		SG Glasses		SP Glasses	
Oxide*	Low	High	Low	High	Low	High
SiO_2	0.491	0.551	0.430	0.590	0.380	0.600
B_2O_3	0.068	0.075	0.050	0.100	0.000	0.120
Al_2O_3	0.024	0.055	0.025	0.080	0.040	0.160
Li_2O	0.043	0.050	0.030	0.060	0.000	0.030
Na_2O	0.078	0.106	0.060	0.110	0.080	0.200
K_2O	0.021	0.026	0.015	0.038	0.000	0.000
MgO	0.013	0.021	0.005	0.025	0.004	0.060
CaO	0.007	0.013	0.003	0.020	0.000	0.000
MnO	0.011	0.028	0.010	0.030	0.000	0.040
NiO	0.001	0.012	0.001	0.020	0.000	0.030
Fe_2O_3	0.085	0.124	0.060	0.150	0.060	0.150
Cr_2O_3	0.000	0.002	0.001	0.003	0.000	0.012
TiO_2	0.002	0.004	0.002	0.006	0.000	0.000
U_3O_8	0.008	0.050	0.000	0.055	0.000	0.000
Others†	—	—	0.000	0.000	0.045	0.070

*SG glasses contained RuO_2 in mass fraction 0.0009. SP glasses contained RuO_2 in mass fraction 0.0003. The estimated RuO_2 mass fraction for the DWPF composition region is 1×10^{-5} to 0.0015.
†Others for SP glasses were a mixture of 22 minor components with ZrO_2, Nd_2O_3, La_2O_3, CdO, MoO_3, F, and SO_3 > 3 wt% of the mix.

B_2O_3, SiO_2) > (K_2O, Na_2O, Li_2O). Cr and Ni strongly increase the T_L, while alkali oxides decrease the T_L. Mg, Ti, Al, and Fe moderately increase the T_L, and U, Mn, Ca, B, and Si have little or no effect on T_L.

The liquidus temperatures for the spinel phase observed in the SG series were analyzed using Eq. (8-3). The data set was then combined with another T_L study by Mika et al. (1997) that consisted of 33 glasses (composition range SP shown in table 8-1) and reanalyzed. Table 8-4 shows the regression coefficients obtained from the individual and combined data set. The SP study varied one component at a time around the baseline glass. Except for MgO, MnO, and Cr_2O_3, the regression coefficients showed a good agreement between data sets. The difference of these three components is attributed to the differences in the composition range not covered by the studies. The T_L regression coefficients using first-order mixture model obtained by Hrma et al. (1994) as shown in table 8-2, are significantly different from the Hrma et al. (1998) or Mika et al. (1997) study (shown in table 8-4). Because the first-order mixture models are valid within a specified composition range, the differences in the regression coefficients between studies are expected.

The application of T_L models discussed in this section is limited because the models are based on a few glass compositions. The T_L depends not only on concentrations of its own components but also on

Table 8-4. Regression coefficients for liquidus temperature (Hrma et al., 1998)

x_i	SG Glass, b_i	SP Glass, b_i	SG and SP Glasses, b_i
Al_2O_3	2,678	3,307	2,897
B_2O_3	453	395	396
CaO	2,033	N/A	1,781
Cr_2O_3	30,313	18,864	21,553
Fe_2O_3	2,643	2,644	2,692
K_2O	-1,152	N/A	-952
Li_2O	-1,504	-1,470	-1,367
MgO	4,839	2,827	3,823
MnO	873	1,870	1,277
Na_2O	-1,673	-1,826	-1,734
NiO	9,959	8,210	9,652
SiO_2	981	834	997
TiO_2	3,554	N/A	3,620
U_3O_8	1,546	N/A	1,622
Others	N/A	4,419	3,492
r^2	0.95	0.94	0.93
adj r^2	0.93	0.87	0.92

concentration of other components in the glass composition, and the effect of a component could be quite different for different crystalline phases. Therefore, the prediction capability of present models is limited to the range of composition studied and crystalline phases observed.

8.4 EFFECT OF MELTER CONDITIONS ON LIQUIDUS TEMPERATURE

Even though T_L is defined by the glass composition, the processing conditions in the melter could influence the formation of secondary phases. These secondary phases could occur because of extremely reducing conditions in the melt, which could precipitate highly conductive phases, such as NiS, CuS, or FeS, or because of phase separation in the melt if the concentration of the components exceeds their solubility limit (e.g., immiscible sodium sulfate phase could form if SO_3 concentration is greater than 0.25 wt% in glass). In addition, limited solubility species such as noble metals and refractory corrosion products could act as nucleating sites for the formation and growth of crystals.

8.5 TANK WASTE REMEDIATION SYSTEM CONCERNS

At Hanford, both LAW and HLW joule-heated melters will be operated at 1,150 °C. The T_L should be below 1,050 °C. The formation of spinel and clinopyroxene crystals in HLW glass composition is more probable compared to LAW glass composition because HLW contains significant concentrations of components such as Fe, Ni, Mn, and Cr, along with Al, Si and Na, which are responsible for spinel and clinopyroxene formation, respectively. In the LAW glass composition, a small concentration of spinel crystals and a higher amount of clinopyroxene crystals are expected.

8.6 SUMMARY

T_L is the highest temperature at which melt and primary crystalline phases can coexist at equilibrium. At temperatures higher than the T_L, no crystalline phases are present in the melt. If the T_L of the melt is higher than the lowest temperature in the melter, crystalline phases can precipitate, perhaps causing processing problems. If the crystalline phases are electronically conductive, electrical shorting could occur in the melter. Experimental vitrification studies using joule-heated melters in the late 1970s at PNNL and SRL produced large amounts of insoluble crystalline phases in the melter. Liquidus temperature is a process property and requires that the lowest temperature in the joule-heated melters be higher than the T_L of the melt. In joule-heated melters operating at an average temperature of 1,150 °C, the T_L limit is set at 1,050 °C. The T_L models—SRL free-energy hydration model, PNNL first-order mixture model, phase-equilibria T_L model, and process constraint model—are based on limited site-specific glass compositions. The T_L depends not only on concentrations of its own components but also on concentration of other components in the glass composition. Also, the effect of a component could be quite different for different crystalline phases. Therefore, the prediction capability of present models is limited to the range of the composition studied and crystalline phases observed. At Hanford, both LAW and HLW joule-heated melters will be operated at 1,150 °C, the T_L should be below 1,050 °C. The formation of spinel and clinopyroxene crystals in HLW glass composition is more probable compared to LAW glass composition because HLW contains significant concentrations of components such as Fe, Ni, Mn, and Cr, along with Al, Si and Na, which are responsible for spinel and clinopyroxene formation, respectively. In the LAW glass composition, a small concentration of spinel crystals and a higher amount of clinopyroxene crystals are expected.

8.7 REFERENCES

Hrma, P.R., G.F. Piepel, M.J. Schweiger, D.E. Smith, D.-S. Kim, P.E. Redgate, J.D. Vienna, C.A. LoPresti, D.B. Simpson, D.K. Peeler, and M.H. Langowski. *Property/Composition Relationships for Hanford High-Level Waste Glasses Melting at 1,150 °C.* Volume 1. Chapters 1–11. PNL–10359. Richland, WA: Pacific Northwest National Laboratory. 1994.

Hrma, P.R., J.D. Vienna, M. Mika, and J.V. Crum. *Liquidus Temperature Data for DWPF Glass.* PNNL–11790. Richland, WA: Pacific Northwest National Laboratory. 1998.

Kim, D.-S and P. Hrma. Models for liquidus temperature of nuclear waste glasses. *Proceedings of the Environmental and Waste Management Issues in the Ceramic Industry II Symposium. 96th Annual Meeting of the American Ceramic Society, Indianapolis, Indiana, April 25–27, 1994.* Ceramic Transactions Volume 45. D. Bickford, S. Bates, V. Jain, and G. Smith, eds. Westerville, OH: American Ceramic Society: 327–337. 1994.

Mika, M., M.J. Schweiger, J.D. Vienna, and P. Hrma. Liquidus. Temperature of spinel precipitating high-level waste glasses. *Scientific Basis for Nuclear Waste Management XX.* Symposium Proceedings 465. Pittsburgh, PA: Materials Research Society: 71–78. 1997.

Jantzen, C.M. First principles process-product models for vitrification of nuclear waste: Relationship of glass composition to glass viscosity, resistivity, liquidus temperature, and durability. *Proceedings of the Fifth International Symposium on Nuclear Waste Management IV. 93rd Annual Meeting of the American Ceramic Society, Cincinnati, Ohio, April 29–May 3, 1991.* G.C. Wicks, D.F. Bickford, and L.R. Bunnell, eds. Ceramic Transactions Volume 23. Westerville, OH: American Ceramic Society: 37–51. 1991.

Pelton, A.D., P. Wu, G. Eriksson, and S. Degtiarev. *Development of Models and Software for Liquidus Temperatures of Glasses of HWVP Products.* PNNL–11037, UC–810. Richland, WA: Pacific Northwest National Laboratory. 1996.

9 REDOX

Redox (reduction-oxidation) reactions involve a transfer of one or more electrons among the different oxidation states of a multivalent element or from one multivalent element to another within a chemical system. Elements that can coexist in multiple valence states are called redox couples, for example, an Fe redox couple can exist as either Fe^{2+}/Fe^{3+} or Fe^{0}/Fe^{2+}, depending on the available oxygen in the system. Knowledge of redox couples participating in chemical reactions in glass melts and the temperature and compositional dependence of redox reactions during vitrification of HLW in joule-heated melters is of great importance.

In this chapter, a brief discussion on redox limits is followed by a discussion of the thermodynamic basis for redox reactions and various variables that affect redox reactions in glass melts. In addition, redox forecasting and control strategies adopted by WVDP and DWPF to predict redox response from the HLW slurry compositions are presented.

9.1 REDOX LIMITS

The redox state in a melter is probably the most important process control parameter. A redox response within a specified range is necessary to avoid process problems that could lead to permanent melter damage. Redox couples that could influence the redox behavior of the nuclear waste glasses are shown in table 9-1. Because Fe is abundant in most wastes and oxidation states can be easily measured, the redox response in waste vitrification systems is determined by the Fe^{2+}/Fe^{3+} ratio. The influence of some minor waste components, such as Cu and Mn, cannot be ignored. A glass melt is defined as extremely reducing if the Fe^{2+}/Fe^{3+} ratio is greater than 1. Under such conditions, sufficient conductive metals and metal sulfides could accumulate and short-circuit the melter. If the Fe^{2+}/Fe^{3+} ratio is less than 0.01, a glass melt is considered to be extremely oxidizing. Under extremely oxidizing conditions, foaming is observed in the melter. Foam creates an insulating layer of gas bubbles between the cold cap and the melt, disrupting the thermal gradients in the melter. If controlled at its onset, foaming typically slows the glass production rate and is not an issue. Left uncontrolled, however, foaming conditions could result in melter shutdown. A much narrower bound between 0.01 and 0.5 is acceptable for processing to avoid foaming or precipitation of metal sulfides Fe^{2+}/Fe^{3+} in the glass.

9.2 THERMODYNAMICS OF REDOX REACTIONS

In simplified form, redox equilibrium of a multivalent element (M) in a glass melt can be represented as

$$M^{m+}_{(melt)} + \frac{n}{2}O^{2-}_{(melt)} \xleftrightarrow{K} M^{(m-n)+}_{(melt)} + \frac{n}{4}O_{2(gas)} \qquad (9\text{-}1)$$

where M^{m+} and $M^{(m-n)+}$ represent oxidized and reduced species of the multivalent element M, n is the number of electrons transferred during redox reaction, O_2 is the oxygen released (the amount of which depends on the furnace atmosphere and/or oxidizing and reducing agents present in the feed materials), and O^{2-} is the basicity (or oxygen ion activity) of the glass melt that depends on the glass composition. Basicity for a given composition is constant.

Table 9-1. Redox couples in nuclear waste glasses

Redox Couple	Reference Electrode Potential for Savannah River Laboratory (SRL–131) Glass at 1,150 °C (Schreiber and Sampson, 1996)*	Enthalpy of Reduction (ΔH) for Savannah River Laboratory (SRL–131) Glass kJ/mol (kcal/mol) (Schreiber et al., 1990)†
Au^{3+}/Au^{0}	>3.00	—
Pd^{2+}/Pd^{0}	+2.30	—
Ni^{3+}/Ni^{2+}	+1.70	—
Rh^{3+}/Rh^{0}	+1.40	—
Co^{3+}/Co^{2+}	+1.40	—
Mn^{3+}/Mn^{2+}	+0.80	54 ± 13 (13 ± 3)
Ag^{1+}/Ag^{0}	+0.50	—
Se^{6+}/Se^{4+}	+0.20	—
Se^{4+}/Se^{0}	+0.20	—
Ce^{4+}/Ce^{3+}	-0.10	46 ± 17 (11 ± 4)
Cr^{6+}/Cr^{3+}	-0.30	42 ± 13 (10 ± 3)
Sb^{5+}/Sb^{3+}	-0.30	—
Cu^{2+}/Cu^{1+}	-0.80	176 ± 42 (42 ± 10)
U^{6+}/U^{5+}	-1.50	172 ± 54 (41 ± 13)
Fe3+/Fe^{2+} (10 percent)	-2.00	243 ± 105 (58 ± 25)
As^{5+}/As^{3+}	-1.70	—
V^{5+}/V^{4+}	-1.90	172 ± 42 (41 ± 10)
U^{5+}/U^{4+}	-2.20	—
Cu^{1+}/Cu^{0}	-3.30	—
Cr^{3+}/Cr^{2+}	-3.40	243 ± 29 (58 ± 7)
Mo^{6+}/Mo^{5+}	-3.80	—
V^{4+}/V^{3+}	-4.00	155 ± 67 (37 ± 16)
Eu^{3+}/Eu^{2+}	-4.30	172 ± 59 (41 ± 14)
Ti^{4+}/Ti^{3+}	-5.00	147 ± 21 (35 ± 05)
Ni^{2+}/Ni^{0}	-5.30	343 ± 63 (82 ± 15)
Sn^{4+}/Sn^{2+}	-5.50	—
Se^{0}/Se^{2-}	-5.70	—
Co^{2+}/Co^{0}	-6.00	—
Fe^{2+}/Fe^{0}	-6.30	335 ± 42 (80 ±10)
Mo^{5+}/Mo^{0}	-15.80	—
S^{6+}/S^{2-}	-19.20	787 ± 0 (188 ± 0)

*Schreiber, H.D., and E.V. Sampson, Jr. A corrosion model for metals in molten slags. *Proceedings of the Corrosion of Materials by Molten Glass Symposium at the 98th Annual Meeting of the American Ceramic Society, Indianapolis, Indiana.* Ceramic Transactions Volume 78. G. Pecoraro, J.C. Marra, and J.T. Wenzel, eds. Westerville, OH: American Ceramic Society: 3–15. 1996.

†Schreiber, H.D., C.W. Schreiber, M.W. Riethmiller, and J.S. Downey. The effect of temperature of the redox constraints for the processing of high-level nuclear waste into a glass waste form. *Proceedings of the Materials Research Society Symposium.* Pittsburgh, PA: Materials Research Society 176: 419–426. 1990.

The equilibrium constant K(T, P) for Eq. (9-1) at a given temperature (T) and pressure (P) can be written as

$$K(T,P) = \frac{[M^{(m-n)+}]fO_2^{n/4}}{[M^{m+}][O^{2-}]^{n/2}} \tag{9-2}$$

where fO_2 is oxygen fugacity. The brackets indicate the activities of the species. For a given glass composition, the oxygen ion activity is constant and can be assumed as unity. Equation (9-2) can be reduced to

$$K(T,P) = \frac{[M^{(m-n)+}]}{[M^{m+}]} fO_2^{n/4} \tag{9-3}$$

Equation (9-3) can be rewritten as

$$-\log fO_2 = \frac{4}{n}\log\frac{[M^{(m-n)+}]}{[M^{m+}]} + E' \tag{9-4}$$

In Eq. (9-4), as long as M is sufficiently dilute the activity ratio can be replaced by the concentration ratio, can be easily measured. A plot of $-\log f(O_2)$ and $M^{(m-n)+}/M^{m+}$ concentration ratio will produce a straight line of slope $\frac{4}{n}$ and intercept E′. The intercept E′ can be related to the relative reduction potential for a given couple in a given glass. The more negative the value of E′, the easier for $M^{(m-n)+}$ to undergo oxidation to M^{m+}. These plots are referred to as electrochemical series diagrams.

If two or more redox components, such as Fe and Mn, are simultaneously present in the melt, the redox equilibrium is attained by internal redox reaction via electron exchange as shown in Eq. (9-5):

$$rM^{m+}_{(melt)} + nQ^{(q-r)+}_{(melt)} \longleftrightarrow rM^{(m-n)+}_{(melt)} + nQ^{q+}_{(melt)} \tag{9-5}$$

where r and n are the number of electrons transferred by multivalent elements M and Q, respectively, in the melt. The degree of two redox couples interaction can be estimated by their relative reduction potentials.

The relationship shown in Eq. (9-4) provides a convenient way of analyzing redox data and is widely used in nuclear waste vitrification processes to study redox behavior. Schreiber and Hockman (1987) developed an electrochemical series of redox couples in SRL–131 (simulated DWPF glass composition) and WV–205 (simulated WVDP glass composition) glasses. Figure 9-1 shows the relationship between $-\log f(O_2)$ and $M^{(m-n)+}/M^{m+}$ for various multivalent ions in a simulated glass composition. In figure 9-2, the same data are replotted as $-\log f(O_2)$ and percentage of redox couple in reduced states. The importance of redox in HLW vitrification is clearly evident from this figure. Key regions that determine the processing range for HLW slurries are marked. Even though Fe precipitation is not observed until the melt attains an oxygen fugacity of 10^{-9}, the upper limit for acceptable redox range is constrained to an oxygen fugacity of 10^{-7}. This oxygen fugacity corresponds to an Fe^{2+}/Fe^{3+} ratio of 0.5. This lowering of the upper limit for acceptable redox range is attributed to the presence of sulfur in the HLW slurries. Sulfur establishes a S^{6+}/S^{2-} redox couple

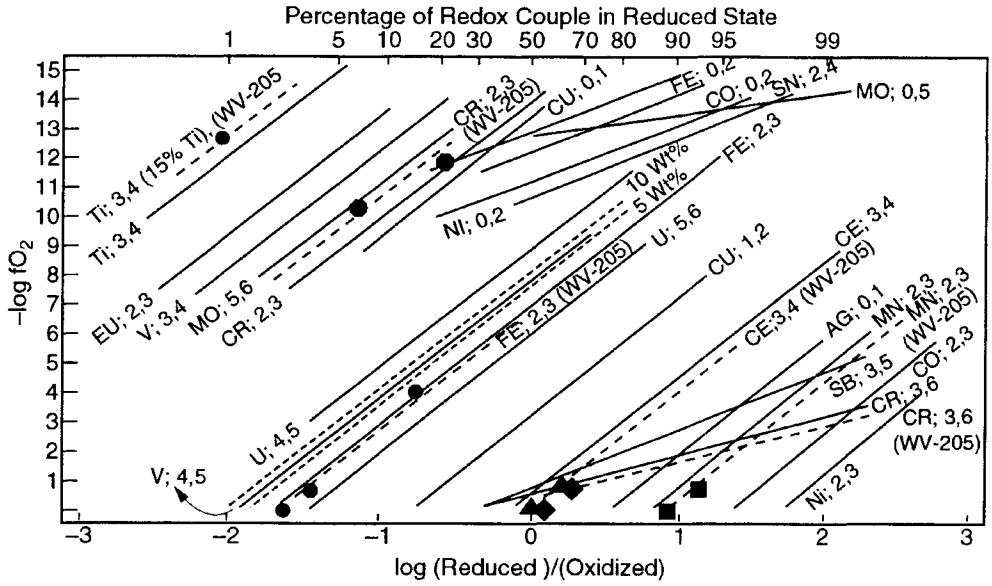

Figure 9-1. Redox chemistry in WV–205 melt at 1,150 °C superimposed on the SRL–131 melt system. Solid lines are SRL–131 at 1,150 °C (broken solid lines labeled 5 and 10 percent are for 5 wt% Fe and 10 wt% Fe in SRL–131); dashed lines with data points are WV–205 at 1,150 °C (Schreiber and Hockman, 1987).

in the system and results in the formation of electrically conductive sulfide phases such as FeS and NiS. These phases could electrically short the melter.

If the oxygen fugacity is less than 10^{-2}, redox couples such as Ce, Mn and Cr start influencing the redox response in the system causing formation of foam in the glass melt. Therefore, the redox response for processing nuclear waste glasses has been bounded between the oxygen fugacity of 10^{-4} and 10^{-7}, which corresponds to Fe^{2+}/Fe^{3+} ratios of 0.01 and 0.5.

From Eq. (9-1), redox equilibrium in glass melts depends on

- Oxygen ion activity
- Equilibrium constant [$K(T, P)$], which is a function of the Gibbs free energy and temperature
- Redox couple activity
- Oxygen [O_2] activity

9.2.1 Oxygen Ion Activity

Oxygen ion activity is also referred to as basicity of the glass melt and is controlled by the base composition of the glass. More oxide ions are produced in the melt as additional network modifiers such as alkali oxides are added into a system of network formers such as B_2O_3 and SiO_2. As the concentration of alkali oxides increases in the glass, the basicity of the glass increases. According to Eq. (9-1), if the equilibrium constant $K(T, P)$ is assumed to be independent of base composition and $f(O_2)$ is assumed to be constant, then higher oxygen ion activity, [O^{2-}], should favor a lower oxidation (reduced) state. However,

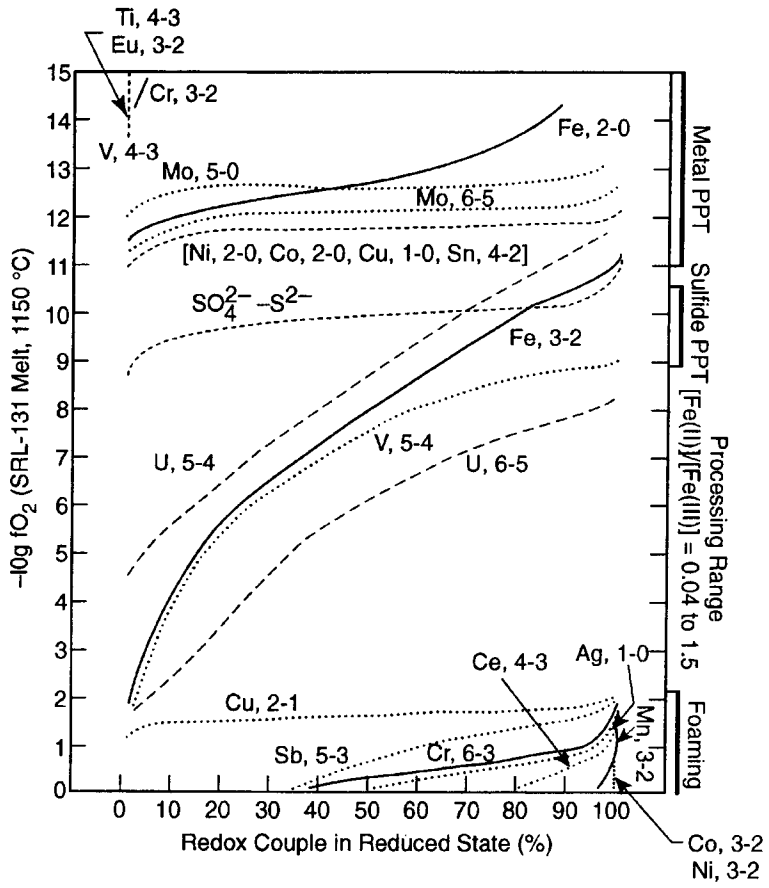

Figure 9-2. The distribution of redox states of various multivalent elements in SRL–131 containing model nuclear waste at 1,150 °C as a function of the imposed oxygen fugacity (Schreiber and Hockman, 1987)

experimental data (Paul and Douglas, 1965) for a series of alkali silicate melts ($M_2O \cdot xSiO_2$), where *M* refers to Li, Na or K ion, as shown in figure 9-3, indicate that, as the alkali content of the glass is increased, the melt becomes more oxidizing. Note that the redox ratio is plotted as an oxidized/reduced ratio instead of a reduced/oxidized ratio. This apparent paradox is resolved by recognizing the fact that the equilibrium constant *K*(T) is different for different glass compositions.

The structure of nuclear waste glass compositions is fairly complex, and the exact determination of oxygen ion activity is not feasible. The effect of composition on redox equilibrium for nuclear waste glasses can be summarized from the studies conducted by Schreiber and Hockman (1987) and Schreiber et al. (1986a,b; 1993). Figure 9-1 shows the effect of increasing Fe concentration in the SRL–131 glass and compares the redox behavior of WVDP and DWPF glasses. For a given redox ratio in the melt, the data indicate that, as the concentration of Fe increases in the glass, the melt becomes more reducing. Because the addition of Fe reduces the basicity of the melt, the results agree with the data shown in figure 9-3 for alkali silicate glasses. The redox data on WVDP WV–205 and DWPF SRL–131 glasses indicate similar redox behavior, despite differences in the compositions of the two glasses. Schreiber and Hockman (1987) have attributed similar redox behavior to probable counterbalancing of oxygen ion activity by the various elements in the glass.

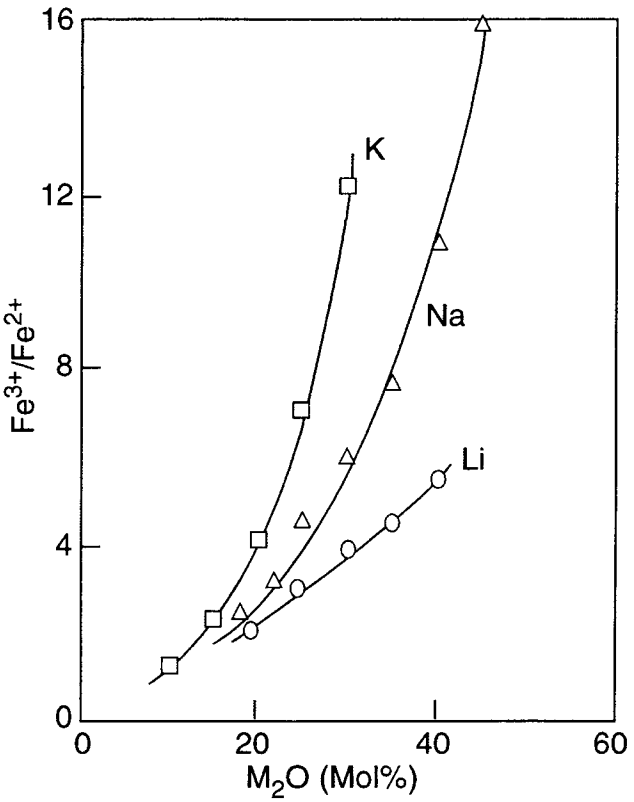

Figure 9-3. Effect of composition of alkali (M) silicate melts on the concentration ratio Fe^{3+}/Fe^{2+} for melts equilibrated with air at atmospheric pressure and 1,400 °C; total Fe in the melt is less than 0.5 percent (Paul and Douglas, 1965)

9.2.2 Effect of Temperature on Redox Equilibrium

The redox equilibrium in glass generally moves toward the reduced side with increasing temperature. The temperature dependence of redox equilibrium in a melt at constant oxygen fugacity can be described by approximation of the Clausius-Clapeyron equation (Schreiber et al., 1986a)

$$\log\frac{[M^{(m-n)+}]}{[M^{m+}]} = \frac{\Delta H_o}{2.303\mathrm{RT}} + B \qquad (9\text{-}6)$$

where ΔH_o is related to the enthalpy change for the reduction reaction in Eq. (9-1). Equation (9-6) is only an approximation because the equilibrium constant is replaced by the redox ratio, and oxygen ion activity is included in constant B and is assumed to be temperature independent.

Schreiber et al. (1986a, b; 1990, 1993) studied the effect of temperature on the redox equilibrium for the DWPF and WVDP glass compositions. Figure 9-4 shows a plot of the redox ratio (Fe^{2+}/Fe^{3+}) versus 1/T for the SRS–131 glass containing 1 and 10 percent Fe. As the temperature increases, the redox equilibria shift to a more reducing state. Figure 9-4 also indicates that, for a given oxygen fugacity, the enthalpy of reduction is endothermic, with ΔH = 189 kJ/mol (45 kcal/mol) and 306 kJ/mol (73 kcal/mol) for 10 percent Fe_2O_3 and 1 percent Fe_2O_3, respectively, in glass. Note that the enthalpy of reduction for 10 percent Fe_2O_3 is lower

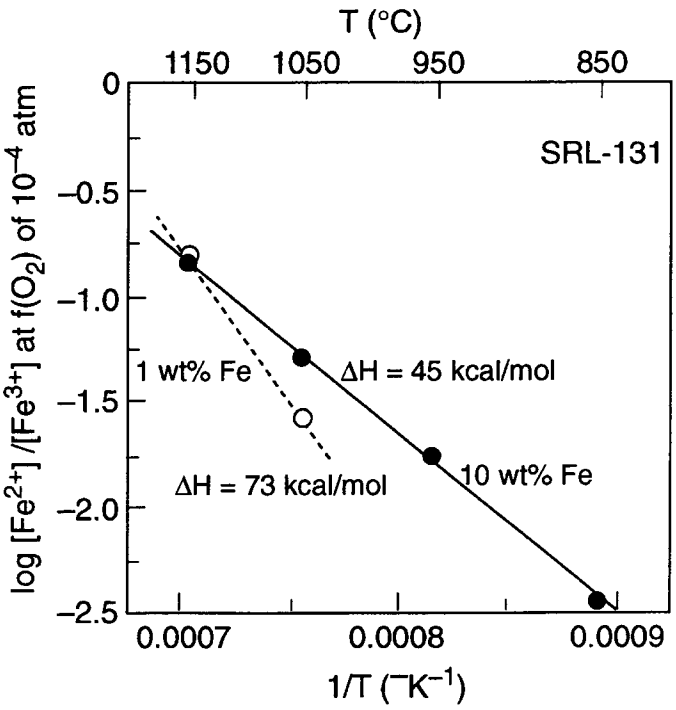

Figure 9-4. The temperature dependence of the Fe^{3+}–Fe^{2+} equilibrium in melt composition (SRL–131) (Schreiber, 1986).

compared to the enthalpy of reduction for 1 percent Fe_2O_3 and is attributed to the basicity of the melt. Average enthalpy of reduction for Fe^{3+} to Fe^{2} and $Fe^{2+}$to Fe^{0} reduction, as shown in table 9-1, for 10 percent Fe_2O_3 in SRL–131 glass is 244 kJ/mol (58 kcal/mol) and 336 kJ/mol (80 kcal/mol), respectively. The enthalpy of reduction for other redox couples, as shown in table 9-1, ranges from 42 to 787 kJ/mol (Schreiber, 1990).

Figure 9-5 shows the effect of increasing temperature on the redox equilibrium for the WVDP glasses (Schreiber et al., 1993). The straight lines relating to $-\log f(O_2)$ and Fe^{2+}/Fe^{3+} and $-\log f(O_2)$ and Fe^{0}/Fe^{2+} are the best fit lines with theoretical slopes of 4 and 2, respectively, as shown by Eq. (9-4).

For a given oxygen fugacity, the data indicate that as the temperature increases, the melt becomes more reducing. In addition, when compared with the DWPF redox data on SRL–131 glass shown in table 9-1, the redox relationships are similar. The relative reduction potentials, E′ in Eq. (9-4), were −2.0 and −6.5 for Fe^{2+}/Fe^{3+} and Fe^{0}/Fe^{2+}, respectively. In addition, the enthalpies of reduction were 150 and 290 kJ/mol (36 and 69 kcal/mol) for the reduction of Fe^{3+} to Fe^{2+} and Fe^{2+} to Fe^{0}, respectively. Slight differences in the enthalpy of reduction between DWPF and WVDP glass melt are attributed to compositional differences.

9.2.3 Effect of Redox Couple Activity

The redox equilibrium established by a multivalent element remains constant, as long as the concentration of the multivalent element dissolved in the glass melt is dilute. Schreiber (1986) has noted that the redox equilibrium is invariant provided the concentration of the multivalent element does not exceed 2–4 wt% in the melt. If the multivalent element becomes a major component of the glass melt, the multivalent element also contributes to the changes in the redox equilibrium because of the changes in the melt basicity.

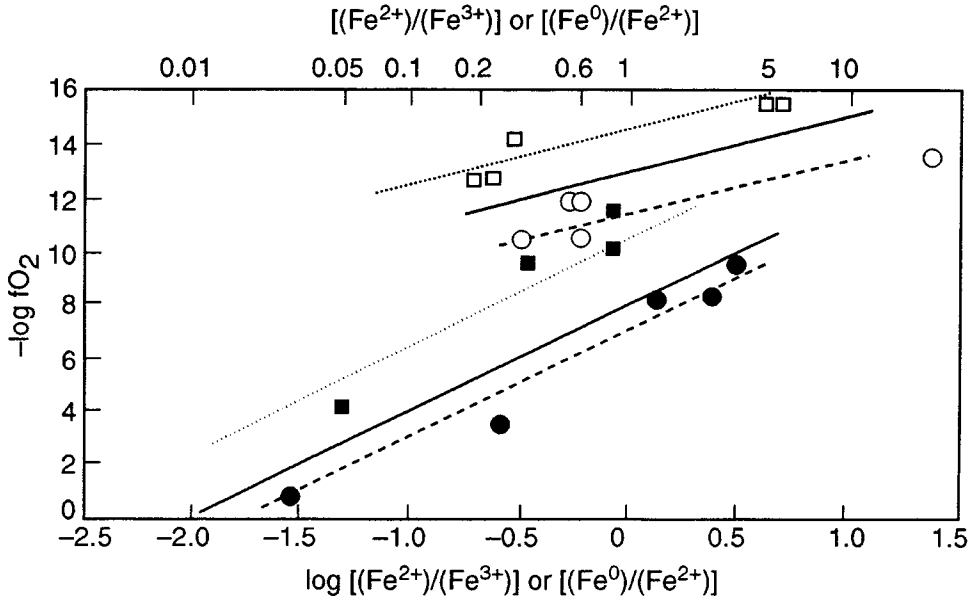

Figure 9-5. The dependence of the redox state of iron on both the imposed oxygen fugacity and the melt temperature in West Valley glass. Circles represent results obtained at 1,250 °C, while squares represent those at 1,050 °C. Solid symbols are the $[Fe^{2+}]/Fe^{3+}]$ ratios, and open symbols are the $[Fe^{0}]/Fe^{2+}]$ ratios. Redox relations at 1,250, 1,150, and 1,050 °C are shown by dashed, solid, and dotted lines, respectively (Schreiber et al., 1993).

Melt basicity, which is a function of oxygen ion activity, increases as the melt becomes more oxidizing. In most of the borosilicate-based nuclear waste glasses, concentration of Fe is sufficient to be considered a major element in the melt. The effect of increasing Fe concentration is clearly shown in figures 9-1 and 9-4 for the SRS–131 glass composition.

As indicated in Eq. (9-5), if two or more multivalent elements are simultaneously present in a melt, the redox couple may interact by internal electron exchange. Schreiber et al. (1993) studied the effect of other redox couples on Fe^{2+}/Fe^{3+} in the WVDP glass melt. Multivalent oxides present the WVDP HLW include Fe (12 wt% Fe_2O_3), Ni (0.25 wt% NiO), Mn (1 wt% MnO_2), Ce (0.16 wt% CeO_2), Cr (0.14 wt% Cr_2O_3) and Cu (0.06 wt% CuO). Individual experimental studies with 1 wt% Cr_2O_3, 1 wt% NiO, 1 wt% CuO, 1 wt% CeO_2, and 4 wt% MnO_2 additions in the WVDP glass melt showed that none of the added metals affected the redox limits established by Fe^{2+}/Fe^{3+} between 0.01 and 0.5. However, the DWPF glass melts that contain similar redox couples as WVDP glasses showed a significant Cu^0 precipitation in glass melts containing more than 0.7 wt % CuO within their redox processing range (Ramsey et al., 1994).

9.2.4 Oxygen Activity in Glass Melts

The oxygen activity, $[O_2]$, in the glass melt depends on the melter atmosphere or the oxidizing and reducing agents present in the feed materials. For simplicity, the activity of oxygen in the melter atmosphere is generally replaced by the partial pressure of oxygen. This assumption is permissible only at low pressures. At high pressures, deviations could be significant, especially in cases where the gas reacts with the melt.

In redox reactions, even though molecular oxygen is present in the gas above the melt, only molecular oxygen dissolved within the melt can react with multivalent element *M*. The dissolved oxygen in the melt establishes an equilibrium with the gaseous oxygen. Redox equilibrium is never completely achieved in melters. The participation of molecular oxygen can be shown by separation of Eq. (9-1) into its half reactions

$$M^{m+}_{(\text{melt})} + ne^- \longleftrightarrow M^{(m-n)+}_{(\text{melt})} \tag{9-7a}$$

$$\frac{n}{2}O^{2-}_{(\text{melt})} \longleftrightarrow \frac{n}{4}O_{2(\text{melt}\rightarrow\text{gas})} + ne^- \tag{9-7b}$$

$$[O_{2(\text{melt})}] = kf(O_2) \tag{9-8}$$

where brackets indicate the activities of the species. The $[O_{2(\text{melt})}]$ is the oxygen activity in the glass melt. The Henry's Law constant, *k*, is dependent on the melt composition and temperature and is expected to be obeyed for relatively low concentrations of dissolved oxygen in the melts. If, in a melter containing multivalent elements, melt conditions such as temperature or atmosphere (oxygen fugacity) are changed, the system, in accordance with LeChatelier's principle, will readjust to achieve a new redox equilibrium. Such readjustment on perturbation in the melt, however, does not happen instantaneously because molecular oxygen has to diffuse into or out of the melt to attain new equilibrium. Because oxygen is a major component of the HLW glass melts, its kinetic behavior could control the final redox equilibrium in the melt or determine the time required to reach steady state.

HLW melter feed, which consists of nitrates, nitrites, sulfates, carbonates, and hydroxides, and other organic components such as sugar or formic acid, undergoes chemical decomposition reactions at different temperatures. The decomposition reactions start as low as 100 °C and continue up to 1,000 °C. Ryan (1994) has tabulated potential reactions for major components that could occur in the melter. As these decomposition reactions occur in the cold cap (a crusty region on the surface of the melt where most of the decomposition reactions occur), reaction products consisting of metal oxides move into the glass melt while gases are released at the surface of the melt. This complex mixture of reaction gases and in-flow of air from melter in-leakage determines the partial pressure of oxygen in the melter. Depending on the size and type of the melter, the time required to attain steady-state redox could range from a few hours to days.

Because the HLW feeds typically contain significant concentrations of oxidizing agents such as nitrates and nitrites, the selection of the proper reducing agent is important. The selection of the type and amount of reducing agent depends not only on its decomposition temperature but also on the decomposition temperature of oxidizing agents. The effectiveness of the reducing agent could be compromised if the difference between decomposition temperatures is large. Starch, sugar, formates, urea, or carbon black could react differently in the same feed. Table 9-2 shows the effect of various reducing agents on the Fe^{2+}/Fe^{3+} ratio (Bickford and Diemer, 1986).

Table 9-2. Effect of various redox compounds in closed crucible tests (Bickford and Diemer, 1986)

Sample	Fe^{2+}/Fe^{3+}	Log (pO_2) at 1,150 °C
90 SRL165 *frit* +10Fe_2O_3 +		
4 NaCOOH + 1 $Ni(NO_3)2.6H_2O$	0.06	-3.20
4 NaCOOH + 1 $NaNO_3$	0.09	-3.72
4 NaCOOH + 2 MnO_2	0.18	-5.02
0.2 C	0.28	-5.79
1.0 phenyl boric acid (PBA)	0.37	-6.29
4 NaCOOH + 1 $Mn(COOH)_2$ + 1 MnO_2 + 1 Ni (NO_3) 2.6 H_2O	0.42	-6.50
4 $Mn(COOH)_2$	0.51	-6.83
2 NaCOOH	0.54	-6.93
5 $Fe(COOH)_3$	0.70	-7.38
6 $Mn(COOH)_2$	0.71	-7.41
2 PBA	1.11	-8.18
5 NaCOOH	1.40	-8.58
1 C	1.45	-8.65
5 PBA + 1 $CaCO_3$	2.00	-9.20
5 PBA (soot in crucible after test)	100.00	-16.00

9.3 REDOX STRATEGY AT HIGH-LEVEL RADIOACTIVE WASTE VITRIFICATION PLANTS

The presence of multiple redox couples as shown in table 9-1, along with a number of reducing and oxidizing agents in the HLW, makes redox control in a HLW melter complex and challenging. Even though most of the HLW stored at West Valley, Savannah River, and Hanford sites originated from the reprocessing of fuel assemblies by the plutonium uranium extraction (PUREX) process, their waste characteristics are different because the fuel assemblies reprocessed at each site were different. While it is accepted by the scientific community that redox, as measured by Fe^{2+}/Fe^{3+}, should be controlled between 0.01 and 1.00 to avoid catastrophic melter failure, a much narrower bound (e.g., between 0.01 and 0.5) is used as processing limits. Applicability of these limits and their relationship to HLW composition and processing characteristics

are discussed in the following sections for WVDP and DWPF. These redox control strategies were developed based on extensive laboratory, pilot, and full-scale studies.

9.3.1 West Valley Demonstration Project Redox Control Strategy

The development of a redox control strategy at the WVDP was divided into two parts. First the redox couples that influence the redox response in a given glass composition were determined and second, the HLW feed variables that influence the redox response of the redox couple were measured.

As discussed in the previous section, Schreiber et al. (1993) systematically studied the redox response in simulated WVDP glasses for the most dominant redox couples and determined that the redox response in the WVDP HLW was bounded by Fe-redox couple. Multivalent oxides present in the WVDP HLW include Fe (12 percent Fe_2O_3), Ni (0.25 wt% NiO), Mn (1 wt% MnO_2), Ce (0.16 wt% CeO_2), Cr (0.14 wt % Cr_2O_3), and Cu (0.06 wt% CuO).

At WVDP, the HLW transferred to the vitrification cell was a homogeneous mixture of washed PUREX sludge, thorium extraction (THOREX) process waste, and Cs-137-loaded zeolite (Jain and Barnes, 1997). Even in this homogeneous HLW, forecasting the redox behavior based on the HLW feed characteristics was complex. Chemical reactions that contribute significantly to the redox response in the melter include decomposition of nitrates, nitrites, hydroxides, sulfates, phosphates, and sugar, and the evaporation of water. The concentration of sulfate, which could interfere in the redox response, was reduced to a concentration below its solubility limit in the HLW.

Since the beginning of nonradioactive operations in 1984, significant resources were devoted to the development of a redox model to forecast redox behavior in the melter. Parallel studies using controlled laboratory tests, pilot-scale melter runs, and full-scale melter runs were conducted. Jain (1993) conducted laboratory-scale studies on simulated HLW feeds to evaluate the effect of oxidizing and reducing agents on redox behavior. A laboratory-scale direct slurry redox test was developed to study the redox behavior. In this test, a known amount of liquid slurry in a covered quartz crucible is placed in a furnace at 1,150 °C for 1 hr. After 1 hr, the crucible is removed, and the glass sample is analyzed for Fe^{2+}/Fe^{3+}. Figure 9-6 shows the effect of adding sugar on the redox ratio. As expected, the addition of sugar increased the Fe^{2+}/Fe^{3+} ratio, but Fe^{2+}/Fe^{3+} stabilized at 1.0. No further increase in Fe^{2+}/Fe^{3+} was observed with additional increases in sugar. Visual examination of the sample revealed the formation of metal nuggets in the glass. This observation established an upper limit for sugar in the feed. In addition, the study examined the effect of dilution (addition of water) on the redox behavior. As water was added to the slurry, more oxidizing conditions were observed in the system. Data are shown in figure 9-7. This study provided information for conducting a series of well-defined tests on pilot-scale and full-scale melters.

Pilot-scale and full-scale melter runs, using simulated feed composition based on the preliminary estimates of the HLW chemical composition, were conducted, and an empirical relationship between oxidizing and reducing components was developed. This relationship was expressed as

$$IFO = \frac{NO_3(1 - TS)}{TOC} \qquad (9\text{-}9)$$

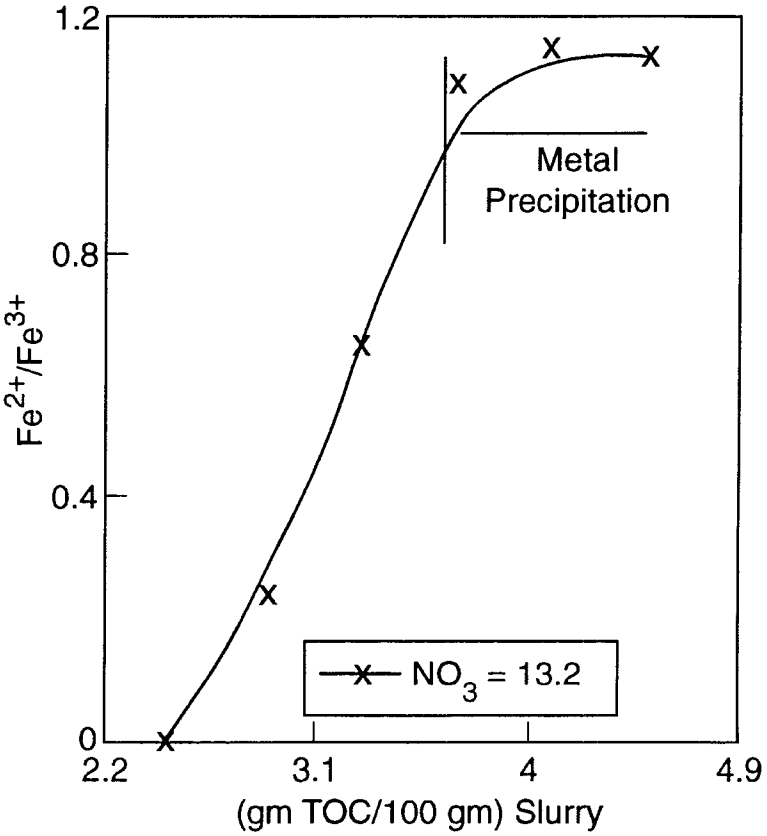

Figure 9-6. Effect of excess total organic carbon on the Fe^{2+}/Fe^{3+} ratio at a fixed NO_3 content (Jain, 1993)

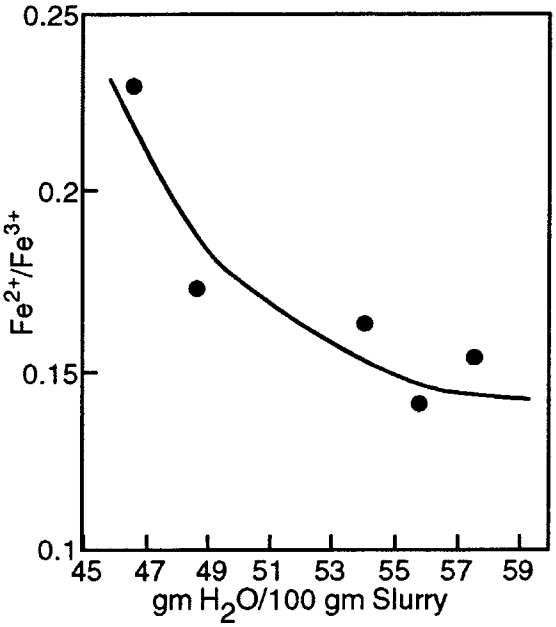

Figure 9-7. Effect of H2O on the Fe^{2+}/Fe^{3+} at a fixed total organic carbon/NO_3 ratio (Jain, 1993)

where Index of Feed Oxidation (IFO) is a measure of feed oxidation, NO_3 is the total nitrate concentration, TS is the fraction of total solids in the feed, and total organic carbon (TOC) is the total organic carbon concentration. The terms TOC and $NO_3(1 - TS)$ represent the net reduction and oxidation potential of the feed, respectively. Note that nitrites were not included in these studies as variables because a significant quantity of nitrites was not expected. Figure 9-8 shows the Fe^{2+}/Fe^{3+} ratio as a function of IFO. Data shown in the figure were collected using scaled vitrification system (SVS)-I and slurry-fed ceramic melter runs (Bowan, 1990). This relationship allowed the amount of sucrose needed to attain a target IFO for known concentrations of NO_3 and TS in the feed to be estimated. For a given simulated WVDP HLW, this forecasting method defined the IFO operating range to be between 1.6 and 2.3, which corresponds to an Fe^{2+}/Fe^{3+} ratio between 0.1 and 0.5.

Prior to beginning radioactive operations in July 1996, additional pilot-scale tests were conducted using SVS–III. The purpose was to reexamine the redox behavior based on new information available on the HLW composition. The new composition contained a significant amount of nitrites in the feed, reflecting the decision made to add sodium nitrite as a tank waste corrosion inhibitor. Figure 9-9 shows the revised redox forecasting curve superimposed on the original curve obtained using feeds without nitrites in the full-scale melter. To account for the nitrites in the feed, total nitrites were converted on a molar basis to an equivalent amount of nitrates and added to the total nitrates. The results indicate that the redox state response to IFO changes was more rapid in the presence of nitrites in the HLW. To avoid this rapid redox response in the melter, a decision was made to process the HLW at IFO > 2.7. Given the uncertainties in the chemical analysis, the target IFO of 3.0 was used to estimate the amount of sucrose required to process the feed and ensure that the Fe^{2+}/Fe^{3+} ratio in the melter remained between 0.01 and 0.20. The upper limit of Fe^{2+}/Fe^{3+} of 0.5 was reduced to 0.2 to account for the effect of nitrites, which cause a sharp increase in Fe^{2+}/Fe^{3+} ratio beyond 0.2.

9.3.2 Defense Waste Processing Facility Redox Control Strategy

Similar to WVDP, the redox strategy at the DWPF evolved as the process flowsheet developed and matured. DWPF HLW contains a high concentration of transition metals such as Fe, Ni, and Mn. Prior to adoption of the precipitate hydrolysis process, precipitation of Ni_3S_2 established the upper operating bound for redox control (Ramsey et al., 1991). The HLW slurry consists of an insoluble portion of the waste, borosilicate glass frit, and precipitate hydrolysis aqueous (PHA) product. PHA contains the radionuclides from the soluble salt waste. Before it is introduced into the melter, the feed has approximately 45 percent solids. The feed contains formate, nitrate, and phenol anions that influence the redox behavior in the melter. An extensive study with laboratory and pilot-scale testing using the scale glass melter (SGM) and integrated DWPF melter system (IDMS) was conducted to model the redox response of the feed and establish the redox relationship between laboratory tests and melter glass. Figure 9-10 shows the correlation between melter feed composition and glass redox. The molar formate minus nitrate (F-N) content is plotted against $Fe^{2+}/Fe_{(total)}$. Also plotted are the data collected from SGM and IDMS runs. Results indicate that redox can be accurately predicted from the F-N value. Note that the redox data plotted here are shown as $Fe^{2+}/Fe_{(total)}$. This nomenclature has been adopted by the DWPF for representing the redox state, and no attempt was made to change the data for consistency purposes between WVDP and DWPF. Figure 9-11 shows the crystalline phases formed in the glass samples as functions of redox and feed composition. For F-N less than 1.2, no Ni_3S_2 is observed in the glass.

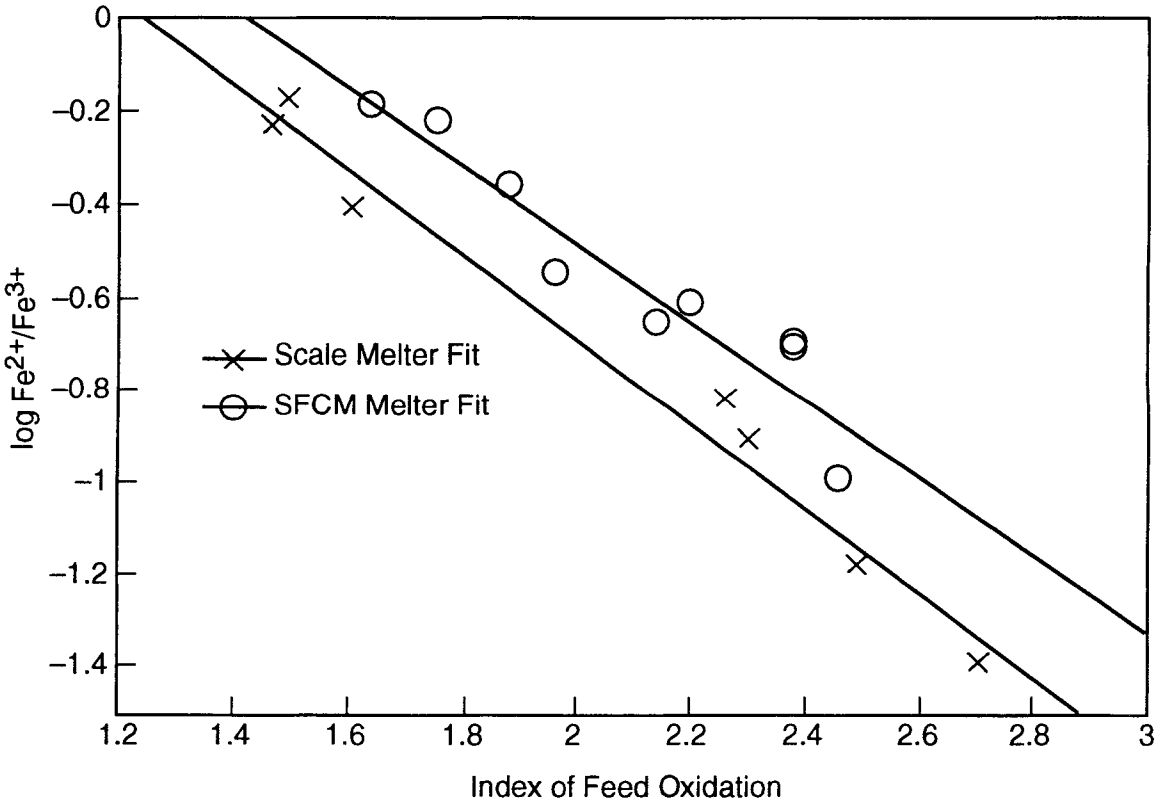

Figure 9-8. The dependence of log Fe^{2+}/Fe^{3+} on the index of feed oxidation: a comparison between slurry fed ceramic melter and pilot-scale melters (Bowan, 1990)

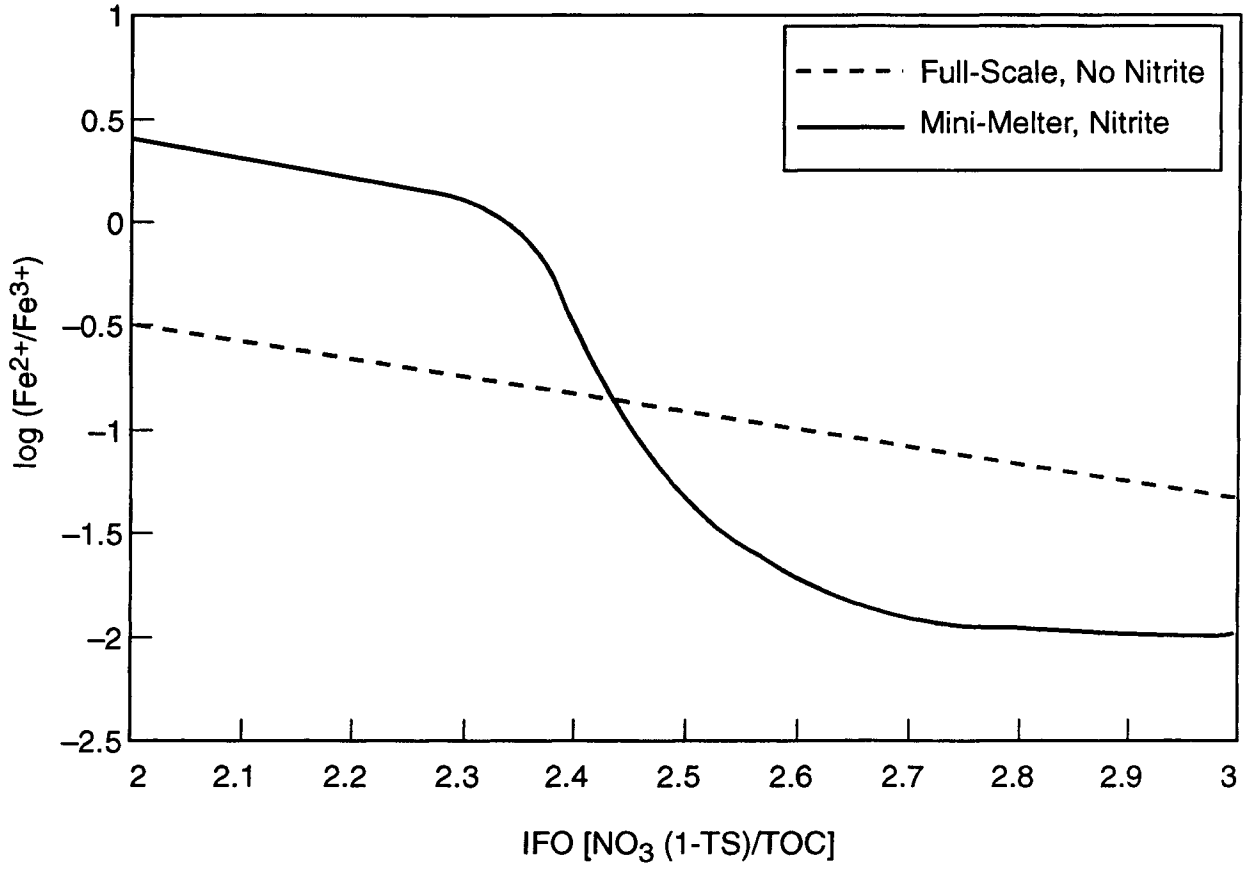

Figure 9-9. West Valley Demonstration Project redox forecasting model revised after addition of nitrites (Barnes and Jain, 1996)

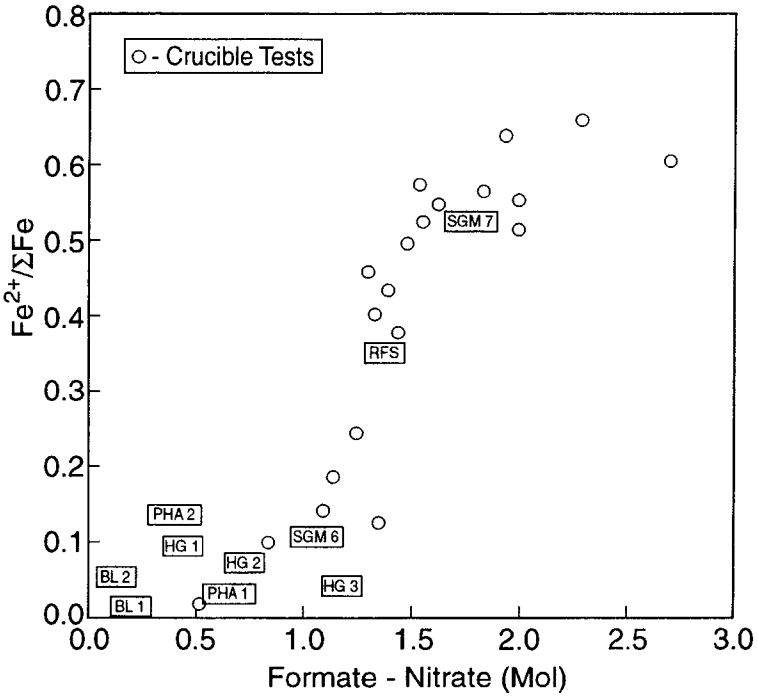

Figure 9-10. Comparison of scale glass melter and integrated Defense Waste Processing Facility melter system campaigns with crucible redox data (Ramsey et al., 1991)

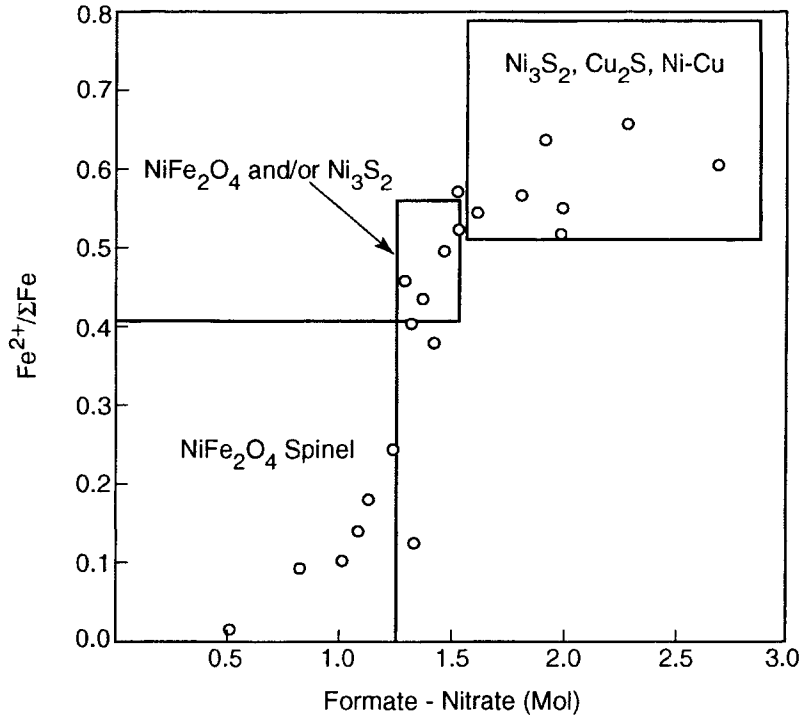

Figure 9-11. Comparison of crystalline phases with slurry (F-N) and glass redox (Ramsey et al., 1991)

As the process matured, DWPF determined that the expected radiation doses from the Cs-137 in the precipitate required additional copper formate catalyst than initially anticipated for complete PHA formation (Schumacker and Ramsey, 1994). This increase in copper concentration in the melter feed increases the potential for precipitation of metallic copper phases in the melter, which could accumulate over a period of time and interfere with the joule heating. Anticipated levels of elemental copper in glass are 0.4 to 0.5 wt%. Figure 9-12 shows a plot of Cu concentration versus F-N. Open circles indicate glasses with no precipitated Cu, while solid circles indicate glasses with precipitated Cu. Boundary lines shown in the figure represents the limits for maintaining Cu as a soluble species in glass. Based on this work, the following limits were established:

- If Cu $\leq$ 0.45 wt%, F-N should not exceed 1.4
- If Cu is between 0.45 and 0.70 wt%, F-N should be $\leq$ 0.5
- Cu should not exceed 0.7 wt%

Because of Cu in the HLW, DWPF is forced to operate the melter in a fairly oxidizing range ($Fe^{2+}/Fe_{(total)} \leq 0.03$). Almost continuous formation of foam in the melter has resulted.

9.4 REDOX ISSUES FOR TANK WASTE REMEDIATION SYSTEM

The flowsheet proposed by BNFL Inc. uses sugar as a reducing agent for controlling redox in the LAW and HLW melters. Separate redox control strategies are needed for LAW and HLW feeds because the characteristics of the two feed streams are quite different. The LAW stream is stripped of almost all multivalent elements and radioactive species, but Fe is added as a glass former. The HLW stream has significant concentration of multivalent elements such as Fe, Mn, Ni, and Cr and has most of the radioactive species. Additional complexity in developing a redox strategy is imposed by the variability in the feed composition at Hanford. Four waste streams of different compositions will be processed and separated into HLW and LAW streams, requiring a different redox control strategy for each waste stream. If waste streams are homogeneously mixed prior to feeding to the melter, one redox strategy could be sufficient. As indicated in the previous section, development of a redox control strategy is a complex process. Attention needs to be focused on all potential reducing and oxidizing agents as well as multivalent elements irrespective of their concentrations. Lessons learned from the development of the redox control strategy at WVDP and DWPF could be beneficial in developing a suitable redox strategy for Hanford wastes. For example, minor additions of material such as nitrite in WVDP HLW or Cu in DWPF HLW could severely restrict the redox operating range.

Recent advances in the development of *in-situ* redox measurement techniques could further facilitate redox measurement in the melter. For example, a redox probe developed by Kuhnreich & Meixner (Korwin and Pye,1995) was tested at WVDP in an SVS–III and used by several commercial glass manufacturers (Muller-Simon and Mergler, 1988). The utility of such probes is limited because they cannot forecast redox and determine the amount of reductant needed to attain target redox in the melter. The redox probe, however, is a useful tool to provide a check on melter redox condition and to allow a prompt shutdown of a melter in case the redox response exceeds the operating range. Thus, the probe should be considered a monitoring sensor.

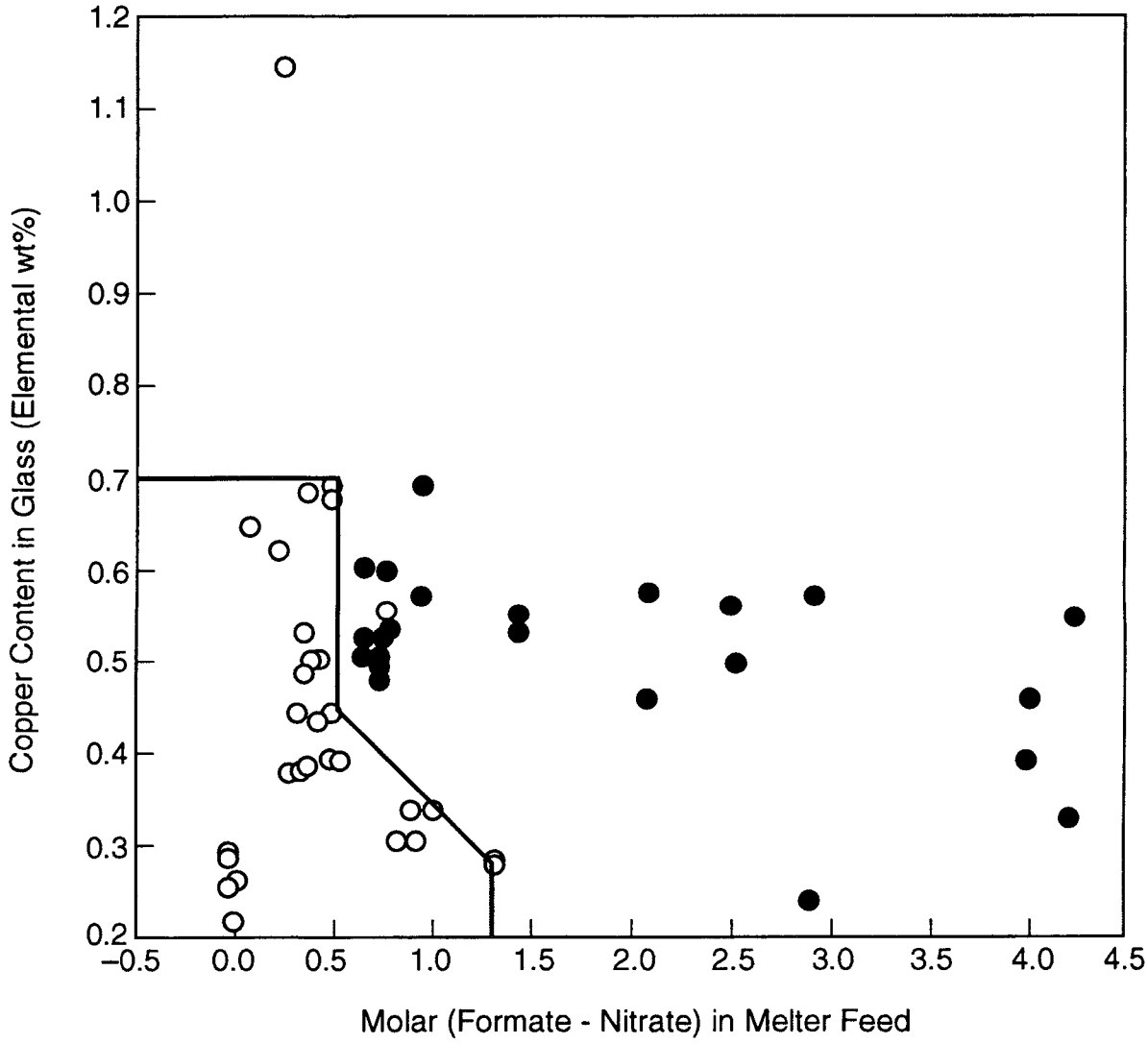

Figure 9-12. Effect of feed chemistry and copper content on the likelihood of formation of insoluble copper precipitates during vitrification (Ramsey et al., 1994)

9.5 SUMMARY

The redox state in a melter is probably the most important process control parameter. A redox response within a specified range is necessary to avoid process problems that eventually could lead to permanent melter damage. The operating range for redox in a melter depends on the amount and type of multivalent elements present in the HLW. Because Fe is abundant in most wastes and oxidation states can be easily measured, the redox response in waste vitrification systems is determined by the Fe^{2+}/Fe^{3+} ratio. However, the influence of some minor components in the waste, such as Cu and Mn, cannot be ignored. A glass melt is defined as extremely reducing if the Fe^{2+}/Fe^{3+} ratio is greater than 1. Under such conditions, sufficient conductive metals and metal sulfides could accumulate and short-circuit the melter. If the Fe^{2+}/Fe^{3+} ratio is less than 0.01, a glass melt is defined as extremely oxidizing. Under extremely oxidizing conditions, foaming is observed in the melter. Foam creates an insulating layer of gas bubbles between the cold cap and the melt, disrupting the thermal gradients in the melter. If controlled at its onset, foaming typically slows the glass production rate and is not an issue. If foaming is not controlled, however, conditions can arise that could lead to melter shutdown. Even though Fe precipitation is not observed until the melt attains an oxygen fugacity of 10^{-9} (Fe^{2+}/Fe^{3+} ratio of 1), the upper limit for acceptable redox range is limited to an oxygen fugacity of 10^{-7}. This value corresponds to an Fe^{2+}/Fe^{3+} ratio of 0.5. This lowering of the upper limit for an acceptable redox range is attributed to the presence of sulfur in the HLW slurries, which establishes a S^{6+}/S^{2-} redox couple in the system and results in the formation of electrically conductive sulfide phases such as FeS and NiS. These phases could electrically short-circuit the melter. If the oxygen fugacity is less than 10^{-2}, redox couples such as Ce, Mn, and Cr begin to influence the redox response in the system causing formation of foam in the glass melt. Therefore, the redox response for processing nuclear waste glasses has been bounded between the oxygen fugacity of 10^{-4} and 10^{-7}, which corresponds to Fe^{2+}/Fe^{3+} ratios of 0.01 and 0.5. Redox equilibrium in glass melts depends on the oxygen ion activity in the melt, the equilibrium constant [K(T)], which is a function of the Gibbs free energy and temperature, the redox couple activity; and the oxygen activity [O_2].

The presence of multiple redox couples, along with a number of reducing and oxidizing agents in the HLW, makes redox forecasting and control in a HLW melter complex and challenging. Because the HLW feeds typically contain significant concentrations of oxidizing agents such as nitrates and nitrites, the selection of a proper reducing agent is important. The selection of the type and amount of reducing agent depends not only on its decomposition temperature, but also on the decomposition temperature of oxidizing agents. The effectiveness of the reducing agent could be compromised if the decomposition temperature differential is large. Starch, sugar, formates, urea, or carbon black could react differently in the same feed.

Both WVDP and DWPF have invested significant resources in understanding and developing redox forecasting and control strategy, and the lessons learned could be beneficial in developing a suitable redox strategy for Hanford wastes. For example, minor additions such as nitrite in WVDP HLW or Cu in DWPF HLW could severely restrict the redox operating range

9.6 REFERENCES

Barnes, S.M., and V. Jain. Vitrification systems testing to support radioactive glass production at the West Valley Demonstration Project. *Proceeding of the Waste Management '96 Symposia*. Tucson, AZ: Waste Management Symposia Inc. 1996.

Bickford, D.F., and R.B. Diemer, Jr. Redox control of electric melters with complex feed compositions. *Journal of Non-Crystalline Solids* 84: 276–284. 1986.

Bowan, B.W. *Redox forecasting correlation developed using a new one-tenth area scale test melter for vitrifying simulated West Valley high-level radioactive wastes.* Master's thesis, Alfred University, Alfred, NY. 1990.

Jain, V. Redox forecasting in the West Valley vitrification system. *Proceedings of the Third International Conference on Advances in Fusion and Processing of Glass, New Orleans, Louisiana, June 10–12, 1992.* Ceramic Transactions Volume 29. A.K. Varshneya, D.F. Bickford, and P.P. Bihuniak, eds. Westerville, OH: American Ceramic Society: 523–533. 1993.

Jain, V., and S.M. Barnes. Radioactive waste glass production at the West Valley Demonstration Project. *Proceedings of the Waste Management '97 Symposia.* Tucson, AZ: Waste Management Symposia Inc. 1997.

Korwin, D.M., and L.D. Pye. *Milestone #3 Final Report on the Oxygen Activity Measurement of Reference 6 Glass.* Alfred, NY: Alfred University. 1995.

Muller-Simon, H., and K.W. Mergler. Electrochemical measurements of oxygen activity of glass melts in glass melting furnaces. *Glastech Ber* 61(10): 293–299. 1988.

Paul, A., and R.W. Douglas. Ferrous-ferric equilibrium in binary alkali silicate glasses. *Physics and Chemistry of Glasses* 6(6): 207–212. 1965.

Ramsey, W.G., C.M. Jantzen, and D.F. Bickford. Redox analyses of SRS melter feed slurry: Interactions between nitrate, formate and phenol based dopants. *Proceedings of the Fifth International Symposium on Nuclear Waste Management IV. 93rd Annual Meeting of the American Ceramic Society, Cincinnati, Ohio, April 29–May 3, 1991.* Ceramic Transactions Volume 23. G.C. Wicks, D.F. Bickford, and L.R. Bunnell, eds. Westerville, OH: American Ceramic Society: 259–265. 1991.

Ramsey, W.G., N.M. Askew, and R.F. Schumacher. *Prediction of Copper Precipitation in the DWPF Melter from the Melter Feed Formate and Nitrate Content.* WSRC–TR–92–385. Revision 0. Aiken, SC: Westinghouse Savannah River Company. 1994.

Ryan, J.L. *Redox Reactions and Foaming in Nuclear Waste Glass Melting.* PVTD–C94–03.02K. Richland, WA: Pacific Northwest National Laboratory. 1994.

Schreiber, H.D. Redox processes in glass-forming melts. *Journal of Non-Crystalline Solids* 84: 129–141. 1986.

Schreiber, H.D., and A.L. Hockman. Redox chemistry in candidate glasses for nuclear waste immobilization. *Journal of the American Ceramic Society* 70(8): 591–594. 1987.

Schreiber, H.D., and E.V. Sampson, Jr. A corrosion model for metals in molten slags. *Proceedings of the Corrosion of Materials by Molten Glass Symposium. 98th Annual Meeting of the American Ceramic Society, Indianapolis, Indiana.* Ceramic Transactions Volume 78. G. Pecoraro, J.C. Marra, and J.T. Wenzel, eds. Westerville, OH: American Ceramic Society: 3–15. 1996.

Schreiber, H.D., S.J. Kozak, R.C. Merkel, G.B. Balazs, and P.W. Jones, Jr. Redox equilibria and kinetics of iron in a borosilicate melt. *Journal of Non-Crystalline Solids* 84: 186–195. 1986a.

Schreiber, H.D., S.J. Kozak, A.L. Fritchman, D.S. Goldman, and H.A. Schaeffer. Redox kinetics and oxygen diffusion in a borosilicate melt. *Physics and Chemistry of Glasses* 27(4): 152–177. 1986b.

Schreiber, H.D., C.W. Schreiber, M.W. Riethmiller, and J.S. Downey. The effect of temperature of the redox constraints for the processing of high-level nuclear waste into a glass waste form. *Symposium Proceedings for the Materials Research Society.* Symposium Proceedings 176. Pittsburgh, PA: Materials Research Society: 87–94. 1990.

Schreiber, H.D., C.W. Schreiber, and C.C. Ward. Redox systematics in model glass compositions from West Valley. *Proceedings for the Materials Research Society Symposium.* Symposium Proceedings 294. Pittsburgh, PA: Materials Research Society: 87–94. 1993.

Schumaker, R.F. and W.G. Ramsey. Conditions for precipitation of copper phases in DWPF glass. *Proceedings of the Symposium on Environmental and Waste Management Issues in the Ceramic Industry, presented at the 95th Annual Meeting of the American Ceramic Society, Cincinnati, Ohio, April 18–22, 1993.* Ceramic Transactions Volume 39. G.B. Mellinger, ed. Westerville, OH: American Ceramic Society: 249–256. 1994.

10 NOBLE METALS IN HIGH-LEVEL WASTE GLASS MELTS

Noble metals such as Ru, Rd, and Pd in the HLW originate from the fission of U-235. Table 10-1 shows the radioactive noble metal isotopes that are present in spent fuel. Ru is the most abundant noble metal in the Hanford HLW.

Noble metals in the borosilicate glass melts have been a major concern in the HLW vitrification process because of their low solubility, high volatilization rate, and high electrical conductivity. In 1985, the accumulation of noble metals on the floor of the Pamela melter, Mol, Belgium, resulted in electrical short-circuiting of a joule-heated melter. Elliott et al. (1994) reviewed various methods for separating noble metals from the HLW. However, efforts to apply noble metal separation methods for Hanford HLW were abandoned because of the complex composition of the HLW that interfered with the separation process. In this chapter, a discussion on behavior of noble metals in glass melts and the melter is followed by a review of various studies on the subject and the implication of noble metals on HLW vitrification at the Hanford site.

10.1 NOBLE METAL SOLUBILITY IN GLASS MELTS

Borosilicate glass-based waste form has a very limited noble metal solubility. In silicate glasses, the solubilities of Rh, Pd, and Ru are about 0.05, 0.03, and 0.01 wt%, respectively. Noble metal concentrations greater than solubility limits produce metal particles suspended in the melt. These metals are either flushed out with the glass melt during pouring or settle on the floor of the melter. Noble metal settling on the melter floor depends on factors such as

- Residence time in the melter. The longer the residence time in the melter, the higher the concentration of the noble metals that settle on the floor of the melter.

- Convective currents in the melter. Stronger convective currents keep the noble metals suspended in the melt. Melter idling is the worst-case scenario. During melter idling, convective currents are weaker, which allow noble metals to slowly settle on the melter floor. The settling rate depends on the particle size of noble metals. The larger the particle size, the quicker the particles reach the melter floor.

Table 10-1. List of noble metal isotopes present in high-level waste (Elliott et al., 1994)

Isotope	Half-Life	Stable Decay Product
Ru-103	39.3 d	Rh-103
Ru-106	372.6 d	Pd-106
Rh-102	2.9 yr	Ru-102
Rh-103m	56.1 min.	Rh-103
Pd-107	6.5 E+6 yr	Ag-107

In addition, both residence time and magnitude of convective currents depend on the viscosity of glass. Noble metal concentrations in various HLW glasses for NCAW, which is now referred to as Envelope B/D waste, DWPF, Kernforschungszentrum Karlsruhe (KfK), Germany, and WVDP are shown in table 10-2.

10.2 NOBLE METAL BEHAVIOR IN THE MELTER

Since the failure of the Pamela melter, Mol, Belgium due to noble metal accumulation on the melter floor, several studies have been performed at various plants and research laboratories. These studies are briefly summarized in this section.

KfK examined noble metal retention in the melter using various melter designs. Their studies are summarized in a report by Elliott et al. (1994). The studies indicated that the accumulation of noble metals can be significantly reduced by increasing the slope of the melter walls. For a flat-bottom melter with a bottom drain, approximately 65 percent of the noble metals were retained in the melter. However, with 75°/60° sloped melter walls, electrical resistance did not indicate any accumulation of noble metals. KfK also compared the effect of a pour system on noble metal retention. The bottom drain retained only 10.3 percent Ru, while the overflow system retained 41.4 percent Ru. An overflow system is currently used in the WVDP and DWPF melter designs for glass pouring. The studies also found that in a melter with 45° sloped walls, convective currents in the glass melt decreased the Ru retention from 38 to 24 percent. In a 75°/60° sloped wall, no measurable effect was observed.

During nonradioactive operations at the WVDP between July 1986 and May 1988, approximately 9.3 kg of RuO_2 was fed to the melter. The analysis of the samples retrieved from the melter floor indicated an almost 6-cm deep sludge layer on the melter floor. Approximately 87 percent of the RuO_2 fed to the melter was flushed from the melter during normal glass pouring. The WVDP melter has sloped walls (Jain et al., 1991). The sludge layer consisted of mostly Fe-Cr spinel and RuO_2 crystals dispersed in the matrix. In addition, crystalline Ce_2O_3 and undissolved phases consisting of Al_2O_3 and Cr_2O_3 were inhomogeneously distributed and were present in trace amounts. Fe-Cr spinel represented almost 33 vol % of the sludge. Based on these results and the total inventory of noble metals in the HLW at WVDP, it was determined that the

Table 10-2. Noble metal concentration in various high-level waste glasses (Elliott et al., 1994)

Noble Metal	Neutralized Current Acid Waste	Defense Waste Processing Facility	Kernforschungszentrum Karlsruhe	West Valley Demonstration Project (Jain et al., 1991)*
RuO_2	0.11	0.1	0.655	0.10
Rh	0.024	0.02	0	0.03 (as oxide)
Pd	0.03	0.03	0.298	0.05 (as oxide)

*Jain, V., S.M. Barnes, T.K. Vethanayagam, and L.D. Pye. Noble metal and spinel deposition on the floor of the joule-heated melter. *Journal of the American Ceramic Society* 74(7): 1,559–1,562. 1991.

entire batch of the HLW containing noble metals can be processed using current melter design (with sloped walls and overflow system for glass pouring) without impacting the electrical resistance of the melter. During radioactive operations, however, electrical resistance between the side and bottom electrodes dropped. This decrease is being attributed to preferential accumulation of noble metals on the melter floor but no reports have been published on the subject.

In 1990, PNNL conducted gradient furnace testing to estimate the behavior of noble metals in a cold cap (Anderson et al., 1994). Dried feed in a long-sample boat was heated in a 590 to 940 °C gradient. The results indicated some agglomeration of noble metals at the cold end (590 °C) of the sample boat, while 1-μm RuO_2 particles with only a few agglomerates were observed at the hot end (940 °C). This study was followed by testing noble metal behavior in the 1/100th scale research scale melter (RSM) in 1992 (Elliott et al., 1994). The RSM operated for 48 d during which time the effects of various operating parameters such as glass and plenum temperature, oxide concentration, redox, and noble metal concentrations were evaluated. A reduction in electrical resistance was observed during the latter part of the campaign. Melter evaluation after operations indicated the presence of a 2–4-mm-thick (0.08–0.16 in.) noble metal layer on the melter floor, which caused one-third of one paddle electrode to corrode or dissolve. The electrode dissolution was attributed to localized heating due to short-circuiting of the electrode to the noble metal layer. In addition, noble metal caused dissolution of 1.3 cm (0.5 in.). of refractory layer on the floor. Mass balance results indicated that 5 percent of the noble metals were retained during segments where noble metal concentration was nominal and 46 percent of the noble metals were retained during the segments with double the nominal concentration of noble metals. Such a large accumulation and its impact on melter components were surprising because the residence time in the RSM is 10 percent of the full-scale melter. The analysis of glass samples poured from the melter indicated 10-μm average diameter needle-like RuO_2 particles with 100–200-μm RuO_2 agglomerates. RuO_2 agglomerates increased with an increase in the noble metal concentration in the feed.

The RSM study was followed by an engineering-scale melter (ESM) study. The ESM melter was one-tenth scale and was operated by KfK in Germany. The ESM operated for 49 d with noble metals. The mass balance results indicated retention of 35 percent of the noble metals on the melter floor. In addition, during the last segment of the campaign, the electrical resistance between the lower set of electrodes decreased by 10 to 15 percent. The glass poured from the melter indicated similar crystals in the glass, but the average diameter of the particles was slightly larger than RSM samples. PNNL also conducted computer modeling using the Transient Energy, Momentum, Pressure Equations Solutions in Three Dimensions (TEMPEST) Code. Results are discussed by Elliott et al. (1994).

Table 10-3. Amount of noble metals processed through integrated Defense Waste Processing Facility melter system (Hutson, 1994)

Noble Metal	Amount (kg)
Ru	15.68
Pd	5.73
Rh	3.12

The DWPF scale melter system, IDMS was used to study noble metal behavior in the Savannah River Site (SRS) and Hanford wastes. Three types of SRS wastes (Blend, HM, and PUREX) and one type of Hanford waste (NCAW) were processed between June 1990 and March 1993. The total amount of noble metals processed through the melter is shown in table 10-3. Pd and Rh were added as nitrate solutions, while Ru was added as nitrosylruthenium hydroxide [$RuNO(OH)_3$]. Samples taken from the melter floor during operations indicated increasing amounts of noble metals on the melter floor with time. In addition, the samples retrieved from the center and from the edges of the melter indicated nonuniform distribution of noble metals on the floor. The samples from the center contained Ru and Rh oxides and large amounts of spinel while the samples from the outer edge contained fewer spinel, metallic Pd and Pd tellurides, Ru and Rh oxides, and RuS_2. After approximately 550 hr of operation, the ratio of upper melt resistance and lower melt resistance increased. The melter floor sample indicated a good correlation between the increase in resistivity ratio and accumulation of noble metals on the floor. The overall mass balance indicated 35-, 21-, and 0-percent retention of Ru, Rh, and Pd in the melter, respectively (Elliott et al., 1994).

Studies indicate that a melter needs to be designed to accommodate anticipated accumulation of noble metals on the melter floor without affecting the current distribution in the melter. The use of sloped walls and positioning electrodes away from the floor could allow significant amounts of noble metals to accumulate on the floor before a resistance drop is observed in the melter. Further, melter idling, which causes suspended noble metals to settle on the floor, should be minimized.

10.3 TANK WASTE REMEDIATION SYSTEM CONCERNS

The settling of noble metals on the floor of the melter could cause premature failure of the melter. At Hanford, HLW will contain most of the noble metals in the feed. The HLW melter should incorporate lessons learned from the failure of the Pamela melter, operation of the radioactive WVDP melter, and other research and pilot-scale melters. Lessons learned include

- Using of sloped walls in the melter
- Positioning electrodes away from the floor
- Minimizing melter idling time
- Regular monitoring of electrode current

10.4 SUMMARY

Noble metals such as Ru, Rd, and Pd in the HLW originate from the fission of U-235. Ru is the most abundant of all the noble metals in the Hanford HLW. During glass melting, these metals have been a major concern because of their low solubility, high volatilization rate, and high electrical conductivity. In 1985, the accumulation of the noble metals on the floor of the Pamela melter in Mol, Belgium, resulted in electrical short-circuiting of a joule-heated melter. Borosilicate glass-based waste form has a very limited noble metal solubility. In silicate glasses, solubility of Rh, Pd, and Ru are about 0.05, 0.03, and 0.01 wt%, respectively. Noble metal concentration greater than solubility limits results in metal particles suspended in the melt. These particles are either flushed out with the glass melt during pouring or then settle on the melter floor. Noble metal settling on the melter floor depends on factors such as residence time in the melter, convective currents in the melter, and melt viscosity. Melter idling is the worst-case scenario for noble metal accumulation. During melter idling, convective currents are weaker, which allows noble metals to settle slowly on the melter floor.

The settling rate depends on the particle size of noble metals. The larger the particle size, the quicker the particles reach the melter floor. Noble metals behavior evaluated at WVDP, KfK, Pamela, DWPF, and PNNL indicates that a melter should be designed to accommodate the accumulation of noble metals on the melter floor without affecting the current distribution in the melter. The use of sloped walls and positioning electrodes away from the floor could allow significant amounts of noble metals to accumulate on the floor before a resistance drop is observed in the melter. Further, noble metal settling can be minimized by reducing the idling time in the melter.

10.5 REFERENCES

Anderson, L.D., T. Dennis, M.L. Elliott, and P. Hrma. Noble metal behavior during melting of simulated high-level nuclear waste glass feeds. *Proceedings of the Symposium on Environmental and Waste Management Issues in the Ceramic Industry. 95th Annual Meeting of the American Ceramic Society, Cincinnati, Ohio, April 18–22, 1993.* Ceramic Transactions Volume 39. G.B. Mellinger, ed. Westerville, OH: American Ceramic Society: 265–272. 1994.

Elliott, M.L., L.L. Eyler, L.A. Mahoney, M.F. Cooper, L.D. Whitney, and P.J. Shafer. *Preliminary Melter Performance Assessment Report.* PNL–9822. Richland, WA: Pacific Northwest National Laboratory. 1994.

Hutson, N.D. The behavior of the platinum group metals in a borosilicate waste glass and their effects on the operation of a joule-heated ceramic melter. *Proceedings of the Symposium on Environmental and Waste Management Issues in the Ceramic Industry. 95th Annual Meeting of the American Ceramic Society, Cincinnati, Ohio, April 18–22, 1993.* Ceramic Transactions Volume 39. G.B. Mellinger, ed. Westerville, OH: American Ceramic Society: 257–254. 1994.

Jain, V., S.M. Barnes, T.K. Vethanayagam, and L.D. Pye. Noble metal and spinel deposition on the floor of the joule-heated melter. *Journal of the American Ceramic Society* 74(7): 1,559–1,562. 1991.

11 SULFUR SOLUBILITY IN WASTE GLASSES

Borosilicate glass-based waste forms have limited sulfur solubility. In the WVDP and DWPF waste forms, SO_3 levels are maintained below 0.25 wt% to avoid formation of an immiscible sodium sulfate phase in the melt. Traditionally, wastes containing high concentrations of sulfur are washed with water to remove soluble sulfate salts. The salt solution is then treated separately as a low-level waste. The HLW at WVDP and at the Pamela vitrification facility, Mol, Belgium, were washed several times with water to reduce SO_3 concentration below 0.25wt%. If the concentration of SO_3 is in excess of 0.25 wt%, the SO_3 concentration limits the waste loading in the glass. Any improvement in increasing the waste loading through better understanding of sulfur solubility could result in significant cost savings. Current plans at Hanford involve development of glass compositions for LAW that can accommodate SO_3 concentration in excess of 1 wt%. Expected concentration of SO_4 from various feed streams at Hanford is shown in table 11-1. In this chapter, a brief discussion on the sulfur solubility limit imposed on the glass composition is followed by a review of various sulfur solubility studies and sulfur solubility implication on the LAW vitrification at the Hanford site.

11.1 SULFUR SOLUBILITY LIMITS IN HIGH-LEVEL WASTE BOROSILICATE GLASSES

Borosilicate glass-based waste forms have limited sulfur solubility. Even though SO_3 solubility under oxidized conditions is approximately 1 wt%, the SO_3 levels in the WVDP and DWPF glasses are maintained below 0.25 wt% to avoid formation of an immiscible sodium sulfate phase in the melt because SO_3 solubility in glass is a strong function of melt redox conditions. SO_3 solubility decreases sharply as glass melts become reducing. The SO_3 solubility limit is established based on the operating redox range of 0.01 and 0.5.

The sodium sulfate phase, usually referred to as "gall," is volatile, water soluble, and floats on the melt surface. Formation of gall could result in undesirable consequences such as

- Partition of radionuclides into the gall phase
- Foam formation in the melter
- Excessive corrosion of refractories and Alloy 690 components in the melter
- Disruption of heat balance in the melter (gall acts as an insulating layer on the surface of the melt)

Table 11-1. SO_4 concentration limits for A, B, and C low-activity waste feed envelopes (Pabalan et al., 1999)

Envelope	SO_4 mol/mol of Sodium
A	9.7×10^{-3}
B	7.0×10^{-2}
C	9.7×10^{-3}

11.2 SULFUR SOLUBILITY STUDIES

11.2.1 Effect of Redox

Schreiber et al. (1994) studied the effects of redox on SO_3 solubility in WVDP and DWPF HLW glasses. Figure 11-1 shows the effect of oxygen fugacity on SO_3 solubility. The relationship between oxygen fugacity and Fe^{2+}/Fe^{3+} ratio in glass is discussed in chapter 9. The V-shaped behavior indicates two different mechanisms by which sulfur is incorporated into the glass melt. Minimum SO_3 solubility occurs at an oxygen fugacity of $10^{-8.8}$. At an oxygen fugacity higher than $10^{-8.8}$, sulfur is incorporated in the glass as sulfate ion.

At an oxygen fugacity lower than $10^{-8.8}$, sulfur is incorporated in the glass as sulfide ion. In glass melts, as oxygen fugacity falls below 10^{-11}, a S^{6+}/S^{2-} redox couple in the system results in the formation of enough electrically conductive sulfide phases such as CuS, FeS and NiS electrically short the melter. At an oxygen fugacity above 10^{-2}, redox couples such as Ce, Mn, and Cr can influence the redox response in the system and cause formation of foam in glass melts.

Sulfur Solubility in Glasses

Sullivan (1995) studied the retention of sulfur in a Hanford HLW glass as a function of sulfur concentration, basicity, Al_2O_3, and P_2O_5 concentration. Figure 11-2 shows the distribution of SO_3 in soluble gall, glass and volatilized fraction as a function of SO_3 added to the batch. Results indicated 100-percent

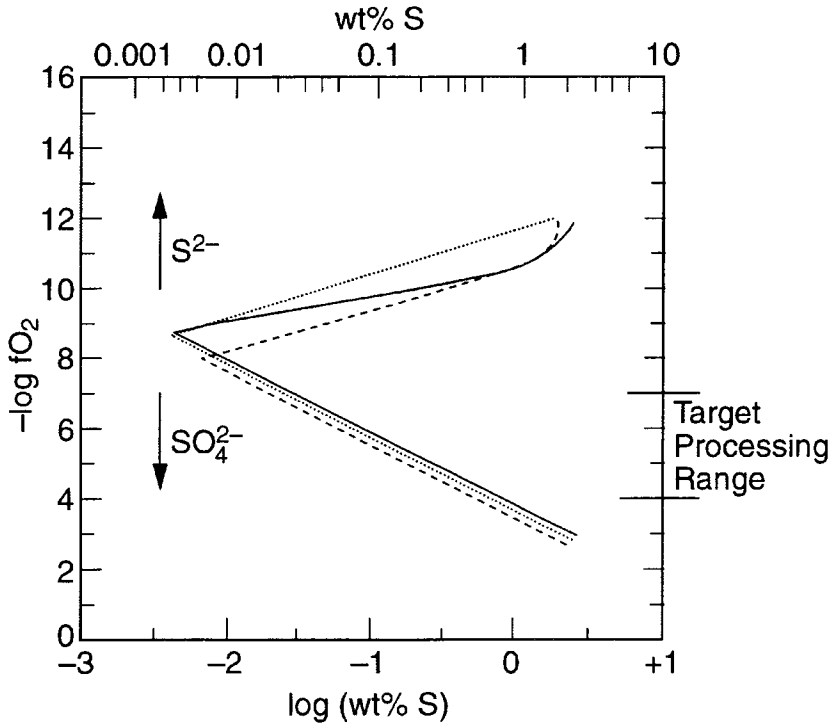

Figure 11-1. Sulfur redox/solubility systematics in WVF–17993 (solid line), in SRL–131 (dotted line) and in SRL–131 + 10 wt% Fe (dashed line) as a function of the imposed oxygen fugacity in an atmosphere of 15 vol% SO_2 at 1,150 °C (Schreiber et al., 1994)

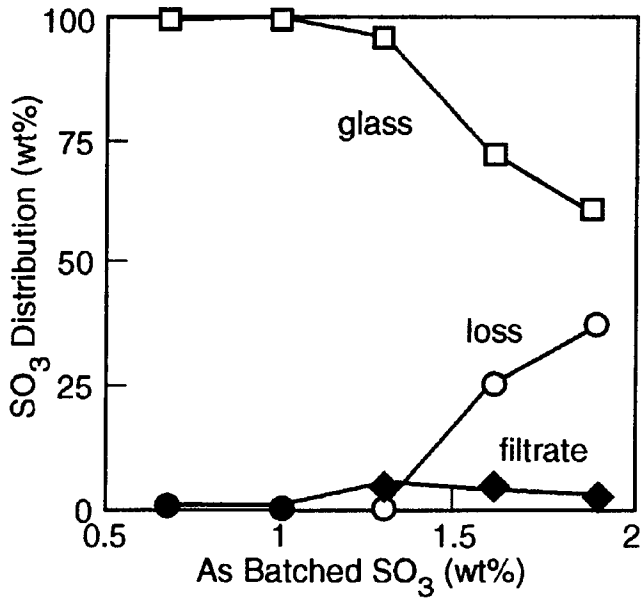

Figure 11-2. SO_3 distribution in soluble gall, glass, and volatilized fraction as a function of SO_3 content (Sullivan, 1995)

retention of sulfur in glasses with SO_3 concentration less than 1.0 wt%. The glass compositions studied had low (1–2 wt%) Fe_2O_3 concentration and were melted in oxidizing conditions (redox was not controlled in the melt). For SO_3 concentrations greater than 1.3, a yellow layer of gall was observed, and 1.1 to 1.2 wt% SO_3 was retained in the glass. In a base glass containing 1.6 wt% SO_3, SO_3 retention decreased with an increase in Al_2O_3 concentration (figure 11-3) and increased with an increase in P_2O_5 concentration (figure 11-4). In all cases, gall was observed on the surface.

Li et al. (1995) studied the kinetics of gall formation using plutonium finishing facility sludge and West Valley glass composition WV–183 spiked with up to 2 wt% sodium sulfate. The glass compositions were classified as high Na_2O and low B_2O_3, and low Na_2O and high B_2O_3. In high Na_2O and low B_2O_3 glasses, phase segregation occurred before melting was complete. In glasses containing low Na_2O and high B_2O_3, no phase segregation was observed during melting. In WV–183 glass, phase segregation did not occur in batches containing ≤ 1 wt% SO_3, while a yellowish phase formed at higher concentrations. The results indicated that phase segregation is a kinetic process occurring in the early stages of batch melting. The glass containing high concentrations of boric acid suppresses sulfate segregation, while Al_2O_3 promotes sulfate segregation. In batches containing both sulfur and phosphorus, the sulfate phase dissolves in the phosphate phase and induces phosphate segregation. While sulfate segregation was suppressed by high boric acid concentration, excessive foaming was observed in the melts.

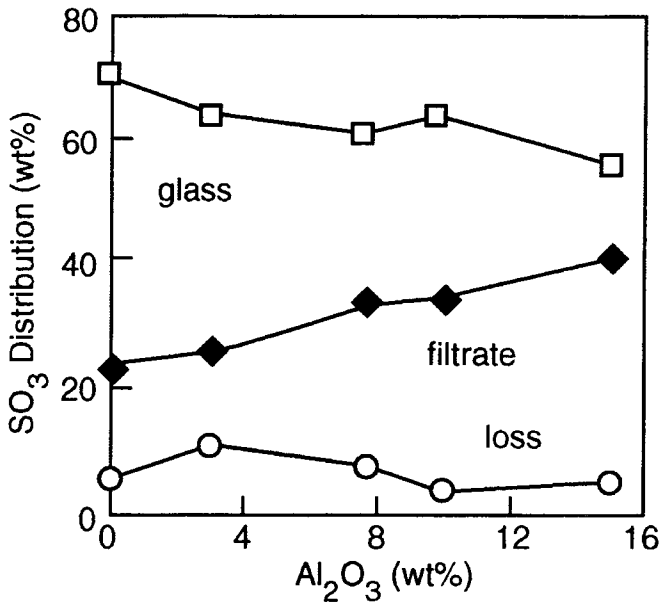

Figure 11-3. SO_3 distribution in soluble gall, glass, and volatilized fraction as a function of Al_2O_3 content (Sullivan, 1994)

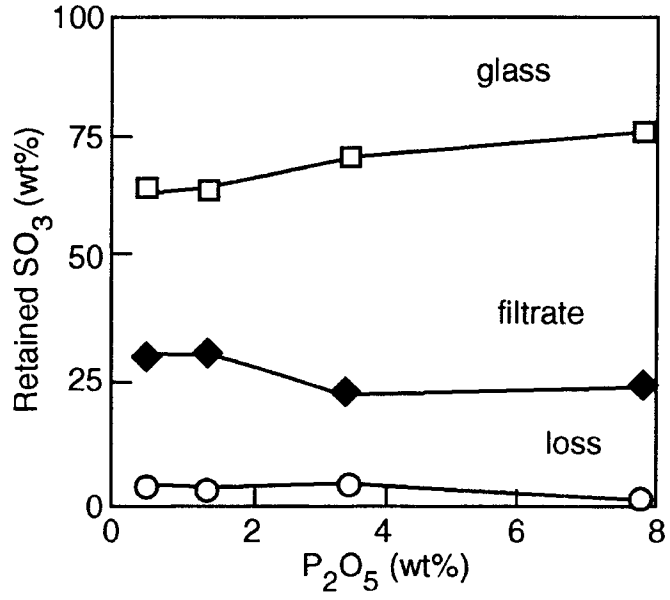

Figure 11-4. SO_3 distribution in soluble gall, glass, and volatilized fraction as a function of P_2O_5 content (Sullivan, 1994)

While sulfate segregation is a kinetic process, the sulfate retention is a thermodynamic process. Li et al.[1] analyzed sulfate retention in the melt and described the dissolution of sulfate melt as

$$\begin{aligned} &\equiv Si-O-Si\equiv + 2Na^+:O^{2-}\,[glass] \xleftrightarrow{k_1} 2(\equiv -O^-:Na^+)[glass] \\ &SO_3\,[gas] + 2Na^+:O^{2-}\,[molten\ salt] \xleftrightarrow{k_2} 2Na^+:SO_4^{2-}\,[molten\ salt] \end{aligned} \tag{11-1}$$

where ≡Si–O–Si≡ and ≡Si–O– are the BO and NBO in glass, respectively, and k_i is the reaction equilibrium constant. Based on the above reaction equilibrium, the solubility ($S_{[SO3]}$) of sulfate in a silicate melt, as expressed in terms of SO_3 concentration is

$$S_{[SO_3]} = p_{SO_3} \frac{k_2}{k_1} \frac{a_{Na^+}^2 a_{NBO}^2}{a_{BO}\gamma_{Na_2SO_4}} = p_{SO_3}\, \psi \frac{C_{NBO}^2}{C_{BO}} \tag{11-2}$$

where k_1 and k_2 are the equilibrium constants of the above reactions, p_{SO_3} is the SO_3 partial pressure, a_i (i = Na, NBO, BO) is the i^{th} species activity, $\gamma_{Na_2SO_4}$ is the Na_2SO_4 activity coefficient, and ψ includes the activity coefficients of Na, Na_2SO_4, NBO, and BO, the reaction equilibrium constants (k_1 and k_2), and concentration of sodium ions. At a given temperature and p_{SO_3}, Eq. (11-1) indicates that S_{SO_3} is a linear function of the $(C_{NBO})^2/C_{BO}$ ratio.

Figure 11-5 shows measured SO_3 retention concentrations in glass versus $(C_{NBO})^2/C_{BO}$. The sulfate retention in glass increases nonlinearly as the $(C_{NBO})^2/C_{BO}$ ratio increases, and the sulfate retention linearly increases as $(C_{NBO})^2/C_{BO}$ decreases with increasing P_2O_5 concentration. While the sulfate retention in these complex systems can be correlated with $(C_{NBO})^2/C_{BO}$, P_2O_5 has a different effect on sulfate retention in the glass. Increase in sulfate retention by adding phosphate is attributed to the formation of a separated phase in which sulfate and phosphate coexist. The figure also includes data for other borosilicate and silicate compositions reported in the literature. Despite differences in the melting temperature of these glasses, sulfate retention concentration falls on the same curve. Li et al.[2] also studied sulfate segregation tendencies and showed that even a melt with high sulfate retention could result in sulfate segregation. They attributed the sulfate segregation tendency to alkali and sulfate reactions occurring prior to the formation of the glass melt.

High SO_3 solubility in phosphate glasses has been observed by Stefanovsky et al. (1995). They studied the $44Na_2O$, $20Al_2O_3$, $(36-x)P_2O_5$, and xSO_3 system for immobilizing high sulfate radioactive wastes. The results indicated that glasses containing up to 8.5 mol% SO_3 were vitreous and showed no sulfate phase segregation. While this system can accommodate higher sulfate concentration in the melt, its applicability to meet product qualification requirements for disposal is not known.

---

[1]Li, H., P.R. Hrma, and J.D. Vienna. Sulfate retention and segregation in simulated waste borosilicate glasses. *Ceramic Transactions of the Environmental Issues and Waste Management Technologies in the Ceramic and Nuclear Industries VI, St. Louis, Missouri, April 30–May 3, 2000.* Ceramic Transactions Volume 119. Westerville, OH: American Ceramic Society. In press.

[2]Ibid.

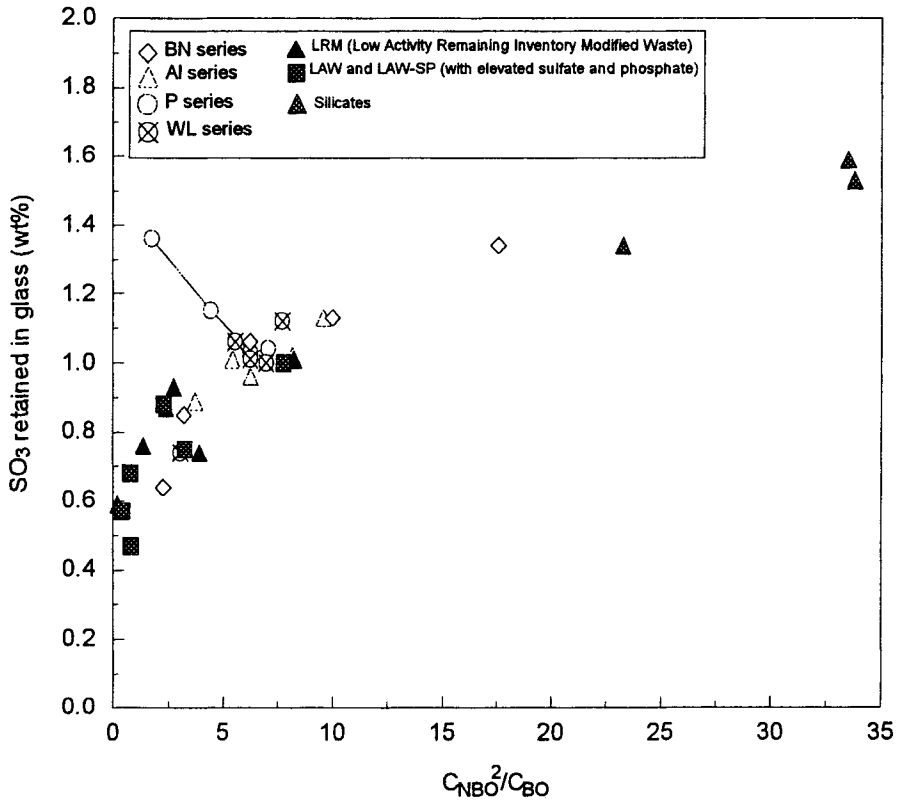

Figure 11-5. Sulfate retention in glass versus $(C_{NBO})^2/C_{BO}$, where C_{NBO} and C_{BO} are calculated mol concentrations of nonbridging oxygen and bridging oxygen[3]

Recently, Davis et al.[4] developed glass compositions for high-sulfate (2–3 wt% SO_3), high-lead (9.0 wt% PbO) wastes stored in Silos 1 and 2 at Fernald. They adjusted the reductant additions and visually observed the salt formation and metal precipitation during vitrification. The data are shown in table 11-2.

The data show that by increasing the reductant addition to the batch, the salt on the surface of the melt decreases and eventually disappears. However, metal droplets start appearing before all salt is dissolved in the melt. These data are in contrast to the sulfate solubility behavior shown in figure 11-1. It is possible that the glass under study contains approximately 9.0 wt% PbO and no B_2O_3, which could result in sulfate solubility behavior different from the typical borosilicate glasses. The applicability of these data to the

---

[3]Li, H., P.R. Hrma, and J.D. Vienna. Sulfate retention and segregation in simulated waste borosilicate glasses. *Ceramic Transactions of the Environmental Issues and Waste Management Technologies in the Ceramic and Nuclear Industries VI, St. Louis, Missouri, April 30–May 3, 2000.* Ceramic Transactions Volume 119. Westerville, OH: American Ceramic Society. In press.

[4]Davis, D.H., D.M. Bennert, and E. Nicaise. Control of batch redox to permit practical manufacturing of Fernald POPT surrogate-based glass. *Ceramic Transactions of the Environmental Issues and Waste Management Technologies in the Ceramic and Nuclear Industries VI, St. Louis, Missouri, April 30–May 3, 2000.* Ceramic Transactions Volume 119. D. Spearing and V. Jain, eds. Westerville, OH: American Ceramic Society. In press.

Table 11-2. Formation of salt layer as a function of redox in S0-1-10 glass (Davis et al., 2000)*

Wt% Equivalent C	Sulfate Salts Present?	Metal Present?	Redox $Fe^{2+}/\Sigma Fe$
0.0	Yes—Heavy Amount	None	0.03
0.1	Yes—Heavy Amount	None	0.10
0.2	Yes—Moderate Amount	None	0.18
0.3	Yes—Minor Amount	Yes	0.19
0.4	None	Yes	0.20

*Davis, D.H., D.M. Bennert, and E. Nicaise. Control of batch redox to permit practical manufacturing of Fernald POPT surrogate-based glass. *Ceramic Transactions of the Environmental Issues and Waste Management Technologies in the Ceramic and Nuclear Industries VI, St. Louis, Missouri, April 30–May 3, 2000.* Ceramic Transactions Volume 119. D. Spearing and V. Jain, eds. Westerville, OH: American Ceramic Society. In press. 2000.

borosilicate borosilicate type is questionable. The sulfate solubility was further improved by adding CaO to the batch. The results, shown in table 11-3, indicate that an increase in CaO concentration decreases the formation of salt layer due to formation of $CaSO_4$, which is a stable liquid. The sulfate solubility in the crucible melt is 0.35 wt% SO_3. When the same batch composition was fed to a melter, the sulfate solubility was 1.2 wt% SO_3 in the glass. The increase was attributed to the adjustments in the glass composition, presence of cold cap in the melter, and a lower melting temperature in the melter compared to crucible tests. Even though this study is not directly applicable to the Hanford glasses, it shows that laboratory and pilot-scale melter tests could yield significantly different results. Conducting laboratory tests followed by pilot-scale tests is strongly recommended.

11.3 EFFECT OF MELTER CONDITIONS ON SULFUR SOLUBILITY

As discussed in section 11.2.1, redox conditions in the melt have significant effects on the sulfur solubility. Since sulfur segregation is a kinetic process, the melter conditions such as temperature and cold cap conditions could have significant effects on the formation of gall. Secondary phases could form due to extremely reducing conditions in the melt, which could precipitate highly conductive phases such as NiS, CuS, or FeS.

11.4 TANK WASTE REMEDIATION SYSTEM CONCERNS

At Hanford, LAW sulfate solubility is a major concern. In traditional HLW borosilicate glasses processed in the redox range of 0.01 to 0.5, the sulfur concentration should be < 0.25 wt% as SO_3 in glass. Laboratory studies have indicated that sulfur solubility under oxidizing conditions could be as high as 1.2 wt% SO_3. Increasing the concentration of P_2O_5 and NBOs (alkali oxides) and decreasing the amount of Al_2O_3 could improve the sulfur solubility in the melt. However, the kinetic behavior of sulfur segregation such as the formation of gall in the cold cap during the melting phase or the formation of secondary phases in the

Table 11-3. Formation of salt layer as a function of redox in glass containing 9 wt% CaO (Davis et al., 2000)*

Wt% Equivalent C	Salts Present After Melting?	Metal Present After Melting?
0.0	Yes—Minimum Amount	None
0.1	None	None
0.2	None	None
0.3	None, but observed during melting	Yes
0.4	None, but observed during melting	Yes

*Davis, D.H., D.M. Bennert, and E. Nicaise. Control of batch redox to permit practical manufacturing of Fernald POPT surrogate-based glass. *Ceramic Transactions of the Environmental Issues and Waste Management Technologies in the Ceramic and Nuclear Industries VI, St. Louis, Missouri, April 30–May 3, 2000.* Ceramic Transactions Volume 119. D. Spearing and V. Jain, eds. Westerville, OH: American Ceramic Society. In press.

presence of P_2O_5 needs further evaluation to ensure safe operations. Proprietary studies to improve sulfur solubility in melts without formation of gall or excessive volatilization of SO_2 are being conducted at Catholic University of America to support the Tank Waste Remediation System project. The results of these studies are not published to date.

11.5 SUMMARY

Borosilicate glass-based waste form has a very limited sulfur solubility. Even though SO_3 solubility under oxidized conditions is approximately 1 wt%, the SO_3 levels in the WVDP and DWPF glasses are maintained below 0.25 wt% to avoid formation of an immiscible sodium sulfate phase in the melt because SO_3 solubility in glass is a strong function of melt redox conditions. SO_3 solubility decreases sharply as glass melts become reducing. The SO_3 solubility limit is established based on an operating redox range of 0.01 and 0.5. The sodium sulfate phase, usually referred to as gall, is volatile, water soluble, and floats on the surface of the melt. The formation of gall could result in undesirable consequences such as partition of radionuclides into the gall phase, foam formation in the melter, excessive corrosion of refractories and Alloy 690 components in the melter, and disruption of heat balance in the melter (gall acts as an insulating layer on the surface of the melt). Studies have indicated that under oxidizing conditions, increasing the concentration of P_2O_5 and NBOs (alkali oxides) and decreasing the amount of Al_2O_3 could improve sulfur solubility in the melt. However, kinetic behavior of sulfur segregation such as formation of gall in the cold cap during melting phase or formation of secondary phases in the presence of P_2O_5 needs further evaluation to ensure safe operations. Any improvement in increasing the waste loading through better understanding of the sulfur solubility could result in significant cost savings. Current plans at Hanford involve development of glass compositions for LAW that can accommodate SO_3 concentration in excess of 1 wt%.

11.6 REFERENCES

Bickford, D.F., and R.B. Diemer, Jr. Redox control of electric melters with complex feed compositions. *Journal of Non-Crystalline Solids* 84: 276–284. 1986.

Li, H., M.H. Langowski, and P.R. Hrma. Segregation of sulfate and phosphate in the vitrification of high-level wastes. *Proceedings of the International Symposium on Environmental Issues and Waste Management Technologies in the Ceramic and Nuclear Industries. 97th Annual Meeting of the American Ceramic Society, Cincinnati, Ohio, May 1–5, 1995.* Ceramic Transactions Volume 61. Westerville, OH: American Ceramic Society: 195–202. 1995.

Pabalan, R.T., M.S. Jarzemba, D.A. Pickett, N. Sridhar, J. Weldy, C.S. Brazel, J.T. Persyn, D.S. Moulton, J.P. Hsu, J. Erwin, T.A. Abrajano, Jr., and B. Li. *Hanford Tank Waste Remediation System High-Level Waste Chemistry Manual.* NUREG/CR–5751. CNWRA 97-008. Revision 2. San Antonio, TX: Center for Nuclear Waste Regulatory Analyses. 1999.

Schreiber, H.D., C.W. Schreiber, E.D. Sisk, and S. J. Kozak. Sulfur systematics in model compositions from West Valley. *Proceedings of the Environmental and Waste Management Issues in the Ceramic Industry II Symposium. 96th Annual Meeting of the American Ceramic Society, Indianapolis, Indiana, April 25–27, 1994.* Ceramic Transactions Volume 45. Westerville, OH: American Ceramic Society: 349–358. 1994.

Stefanovsky, S.V., I.A. Ivanov, and A.N. Gulin. Aluminophosphate glasses with high sulfate content. *Proceedings of the Materials Research Society Symposium.* Symposium Proceedings 353. Pittsburgh, PA: Materials Research Society: 101–106. 1995.

Sullivan, G. K. Sulfate segregation in vitrification of simulated Hanford nuclear waste. *Proceedings of the International Symposium on Environmental Issues and Waste Management Technologies in the Ceramic and Nuclear Industries. 97th Annual Meeting of the American Ceramic Society, Cincinnati, Ohio, May 1–5, 1995.* Ceramic Transactions Volume 61. Westerville, OH: American Ceramic Society: 187–193. 1995.

12 CHEMICAL DURABILITY

When a glass comes in contact with an environment, such as flowing or stagnant groundwater, corrosive gases and vapors, or aqueous solutions, chemical reactions occur at the surface, and then spread to the whole of the glass, depending on its composition, the pH of the solution, and the temperature of the environment. Newton (1985) provides an excellent historical review, dating back to 1660, of the chemical durability of glasses. The modern understanding of chemical durability of glasses has developed in the last 30 yr. These studies have focused on understanding two aspects of chemical durability of nuclear waste glasses. First, the ability to predict glass durability and produce glasses to meet specific leaching criteria based on short-term tests, and, secondly, the ability to predict the long-term (on the order of 10,000 yr or more) dissolution behavior of glasses. In recent years, studies attempt to measure the durability of glasses developed for the disposal of high-level radioactive wastes. Various aspects of the chemical durability of glasses have been reviewed by Paul (1977), Jantzen (1992), Ellison et al. (1994), Bourcier (1994), and the U.S. Department of Energy (1994).

This chapter provides an overview of the current understanding of glass dissolution behavior. Since glass corrosion is not an intrinsic property of the materials, the observed dissolution behavior depends on the test conditions and test methods. Several methods have been developed for accelerated testing to determine the corrosion behavior of glasses. A few test methods that form the basis of current understanding are discussed, as well as relationships between glass composition and environment (pH, temperature, and nature of solution). A careful evaluation is required before drawing conclusions regarding the chemical durability of a glass based solely on data. In this report, the terms glass durability, corrosion of glass, or dissolution of glass are interchangeably used to refer to glass corrosion.

12.1 CATION RELEASE SPECIFICATION

12.1.1 Production Specification

The WAPS require, at the time of shipment, the producer to demonstrate control of waste form production by comparing, either directly or indirectly, production samples to the EA benchmark glass. The consistency of the waste form must be demonstrated using PCT. For acceptance, the mean concentrations of lithium, sodium, and boron in the leachate, after normalizing for the concentrations in the glass, must each be less than those of the benchmark glass. One acceptable method of demonstrating that the acceptance criteria are met would be to ensure that the mean PCT results for each waste type are at least two standard deviations below the mean PCT of the EA glass.

12.1.2 Geologic Disposal Specification

The long-term performance of the HLW vitrified waste form and the overall performance of the repository are independent, though there are no limits placed on the radionuclide release from the glass waste form. The NRC, in Draft 10 CFR Part 63, has proposed a limit of 0.25 mSv (25 mrem) as the total effective dose equivalent received in a single year, by the average member of the critical group, weighted by the probability of occurrence as the overall system performance objective for the repository following permanent closure. The review of repository performance is outside the scope of this report.

12.2 GLASS CORROSION MECHANISM

Glass reactions in aqueous environments are complex and depend on glass composition and contact solution chemistry. Figure 12-1(a) shows a schematic of reactions occurring at various stages of the glass dissolution process. The processes involved in glass dissolution include ion-exchange, water diffusion, hydrolysis, and precipitation. Even though dissolution may start by simple ion-exchange or hydrolysis reaction, the simultaneous occurrence of the stated processes is not uncommon. The initial reaction on the glass surface depends on the contact-solution chemistry. In contact with water at neutral pH, the dissolution behavior of a simple alkali silicate glass is controlled by the hydrolysis reaction expressed by Eq. (12-1). Alkaline pH involves network hydrolysis of Si-O-Si bonds, as shown by Eqs. (12-2) and (12-3). In acidic pH, the reaction begins with an ion-exchange reaction between alkali ions (M^+ ions) in the glass and the hydrogen ions (hydronium ions, H_3O^+) in the solution, as shown by Eq. (12-4). In 1980, Enrsberger pointed out that the field intensity of the bare proton is so high that it cannot exist in a condensed phase, and the proton is probably associated with water molecules (H_3O^+). The interrelationship between reactions was described by Paul (1982). He stated that, in neutral solutions, water reacts with alkali ions at the NBO site to produce hydroxyl bonds and release alkali ions into solution, which increases the pH of the solution, as shown by Eq. (12-1). Next, the OH^- ion disrupts the siloxane bonds, as shown by Eq. (12-2). The ≡ Si-O-formed in reaction (12-2) further reacts with H_2O producing an OH^- ion [Eq. (12-3)], which is free to repeat the reaction in Eq. (12-2). The release of Si from the glass into the contact solution, as silicic acid, occurs when BO bonds associated with Si are hydrolyzed, as shown by Eqs. (12-5) and (12-6).

$$\equiv Si - O - M + H_2O \rightarrow \equiv Si - O - H + M^+ + OH^- \quad (12\text{-}1)$$

$$\equiv Si - O - Si \equiv + OH^- \rightarrow \equiv Si - O - H + \equiv SiO^- \quad (12\text{-}2)$$

$$\equiv Si - O^- + H_2O \rightarrow \equiv Si - O - H + OH^- \quad (12\text{-}3)$$

$$\equiv Si - O - M + H_3O^+ \rightarrow \equiv Si - O - H + M^+ + H_2O \quad (12\text{-}4)$$

$$= Si - OSi(OH)_3 + OH^- \rightarrow = Si - O^- + Si(OH)_4 \quad (12\text{-}5)$$

$$= Si - O - Si(OH)_3 + H_2O \rightarrow = Si - OH + Si(OH)_4 \quad (12\text{-}6)$$

As the corrosion front progresses inside the glass, more and more alkali ions are released from the glass into the solution and the solution, pH continues to rise. However, the increase in pH is counteracted by the release of a weak acid (silicic acid). The release of silicic acid increases sharply at pH > 9, as shown in figure 12-2. The initial rate of glass corrosion depends on the mass transport rate of H_2O or H_3O^+ to the alkali site and removal of alkalis out of the glass into the contact solution. In acidic pH, the ion-exchange reaction progresses at a much higher rate compared to the network hydrolysis reactions, as shown in figure 12-3.

As the reaction progresses, reaction layers are formed on the surface. The formation of reaction layers on the surface of the glass in contact with leachate plays a significant role in determining the leaching behavior of the glass components. Figure 12-1(b) shows a schematic of the surface layers formed on the surface of the glass. The outermost surface layer is called the precipitation layer, while the innermost layer is called the diffusion layer. The layer sandwiched between the diffusion and precipitation layers is called the gel layer. The formation of the diffusion layer occurs through ion-exchange reactions shown by Eqs. (12-1)

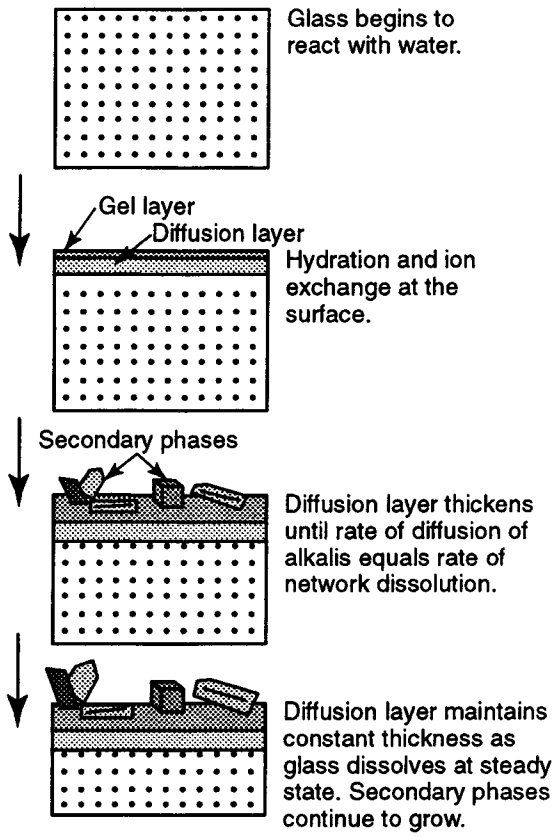

(a)

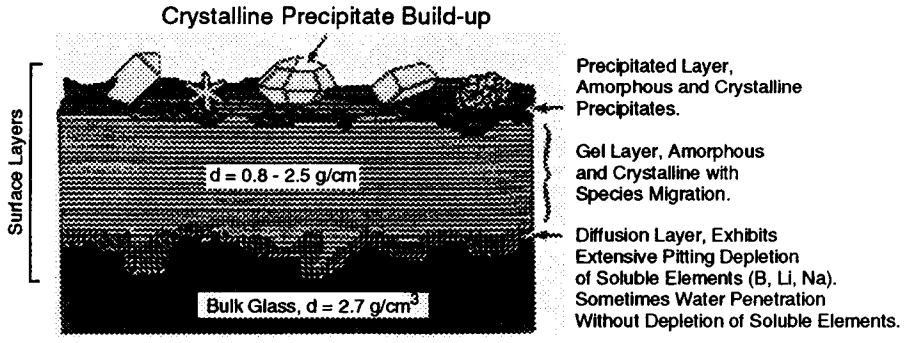

(b)

Figure 12-1. (a) Glass dissolution mechanism, (b) Schematic of surface layer on leached glass

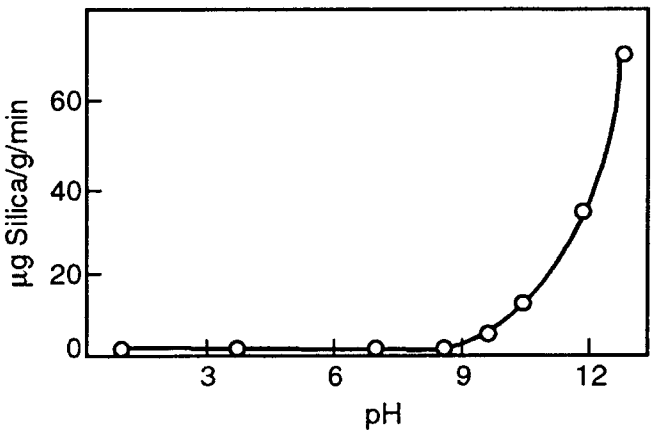

Figure 12-2. Effect of pH on the rate of extraction of silica from fused silica powder at 80 °C (Paul, 1982)

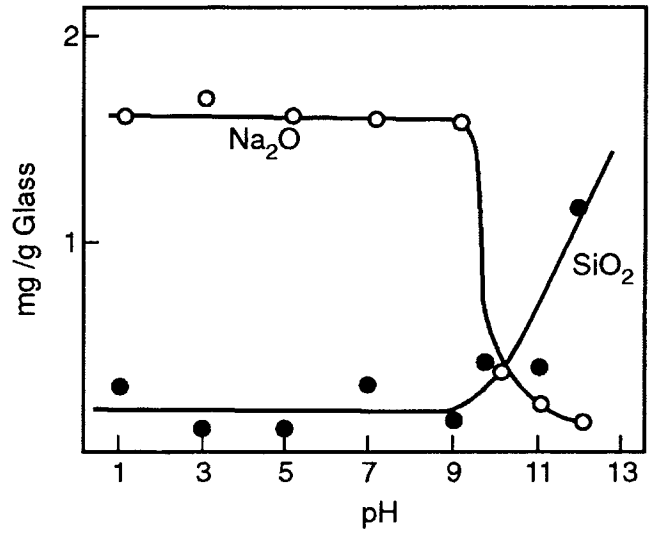

Figure 12-3. Effect of pH on the extraction of soda and silica from a $Na_2O{\cdot}3SiO_2$ glass at 35 ° C (Paul, 1982)

and (12-2), while the formation of the gel layer occurs through a hydrolysis reaction, shown by Eqs. (12-3) and (12-4). As the glass corrodes and its components are released into solution, the leachate may become supersaturated with some components, leading to precipitation of the secondary phases on the surface of the glass or the walls of the test container.

The thickness of the gel layer remains constant if the pH of the contact solution does not change. If the contact solution becomes more alkaline, the Si dissolution increases, which may reduce the thickness of the gel layer. In a more complex system containing more than one glass-forming oxide such as B_2O_3 or Al_2O_3 (depending on the glass composition), the corrosion mechanism is further complicated by the release rate of various cations from the glass and their solubility in the contact solution.

The properties of the surface layer depend on the glass composition, contact solution chemistry, test parameters, and reaction time. The surface layers can provide a sink or reservoir for components in solution and act as a physical barrier to the transport of reactants and corrosion products. In addition, the surface layers can influence the chemical affinity of the glass reactions.

Depending on the test conditions, surface layers could either increase or decrease the corrosion rate. Chick and Pederson (1984) showed that even though surface layers provide some transport barrier to glass reaction, the leaching behavior is controlled by the contact solution. Conradt et al. (1985) showed that surface layers in glass corroded in brine solutions (pH=5.7) at 120 and 200 °C had no effect on the corrosion rate, but when the glass was tested in 0.1 M NaOH (pH=12), glass corrosion was completely controlled by surface layers. Grambow and Strachan (1984) tested simulated waste glass PNL 76–68 in deionized water and 0.001 M $MgCl_2$ solution and showed that the formation of surface layers in the $MgCl_2$ solution dominated the corrosion behavior of the glass. The experimental evidence suggests that the surface layers provide a barrier to glass corrosion. However, the extent of this effect depends on the glass composition, characteristics of reaction layers, contact solution, temperature, and test conditions.

Surface layers that act as sinks reduce the concentration of corrosion species in the solution and increase the affinity for glass dissolution. The dissolution affinity is influenced by factors such as (Feng, 1994)

- Precipitated crystalline phases
- Amorphous silica phase(s)
- Gel layer
- Bulk glass components

12.3 GLASS DURABILITY MEASUREMENTS

Glass durability is not an intrinsic material property. Glass durability is dictated by the parameters controlled during testing. Typically the test is either dominated by the solution chemistry or the glass chemistry. The tests conducted using a low surface area/volume (SA/V) ratio are referred to as glass-dominated conditions. In this case, a monolithic sample is placed either in a large amount of water in closed system or in a periodic or continuous flowing condition. The corrosion behavior is not influenced by the glass components leached into the contact solution. The tests conducted using a high SA/V ratio are referred to as solution-dominated conditions. In this case, the contact solutions quickly attain saturation with the glass components, and the test results are dominated by the glass components leached into the contact solution. The glass components exceeding solubility limits in the solution often precipitate on the surface of

the glass and lead to the formation of secondary phases. Depending on their characteristics, these secondary phases could either increase or decrease the dissolution rate. These tests are used to provide accelerated corrosion of glasses.

The corrosion of glass is usually determined by measuring the amounts of various glass components that are released into the solution in contact with the glass. The components are released at different rates depending on the characteristics of the contact solution and the chemical composition of the glass. In alkali borosilicate glasses, alkali and boron are released at the fastest rate and are often used to measure corrosion. Boron and alkali have high solubility in solution and are not incorporated into the secondary phases that are formed on the surface of the glass. Boron is preferred over alkalis because, a boron release is more sensitive to reaction kinetics such as temperature and pH. However, to study the reaction mechanisms, additional components such as Al, Si, and others involved in the reactions are monitored. Table 12-1 shows different techniques and protocols used in determining glass durability. The test methods are generally categorized as static tests and dynamic tests. In static tests, the leachate is not refreshed or replaced, while in dynamic tests, the leachate is continuously or periodically refreshed or replaced.

12.3.1 Static Tests

The most widely used static tests to compare durabilities of various glasses, and the accepted test method for determining corrosion behavior, are Materials Characterization Center (MCC)–1 and MCC–3 (U.S. Department of Energy, 1982), and the PCT (ASTM C1285-97) durability test. In MCC–1, a monolithic glass sample is used in test solutions such as deionized water, brine, and silicate solution. The reference conditions include the SA/V ratio of 10 m^{-1} at 90 °C for 28 d. However, the conditions can be varied. The glass corrosion is determined by analyzing the concentration of the glass components in the leachate. The samples for the test are prepared by fracturing, cutting, or grinding. The surface finish has a measurable effect on the corrosion rate. The rougher sample has a larger surface area and, therefore, a higher corrosion rate. The test sample and the contact solution are placed in a closed vessel, usually perfluoroalkoxy (PFA) Teflon®, and placed in a oven equilibrated at the test temperature. The PCT method is an ASTM standard (Test Method C 1285–97), a modified version of the MCC–3 test, and is exclusively developed to monitor the performance of the HLW glasses during production. This method uses a crushed sample, which provides a high SA/V ratio (2,000 m^{-1}) instead of the monolithic sample in MCC-1 (10 m^{-1}). The method details two versions of the test. The PCT-A method uses a crushed glass specimen with a particle size distribution between -100 and +200 (0.149 and 0.074 mm) mesh, placed in an airtight 304L stainless-steel vessel containing deionized water, which is ten times the mass of the crushed sample. This provides a SA/V of 2,000 m^{-1}, and the test is conducted at 90 °C for a fixed duration of 7 d. The normalized release concentration for element *i*, NC_i, in the leachate can be calculated by Eq. (12-7).

$$NC_i = \frac{C_i}{F_i} \tag{12-7}$$

where NC_i is in g-glass/m^3, C_i is the concentration of element i in solution in g/m^3, and F_i is the mass fraction of element *i* in glass. The PCT-B method allows variation in the SA/V ratio, particle size, leachate composition, temperature and time. This method is used for investigating the effect of various parameters on glass corrosion. The test uses either stainless steel or PFA Teflon® vessels. The high SA/V ratio accelerates saturation of glass components in the contact solution. A PCT can reach saturation in a few days while an

Table 12-1. Summary of leach test methods (U.S. Department of Energy, 1994)

Name of Test	Temperature (°C)	Leachant	Flow Rate	Sample Description	Reference
Soxhlet	50–100	Distilled water	1.5 cm^3/min	Plate, SA = 3 cm^2	1
Modified soxhlet	35–100	Distilled water	Variable	Grains or plate SA = Variable	2
Hot-cell soxhlet	100	Distilled water	80 cm^3/hr	Beads/plates/chips SA = Variable	3
MCC–5 soxhlet	100	Distilled water	~1.5 cm^3/min	Plate, S = 4 cm^2	4
Soxhlet (PNC)	70,100	Distilled water	60–225 cm^3/hr	Bar, SA = 2 cm^2	5
HIPSOL (HT soxhlet)	100–300	Distilled water	100–900 cm^3/hr	Powder or block	6
IAEA	25	Distilled water	Periodic replacement	Cylinder with exposed surfaces	7
ISO Buffer	23–100	Distilled water, buffers, and seawater	Periodic replacement	Monoliths	7
Powder (P1)	95–200	Distilled water	Periodic replacement	Powder, 100–200 μm	8
Powder (P2)	40–100	Deionized water	Daily replacement	Powder, 100–150 mesh	9
MCC–4	40, 70, 90	Distilled water and reference groundwater	0.1–0.001 cm^3/min	Plate, SA = 4 cm^2	4
Low-flow	25–90	Distilled water	1 cm^3/wk	Plate, SA = 3 cm^2 (radiotracers)	10
Dynamic	35–90	Distilled water	3–1,200 cm^3/hr	Grains or monoliths	11
Grain Titration	100	Distilled water	Static	Powder	12
Time-Dependent Method	20– ~60	Buffered water	Static	Disc	10
MCC–1	40, 70, 90	Distilled water and reference groundwater	Static	Monolith SA/V = 10 m^{-1}	4
MCC–2	110, 150, 190	Distilled water and reference groundwater	Static	Monolith SA/V = 10 m^{-1}	4

Table 12-1. Summary of leach test methods (U.S. Department of Energy, 1994) (cont'd)

Name of Test	Temperature (°C)	Leachant	Flow Rate	Sample Description	Reference
MCC–3	40, 90, 110, 150, 190	Distilled water and reference groundwater	Static (agitated)	Crushed (1) 149–175 μm (2) <45 μm	4
HTLT (CEC)	90, 110 150, 190	Distilled water	Static	SA = 4 cm^2	13
Autoclave (HMI)	150–200	Distilled water and brines	Static	Beads, chips	14
Autoclave (KfK)	100, 150, 200, 250	Distilled water and brines	Static	Cylinders SA = 20 or 5 cm^2	15
Repository Simulation	25–90	Granite equilibrated water	None (sampling equivalent to 1 cm^3/mo)	Plate SA = 3 cm^2	10
Waste/Water/ Rock Leach	98	Distilled water or granite water		Glass cube: SA = 6 cm^2 20 g granite powder: 250–710 μm, 60 cm^2 water	5
MCC–14	25–250	Repository groundwaters	Static or periodic sampling	Monoliths and powders	4
PCT	90	Deionized water	Static	Crushed 74–149 μm	16

1 Nakamura H., and S. Toshiro. *Safety Research of High-Level Waste Management for the Period April 1982 to March 1983.* Progress Report JAERI–M–83–076. Japan Atomic Energy Research Institute. 1983.

2 Hussain, M., and L. Kahl. Incorporation of precipitation from treatment of medium-level liquid radioactive waste in glass matrix or ceramics together with high-level waste. *Symposium Proceedings for the Ceramic in Nuclear Waste Management.* 1979.

3 Commission of the European Communities. *Testing and Evaluation of Solidified High-Level Waste Forms.* Joint Annual Progress Report EUR 10038. Commission of European Communities (CEC). 1983.

4 U.S. Department of Energy. *Nuclear Waste Material Handbook (Test Methods) Technical Information Center.* DOE/TIC–11400. Washington, DC: U.S. Department of Energy. 1981.

5 Igarashi, H. et al. Leaching test of simulated HLW glass in the presence of rock. *Atomic Energy Society of Japan—1983 Annual Meeting.* 1983.

6 Senoo, M. et al. *High-Pressure Soxhlet-Type Leachability Testing Device and Leaching Test of Simulated High-Level Waste Glass at High Temperature.* JAERI–M–8571. Japan Atomic Energy Research Institute. 1979.

7 Draft International Standard Report. ISO/DIS–6961. 1979.

8 Oversby, V.M., and A.E. Ringwood. Leaching studies on Synroc at 95 and 200 °C. *Radioactive Waste Management* 23: 223. 1982.

9 Reeve, K.D., et al. The development of testing of Synroc for high-level radioactive waste fixation. *Symposium Proceedings for the Waste Management* 1: 249–266. 1981.

Table 12-1. Summary of leach test methods (U.S. Department of Energy, 1994) (cont'd)

Name of Test	Temperature (°C)	Leachant	Flow Rate	Sample Description	Reference
10 Van Iseghem, P., et al. Chemical Stability of Simulated HLW Forms in Contact with Clay Media. EUR–8424. CCC. 1983.					
11 Vaswani, G.A., et al. Development of Improved Leaching Techniques for Vitrified Radioactive Waste Products. BARC–1032. Bhabba Atomic Research Center. 1978.					
12 Deutsches Institut for Normung. *DIN Leach Test.* Report 12111. Deutsches Institut for Normung. 1976.					
13 European Community Static High Temperature Test Summary. CEC Report EUR 9772. 1985.					
14 Altenhein, F.K., et al. Scientific Basic International Symposium Proceedings for the Nuclear Waste Management: 363–370. 1981.					
15 Kahl, L., M.C. Ruiz-Lopez, J. Saidl, and T. Dippl. Preparation and Characterization of an Improved Borosilicate Glass for Solidification of High-Level Radioactive Fission Product Solutions. Part 2: Characterization of the Borosilicate Glass Product. GP 98/12. Kernforschungszentrum Karlsruhe Report KFK–3251e. 1982.					
16 American Society for Testing and Materials. *Determining Chemical Durability of Nuclear, Hazardous, and Mixed Waste Glasses: The Product Consistency Test.* Annual Book of ASTM Standards. ASTM C 1285-97. Volume 12.01. 774–91. West Conshohocken, PA: American Society for Testing and Materials. 1997.					

MCC–1 test, which is a solution-dominated system (low SA/V ratio), may take significant time to reach saturation.

12.3.2 Dynamic Tests

The Soxhlet (Delage and Dussossoy, 1991), single-pass, flow-through (SPFT) test (McGrail et al., 1997) and periodic replacement tests are widely used as dynamic tests. The Soxhlet test can be conducted over a temperature range of 90 to 250 °C. The test apparatus consists of a stainless steel reactor with a boiler supported by a condenser. The leaching vessel is located in the upper portion of the boiler. The water evaporating from the boiler is condensed in a reflux tube and is allowed to drip into the leaching vessel, which contains either a monolithic or crushed glass sample. The excess water from the leaching vessel overflows into the boiler. The corrosion rate is measured by periodically removing and analyzing the sample from the boiler. Since the leachate solution is recondensed, only deionized water can be used as a leachate solution. While the test allows studying a wide temperature and pressure range, the testing apparatus is quite complex. The test is useful where high flow rates are required.

The SPFT test is used to measure forward reaction rate. In this test, leachate solution is passed at a constant rate, using a peristaltic pump, into a cell containing a monolith or crushed glass. The solution leaving the cell is periodically collected and analyzed. The corrosion rate is determined by Eq. (12-8).

$$NR_{i,j} = (C_{i,j} - \overline{C}_{i,b})\frac{q_j}{f_i s_j} \tag{12-8}$$

where $NR_{i,j}$ is the normalized release rate of i^{th} element at the j^{th} sampling, q_j is the flow rate at the time period j in m^3/s, $C_{i,j}$ is the concentration of component i at the time period j, $C_{i,b}$ is the mean background concentration of component i, f_i is the mass fraction of component i in glass, and s_j is the surface area over the time period j-1 and j, m^2. In glasses, the corrosion rate increases to a maximum value as the flow rate

increases. This maximum corrosion rate is called the forward reaction rate. In this test, conditions such as leachate composition, temperature, and pH can be varied to measure the reaction characteristics.

In periodic replenishment tests, leachate solutions are periodically removed from the ongoing static tests. The static tests, such as MCC–1, MCC–3, and PCT, can be used to conduct periodic replenishment tests. The time of replenishment can be determined based on the aforementioned test conditions. The corrosion behavior of the glass depends on the amount of leachate replaced and the frequency of replacement.

The selection of a test method depends on the characteristics of the system under study. For example, if the interactions between the glass and contact solution are important without the influence of solution chemistry, tests such as MCC–1 or dynamic tests are recommended. If the effect of solution chemistry on the glass corrosion behavior is important, then tests such as PCT are more useful. Most of the literature data on glass durability are collected using either the MCC–1 or PCT method. Selecting the test method that duplicates the performance requirements (or meets the anticipated environmental conditions during use) of a glass is the key to conducting relevant tests.

12.4 PARAMETERS AFFECTING LEACHING BEHAVIOR

Test parameters such as SA/V ratio, flow rate, and temperature for a given method could limit the usefulness of the data for the desired application.

12.4.1 Effect of Surface Area to Volume Ratio

Glass dissolution initiates on the surface. The greater the surface area, the greater the dissolution of glass in the contact solution. However, the effect of surface area on glass dissolution is not linear. Ebert and Bates (1993) studied the dissolution of two reference DWPF borosilicate glasses, SRL–131A and SRL–202A, with SA/V ratios of 10; 2,000; and 20,000 m^{-1}. The results shown in figure 12-4 indicate that B release cannot be linearly scaled as a function of SA/V·t. The higher, nonlinear release at the high SA/V ratio has been attributed either to the differences in the contact solution chemistry or mass transport effects. The changes in solution chemistry (i.e., the evolution of pH as a function of time) are shown in figure 12-5. Pederson et al. (1983) hypothesized that thicker surface layers are formed in tests with low SA/V ratio, which affects the mass transport to a greater degree compared to the thinner surface layers formed in high SA/V tests, which is responsible for higher B release from high SA/V samples. In addition, long-term tests can be affected by the changes in surface area. The release from the glass should be corrected to include the change in surface area of the glass with time due to pulverization from stresses, formation of secondary phases, or normal dissolution of glass. If the effects of solution chemistry, surface area, and nature of surface layers is not properly accounted for in the analysis, the extrapolation of short-term data to long-term behavior could be biased.

12.4.2 Effect of Flow Rates

In the dynamic tests, the leachate solution is continuously flushed at a given flow rate or periodically exchanged. The increase in ions released from the glass is counteracted by their removal through continuous or periodic leachate exchanges. The maximum corrosion will occur if the flow rate is such that the

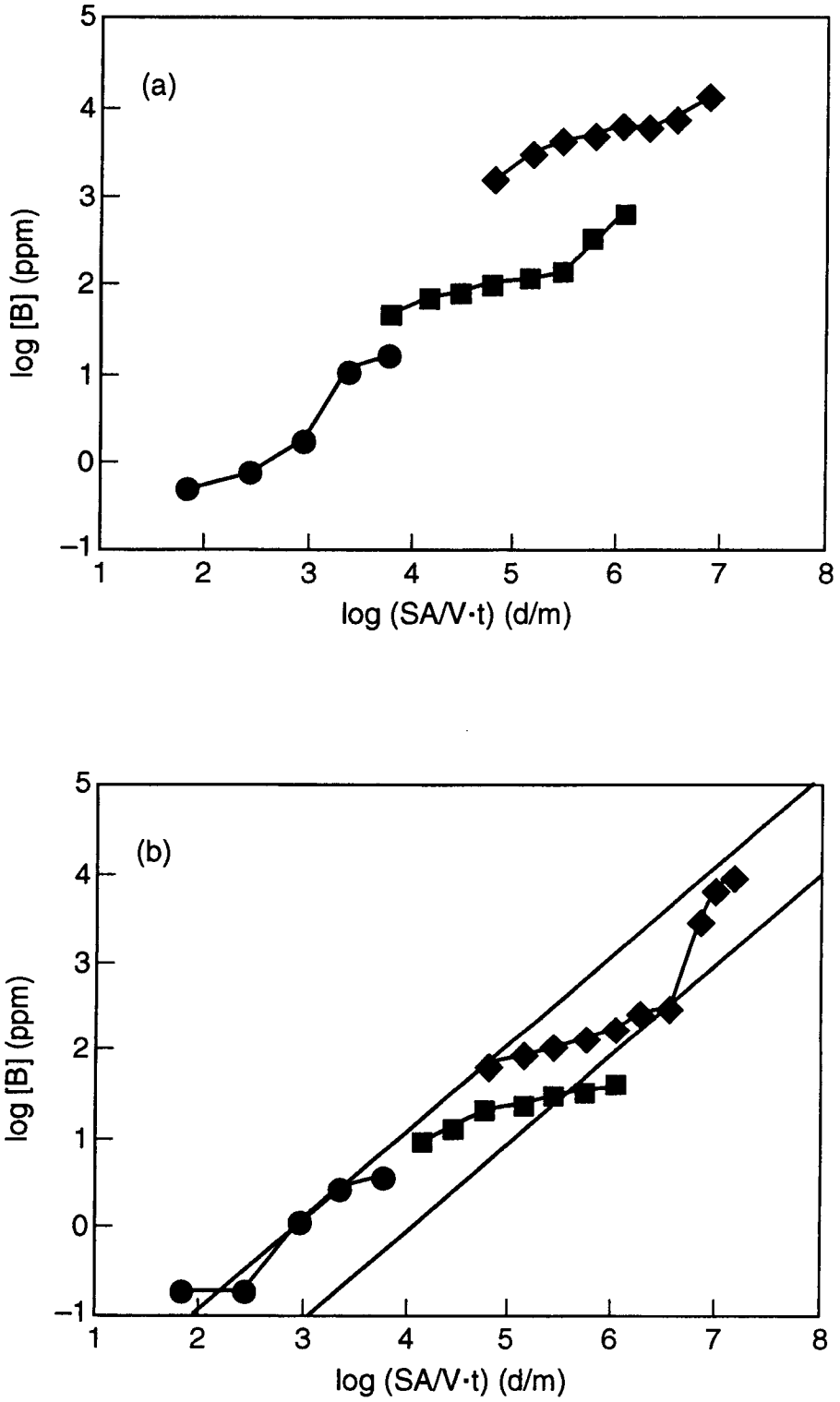

Figure 12-4. Concentration versus (SA/V)•time for release of B from (a) SRL–131 glass and (b) SRL–202 glass at 90 °C at (●) 10, (■) 2,000, and (◆) 20,000 m^{-1} (Ebert and Bates, 1993)

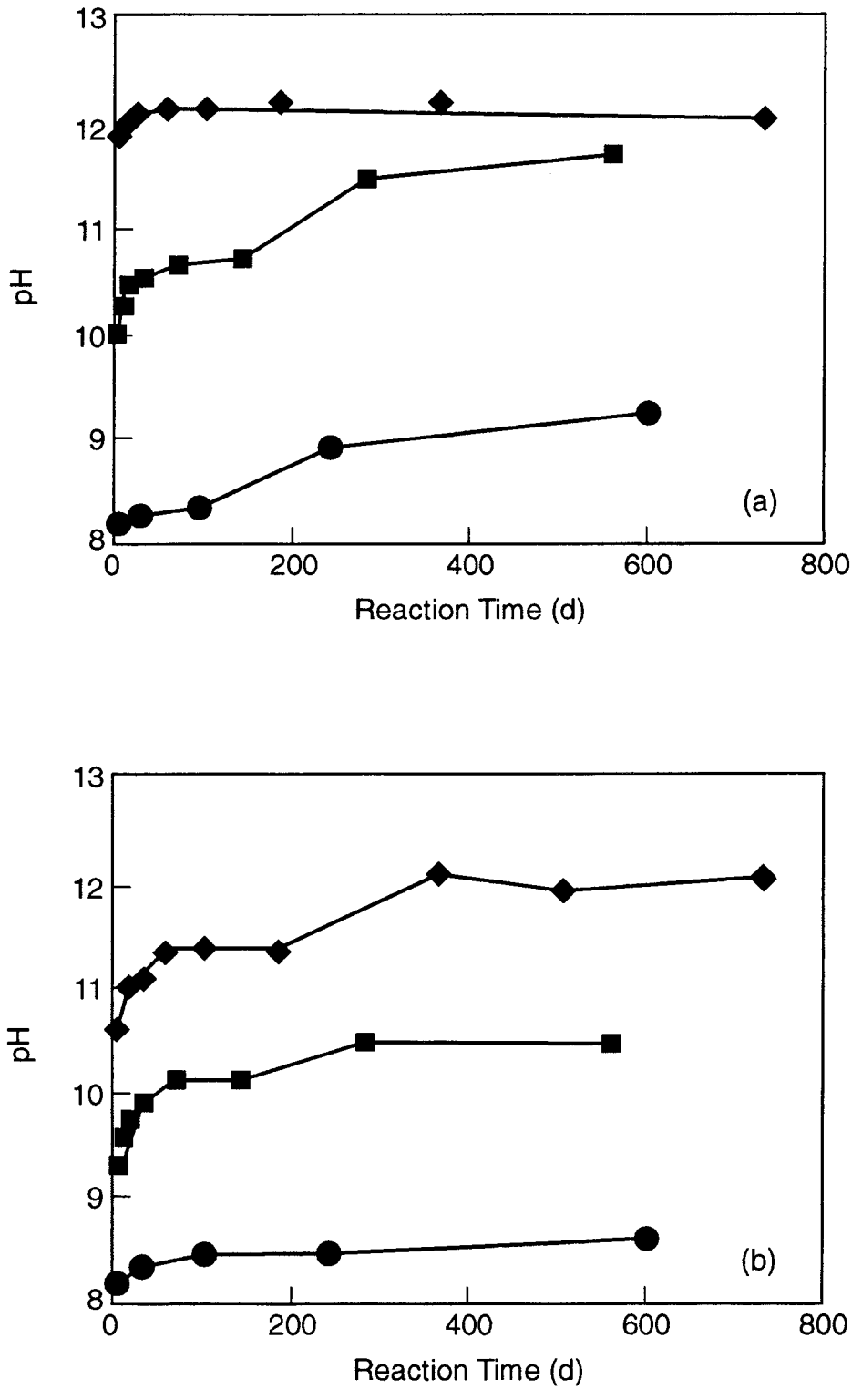

Figure 12-5. Leachate pH values (25 °C) versus reaction time for (a) SRL–131 glass and (b) SRL–202 glass reacted at 90 °C at (●) 10, (■) 2,000, and (◆) 20,000 m^{-1} (Ebert and Bates, 1993)

components released from the glass do not exceed the solubility limit. Figure 12-6 shows the normalized Na and Si release rates as a function of flow rate in SRL–131 glass. The curve shows two regions of leaching behavior. In region 1 the leach rate is proportional to flow rate up to 1 ml/hr, while, in region 2 beyond 10 ml/hr, the leach rate is nearly independent of flow rate. Figure 12-7 shows the time dependence on corrosion at various flow rates. At high flow rates, the corrosion proceeds at a maximum rate that depends on the leachate composition, pH, and temperature but is independent of the flow rate. At a low flow rate, reaction rate decreases with time. The flow rate representing the maximum corrosion rate is referred to as a forward reaction rate.

12.4.3 Effect of Temperature

In general, the temperature dependence of reaction rate is expressed through an Arrhenius equation of the type shown by Eq. (12-9).

$$k = A \times \mathrm{e}\frac{E}{RT} \tag{12-9}$$

where

- k — reaction rate constant or normalized release
- A — preexponential constant,
- E — activation energy,
- T — temperature
- R — gas constant.

Higher temperature is usually used as a method of accelerating the reactions, provided the reaction mechanism does not change over the range of temperature studied. Glass corrosion studies have been conducted from ambient temperatures to as high as 300 °C. However, most of the test methods are designed to study glass corrosion at 90 °C. Vernaz et al. (1988) studied the effect of temperature between 100 and 300 °C on R7T7 French HLW borosilicate glass. The glass samples were corroded for various time intervals. The data shown in figure 12-8 indicate two distinct corrosion mechanisms between 100 and 250 °C. The activation energy for the corrosion process was about 30 kJ/mol, while for a temperature greater than 250 °C, the activation energy increased to 150 kJ/mol. The corroded samples showed an increase in the thickness of the secondary phase layer from 1.5 to 30 μm when the temperature increased from 100 to 250 °C. The thickness of the secondary layer was almost 3 mm at 300 °C.

In addition, the leachate analysis showed that the effect of temperature on the release of various elements from the glass was not the same. Figure 12-9 shows the distribution of activation energies observed in various nuclear waste and natural glasses. The reported activation energy for glass corrosion ranges from 22 to 150 kcal/mol (U.S. Department of Energy, 1994). The wide range of activation energies is attributed not only to the complex nature of the glass corrosion mechanism but also to the effects of glass composition, contact solution chemistry, reaction time, and temperature. Therefore, temperature data should be extrapolated with care to assure the corrosion mechanisms do not change over the extrapolation range.

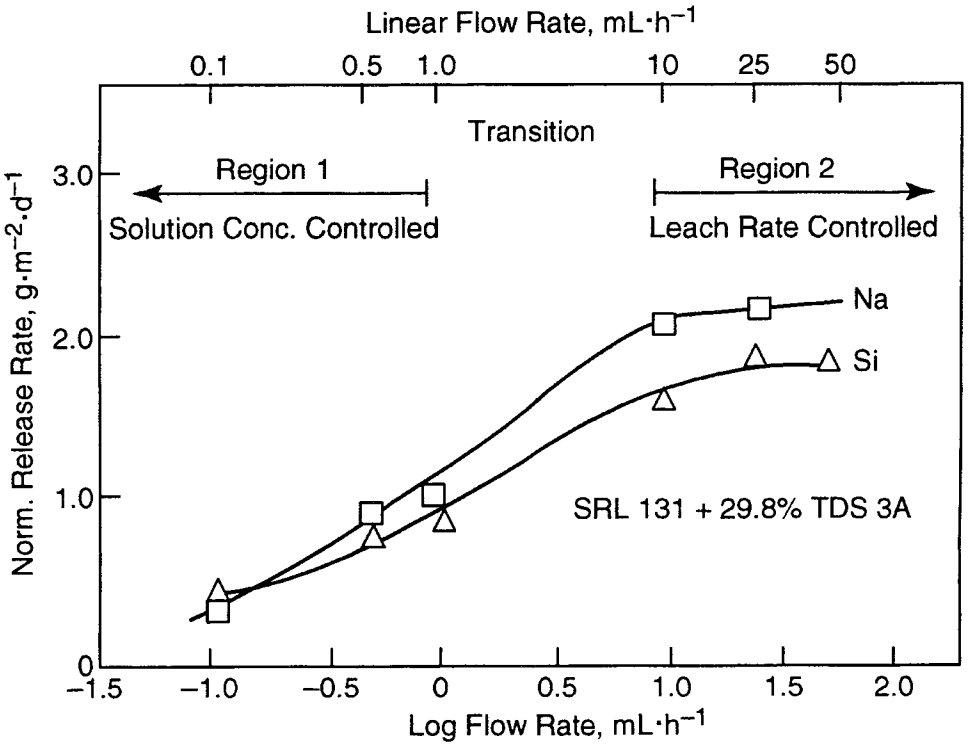

Figure 12-6. Normalized release rates of sodium and silicon as a function of leachant flow rates (Hench et al., 1986)

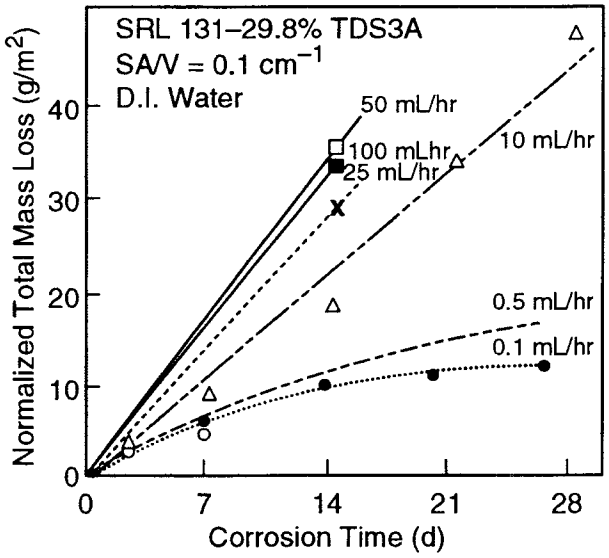

Figure 12-7. Normalized total mass loss versus leach time for various flow rates (Adiga et al., 1985)

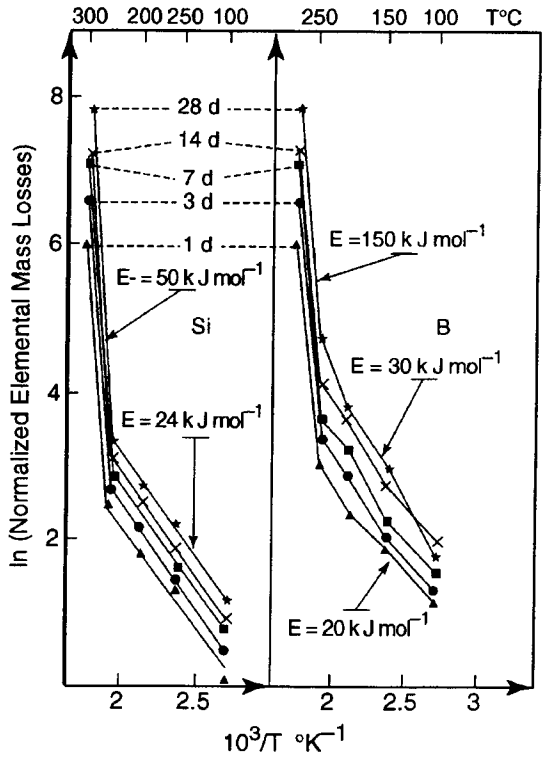

Figure 12-8. Normalized elemental mass loss versus temperature for different leaching durations (Vernaz et al., 1988)

12.4.4 Effect of Glass Composition

The chemical durability of a glass depends on its components. Because of the lack of a uniform testing and measurement approach to study durability-composition relationships, the data from various studies are difficult to compare quantitatively. Chemical durability-composition trends observed in various glass compositions are summarized here.

The chemical durability behavior of fused silica glass powder at 80 °C as a function of pH is shown in figure 12-2. Silica is a major component of all glass-forming systems. The data indicate that fused silica is fairly stable up to a pH of 9. Beyond pH 9, the network dissolution reactions, shown by Eqs. (12-5) and (12-6), are responsible for Si dissolution from glass. In glass systems xNa$_2$O•10CaO•(90−x)SiO$_2$ containing alkali ions, Clark et al. (1976) showed that as Na concentration increases, the durability sharply decreases. In Na-Ca silicate glass, Das (1980) showed that the rates of Na and Si release were different as a function of pH. The highest Na release rates were obtained in acidic conditions, while the highest Si release rates were obtained in alkaline solutions, as shown in figure 12-3. The chemical durability also depends on the particular alkali ion present. Dilmore et al. (1978a) showed that 15K$_2$O•10CaO•75SiO$_2$ glasses leach at a higher rate than 15Na$_2$O•10CaO•75SiO$_2$ glass and that mixed alkali glasses such as (15−x)Na$_2$O•xK$_2$O•10CaO•75SiO$_2$ are more durable than either Na or K end-members. The presence of more than one type of alkali in the glass suppresses the alkali leaching from the glass. This behavior is called the mixed-alkali effect. Clark et al. (1976) showed that the addition of a divalent cation, such as Ca, in glass significantly improves durability. The concentrations of Na and Si from 20Na$_2$O•80SiO$_2$ were 2.5 × 10^5 and 8.5 × 10^5 ppm after 12 hr, but in 20Na$_2$O•10CaO•70SiO$_2$ glass, the concentration was only 566 ppm after 9 d. Similarly, Smets and

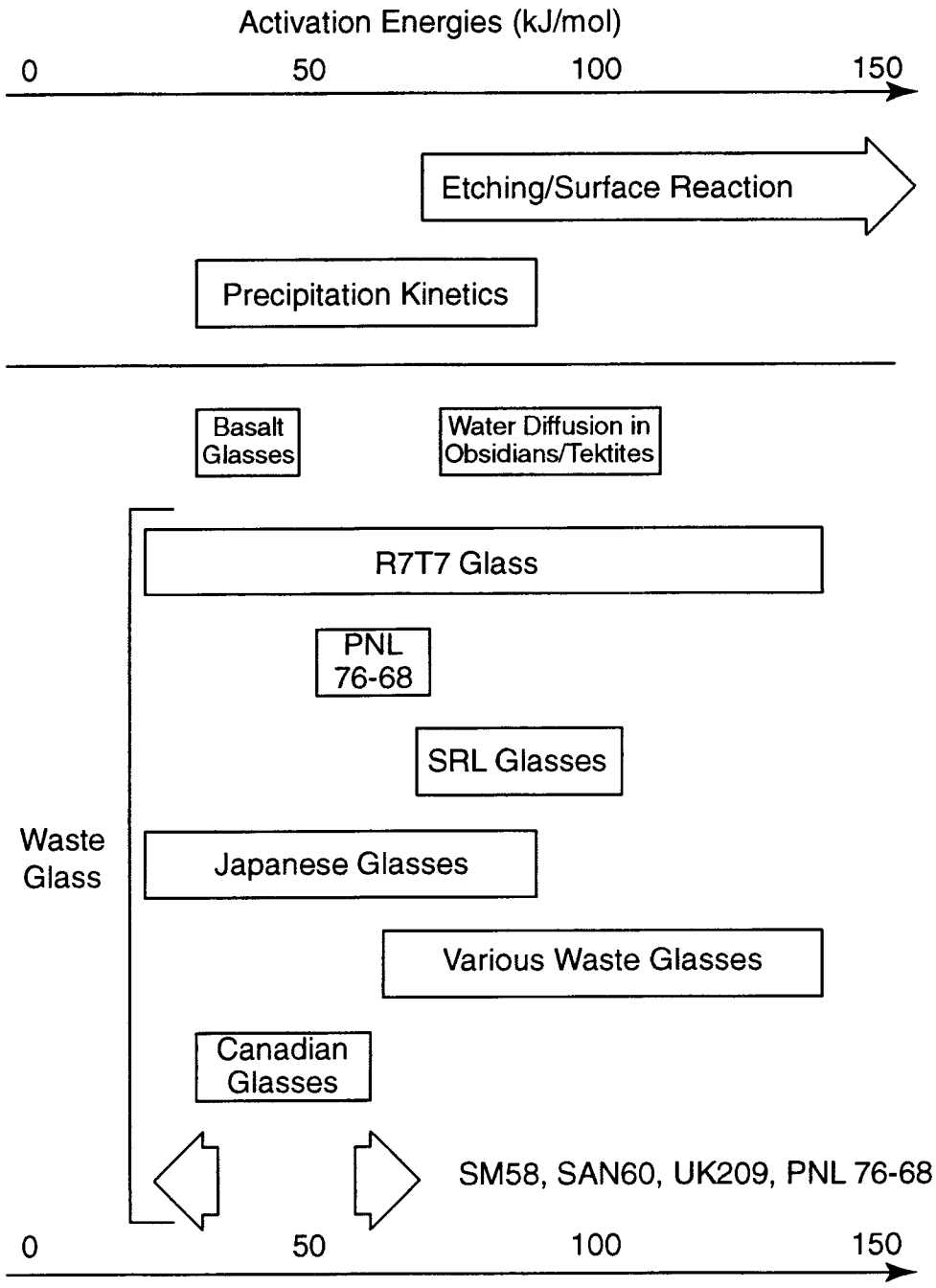

Figure 12-9. Summary diagram indicating reported activation energies for individual reaction processes and overall activation energies for high-level waste glass studies (U.S. Department of Energy, 1994)

Tholen (1984) showed that in $20Na_2O•10MO•70SiO_2$ glass (where M = Ca, Mg, or Zn), glass durability as measured by Na remaining in the glass decreased with the presence of Ca, Mg, and Zn, in order. This study also indicated that the most drastic changes were observed at low concentrations of the divalent ions.

In alkali borosilicate glasses, depending on the alkali/boron ratio, boron is either incorporated in the structure as tetrahedrally coordinated BO_4 species or trigonally coordinated BO_3 species. Adams and Evans (1978) studied durability/composition relationships by reacting the glasses in a Na_2O-B_2O_3-SiO_2 system at 25 °C for 24 hr. Their study showed that the glass compositions that maximize the concentration of BO_4 tetrahedra tend to have the highest durabilities. Bunker et al. (1986) reached a similar conclusion in their durability study on a Na_2O-B_2O_3-SiO_2 glass system containing 60 mol% SiO_2 as a function of Na_2O/B_2O_3 ratio and as a function of SiO_2 for $Na_2O/B_2O_3 = 1$. They showed that in samples with Na_2O/B_2O_3 ratios $<<1$, Na and B were preferentially leached from the glasses. However, in glasses with $Na_2O/B_2O_3 \geq 1$, Na and B leached congruently in alkaline solutions. In addition, the glasses with $Na_2O/B_2O_3 = 1$ were orders of magnitude more durable than glasses with a lower or higher Na_2O/B_2O_3 ratio.

In short-term durability tests (less than 1 hr) of an alkali aluminosilicate [$20Na_2O•xAl_2O_3•(1-x)SiO_2$] system, Smets and Lommen (1982) showed the depth of the Na depletion decreased significantly with an increase in the Al_2O_3 concentration. The greatest change in depth of Na depletion was obtained with small amounts of added Al_2O_3, while for $x = 5$ or 10, the Na profile showed no measurable change. Similarly, for Li_2O-Al_2O_3-SiO_2 glasses, Dilmore et al. (1978b) conducted durability tests at 100 °C for 41 d and showed that as the Al_2O_3 concentration increases in the glass, Li ions released in the leachate solution decreased. In alkali borosilicate glasses, depending on the alkali/alumina ratio, alumina is incorporated in the structure either as a tetrahedrally coordinated AlO_4 species (similar to B) or as a six-fold coordinated modifier in the absence of alkali ions in the glass structure. The improvement in durability is attributed to the formation of AlO_4 tetrahedra whose charge is balanced by alkali ions and forms an AlO_4Na bond, which is much stronger than NBO (≡Si-O-Na) bond.

In alkali iron silicates, the fraction of Fe^{3+} ions that are stabilized by alkali ions in tetrahedra coordination depends on the redox [Fe^{2+}/Fe^{3+} or $Fe^{2+}/Fe^{(total)}$] ratio in the glass. As the redox ratio increases or Fe^{3+} ions decrease, the number of FeO_4 tetrahedra decreases. Feng et al. (1988) studied the effect of the redox ratio [$Fe^{2+}/Fe^{(total)}$] on durability using the MCC–3 test on WV–205 simulated nuclear waste glass. The durability behavior is shown in figure 12-10. The normalized Na concentration increases sharply as the samples are reduced. The decrease in durability is attributed to the fact that, as the redox ratio increases, more alkali ions attach as NBO (≡Si-O-Na) to Si and fewer attach to the FeO_4 (FeO_4-Na) tetrahedra in the glass.

Feng et al. (1989) performed a study on WV–205 glass by systematically varying major components by small concentrations and measuring durability using the MCC–3 test at 90 °C at various time intervals up to 180 d in deionized water. Figures 12-11, 12-12, and 12-13 show the effect of small additions of SiO_2, ZrO_2 and Al_2O_3, respectively, to WV–205 glass. The trends indicate that a significant increase in durability occurs with small additions of SiO_2, ZrO_2, and Al_2O_3, followed by a plateau region with a constant high durability. Feng et al. (1989) explained the effect based on the deficiency of network formers. In the nondurable glass region, the glasses can be considered deficient in network formers and, therefore, can be quickly attacked by water. Ellison et al. (1994) analyzed Feng et al. (1989) data and showed that WV–205 composition had a (Na+K+Li)/(B+Al) ratio of 1.8 and (Na+K+Li)/(B+Al+Fe) ratio of 1.3, which is significantly higher

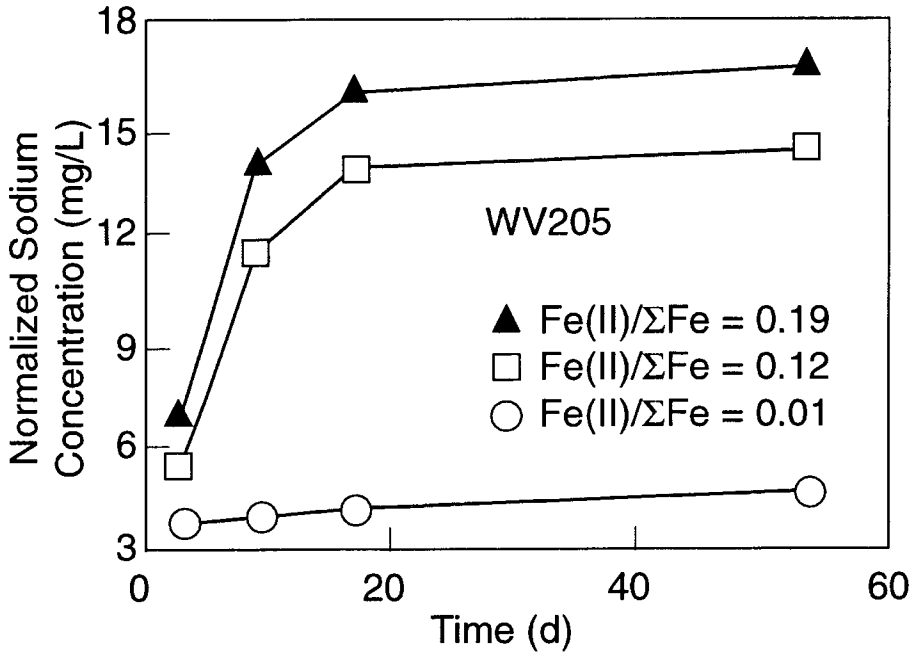

Figure 12-10. Leaching (MCC–3 test, 90 °C) of WV–205 glass as a function of glass redox state (Feng et al., 1988)

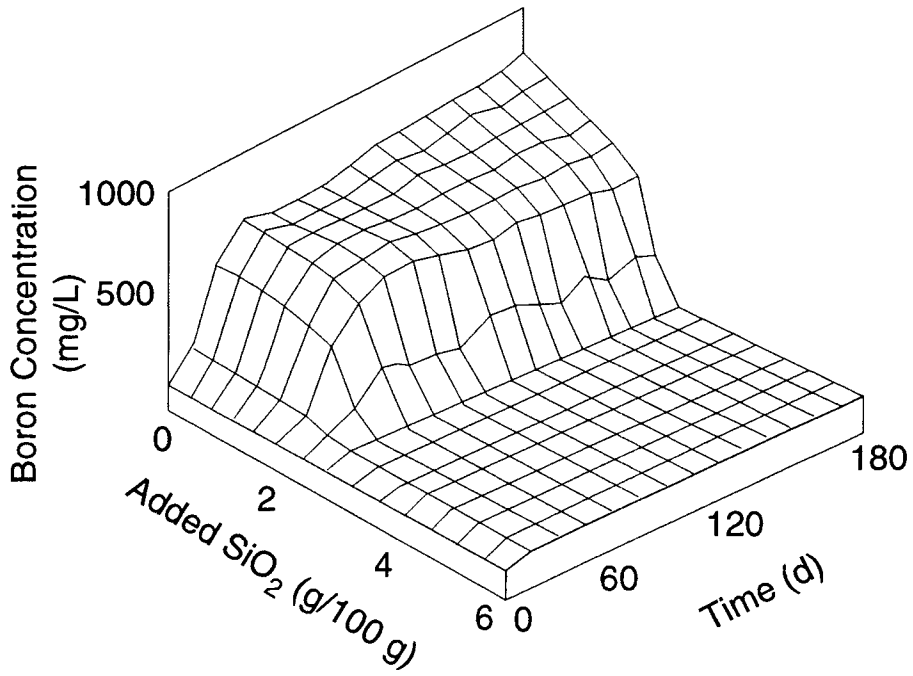

Figure 12-11. Interpolated surface showing the dependence of MCC–3 boron concentration on test time and amount of SiO_2 added to WV–205 (Feng et al., 1989)

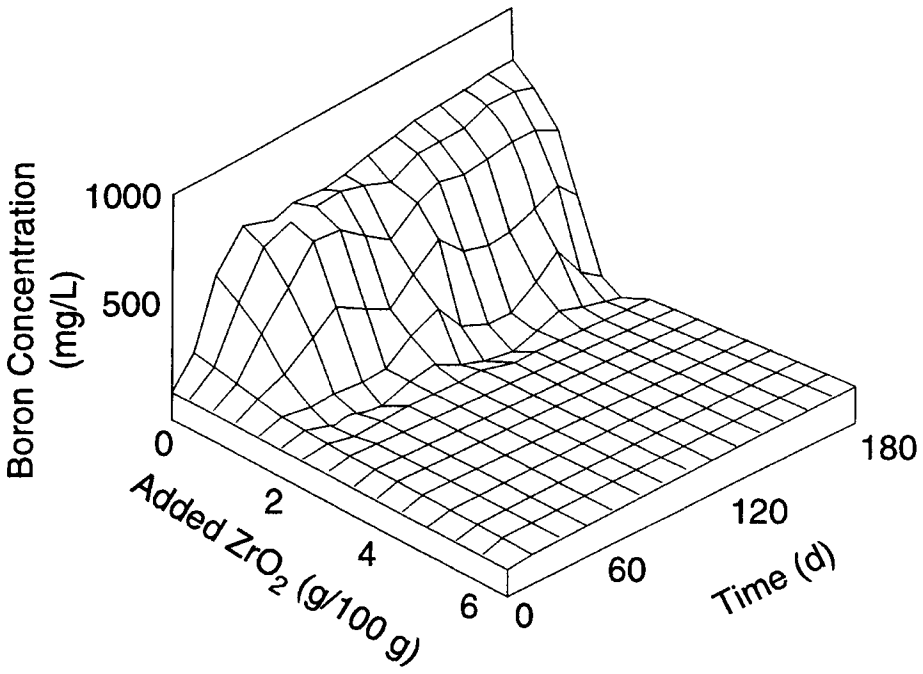

Figure 12-12. Interpolated surface showing the dependence of MCC–3 boron concentration on test time and amount of ZrO_2 added to WV–205 (Feng et al., 1989)

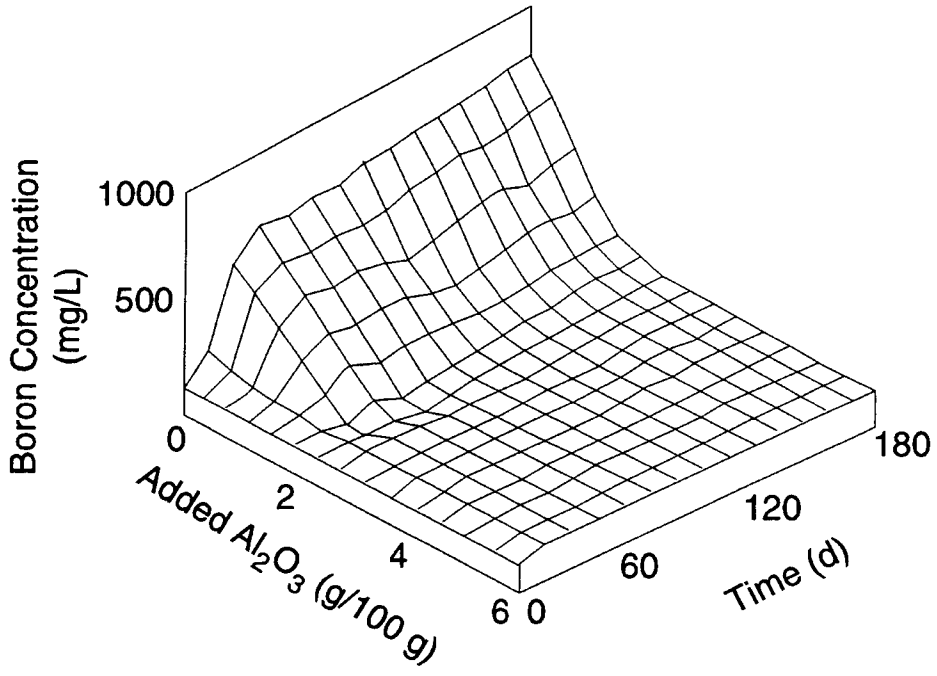

Figure 12-13. Interpolated surface showing the dependence of MCC–3 boron concentration on test time and amount of Al_2O_3 added to WV–205 (Feng et al., 1989)

than one. Thus, small additions of network formers were able to significantly improve the durability of the glasses.

Nuclear waste glasses contain alkalis (Li, Na, K, Cs), oxides, divalent (Ca, Mg, Sr, Ba) oxides, Al_2O_3, B_2O_3, Fe_2O_3, SiO_2, ZrO_2, and many minor components. The interactions between components make the assessment of the composition/durability relationship challenging. Extensive work has been done to evaluate composition effects in nuclear waste glasses. The review of every waste glass system is beyond the scope of this report. Table 12-2 summarizes the effect of various components on glass durability from several studies. The composition/durability studies indicate that the greatest improvements in durability result from the components that form the strongest bonds. For example, the durability of alkali silicate glass is improved by adding Al_2O_3, B_2O_3, Fe_2O_3, ZrO_2, or divalent cations (Ca, Mg, Zn, etc.) (shown in order of decreasing effect). The mechanism in each case is a formation of bonds stronger than the alkali-NBO bond in simple alkali silicate glass. The addition of Al_2O_3, B_2O_3, or Fe_2O_3 removes one NBO bond and, to compensate, alkali ions attach to AlO_4, BO_4, or FeO_4 tetrahedras.

12.4.5 Effect of Contact Solution

The nature of the solution in contact with glass has a significant effect on chemical durability. Feng and Pegg (1994) leached simulated nuclear waste glass, WV–205, in the presence of various alkali nitrate solutions at 90 °C. Figure 12-14 shows the effect of various alkali nitrates on the Si leach rate. The Si leach rates in various solutions were less than half those in deionized water. Reduced leaching in the presence of a salt solution is attributed to the ion-exchange reaction shown in Eq. (12-10)

$$\equiv \mathrm{Si} - \mathrm{O}^- M_2^+ + M_1^+ \leftrightarrow \equiv \mathrm{Si} - \mathrm{O}^- M_1^+ + M_2^+ \qquad (12\text{-}10)$$

where M_1 is the alkali cation in solution and M_2 is the alkali cation in glass. The ion-exchange reaction shown by Eq. (12-10) does not result in network hydrolysis as shown by Eqs. (12-3) and (12-4), or increase the pH of the solution. However, the reaction competes with and suppresses the network hydrolysis reaction, thus lowering the Si dissolution rate. Barkett et al. (1989) showed that simulated nuclear waste glasses leached in Pacific Coast seawater have almost two orders of magnitude lower Si and Al release rates and one order of magnitude lower B and alkali compared to the leach rates observed in deionized water. However, a recent study by Wickert et al. (1999) showed a significant increase in the dissolution rate of soda lime silicate glass with increasing NaCl concentration in the leachate. Wickert et al. (1999) attributed the increase in the leaching rate to the replacement of H ions by alkali, ions on the surface sites, which facilitates the access of aqueous medium in to Si-O-Si network.

Several studies have been conducted to determine the effect of container materials and corrosion products on glass dissolution behavior. McVay and Buckwalter (1983) and Burns et al. (1986) studied the effect of metals on glass dissolution behavior. While the former showed higher glass dissolution in the presence of ductile iron, the latter showed no significant effect on glass dissolution from 304L stainless steel and 409 and 430 ferrite steels. In addition, Burns et al. (1986) showed that A516 carbon steel had a significant detrimental effect on glass dissolution. Inagaki et al. (1996), Bart et al. (1997), and Werme et al. (1983) studied the effect of magnetite on glass dissolution behavior. Magnetite is considered a primary corrosion product, and for many disposal systems these studies showed that glass dissolution is enhanced by the presence of magnetite. Werme et al. (1983) also studied the effect of FeOOH and concluded that glass

Table 12-2. Leaching experimental results after varying composition (U.S. Department of Energy, 1994)

Composition Change	Durability	Glass Composition	Reference
(Ca, Mg, Zn) for Si	Increases	Simple glass	1
(Mg, Ca) for Si	Increases	Simple glass	2
Ca for Si	Increases	Simple glass	3
(Sr, Ba) for Si	Decreases	Simple glass	2
(Na, K, Li) for Si	Decreases	Simple glass	4
Na for Si	Negligible	Waste glass	5
Al for Si	Increases	Simple glass	6
Ca for (Na, K)	Decreases	Waste glass	5
Na for Al	Negligible	Waste glass	5
Na for K	Variable	Mixed alkali effect	7
Na for K	Negligible	No mixed alkali effect	5
Al for Fe	Increases	Waste glass	8
Fe^{3+} for Zn	Decreases	Waste glass	9
Increase (Si, Al, Zr)	Increases	Waste glass	10, 11
Increase Al	Increases	Waste glass	12
Increase (Al, Cr, Si)	Increases	Waste glass, MCC–1 tests	13
Increase Al	Decreases	Waste glass, acid leachate	13
Increase B	Decreases	Waste glass	13
Increase B	Increases	Waste glass	10
Increase (Na, Li)	Decreases	Waste glass	14
Increase Alkali	Decreases	Waste glass	10, 11
Increase (Na, Ca)	Decreases	Waste glass, MCC–1 tests	13
Increase (Mg, Ca)	Negligible	Waste glass	10
Increase Ti	Variable	Waste glass	11

Table 12-2. Leaching experimental results after varying composition (U.S. Department of Energy, 1994) (cont'd)

Composition Change	Durability	Glass Composition	Reference
Increase Ti	Increases	Waste glass	13
Increase (Cu, Cr, Ni)	Negligible	Waste glass	11
Increase La	Increases	Waste glass	11
Increase Zn	Decreases	Waste glass, MCC–1 tests	13
Increase Zn	Decreases	Waste glass	11
Fe^{3+} for Fe^{2+}	Increases	Waste glass	10
Fe^{3+} for Fe^{2+}	Negligible	Waste glass	8

1 Smets, B.M., M.G.W. Tholen, and T.P.A. Lommen. The effect of divalent cations on the leaching kinetics of glass. *J. Non-Crys. Sol.* 65: 319–332. 1984.

2 Isard, J.O., and W. Muller. Influence of alkaline earth ions on the corrosion of glasses. *Phys. Chem. Glasses* 27(2): 55–58. 1986.

3 Rana, M.A., and R.W. Douglas. The reaction between glass and water—Part I: Experimental methods and observations. *Phys. Chem. Glasses* 2(6): 179–195. 1961a.
Rana, M.A., and R.W. Douglas. The reaction between glass and water—Part 2: Discussion of the results. *Phys. Chem. Glasses* 2(6): 196–204. 1961b.

4 Douglas, R.W., and T.M.M. El-Shamy. Reactions of glasses with aqueous solutions. *J. Am. Ceram. Soc.* 50(1): 1–8. 1967.

5 Tait, J., and D.L. Mandelosi. *The Chemical Durability of Alkali Aluminosilicate Glasses.* Atomic Energy of Canada Limited Report AECL–7803. Pinawa Manitoba, Canada: Atomic Energy of Canada Limited. 1983.

6 Smets, B.M.J., and T.P.A. Lommen. The leaching of sodium aluminosilicate glasses studied by secondary ion mass spectrometry. *Phys. Chem. Glasses* 23(3): 83–87. 1982.

7 Dilmore, M.F., D.E. Clark, and L.L. Hench. Chemical durability of Na_2O-K_2O-CaO-SiO_2 glasses. *J. Am. Ceram. Soc.* 61: 439–443. 1978.

8 Van Iseghem, P., and R. de Batist. Corrosion mechanisms of simulated high level nuclear waste glasses in distilled water. *Riv. Della Staz. Sper. Vetro* 5: 163–170. 1984.

9 Nogues, J.L., and L.L. Hench. Effect of Fe_2O_3/ZnO on two glass compositions for solidification of Swedish nuclear wastes. *Proceedings of the Materials Research Society Symposium.* Symposium Proceedings 11. Pittsburgh, PA: Materials Research Society: 273–278. 1982.

10 Feng, X., I.L. Pegg, Y. Guo, Aa. Barkatt, P.B. Macedo, S.J. Cucinell, and S. Lai. Correlation between composition effects on glass durability and the structural role of the constituent oxides. *Nucl. Technol.* 85: 334–345. 1989.

11 Macedo, P.B., S.M. Finger, A.A. Barkatt, I.L. Pegg, X. Feng, and W.P. Freeborn. *Durability Testing with West Valley Borosilicate Glass Composition—Phase II.* West Valley Nuclear Services Topical Report DOE/NE/44139-48. West Valley, NY: West Valley Nuclear Services, Inc.. 1988.

12 Nogues, J.L., L.L. Hench, and J. Zarzycki. Comparative study of seven glasses for solidification of nuclear wastes. *Proceedings of the Materials Research Society Symposium.* Symposium Proceedings: 11. Pittsburgh, PA: Materials Research Society: 211–218. 1982.

13 Chick, L.A., G.F. Piepel, G.B. Mellinger, R.P. May, W.J. Gray, and C.Q. Buckwalter. *The Effects of Composition on Properties in an 11-Component Nuclear Waste Glass System.* Pacific Northwest Laboratory Report PNL–3188. Richland, WA: Pacific Northwest National Laboratory. 1981.

14 Diebold, F.E., and J.K. Bates. Glass-water vapor interaction. *Adv. in Ceram.* 20: 515–522. 1986.

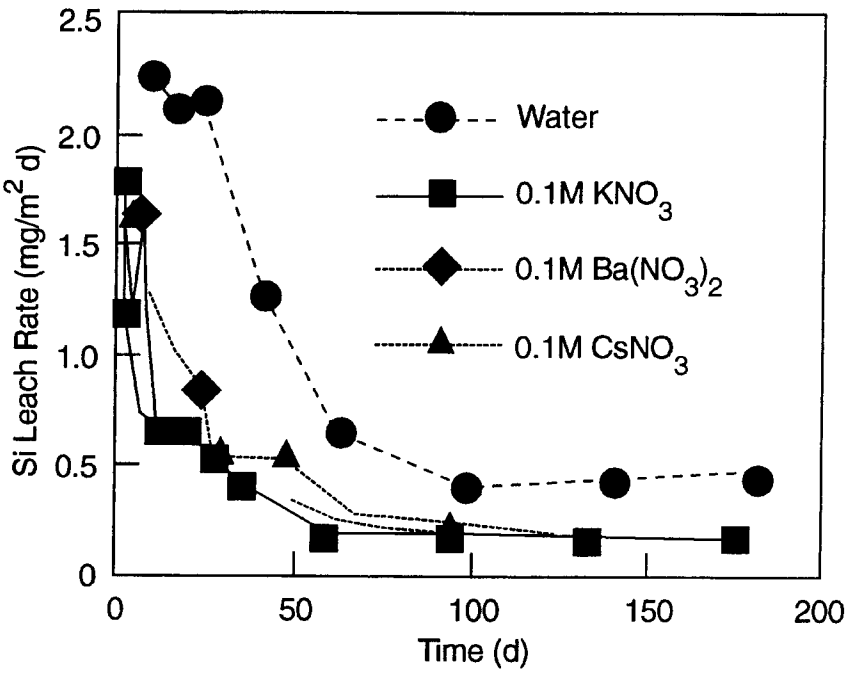

Figure 12-14. The Si leach rates (mg/m²/d) of glass WV–205 in deionized water, 0.1 M KNO_3, 0.1 M $Ba(NO_3)_2$ and 0.1 M $CsNO_3$ solutions at neutral pH for up to 200 d of leaching

dissolution is higher in the presence of FeOOH than in the presence of the same amount of magnetite. These studies clearly establish the effect of magnetite and FeOOH on enhancing glass dissolution. Pan et al.[1] studied the behavior of simulated waste glass samples from WVDP and DWPF by subjecting them to long-term leaching tests in the presence of $FeCl_2$ and $FeCl_3$ at 90 °C, to simulate a corroded waste package (WP) environment. Ferrous and ferric chlorides were selected because chloride is the primary ion responsible for WP corrosion. Results, as indicated in figure 12-15, showed substantially higher initial normalized release for B and alkali, approximately a factor of 50 to 70 times greater than those in deionized water in 0.25-M $FeCl_3$ solutions. The initial leaching rate (figure 12-16) for B and alkali was found to be pH-dependent and decreased as the leachate pH was increased. While the leach rate for Si did not show any significant change in the pH range studied, the leach rate for Al showed a minimum. The minimum for the leach rate of Al occurred at different pH values. The study indicates that elements in the glass matrix are released incongruently.

As indicated by several studies, the contact solution has a significant effect on the glass dissolution. Studies, however, fail to indicate specific trends in the dissolution behavior in the presence of various salts or components in the contact solution.

---

[1]Pan, Y.-M., V. Jain, M. Bogart, and P. Deshpande. Effect of iron chlorides on the dissolution behavior of simulated high-level waste glasses. *Ceramic Transactions of the Environmental Issues and Waste Management Technologies in the Ceramic and Nuclear Industries VI, St. Louis, Missouri, April 30–May 3, 2000.* Ceramic Transactions Volume 119. D. Spearing and V. Jain, eds. Westerville, OH: American Ceramic Society. In press.

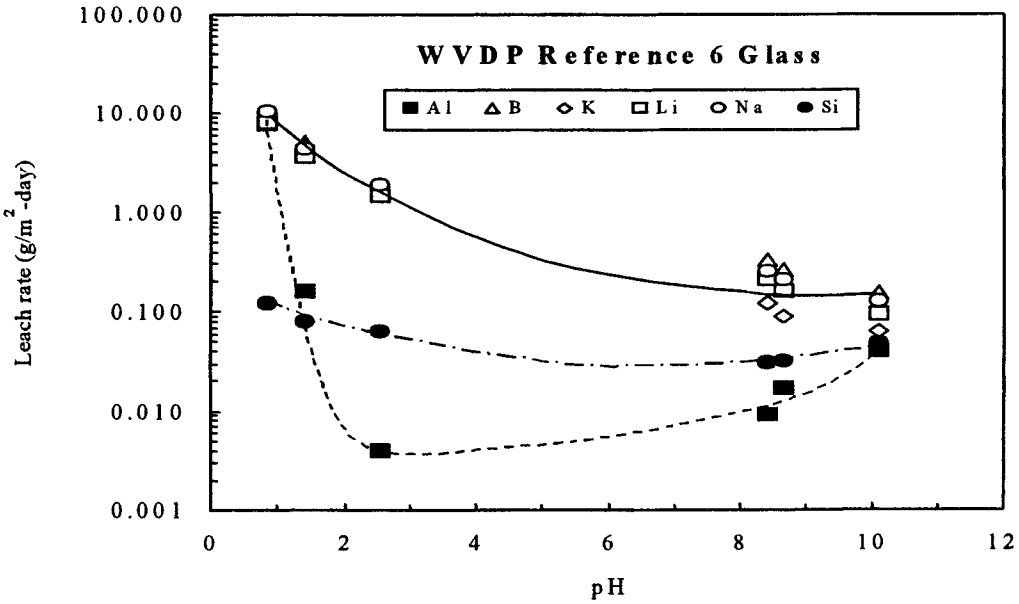

Figure 12-15. Cumulative normalized leach concentration for boron versus time for the West Valley Demonstration Project (WVDP) glass in various solutions[2]

12.5 CHEMICAL DURABILITY MODELS

12.5.1 General Chemical Durability Models

Several attempts have been made to correlate chemical durability and glass composition. In this section, proposed empirical and thermodynamic relationships for durability behavior are reviewed. The models discussed assume that the glass is homogeneous and crystal free. In addition, the models only apply to normalized release measured in static tests of fixed duration, and there is no correlation between data collected using static tests and long-term durability. Static tests can only verify product consistency and can not be regarded as an accurate measure of relative durability of a glass.

The free energy of hydration (FEH) model was initially developed by Paul (1977) for simple alkali silicate glasses and later extended by Jantzen (1992) to complex borosilicate-based waste glasses. FEH relates the thermodynamic properties of glasses to their dissolution rates as measured in short-term, closed-system tests such as MCC–1 and PCT. FEH treats glasses as solids composed of mechanical mixtures of silicate and oxide components as shown in table 12-3. The net free energy change (ΔG_{hyd}) is calculated as

$$\Delta G_{hyd} = \Sigma x_i \bullet (\Delta G_{hyd})_i \qquad (12\text{-}11)$$

[2]Jain, V., and Y.-M. Pan. High-Level waste glass dissolution in simulated internal waste package environments. *Proceedings of the Atalante 2000 Conference, October 24–26, 2000.* Avignon, France. In press.

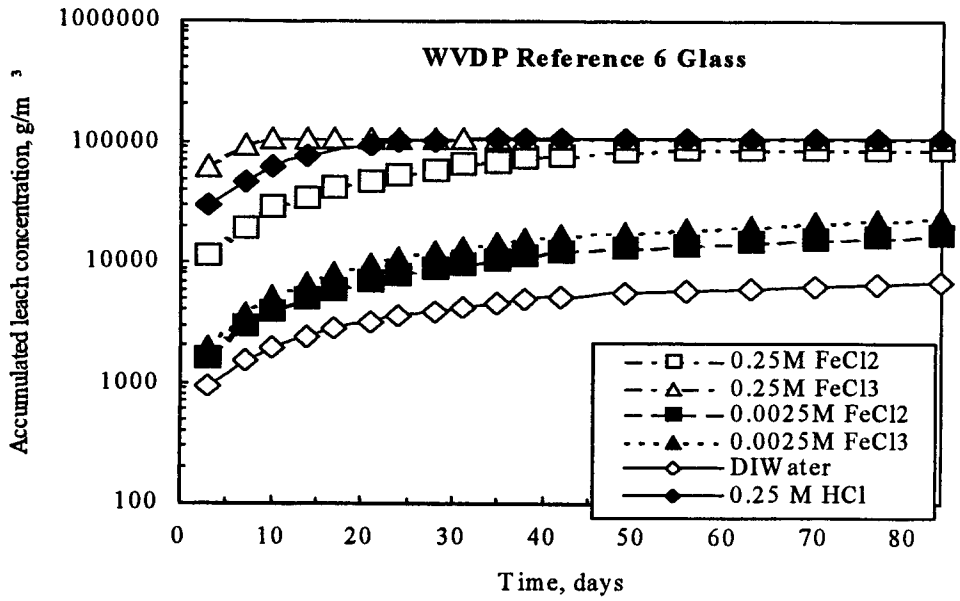

Figure 12-16. Normalized leach rate for various elements versus leachate pH after the first solution replacement for West Valley Demonstration Project (WVDP) glass[3]

where $(\Delta G_{hyd})_i$ is the free energy change in kcal/mol of the thermodynamically most stable hydration reaction of the structurally associated silicate and oxide of component i having mol fraction x_i. The model assumes that the choice of structural units is adequate and that free energy of mixing of the components in the glass can be neglected. The original approach of Paul (1977) assumed that the silicate and borate components of a glass hydrate to silicic and boric acid. However, for low-durability glasses where alkali released from the glass increases the pH of the solution >9.5, the solubilities of silica and borate rapidly increase. Therefore, additional contribution to the FEH should be included to account for silicic and boric acid dissolution at pH 9.5. The additional contribution is calculated by

$$\Delta(\Delta G_{hyd}) = 1.364\left[-\log\left(1+\frac{10^{-10}}{10^{-pH}}+\frac{10^{-21.994}}{10^{-2pH}}\right)\right] \text{ for } \quad H_2SiO_3 \qquad (12\text{-}12)$$

and

$$\Delta(\Delta G_{hyd}) = 1.364\left[-\log\left(1+\frac{10^{-9.18}}{10^{-pH}}+\frac{10^{-21.89}}{10^{-2pH}}+\frac{10^{-35.69}}{10^{-3pH}}\right)\right] \text{ for } \quad H_2BO_3 \qquad (12\text{-}13)$$

[3]Jain, V., and Y.-M. Pan. High-Level waste glass dissolution in simulated internal waste package environments. *Proceedings of the Atalante 2000 Conference, October 24–26, 2000.* Avignon, France. In press.

Table 12-3. Primary basis set of partial molar hydration free energies, ΔG_i, for glass in oxidized pH regimes >7 (Jantzen et al., 1998)*

Hydration Reactions	ΔG_i kcal/mole	pH Range
$Al_2O_3 + H_2O \leftharpoondown 2AlO_2^-{}_{(aq)} + 2H^+{}_{(aq)}$	+37.68	7–14
$AmO_2 + 3H_2O \leftharpoondown Am(OH)_5^-{}_{(aq)} + H^+{}_{(aq)}$	+23.68	7–14
$As_2O_3 + 3H_2O + O_2 \leftharpoondown 2HAsO_4^{-2}{}_{(aq)} + 4H^+{}_{(aq)}$	-33.65	7–11
$B_2O_3 + 3H_2O \leftharpoondown 3H_3BO_{3(aq)}$	-10.43	7–10
$\{BaO + SiO_2\} + 2H_2O \leftharpoondown Ba(OH)_2 + H_2SiO_{3(aq)}$	-19.13	7–14
$\{CaO + SiO_2\} + 2H_2O \leftharpoondown Ca(OH)_2 + H_2SiO_{3(aq)}$	-9.74	7–14
$\{CdO + SiO_2\} + 2H_2O \leftharpoondown Cd(OH)_2 + H_2SiO_{3(aq)}$	+2.31	7–14
$Ce_2O_3 + 3H_2O \leftharpoondown 2Ce(OH)_3$	-44.99	7–14
$\{CoO + SiO_2\} + \frac{5}{2}H_2O + \frac{1}{4}O_2 \leftharpoondown Co(OH)_3 + H_2SiO_{3(aq)}$	-2.33	7–14
$Cr_2O_3 + 3H_2O \leftharpoondown 2Cr(OH)_3$	+11.95	7–14
$\{Cs_2O + SiO_2\} + 2H_2O \leftharpoondown 2Cs^+{}_{(aq)} + 2OH^-{}_{(aq)} + H_2SiO_{3(aq)}$	-76.33	7–14
$\{Cu_2O + SiO_2\} + \frac{1}{2}O_2 + 3H_2O \leftharpoondown 2Cu(OH)_2 + H_2SiO_{3(aq)}$	-18.85	7–14
$\{CuO + SiO_2\} + 2H_2O \leftharpoondown Cu(OH)_2 + H_2SiO_{3(aq)}$	+5.59	7–14
$\{FeO + SiO_2\} + \frac{1}{4}O_2 + \frac{5}{2}H_2O \leftharpoondown Fe(OH)_3 + H_2SiO_{3(aq)}$	-17.28	7–14
$Fe_2O_3 + 3H_2O \leftharpoondown 2Fe(OH)_3$	+14.56	7–14
$\{K_2O + SiO_2\} + 2H_2O \leftharpoondown 2K^+{}_{(aq)} + 2OH^-{}_{(aq)} + H_2SiO_{3(aq)}$	-72.36	7–14
$La_2O_3 + 3H_2O \leftharpoondown 2La(OH)_3$	-48.59	7–14
$\{Li_2O + SiO_2\} + 2H_2O \leftharpoondown 2Li^+{}_{(aq)} + 2OH^-{}_{(aq)} + H_2SiO_{3(aq)}$	-19.99	7–14
$\{MgO + SiO_2\} + 2H_2O \leftharpoondown Mg(OH)_2 + H_2SiO_{3(aq)}$	-2.52	7–14
$\{MnO + SiO_2\} + \frac{1}{2}O_2 + H_2O \leftharpoondown MnO_2 + H_2SiO_{3(aq)}$	-20.39	7–14
$MoO_3 + H_2O \leftharpoondown 2H^+{}_{(aq)} + MoO_4^{-2}{}_{(aq)}$	+16.46	7–14

Table 12-3. Primary basis set of partial molar hydration free energies, ΔG_i, for glass in oxidized pH regimes >7 (Jantzen et al., 1998)* (cont'd)

Hydration Reactions	ΔG_i kcal/mole	pH Range
$\{Na_2O + SiO_2\} + 2H_2O \rightarrow 2Na^+_{(aq)} + 2OH^-_{(aq)} + H_2SiO_{3(aq)}$	-49.04	7–14
$Nd_2O_3 + 3H_2O \rightarrow 2Nd(OH)_3$	-37.79	7–14
$\{NiO + SiO_2\} + 2H_2O \rightarrow Ni(OH)_2 + H_2SiO_{3(aq)}$	+4.42	7–14
$P_2O_5 + 3H_2O \rightarrow 2HPO_4^{-2}{}_{(aq)} + 4H^+_{(aq)}$	-26.55	7–12
$\{PbO + SiO_2\} + 2H_2O \rightarrow HPbO_2^-{}_{(aq)} + H_2SiO_{3(aq)} + H^+_{(aq)}$	+25.10	7–14
$PuO_2 + 3H_2O \rightarrow Pu(OH)_5^-{}_{(aq)} + H^+_{(aq)}$	+30.75	7–14
$\{Rb_2O + SiO_2\} + 2H_2O \rightarrow 2Rb^+_{(aq)} + 2OH^-_{(aq)} + H_2SiO_{3(aq)}$	-82.18	7–14
$RuO_2 + \frac{1}{2} O_2 + H_2O \rightarrow RuO_4^-{}_{(aq)} + 2H^+_{(aq)}$	+57.30	7–10
$Sb_2O_3 + O_2 + H_2O \rightarrow 2SbO_3^-{}_{(aq)} + 2H^+_{(aq)}$	-37.56	7–14
$SeO_2 + \frac{1}{2} O_2 + H_2O \rightarrow SeO_4^{-2}{}_{(aq)} + 2H^+_{(aq)}$	-7.80	7–14
$SiO_2\ H_2O \rightarrow H_2SiO_{3(aq)}$	+4.05	7–10
$SnO_2 + 2H_2O \rightarrow Sn(OH)_4$	+10.16	7–12
$\{SrO + SiO_2\} + 2H_2O \rightarrow Sr(OH)_2 + H_2SiO_{3(aq)}$	-15.16	7–14
$TcO_2 + \frac{1}{2} O_2 + H_2O \rightarrow TcO_4^-{}_{(aq)} + 2H^+_{(aq)}$	-2.04	7–14
$TeO_2 + \frac{1}{2} O_2 + H_2O \rightarrow TeO_4^{-2}{}_{(aq)} + 2H^+_{(aq)}$	+12.02	7–14
$ThO_2 + H_2O \rightarrow Th(OH)_4$	+19.23	7–14

*Jantzen, C.M., J.B. Pickett, K.G. Brown, and T.B. Edwards. *Method of Determining Glass Durability*. Patent No. 5,846,278. Aiken, SC: Westinghouse Savannah River Company. 1988.

Linear relationships shown by Eqs. (12-12) and (12-13) were developed between the logarithmic normalized release from the glass in g-glass/m^2 and the calculated ΔG_{hyd} including the effect of silicic and boric acid. Figure 12-17 shows normalized B and Si release for more than 300 data points collected using the MCC–1 test for 28 d at 90 °C as a function corrected FEH. The relationship statistically showed that release rate was better correlated with corrected FEH than uncorrected FEH. The more negative the FEH, the less durable the glass. Glasses, such as natural obsidians, tektites, basalts, silica, pyrex, window glass, and ancient Roman and Islamic glasses, were included in the study. The relationship between the Si and B normalized release and the adjusted ΔG_{hyd} is

$$\log(NL_{Si}) = -0.2240\Delta G_{hyd} - 0.0448 \qquad r^2 = 0.73 \tag{12-14}$$

$$\log(NL_{B}) = -0.2795\Delta G_{hyd} + 0.2147 \qquad r^2 = 0.59 \tag{12-15}$$

where N_{Li} is the normalized release in g-glass/m^2 for component *i*. Jantzen et al.[4] refined the FEH model for predicting durabilities of the HLW glasses produced at DWPF. The refined thermodynamic hydration energy reaction model (THERMO) calculates the FEH, ΔG_f, as

$$\Delta G_f = \Delta G_p + \Delta G_a^{WA} + \Delta G_a^{SB>11} + \Delta G_a^{SB>12} \tag{12-16}$$

where, ΔG_p is the FEH, in kcal/100 gm-glass, represented by Eq. (12-11), and the $\Delta G_a{}^i$ terms are the contributions from the accelerated dissolution reactions. The $\Delta G_a{}^{WA}$ represents the weak acid (WA) disequilibrium effect, and $\Delta G_a{}^{SB>11}$ and $\Delta G_a{}^{SB>12}$ terms represent strong base effects at pH>11 and >12. The $\Delta G_a{}^{WA}$ is sum of contributions from Eqs. (12-12) and (12-13). The relationship between the normalized release (g/L) and the ΔG_f was developed using the PCT-A (7 d at 90 °C) as

$$\log[NL_{Na}(g/L)] = -0.0981\Delta G_f - 1.448 \qquad r^2 = 0.88 \tag{12-17}$$

$$\log[NL_{B}(g/L)] = -0.104\Delta G_f - 1.535 \qquad r^2 = 0.86 \tag{12-18}$$

Note that the FEH and THERMO not only use different units for data analysis but also use different test methods. A step-by-step method for calculating FEH for the THERMO model is provided in Jantzen et al.[5]

For vitrified HLW, Hrma et al (1994) conducted a multiyear statistically designed CVS to characterize the relationship between composition and properties. Table 5-1 shows target composition and upper and lower limits for various components in the study. The target composition, HW–39–4, is based on the proposed Hanford HLW glass composition for the NCAW waste (now known as envelope B/D waste). Glass durability was measured on 120 glasses using 28 d MCC–1 and 7 d PCT methods. Compositional dependence on normalized release was determined by the first-order mixture models as

$$NR = \sum_{1}^{10} b_i x_i \tag{12-19}$$

---

[4]Jantzen, C.M., J.B. Pickett, K.G. Brown, and T.B. Edwards. *Method of Determining Glass Durability*. U.S. Patent No. 5,846,27. Issued on December 8, 1988.

[5]Ibid.

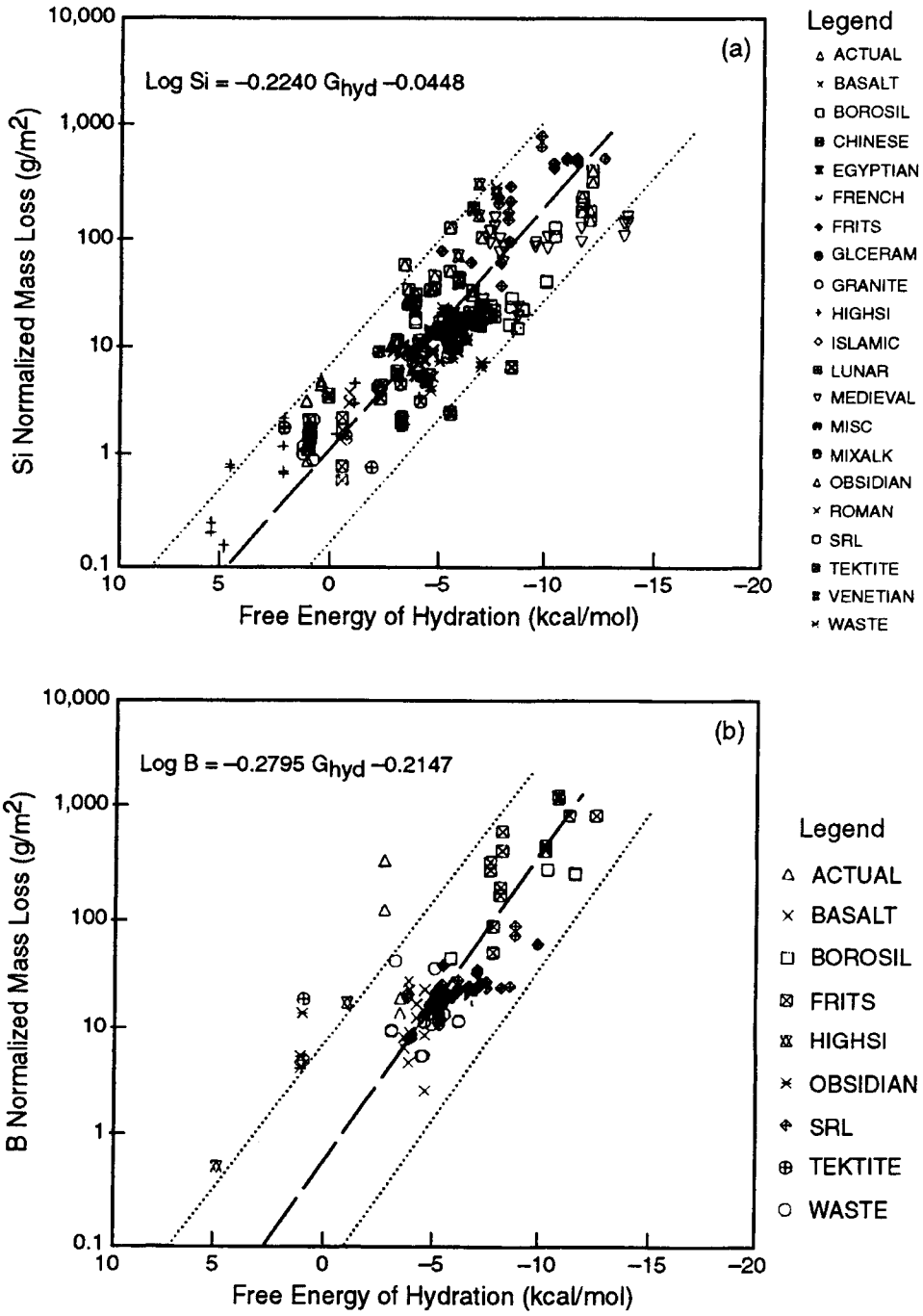

Figure 12-17. (a) Linear regression plots of the ΔG_{hyd} term versus silicon release to the leachant in a 28-d static leach test. The ΔG_{hyd} term has been adjusted for pH changes, as discussed in the text. (b) Linear regression plots of the ΔG_{hyd} term versus boron release to the leachant in a 28-d static leach test. The ΔG_{hyd} term has been adjusted for pH changes, as discussed in the text.

where

NR — the normalized release in g/m^2
x_i — mass fraction
b_i — regression coefficients for component i

The estimated regression coefficients for B, Si, Na, and Li are shown in tables 12-4 and 12-5 for MCC–1 and PCT data, respectively. For MCC–1 data, seven data points representing high B release were removed from the analysis. Their removal was attributed to nonlinear or interactive effects of components, which cannot be addressed by first-order mixture models. The r^2 statistics indicate that the first-order mixture model for MCC–1 data provides some predictive ability. Based on the regression coefficients provided in table 12-4, a component effects plot using normalized boron release was developed centered around composition HW–39–4 (figure 12-18). The analysis predicts that normalized B release is increased by Li_2O, Na_2O, and B_2O_3 (in the order written) and decreased by Al_2O_3 and SiO_2. For the PCT data set, no data points were removed. The r^2 values for the PCT data set were higher than the MCC–1 data set, indicating that the first-order mixture model for PCT data provides better predictive ability than MCC–1 data. Based on the regression coefficients provided in table 12-5, a component effects plot using normalized boron release was developed centered around composition HW–39–4, shown in figure 12-19. The analysis predicts that normalized B release is increased by Li_2O, B_2O_3, and Na_2O and decreased by Al_2O_3 and SiO_2. The MCC–1 and PCT data were analyzed using first-order mixture model terms along with several second-order terms

Table 12-4. Regression coefficients for normalized release and pH using 28-d MCC–1 method (Hrma et al., 1994)

x_i	b_i (Si)	b_i (B)	b_i (Li)	b_i (Na)	b_i (pH)
SiO_2	0.9025	-0.0993	-0.2319	-0.0587	7.3144
B_2O_3	6.8360	9.6800	9.4346	9.6671	9.1180
Na_2O	7.1851	9.5454	9.1998	8.9623	17.8061
Li_2O	9.6783	11.8108	10.5425	12.2173	24.4490
CaO	2.0185	3.7572	4.7685	3.6144	13.3174
MgO	1.8500	5.1079	4.9844	5.0078	13.1459
Fe_2O_3	4.6516	5.7008	6.0434	5.7557	10.1817
Al_2O_3	-4.6186	-6.2911	-5.6794	-6.0434	4.0454
ZrO_2	-2.1819	-0.6283	-0.2328	-0.7562	7.5917
Others	1.9548	3.6529	4.1125	3.4126	8.6750
# points	114	114	114	114	120
r^2	0.5996	0.6520	0.6525	0.6532	0.7487

Table 12-5. Regression coefficients for normalized release and pH using the 7-d product consistency test method (Hrma et al., 1994)

x_i	b_i (Si)	b_i (B)	b_i (Li)	b_i (Na)	b_i (pH)
SiO_2	-2.9671	-4.3173	-3.2278	-4.4118	8.1926
B_2O_3	-0.6148	11.9791	10.1496	9.4049	3.3332
Na_2O	10.7384	17.6068	14.0017	19.4013	23.6171
Li_2O	19.7370	22.5791	18.4159	19.0635	31.2448
CaO	-6.0415	-8.7114	-5.3528	-1.9567	17.2056
MgO	2.9296	10.9210	7.1181	11.8228	15.3354
Fe_2O_3	-4.2315	-3.2009	-4.5113	-4.0953	8.5939
Al_2O_3	-17.3377	-25.4071	-22.3095	-25.4294	5.3578
ZrO_2	-10.8139	-10.5613	-10.0618	-11.4209	7.6111
Others	-0.7297	0.1587	0.6181	0.6647	9.2689
# points	123	123	123	123	123
r^2	0.7377	0.8114	0.7905	0.8457	0.9092

selected using statistical variable selection techniques to improve the relationship between normalized release for B, Si, Na, and Li, and composition. The second-order mixture model provided a slightly better fit than the corresponding first-order mixture models.

Tables 12-4 and 12-5 also show first-order mixture model regression coefficients for pH. The r^2 statistics for the MCC–1 and PCT pH models show that the first-order mixture model for PCT data provides better predictive ability than for MCC–1 data.

Feng and Barkatt (1988) developed a structural bond strength (SBS) that assumes the dissolution of glass is controlled by the breaking of network bonds such as Si-O-Si. The energy of formation that represents an average structural strength of the glass is calculated by Eq. (12-20).

$$\Delta H = \sum_i x_i \Delta H_i \qquad (12\text{-}20)$$

where ΔH is the total energy of formation, and ΔH_i is the energy of formation for component i having mol fraction x_i in glass. The methodology of calculating the energy of formation of various glass components is discussed in chapter 6. The model was applied to various nuclear waste glasses from West Valley, SRL, and PNNL; commercial glasses, such as aluminosilicate and soda lime silica; and natural glasses such as basalts and tektites. The tests were conducted using the modified MCC–3 test. The MCC–3 test is a closed-system

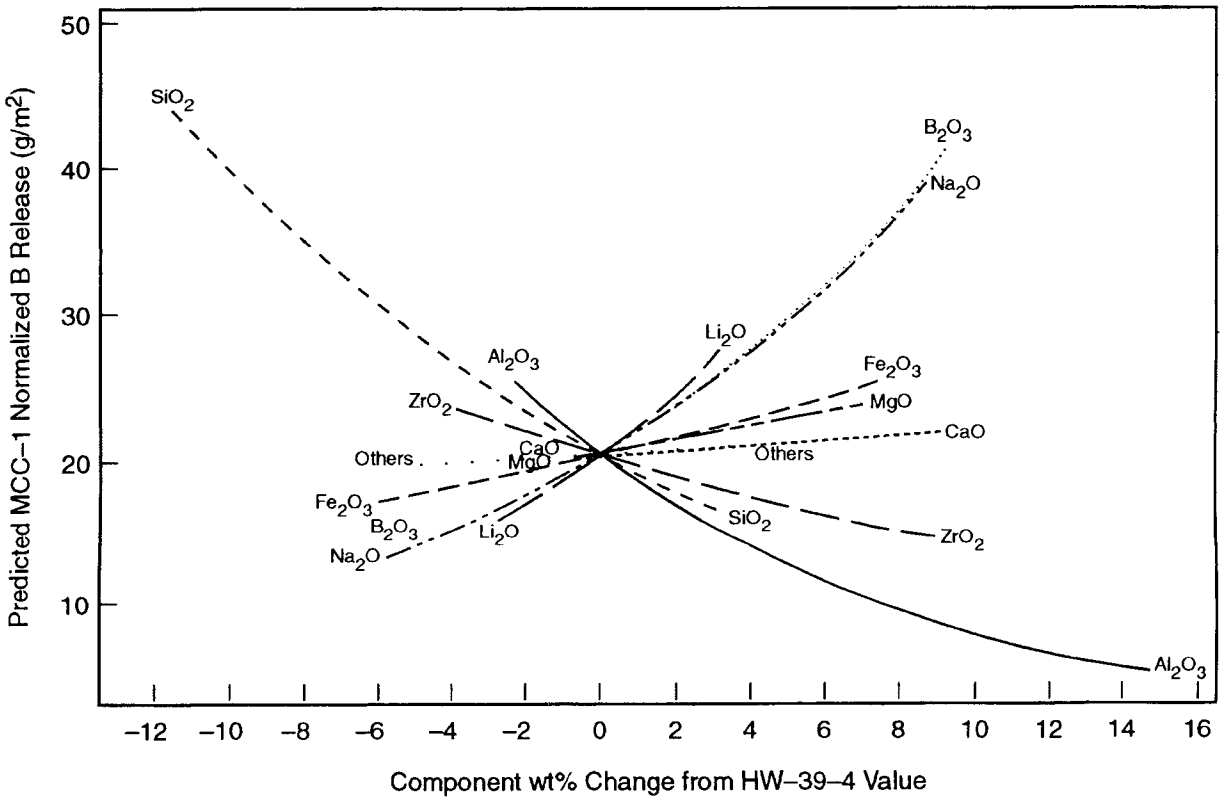

Figure 12-18. Predicted component effects on MCC–1 release relative to the HW–39–4 composition, based on the first-order mixture model using mass fractions fitted to the reduced data set (Hrma et al., 1994)

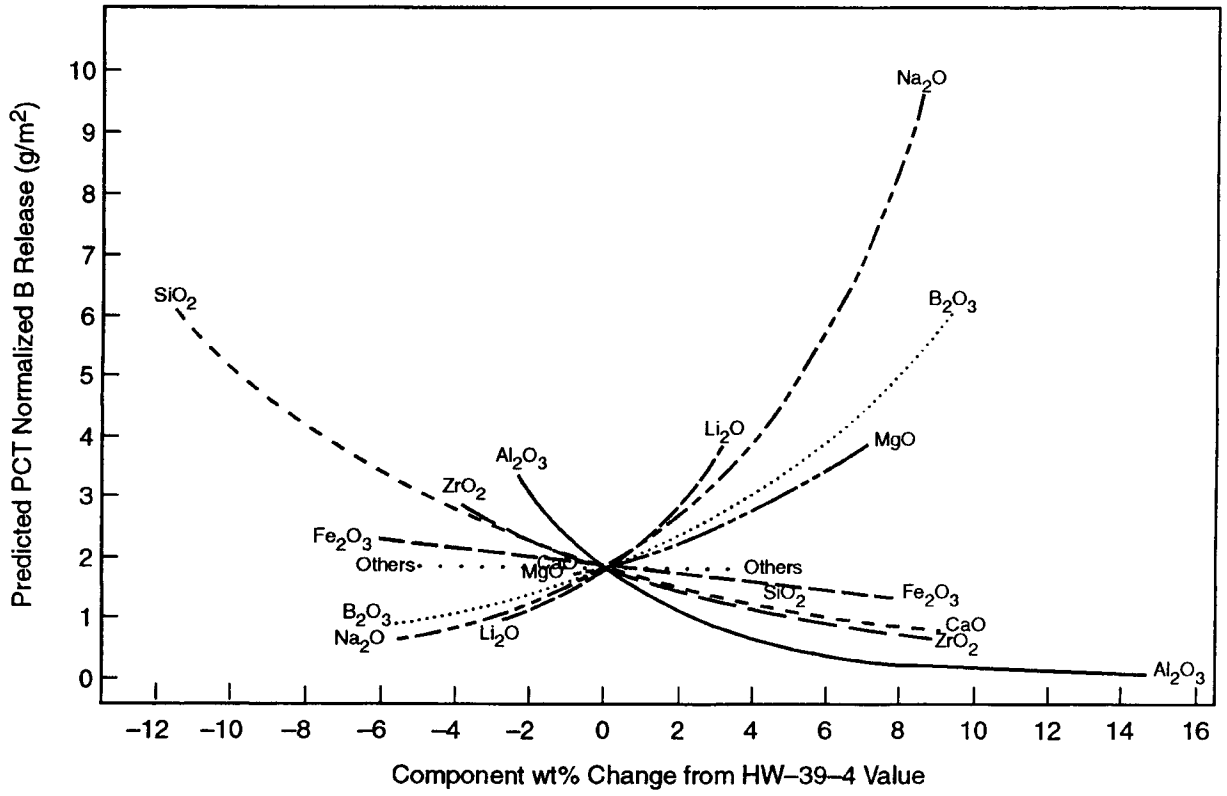

Figure 12-19. Predicted component effects on PCT B release relative to the HW–39–4 composition, based on the first-order mixture model using mass fractions (Hrma et al., 1996)

test using a crushed sample. Linear relationship shown by Eqs. (12-21) and (12-22) were developed between the logarithmic normalized release from the glass and the calculated ΔH.

$$\log(NL_{B-7day}) = -0.0193\Delta H + 5.2667 \qquad r^2 = 0.705 \tag{12-21}$$

$$\log(NL_{B-28day}) = -0.02865\Delta H + 8.358 \qquad r^2 = 0.723 \tag{12-22}$$

Ellison et al. (1994) used an independent data set consisting of normalized release data using the MCC–1 test at 90 °C for 28 d for 300 glasses and evaluated prediction capabilities of the FEH, THERMO, CVS, and SBS models. The data set included waste glasses (alkali boroaluminosilicate, alkali borosilicate, alkali aluminosilicate, and alkali lime silicates), natural glasses, and historical glasses. Results showed that FEH provided the best correlation between glass composition and durability among various models. FEH provided the best results for alkali boroaluminosilicate glasses having high mass losses, but provided poor correlation for highly durable glasses. For the SBS model, regression analysis showed the best correlation for alkali boroaluminosilicate glasses ($r^2 = 0.80$) and the worst for alkali borosilicate glasses ($r^2 = 0.05$). Compared to the FEH model, the SBS model provided a better correlation for predicting normalized release for highly durable glasses. Neither the SBS nor the FEH models provided a good correlation for alkali borosilicate glasses.

Tovena et al. (1994) used normalized release data for 32 waste glass samples (6 R7T7 and 26 SON) to test the FEH and SBS models. Both the FEH and SBS models provided satisfactory approximation of initial release rate. However, the models underpredicted the normalized release rate for glasses containing >15 wt% B_2O_3 with little Al_2O_3. This departure was attributed to the phase separation and complete dissolution of the borate phase in the absence of Al_2O_3.

The thermodynamic, structural, and empirical models reviewed in this chapter were developed for a specific range of glass compositions and glass components. Even though the applicability of these models can be extended to other wastes, as shown by Ellison et al. (1994) and Tovena et al. (1994), the user is cautioned to perform a careful and rigorous evaluation prior to using any model for predicting normalized release from the glass. In addition, the models predict glass performance under given test conditions at a single time; therefore, the results cannot be used for predicting time-dependent durability behavior.

12.5.2 Long-Term Chemical Durability Models

The release of components from glass follows a complex nonlinear behavior as a function of time. The behavior is a combination of glass composition effects, changes in solution chemistry with time, formation of secondary phases, and temperature. The long-term corrosion behavior can be divided into three distinct stages as reviewed by Ellison et al. (1994). In stage I, referred to as the short-term stage, the chemical potential gradient between the glass components and local environment is the steepest. The glass components are released into the local environment at a comparatively high rate. The soluble components, such as boron and alkalis, are released at a higher rate compared with components such as silica and aluminum oxide. This higher release rate results in the formation of a layer on the glass surface depleted of soluble components, compared with the bulk glass. This layer is often called the altered surface layer. In stage II, the intermediate stage, the corrosion rate decreases as the concentration of reaction products, particularly silica, increases in the solution that is in close contact with the glass. In addition, the reaction products in the altered surface layer

reach saturation concentration of their crystalline phases and result in the formation of secondary phases, such as zeolites and clays. In stage III, the long-term stage, glass corrosion rate is further affected because of the reprecipitation of secondary phases that exceed solubility limits at the altered zone. Physical processes, such as crystallization, cracking, or exfoliation of the altered surface layers, that occur in stage III, could influence the glass corrosion rate, as well as the release and transport of colloids and radionuclides. The change in dissolution rate also depends on the identity, distribution, and surface area of the secondary phases. In most cases, the dissolution rate increases as a result of crystallization, exfoliation, and cracking of the altered surface layers. The transition from one stage to another is dependent on the glass composition and the local environment. A highly durable glass may take months to years to reach stage II, whereas a nondurable glass may reach stage II within hours or days.

The long-term dissolution models use a rate equation consistent with the transition state theory (Bourcier, 1994)

$$\frac{dn_i}{dt} = An_i k_r \prod_j a_j^{-n} \left(1 - e^{\left(-\frac{A_f}{\sigma RT}\right)}\right) \tag{12-23}$$

where

n_i — is the number of mols of species i in solution released from the glass
t — time
A — reactive surface area of glass
v_i — concentration of species i in the glass
k_r — rate coefficient for the rate-limiting reaction for glass dissolution
$\prod_j a_j^{-n}$ — the product of the activities (concentrations) of dissolved aqueous species, that contributes to the activated complex of the rate-limiting microscopic dissolution reaction
A_f — reaction affinity, defined as $RT\ln(Q/K)$, where Q is the activity product and K is the equilibrium constant for the rate-determining glass dissolution reaction
σ — a stoichiometric factor that relates the rate-controlling microscopic reaction to the overall solid dissolution reaction (usually it is assumed $\sigma = 1$)
R — gas constant
T — temperature in kelvin.

The Eq. (12-23) implies that, at equilibrium, there is a reversible dissolution reaction. Since the glass is considered as thermodynamically metastable, the rate law cannot be applied to the overall glass dissolution but to some rate-limiting microscopic reversible reaction. Several parameters shown in Eq. (12-23) are not known either from theory or experiments. Therefore, the rate equation is simplified to the form

$$\frac{dn_i}{dt} = An_i k(\mathrm{pH})\left(1 - \left(\frac{Q}{K}\right)^r\right)^\sigma \tag{12-24}$$

Equation (12-24) is commonly used for determining release rate. The parameters k, K, r, and σ are determined by fitting experimental data. Grambow further simplified Eq. (12-24) to include only silica in the affinity term and expressed glass dissolution rate as

$$R_m = k_+\left(1-\left(\frac{a_{SiO_2(aq)}}{K}\right)\right) + R_{final} \qquad (12\text{-}25)$$

where

R_m — matrix dissolution rate
k_+ — rate coefficient
$a_{SiO2(aq)}$ — the activity of aqueous silica at the reacting surface
K — glass saturation activity
R_{final} — residual rate after silica saturation is achieved

The parameters K and k_+ are regressed from experimental data. Geochemical modeling codes, such as PHREEQE/GLASSOL, EQ3/6, DISSOL, REACT, and LIXIVER, use an expression shown by Eqs. (12-24) and (12-25). Grambow's model has been applied to several closed- and open-system dissolution tests for a variety of glass compositions. In most cases, the model predicts observed trends and agrees with measured solution compositions to within a factor of two or three. The model, however, requires that parameters such as K and k_+ be determined for each glass composition. In addition, the release of components can only be modeled assuming congruent dissolution; the model does not provide a mechanistic basis for predicting the long-term dissolution rate of glasses. The long-term models have no capability to predict how the rate may change as the environmental parameters change during the lifetime.

12.6 GLASS BEHAVIOR IN THE REPOSITORY ENVIRONMENT

Several long-term HLW glass corrosion studies have been conducted in the previous 20 yr on simulated glasses doped with plausible radionuclides, and fully radioactive glasses. Drip tests, designed to simulate slow flow through the breached canisters, have been used by Fortner and Bates (1996) and Fortner et al. (1997) to study the long-term performance of actinide-doped WVDP and DWPF HLW glasses. The long-term PCT-B, designed to simulate fully immersed conditions, has been used by Ebert and Tam (1997) to study the long-term performance of DWPF glasses. In addition, vapor hydration tests (VHT), designed to replicate a natural alteration process, are used by Luo et al. (1997) to compare the dissolution behavior of DWPF glasses with that of naturally occurring basalt glasses.

The dissolution rate of the HLW glass decreases as the groundwater environment in close contact with the WPs becomes saturated with glass matrix components, such as silica. Even though the glass corrosion studies discussed previously confirmed that net dissolution rate decreases as the surrounding environment becomes rich in HLW glass matrix components, the drip test studies show a steep increase in radionuclide release rate for Pu and Am after 400 wk. The steep increase in radionuclide release rate was attributed to the spalling of radionuclide-containing colloids from the exposed HLW glass surface. The HLW glass corrosion models currently proposed do not account for such excursions in corrosion behavior, although they can have a significant effect on radionuclide release.

The concentration of silica in the near-field environment may affect the degradation of SNF WPs. If there is abundant silica during SNF dissolution, uranosilicates may eventually form. If silica is depleted and groundwater contact with WPs is limited, schoepite may form. Because the retention factors of radionuclides in uranosilicates and schoepite may be different, the silica release from HLW glass corrosion may affect the release behavior of radionuclides from SNF dissolution. The effects of HLW glass corrosion on radionuclide retention in secondary minerals during SNF dissolution should be considered.

Long-term corrosion studies of HLW glasses indicate formation of secondary phases on the exposed surface of the HLW glasses. This process is dependent on the external environment. Long-term PCTs in J-13 water show formation of clay, Ca-phosphate, and (Th, U, and Ca) titanate as secondary phases (Bates, 1998), whereas, the VHTs show accumulation of clay, zeolites, Ca-silicates, weeksite, and K-feldspar as secondary phases (Bates, 1998). The formation of different phases under diverse test conditions is attributed to varying solution chemistries. The formation of secondary phases may also be influenced by the corroding container materials. Secondary minerals play an important role in radionuclide release because they can incorporate low-solubility radionuclides, such as Pu and Am, and control their solubility limits. They may also act to block the reactive surface area of the primary phase.

It is important that the long-term radionuclide release rate in the corrosion models includes the influence of stage III behavior. Experimental data on the formation of secondary phases under anticipated repository conditions are necessary if the contribution of the HLW glass to the estimated receptor dose is significant. If the models are simply based on experimental dissolution data for stages I or II that exhibit significant retention of radionuclides in the secondary phases, evaluation of the long-term radionuclide release rates could be erroneous.

Natural analog studies, coupled with experimental data and geochemical modeling, provide other methods of gaining confidence in predicting long-term corrosion behavior of glasses. Natural analog studies are useful in evaluating the merits of extrapolating short-term experiments to longer time frames. Several natural glasses, especially basalt, have compositions comparable to the HLW glasses and have been subjected to conditions similar to those expected in the proposed Yucca Mountain repository (Ewing et al., 1998). The characterization of secondary phases formed on these natural glasses can provide insights into the long-term dissolution behavior of HLW glasses.

A recent study by Luo et al. (1997) compared the formation of secondary phases in the naturally occurring Hawaiian basaltic glasses with the results of VHTs conducted for 7 yr on simulated basaltic and HLW borosilicate glasses. Luo et al. (1997) concluded that secondary phases formed on both simulated natural glasses and HLW borosilicate glasses were similar to secondary phases observed in naturally occurring basaltic glasses, and VHTs could be used to simulate naturally occurring conditions.

Field data on naturally occurring glasses, combined with experimental data and models on dissolution of HLW glasses, could be useful to demonstrate that long-term dissolution behavior under repository conditions can be represented by extrapolation of results from short-term laboratory tests. Such data can be important to supplement and support the validity of the existing glass-dissolution data generally obtained by short-term experiments.

12.7 TANK WASTE REMEDIATION SYSTEM CONCERNS

Chemical durability is an important specification for the vitrified HLW. The target glass composition should be designed to meet the specification and to accommodate variability in leachate concentrations caused by composition variability. A robust glass composition enveloping composition variability should be able to meet the WAPS.

12.8 SUMMARY

When a glass comes in contact with an environment, such as flowing or stagnant groundwater, corrosive gases and vapors, or aqueous solutions, chemical reactions occur at the surface, which then spread to the whole of the glass, depending on its composition, the pH of the solution, and the temperature of the environment. Several studies have focused on understanding two aspects of nuclear waste glasses. First, the ability to produce glasses to meet production specifications based on short-term tests and second, predicting the long-term dissolution behavior of glasses on the of 10,000 yr or more. Several methods have been developed to perform accelerated testing to determine corrosion behavior of glasses. Since glass corrosion is not an intrinsic property of the materials, the observed dissolution behavior depends on the test conditions and test methods. A careful evaluation is required in drawing conclusions regarding the chemical durability of a glass based solely on data. A few test methods that form the basis of current understanding are discussed, including relationships between glass composition and environment (pH, temperature, and nature of solution) as a function of time. The processes involved in glass corrosion include ion-exchange, water diffusion, hydrolysis, and precipitation. Even though dissolution may start by simple ion-exchange or the hydrolysis reaction, the simultaneous occurrence of stated processes is not uncommon.

The initial reaction on the glass surface is dominated by the initial pH of the contact solution. As the reaction progresses, reaction layers are formed on the surface. The formation of reaction layers on the surface of the glass in contact with leachate plays a significant role in determining the leaching behavior of the glass components. As the glass corrodes and its components are released in the solution, the leachate may become supersaturated with respect to some components, leading to precipitation of the secondary phases on the surface of the glass or the walls of the test container. The thickness of the gel layer remains constant provided the pH of the contact solution does not change. If the contact solution becomes more alkaline, the Si dissolution increases, which may reduce the thickness of the gel layer. In a complex system containing more than one glass forming oxides, such as B_2O_3 and Al_2O_3 (depending on the glass composition), the corrosion mechanism is further complicated by the release rate of various cations from the glass and their solubility in the contact solution. The properties of the surface layer depend on glass composition, contact solution chemistry, test parameters, and reaction time. The surface layers can provide a sink or reservoir for components in solution and act as a physical barrier to the transport of reactants and corrosion products. In addition, surface layers can influence the chemical affinity of the glass reactions.

The selection of a test method depends on the characteristics of the system to be studied. For example, if the interactions between the glass and contact solution are important without the influence of solution chemistry, tests such as MCC–1 or dynamic tests are recommended. If the effect of solution chemistry on the glass corrosion behavior is important, tests such as PCT are more useful. Most of the literature data on glass durability was collected using either the MCC–1 or the PCT method. Test parameters

such as SA/V ratio, flow rate, and temperature for a given method could limit the usefulness of the data for the desired application.

The chemical durability of a glass depends on its components. Because of the lack of a uniform testing and measurement approach to study durability-composition relationships, data from various studies are difficult to compare quantitatively. The composition/durability studies indicate that the greatest improvements in durability result from adding components that form the strongest bonds. For example, the durability of alkali silicate glass is improved by adding Al_2O_3, B_2O_3, Fe_2O_3, ZrO_2, or divalent cations (Ca, Mg, Zn). The mechanism in each case is formation of bonds stronger than the alkali-NBO bond in simple alkali silicate glass. In addition, the nature of the solution in contact with glass has a significant effect on chemical durability.

Several attempts have been made to correlate chemical durability and glass composition. The models assume that the glass is homogeneous and crystal free. The thermodynamic, structural, and empirical models discussed in this report were developed for a specific range of glass compositions and glass components. Even though the applicability of these models can be extended to other wastes, the user is cautioned to perform a careful and rigorous evaluation prior to using any model for predicting normalized release from the glass. In addition, the models predict glass performance under given test conditions at a single time; therefore, the results cannot be used for predicting time-dependent durability behavior. The long-term dissolution models use rate equations consistent with the transition state theory. Grambow's model has been applied to several closed- and open-system dissolution tests for a variety of glass compositions. In most cases, the model predicts observed trends and agrees with the measured solution compositions to within a factor of two or three. However, the model does not provide a mechanistic basis for predicting the long-term dissolution rate of glasses. The long-term models have no capability to predict how the rate may change as the environmental parameters change during the performance period for the glass.

12.9 REFERENCES

Adams, P.B., and D.L. Evans. Chemical durability of borate glasses. *Borate Glasses: Structure, Properties, Applications*. New York: Plenum Press. 1978.

Adiga, R.B., E.P. Akomer, and D.E. Clark. Effects of flow parameters on the leaching of nuclear waste glass. *Ceramic Transactions of the Materials Processing and Design: Grain-Boundary-Controlled Properties of Fine Ceramics II, Aichi, Japan.* Ceramic Transactions Volume 44. K. Niihara, K. Ishizaki, and M. Isotani, eds. Pittsburgh, PA: Materials Research Society: 45–54. 1985.

American Society for Testing and Materials. *Determining Chemical Durability of Nuclear, Hazardous, and Mixed Waste Glasses: The Product Consistency Test.* Annual Book of ASTM Standards. ASTM C 1,285–1,297. Ceramic Transactions Volume 12.01. 774-91. West Conshohocken, PA: American Society for Testing and Materials. 1999.

Barkatt, A.A., E.E. Saad, R. Adiga, W. Sousanpour, A.L. Barkett, M.A. Adel-Hadadi, J.A. O'Keefe, and S. Alterescu. Leaching of natural and nuclear waste glasses in sea water. *Appl. Geochem* 4: 593–603. 1989.

Bart, G., H.U. Zwicky, E.T. Aerne, T.H. Graber, D. Z'Berg, and M. Tokiwai. Borosilicate glass corrosion in the presence of steel corrosion products. *Proceedings of the 99th Annual Meeting of the American Ceramic Society, Cincinnati, Ohio.* Ceramic Transactions Volume 84. W. Wong-Nu, U. Balachandran, and A. Bhalla, eds. Westerville, OH: Materials Research Society: 459–470. 1997.

Bates, J.K. Distribution and stability of secondary phases. *Workshop on Preliminary Interpretations Waste Form Degradation and Radionuclide Mobilization Expert Elicitation Project.* San Francisco, CA. 1998.

Bourcier, W.L. *Critical Review of Glass Performance Modeling.* ANL–94/17. Argonne, IL: Argonne National Laboratory. 1994.

Bunker, B.C., G.W. Arnold, D.E. Day, and P.J. Bray. The effect of molecular structure on borosilicate glass leaching. *Journal of Non-Crystalline Solids* 87: 226–253. 1986.

Burns, D.B., B.H. Upton, and G.G. Wicks. Interactions of SRP waste glass with potential canister and overpack metals. *Journal of Non-Crystalline Solids* 84: 258–267. 1986.

Chick, L.A., and L.R. Pederson. The relationship between reaction layer thickness and leach rate for nuclear waste glasses. *Proceedings of the Materials Research Society Conference.* Symposium Proceedings 26. Pittsburgh, PA: Materials Research Society: 635–642. 1984.

Clark D.E., M.F. Dilmore, E.C. Ethridge, and L.L. Hench. Aqueous corrosion of soda-lime-silica glass. *Journal of American Ceramic Society* 59: 62–65. 1976.

Conradt, R., H. Roggendorf, and H. Scholze. Investigations of the role of surface layers in HLW glass leaching. *Proceedings of the Materials Research Society Conference.* Symposium Proceedings 50. Pittsburgh, PA: Materials Research Society: 203–210. 1985.

Das, C.R. Diffusion controlled attack of glass surfaces by aqueous solutions. *Journal of American Ceramic Society* 63: 160–165. 1980.

Delage, F., and J.L. Dussossoy. R7T7 Glass dissolution measurements using high-temperature soxhlet device. *Proceedings of the Materials Research Society Conference.* Symposium Proceedings 212. Pittsburgh, PA: Materials Research Society: 41–47. 1991.

Dilmore, M.F., D.E. Clark, and L.L. Hench. Chemical durability of Na_2O-K_2O-CaO-SiO_2 glasses. *Journal of the American Ceramic Society* 61: 439–443. 1978a.

Dilmore, M.F., D. E. Clark, and L.L. Hench. Aqueous Corrosion of Lithia-Alumina-Silicate Glasses. *Journal of the American Ceramic Society* 57: 339–353. 1978b.

Ebert, W.L. and J.K. Bates. A comparison of glass reaction at high and low SA/V. *Nuclear Technology* 104(3): 372–384. 1993.

Ebert, W.L., and S.W. Tam. Dissolution rates of DWPF glasses from long-term PCT. *Proceedings of the Materials Research Society Conference*. Symposium Proceedings 465. Pittsburgh, PA: Materials Research Society: 149–156. 1997.

Ellison, A.J.G., J.J. Mazar, and W.L. Ebert. *Effect of Glass Composition on Waste Form Durability: A Critical Review.* ANL–94/28. Argonne, IL: Argonne National Laboratory. 1994.

Ewing, R.C., W. Lutze, and A. Abdelouas. Natural glasses and the 'verification' of the long-term durability of nuclear waste glasses. *Proceedings of the XVIII International Congress on Glass (CD Rom Edition)*. Westerville, OH: American Ceramic Society. 1998.

Feng, X., and A. A. Barkatt. Structural thermodynamic model for durability and viscosity of nuclear waste glasses. *Proceedings of the Materials Research Society Conference*. Symposium Proceedings 112. Pittsburgh, PA: Materials Research Society: 543–554. 1988.

Feng, X., A.A. Barkett, and T. Jiang. Systematic composition studies on the durability of waste glass WV205. *Proceedings of the Materials Research Society Conference*. Symposium Proceedings 112. Pittsburgh, PA: Materials Research Society: 673–683. 1988.

Feng, X., I.L. Pegg, A.A. Barkatt, P.B. Macedo, S.J. Cucinel, and S.Lai. Correlation between composition effects on glass durability and structural role of the constituent oxides. *Nuclear Technology* 85: 334–345. 1989.

Feng, X. Surface layer effects on waste glass corrosion. *Proceedings of the Materials Research Society Conference.* Proceedings 333. Pittsburgh, PA: Materials Research Society: Symposium: 55–67. 1994.

Feng, X., and I.L. Pegg. Effects of salt solutions on glass dissolution. *Physics and Chemistry Glasses* 35(2). England. 1994.

Fortner, J.A., and J.K. Bates. Long-term results from unsaturated durability testing of actinide-doped DWPF and WVDP waste glasses. *Proceedings for the Materials Research Society Conference.* Symposium Proceedings 412. Pittsburgh, PA: Materials Research Society: 205–211. 1996.

Fortner, J.A., S.F. Wolf, E.C. Buck, C.J. Mertz, and J.K. Bates. Solution-borne colloids from drip tests using actinide-doped and fully-radioactive waste. *Proceedings for the Materials Research Society Conference*. Symposium Proceedings 465. Pittsburgh, PA: Materials Research Society: 165–172. 1997.

Grambow, B., and D.M. Strachan. Leach testing of waste glasses under near-saturation conditions. *Proceedings for the Materials Research Society Conference*. Symposium Proceedings 26. Pittsburgh, PA: Materials Research Society: 623–634. 1984.

Hench, L.L., D.E. Clark, and A.B. Harker. Review: Nuclear waste solids. *Journal of Material Science* 21: 1,457–1,478. 1986.

Hrma, P.R., G.F. Piepel, M.J. Schweiger, D.E. Smith, D.-S. Kim, P.E. Redgate, J.D. Vienna, C.A. LoPresti, D.B. Simpson, D.K. Peeler, and M.H. Langowski. *Property/Composition Relationships for Hanford High-Level Waste Glasses Melting at 1,150 °C*. Volume 1 (Chapters 1–11). PNL–10359. Richland, WA: Pacific Northwest National Laboratory. 1994.

Inagaki, Y., A. Ogata, H. Furuya, K. Idemistu, T. Banba, and T. Maeda. Effects of redox condition on waste glass corrosion in the presence of magnetite. *Proceedings for the Materials Research Society Conference*. Symposium Proceedings 412. Pittsburgh, PA: Materials Research Society: 257–264. 1996.

Jantzen, C.M. Nuclear waste glass durability: I, predicting environmental response from thermodynamic (Pourbaix) diagrams. *Journal of the American Ceramic Society* 75(9): 2,433–2,448. 1992.

Luo, J.S., W.L. Ebert, J.J. Mazer, and J.K. Bates. Dissolution rates of DWPF glasses from long-term PCT. *Proceedings of the Materials Research Society Conference*. Symposium Proceedings 465. Pittsburgh, PA: Materials Research Society: 157–163. 1997.

McGrail, B.P., W.L. Ebert, A.J. Bakel, and D.K. Peeler. Measurement of kinetic rate law parameters on a Na-Ca-Al borosilicate glass for low-activity waste. *Journal of Nuclear Materials* 249: 175–189. 1997.

McVay G.L., and C.Q. Buckwalter. Effect of iron on waste-glass leaching. *Journal of the American Ceramic Society* 66(3): 170–174. 1983.

Newton, R.G. The durability of glass—A review. *Glass Technology* 26(1): 21–28. 1985.

Paul, A. Chemistry of glass—A thermodynamic approach. *Journal of Material Science* 12: 2,246–2,268. 1977.

Paul, A. *Chemistry of Glass*. New York: Chapman and Hall, Ltd. 1982.

Pederson, L.R., C.Q. Buckwalter, G.L. McVay, and B.L. Riddle. Glass surface area to solution volume ratio and its implication to accelerated leach testing. *Proceedings of the Materials Research Society Conference*. Symposium Proceedings 15. Pittsburgh, PA: Materials Research Society: 47–54. 1983.

Smets, B.M., and T.P.A. Lommen. The leaching of sodium aluminosilicate glasses studied by secondary ion mass spectroscopy. *Physics and Chemistry, Glasses 23*: 83–87. 1982.

Smets, B.M., and M.G.W. Tholen. Leaching of glasses with molar compositions $20Na_2O \cdot 10CaO \cdot xAl_2O_3 \cdot (1\text{-}x)SiO_2$. *Journal of American Ceramic Society* 67: 281–284. 1984.

Smets, B.M.J., and M.G.W. Tholen. The pH dependence of the aqueous corrosion of glass. *Physics and Chemistry, Glasses* 26: 60–63. 1985.

Tovena, I., T. Advocat, D. Ghaleb, E. Vernaz, and F. Larche. Thermodynamic and structural models compared with the initial dissolution rates of "SON" glass samples. *Proceedings for the Materials Research Society Conference*. Symposium Proceedings 333. Pittsburgh, PA: Materials Research Society: 595–602. 1994.

U.S. Department of Energy. *Nuclear Waste Materials Handbook—Test Methods*. DOE/TIC–11400. Richland, WA: Pacific Northwest National Laboratory. 1982.

U.S. Department of Energy. *High-Level Waste Borosilicate Glass: A Compendium of Corrosion Characteristics*. (Volumes 1, 2, and 3). DOE–EM–0177. Washington, DC: Office of Waste Management, U.S. Department of Energy. 1994.

Vernaz, E.Y., J.L. Dussossoy, and S. Fillet. Temperature dependence of R7T7 nuclear waste glass alteration mechanisms. *Proceedings of the Materials Research Society Symposium*. Symposium Proceedings 112. Pittsburgh, PA: Materials Research Society: 555–563. 1988.

Werme, L., I.K. Bjorner, G. Bart, H.U. Zwicky, B. Grambow, W. Lutze, R.C. Ewing, and C. Magrabi. Chemical corrosion of highly radioactive borosilicate nuclear waste glass under simulated repository conditions. *Journal of Materials Research* 5(5): 1,130–1,146. 1983.

Wickert, C.L., A.E. Vieira, J.A. Dehne, X. Wang, D.M. Wilder, and A. Barkatt. Effects of salts on silicate glass dissolution in water: kinetics and mechanisms of dissolution and surface cracking. *Physics and Chemistry of Glasses* 40(3): 157–170. 1999.

13 PHASE STABILITY

The phase stability of glasses used for the immobilization of HLW is of concern during melting and long-term storage. The requirements for phase stability have been outlined in the WAPS. Phase instability in glass can be induced by either liquid-liquid phase separation or crystallization on cooling from the melt. While crystallization occurs only at temperatures below the T_L, liquid-liquid phase separation occurs in the fields of immiscibility defined by the equilibrium or metastable phase relations, which may be above or below the liquidus. These processes have been carefully controlled in many engineered glass products to achieve properties not available in a homogeneous glass.

- High-silica Vycor™ glass is made at lower temperatures than an equivalent fused silica by a process involving phase separation of a sodium borosilicate glass, chemical leaching of the high-alkali phase, and viscous sintering of the remaining high-silica network.

- Pyroceram™ glass ceramics are first melted and formed as glasses and subsequently crystallized to contain more than 95 percent by volume of crystalline phases in the lithium aluminosilicate system that lend a low thermal expansion coefficient and high degree of thermal shock resistance to the product.

For the glass waste form, however, phase separation and crystallization can result in the development of an inhomogeneous microstructure that may affect the reliability of the production process and product performance. A time-temperature-transformation (TTT) diagram is a useful method for defining the heat treatment conditions for crystallization, and for predicting the types and quantities of phases that can form in HLW glasses. From the nose of a TTT curve, one is able to calculate the rate of cooling needed at each temperature to avoid a specific volume fraction of crystalline phases. This information can provide guidance about conditions to be avoided during processing of the waste glasses such as melter idling, and shipping, handling, and storage of canistered waste forms. An overview of the phase separation and crystallization behavior in HLW glasses and their effect on glass performance is the subject of this chapter.

13.1 PHASE STABILITY SPECIFICATION

Specification 1.4 of the WAPS requires that TTT diagrams be developed for each of the targeted HLW glass compositions. The TTT diagrams identify the temperatures and durations of exposure at these temperatures that cause significant changes in phase structure and phase composition of the glass waste form.

13.2 PHASE SEPARATION

Liquid-liquid phase separation is the growth of two or more noncrystalline glassy phases, each of which has a different composition from the overall melt. The occurrence of phase separation is confined within a region of composition and temperature in the phase diagram known as the immiscibility dome phase boundary, as shown in figure 13-1. The dashed line delineates the metastable extension of the immiscibility boundary. Single-phase glasses with a homogeneous composition within the phase boundary can lower their free energy by separating into two immiscible glass phases. The compositions of these two glass phases can be determined by drawing a common tangent between the energy minima of the free energy versus

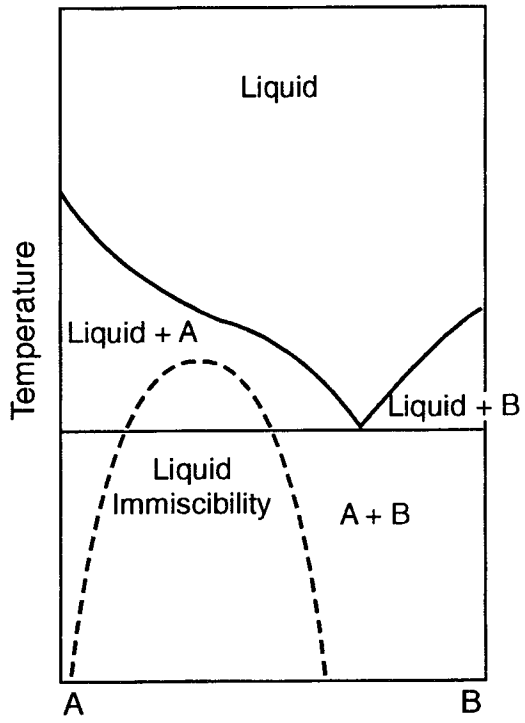

Figure 13-1. Liquid immiscibility in a binary eutectic diagram of components A and B. X_B is the mole fraction of B.

composition curve. There are two types of phase separation kinetics: nucleation/growth and spinel decomposition. While the former is large in composition fluctuation but small in spatial extent, the latter is small in composition fluctuation and large in spatial extent. These two processes often result in different microstructures. Tomozawa (1979) classified the microstructure of the phase-separated glasses into three types, depending on the separation kinetics governed by nucleation/growth or spinel decomposition:

- Interconnected microstructure
- Chemically more durable phase dispersed as discrete droplets in a continuous matrix of the less durable phase
- Chemically less durable phase dispersed as discrete droplets in a continuous matrix of the more durable phase

Borosilicate glasses are prone to liquid-liquid phase separation. The phase-separated glass usually forms one phase rich in silica and a second one enriched in most of the other components. The latter is usually less durable than either the silica-rich phase or the homogeneous glass. Depending on the developed microstructure, phase separation can profoundly affect glass durability. Controlling the glass chemistry in compositional regions that avoid phase separation is the key to achieving waste glass durability control during processing.

13.2.1 Immiscibility Boundary Measurements

Immiscibility boundaries can be mapped on phase diagrams by the visible opalescence in most phase-separated glasses. If a glass changes from transparent to uniformly opalescent after heating at a given temperature for sufficient time, this indicates that the heat treatment temperature used is inside the immiscibility boundary. For a given glass composition, the maximum heat-treatment temperature at which the opalescence is detected can be defined as the critical (or immiscibility) temperature. A series of heat treatments on selected glass compositions can thus be used to map the immiscibility boundary. Care is needed to assure the opalescence is indeed caused by liquid-liquid phase separation rather than crystallization. The accuracy of the immiscibility boundary using the opalescence method is approximately ±10 °C. A more accurate determination can be made by checking the existence of the microstructure in the quenched sample using various instruments such as electron microscopy, X-ray diffraction, and the small angle neutron scattering method.

13.2.2 Phase Separation in High-Level Waste Glasses

Taylor (1990) suggested a simple approach to predicting immiscibility in complex borosilicate systems with a special reference to nuclear waste immobilization. His approach is based on the observation that the extent of immiscibility is related to the polarizing power of the modifier cation, which is a function of its charge and radius. In general, as the polarizing power increases, the attraction between the cation in negatively charged nonbridging oxygens strengthens, and the tendency toward clustering of these species and phase separation increases. Figure 13-2 shows miscibility limits in a variety of binary silicate systems involving monovalent and divalent cations. As expected, the extent of the immiscibility dome increases with increasing polarizing power. This relationship between the extent of immiscibility and polarizing power breaks down with the most polarizing cation (i.e., Al^{3+}, which enters the silicate structure as a network-former rather than a modifier). Consequently, a suppression of liquid-liquid phase separation results when sufficient Al_2O_3 is incorporated into the glass composition. To a lesser extent, additions of TiO_2 and ZrO_2 will also suppress the development of liquid-liquid phase separation. Taylor used the location of the Na_2O-B_2O_3-SiO_2 submixture from the multicomponent glass from the immiscibility dome to predict the development of liquid-liquid phase separation. The effects of individual components on the occurrence of phase separation in a variety of multicomponent borosilicate glasses have been reviewed by Taylor (1990). Based on the observations of this review report, there are a large number of oxides of cations more polarizing than Na^+, such as oxides of Li, Mg, Ca, Ba. Taylor predicted that the addition of various oxides will induce phase separation when added to a submixture composition lying within the sodium borosilicate immiscibility dome but will not promote phase separation when added to a submixture composition lying outside the dome.

Hrma et al. (1994) conducted a composition variation study to characterize the relationships between glass composition and properties of a total of 123 glasses in support of the HLW glasses development at the Hanford site. The authors applied Taylor's model to the Hanford simulated HLW glasses for the prediction of liquid-liquid phase separation in complex, multicomponent systems. Figure 13-3 shows the durability data of all the tested glasses within various normalized sodium borosilicate submixtures with an immiscibility boundary for the Na_2O-B_2O_3-SiO_2 system. In all three submixtures, glasses located near the SiO_2-rich apex were generally more durable because of a continuous 3D network, whereas glasses positioned in the SiO_2-deficient regions produced low durability. The use of the normalized sodium borosilicate submixture (figure 13-3a) appears to be inadequate to predict phase separation for Hanford's glasses, in which many of

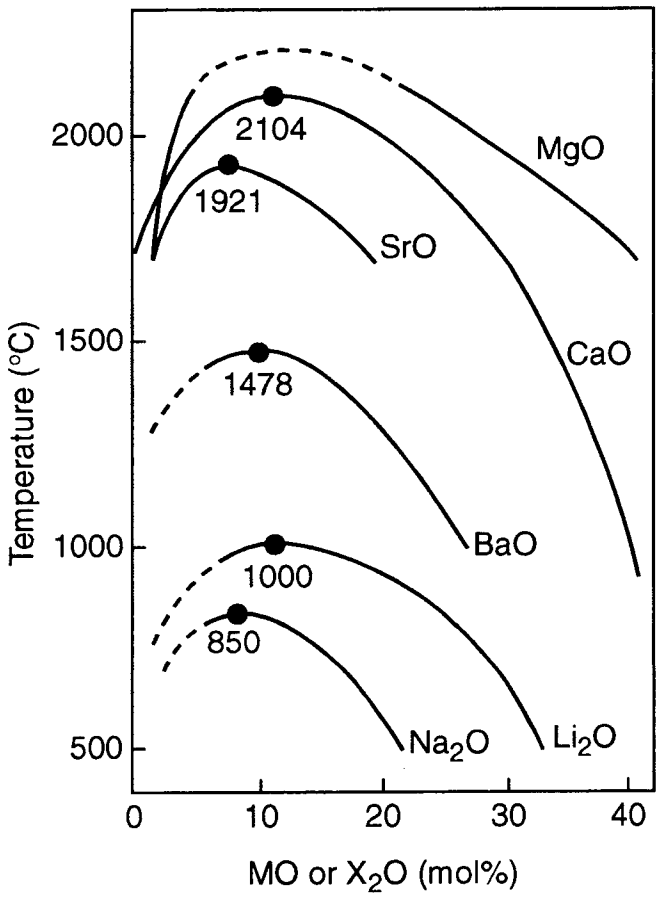

Figure 13-2. Miscibility limits in a variety of binary silicate systems involving monovalent (X^+) and divalent (M^{2+}) cations (Kawamoto and Tomozawa, 1981)

the high-durability, nonphase-separated glasses remained within the immiscibility boundary. With the addition of Li_2O to the alkali corner of the sodium borosilicate submixture (figure 13-3b), the experimental results indicated that phase separation can be more accurately predicted for the multicomponent systems. As predicted by the modified model, nine glasses located within the immiscibility boundary were prone to liquid-liquid phase separation. The sodium borosilicate submixture with an equivalent Na_2O content (figure 13-3c) further improved the ability to predict immiscibility within these glass systems. The equivalent Na_2O content is defined as

$$Na_2O(\text{equivalent}) = k \times Li_2O + Na_2O \qquad (13\text{-}1)$$

where $k = 61.98/29.88$, the ratio of the molecular masses of Na_2O and Li_2O, respectively. In this equivalent submixture, only eight glasses remained within the immiscibility boundary, four which were experimentally characterized to be phase-separated. The modified submixture systems, both the addition of Li_2O on a mass fraction basis and the equivalent Na_2O content on a molar basis, demonstrated the capacity to discriminate the phase-separated glasses from the homogeneous glasses. A few glasses, however, did not follow the

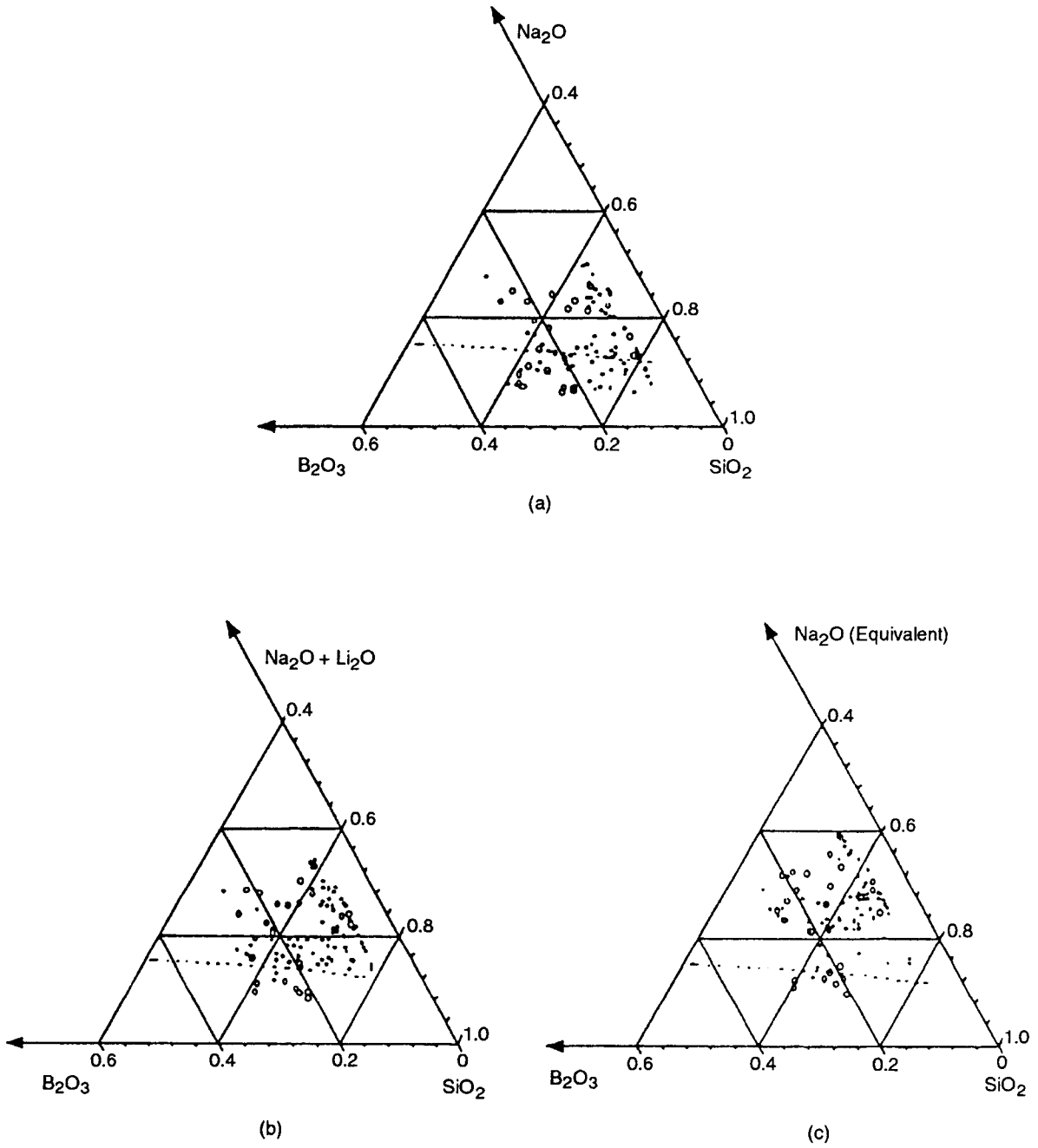

Figure 13-3. Prediction of phase separation using various normalized submixtures of (a) Na_2O-B_2O_3-SiO_2, (b) (Na_2O+Li_2O)-B_2O_3-SiO_2, and (c) Na_2O(equivalent)-B_2O_3-SiO_2. The dashed line is the immiscibility boundary. Solid points and open circles represent high- and low-durability glasses, respectively (Hrma et al., 1994).

modified models for predicting immiscibility. Evaluation of other submixtures for immiscibility prediction was therefore suggested.

Jantzen et al. (2000) investigated the compositional nature of phase separation in HLW glasses in an attempt to improve the predictability of the glass durability model by eliminating phase-separated glasses from the DWPF databases. An analysis of the compositional differences of 110 homogeneous and phase-separated glasses indicated that the phase-separated glasses were significantly lower in Al_2O_3 while being somewhat higher in B_2O_3. Good discrimination between the homogeneous and phase-separated glasses was achieved by plotting the sum of the lighter density alkali oxide components versus the denser sludge components, as shown in figure 13-4. From these results, a composition-dependent phase separation discriminator has been defined. This discriminator function is mathematically derived based on a discriminant analysis of 110 waste glasses in 14 component composition spaces, and is expressed as

$$-1.6035x - 5.6478y + 210.9203 < 0 \qquad (13\text{-}2)$$

where x and y are defined as the sum of the wt% of less dense and dense oxide components, respectively, and are expressed as

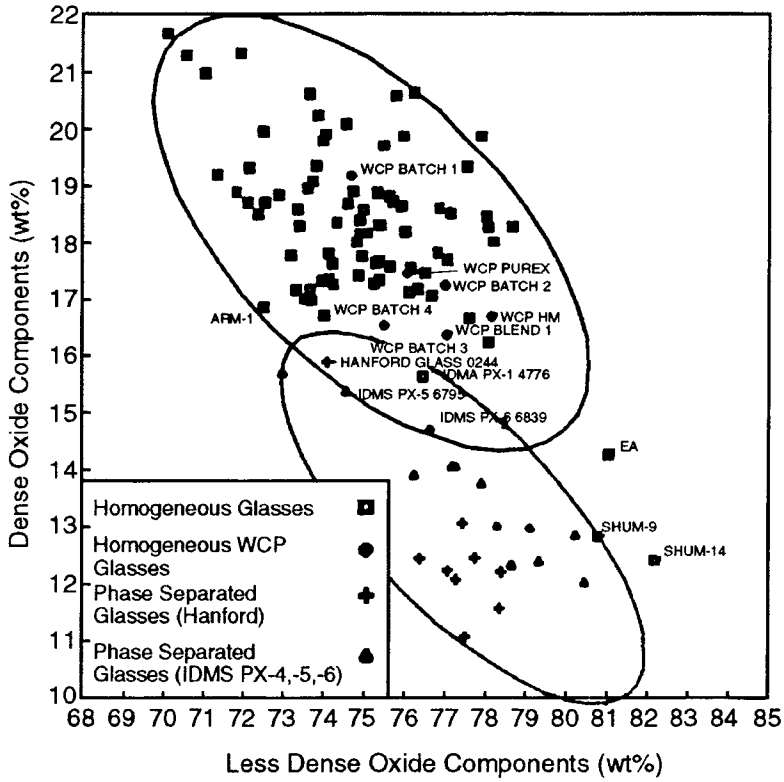

Figure 13-4. Compositional distinction between homogeneous and phase-separated glasses with 95-percent confidence ellipsoids (Jantzen et al., 2000)

$$x = \sum \text{wt\%}(Na_2O + Li_2O + K_2O + CsO_2 + SiO_2 + B_2O_3)$$

$$y = \Sigma \text{wt\%}(Al_2O_3 + Fe_2O_3 + Nd_2O_3 + Ce_2O_3 + La_2O_3 + Y_2O_3 + CaO + MoO_3)$$

Glasses will be homogeneous if the criterion defined in Eq. (13-2) is satisfied. The phase separation discriminator has been validated with a 95-percent accuracy by applying it to a group of 53 validation glasses that cover a wide composition range.

13.3 CRYSTALLIZATION

Glass-crystal transformation follows a two-step process: crystal nucleation and growth. When a liquid is cooled below its freezing point, crystallization occurs by the growth of crystals at a finite rate from a finite number of nuclei. Glass formation may be attributed to a low rate of crystal growth, a low rate of nuclei formation, or a combination of both. The nucleation rate and crystal growth rate as a function of temperature can be plotted in the form of skewed bell-shaped curves, as shown in figure 13-5. In both cases, the rate reaches a maximum at a certain temperature below the melting point and decreases to zero at both ends of high and low temperatures. However, the maximum crystal growth rate occurs at much smaller undercoolings than the case for the maximum nucleation rate. The extent of the overlap between the two curves determines the capability of glass formation upon cooling: the smaller the overlap, the easier the glass formation.

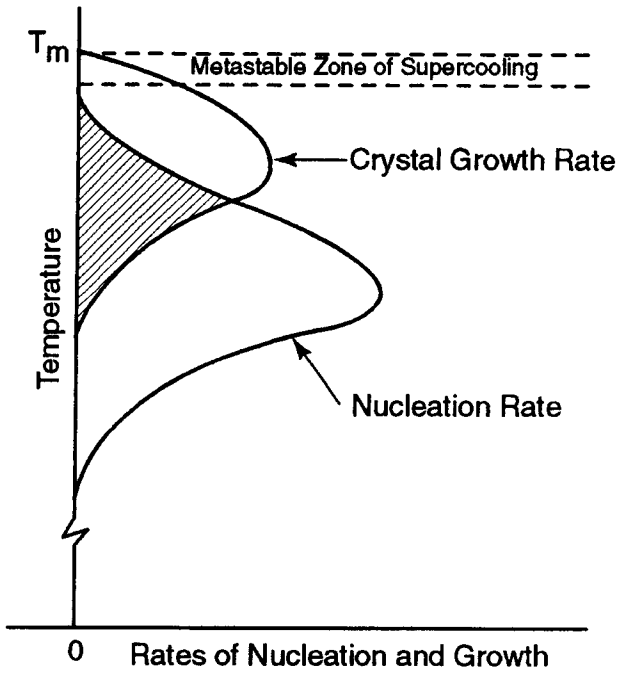

Figure 13-5. Variation of nucleation rate and crystal growth rate with temperature. T_m represents melting point.

A stable crystalline phase will only form when the liquid is sufficiently undercooled. The metastable zone of supercooling near the melting point with small undercoolings in figure 13-5 represents a region where few nuclei are present and the rate of crystal growth is low because of a reduced driving force for crystallization. Contrarily, at large undercoolings below the melting point, the nucleation rate may be very high but, in the absence of crystal growth, the overall crystallization rate remains low. A combination of nucleation rate and crystal growth rate is required for crystallization. Crystallization of nuclear waste glasses can occur during continuous cooling of pour canisters, or during annealing of quenched glasses. The degree of crystallinity and crystalline phases that may be produced will depend on factors such as the specific cooling rates and the waste glass compositions.

Glass crystallization affects both waste glass processability and acceptability. The formation of crystalline phases affects chemical durability, thus influencing the acceptability of the waste glass product for isolation in a geological repository. Crystallization can affect chemical durability as a result of a change of residual glass composition and structure. If the crystalline phases are more durable than the glass, the chemical durability of the partly crystallized glass is determined predominantly by the durability of residual glass. Crystalline phases in the melter can also cause processing problems, such as sludge formation on the melter bottom or melter electrode shorting if the phases are highly conductive. The TTT diagram is a useful method for defining the heat treatment conditions for crystallization, and for predicting the types and quantities of phases that can form in nuclear waste glasses. By combining the time and temperature dependencies of the nucleation and growth rates, the TTT diagram can be determined. The development of TTT diagrams for HLW glasses is a requirement of the WAPS.

13.3.1 Crystallization Kinetics Model

A quantitative model for the kinetics of crystallization can be developed by combining the phase transformation theory of nucleation and growth based on the Johnson-Mehl-Avrami equation. Reynolds and Hrma (1994) established an analytical kinetic model for spinel crystallization in a blended Hanford Site waste. The spinel volume fraction in molten glass, C, can be expressed in the form of the Johnson-Mehl-Avrami equation

$$\frac{C}{C_o} = 1 - \exp[-\left(\frac{t}{\tau}\right)^n] \qquad (13\text{-}3)$$

where

C_o — equilibrium value
t — time
τ — time constant
n — Avrami exponent

Both C_o and τ are functions of temperature and expressed as

$$\frac{C_o}{C_{max}} = 1 - \exp[-B_L(\frac{1}{T} - \frac{1}{T_L})] \qquad (13\text{-}4)$$

$$\tau = \tau_o \exp\left(\frac{B\tau}{T}\right)$$

where B_L, B_τ, C_{max}, and τ_o are constants, and T_L is the liquidus temperature. The above kinetic and thermodynamic parameters can be determined by fitting the vol% of crystallization data, and then be used to construct the TTT diagram, as discussed in section 13.3.3.

13.3.2 Time-Temperature-Transformation Diagram Measurements

A TTT diagram can be determined experimentally by means of isothermal and nonisothermal heat treatments. For isothermal heat treatments, glass samples are heat-treated at specific temperatures for certain time periods and then quenched to reserve the microstructure. Generally, the heat treatment temperatures range from T_g to T_L. Nonisothermal heat treatments involve a simulation of canister cooling curves and critical cooling. The canister cooling curve simulates the thermal history of glasses in the canister, while critical cooling simulates the glass at a specific cooling rate. In general, because the time required for crystallization to begin and end is delayed during nonisothermal heat treatments, the isothermal diagrams tend to shift to longer times and lower temperatures.

A variety of analytical techniques has been used to characterize the crystal phases in the heat-treated glass samples, including optical microscopy, electron microscopy, and X-ray diffraction. The structure and composition of the crystalline phases can be identified by X-ray diffraction and an energy dispersive spectroscopy attachment to scanning/transmission electron microscopy. The vol% crystallization data of glass samples are generally measured by image analysis using reflected-light optical microscopy. With these vol% crystallization results, a TTT diagram can be constructed.

13.3.3 Time-Temperature-Transformation Diagrams for High-Level Waste Glasses

TTT diagrams for various waste glass compositions have been developed to determine the effect of composition on crystallization. Bickford and Jantzen (1986) reported TTT diagrams for simulated glasses (SRS 131 and SRS 165) bounding the compositional range in the DWPF. Formulations included all of the minor constituents such as RuO_2 and chromium, which have limited solubility in borosilicate glasses. Crystallization of these waste glasses under isothermal heat treatments was observed to be heterogeneous nucleation of spinel on RuO_2 and subsequent nucleation of acmite on spinel. A similar crystallization path was also observed in the glasses subjected to a canister centerline cooling heat treatment. The total vol% of spinel in these glass samples, however, was slightly higher than those on isothermal annealing.

The TTT diagrams for seven HLW waste glass target compositions to be produced in the DWPF have been determined by Cicero et al. (1993). The glass samples were isothermally heat-treated at temperatures varying from 500 to 1,100 °C with times varying from 0.75 to 768 hr. All glass compositions contained trevorite, acmite, lithium metasilicate, and nepheline in various amounts, except the PUREX glasses, which did not contain any lithium metasilicate. Different phase regions in the TTT diagrams were then constructed according to the occurrence of each phase in the time-temperature domain. Figure 13-6 shows a representative TTT diagram for the Blend composition of the DWPF glasses. As displayed in the figure, the trevorite region was predominant at higher temperatures. Acmite began to form with the trevorite from 750 to 850 °C above 0.75-hr annealing times and led to the ingrowth of lithium metasilicate at longer annealing

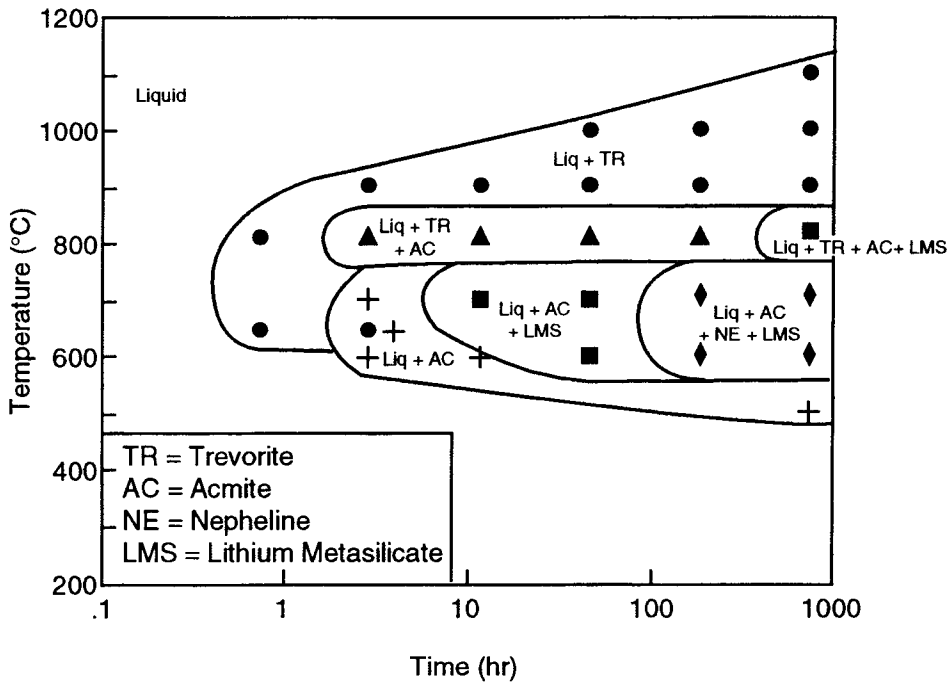

Figure 13-6. Time-temperature-transformation diagram for the Defense Waste Processing Facility Blend glass (Cicero et al., 1993)

times. The normal growth sequence of acmite, lithium metasilicate, and then nepheline occurred at the lower temperatures.

Joseph et al. (1988) established TTT diagrams for the fully simulated reference borosilicate glass (WVCM50), both in the fully oxidized and partially reduced forms, developed for the WVDP. While the oxidized glass sample was directly melted in air, the reduced glass was subsequently processed in a controlled reducing atmosphere. Crystallization behavior of these glasses was investigated using glass samples isothermally heat-treated over the temperature range of 500 to 1,000 °C for time periods of 1 to 384 hr. The major crystalline phases observed in the heat-treated samples were spinel, acmite, and cerium-thorium oxide. The total vol% crystallization data, determined by image analysis, were used to construct TTT diagrams at various levels of vol% crystals.

Simpson et al. (1994) constructed TTT diagrams for the oxidized and reduced versions of the WVDP target Reference 6 glass with the consideration of statistical confidence intervals. A 95-percent confidence interval for the time to achieve a given vol% crystallization in the region of the nose of the TTT diagrams was estimated. Spinel was identified in all of the glass samples. The reduced glass showed a greater extent of crystallization than the oxidized glass. The vol% crystallization in both glasses, however, was very low and did not affect the processing of the WVDP Reference 6 glass. Figure 13-7 shows the TTT diagrams for the oxidized WVDP Reference 6 glass for 2 and 4 vol% crystallization. The 95-percent confidence intervals for the time periods to achieve the respective crystallization are shown as horizontal bars.

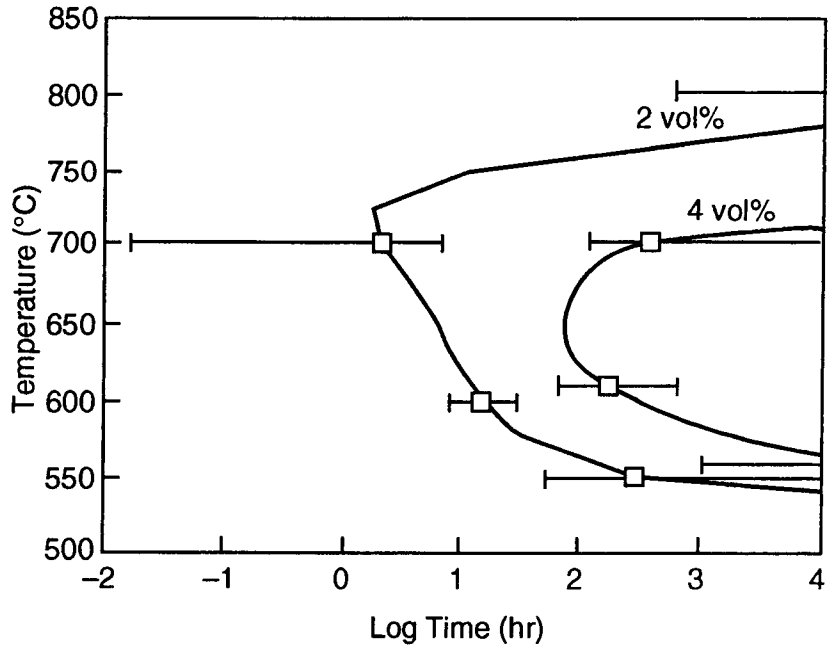

Figure 13-7. Time-temperature-transformation diagrams for 2 and 4 vol% crystallization of the oxidized West Valley Demonstration Project Reference 6 Glass. Horizontal bars represent 95-percent confidence intervals (Simpson et al., 1994).

Using the Johnson-Mehl-Avrami Eq. (13-3), Reynolds and Hrma (1997) obtained the kinetic parameters by fitting isothermal data for spinel crystallization of a simulated HLW glass for the Hanford site. From these numerical values of coefficients, the TTT diagram for isothermal crystallization was calculated as shown in figure 13-8a. In a similar way, nonisothermal kinetics of spinel crystallization during cooling at constant rates was also predicted by Casler and Hrma (1999). The TTT diagram for nonisothermal crystallization is shown in figure 13-8b. A comparison of the TTT diagrams was made by overlapping the isothermal TTT curve for 0.004 volume fraction of spinel in the nonisothermal diagram (figure 13-8b). The nose of the nonisothermal curve was slightly shifted to a longer time and lower temperature than that for the isothermal curve.

13.4 EFFECT OF PHASE STABILITY ON GLASS DURABILITY

13.4.1 Effect of Phase Separation

Liquid-liquid phase separation has been shown to be detrimental to the stability and durability of nuclear waste glasses (Hrma et al., 1994; Tovena et al., 1994). From the composition variation study performed by Hrma et al. (1994), liquid-liquid phase separation was assessed using the plots of the MCC–1 durability data within various normalized submixtures, as shown in figure 13-1. Glasses within the immiscibility boundary generally showed low durability. These low-durability glasses were characterized by either liquid-liquid phase separation or by a high degree of crystallinity.

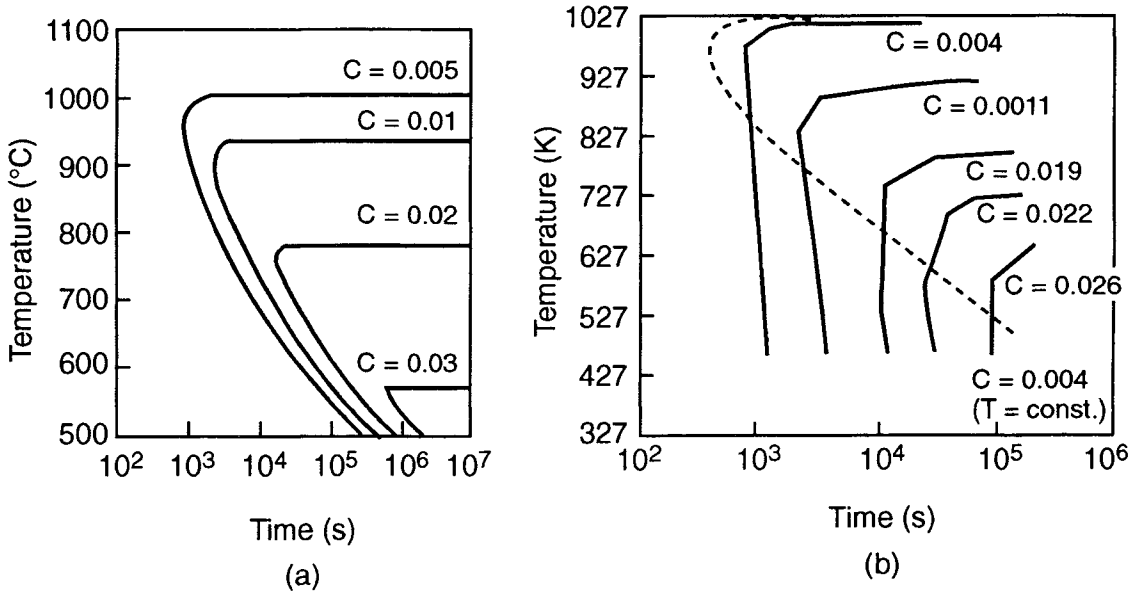

Figure 13-8. Time-temperature-transformation diagrams for (a) isothermal and (b) nonisothermal crystallization for a simulated Hanford glass with various volume fraction of spinel (Casler and Hrma, 1999)

Tovena et al. (1994) reported dissolution rates of HLW glasses developed in France. Experimental analysis indicated that phase separation also resulted in a high glass dissolution rate. In addition, glass durability of these glasses was assessed using various thermodynamic and structural models in the literature. The calculated dissolution rates were largely underestimated for the phase-separated glasses. The underprediction of the glass durability models was attributed to the development of inhomogeneous microstructure in the phase-separated glasses.

13.4.2 Effect of Crystallization

Glass durability can be increased, decreased, or unaffected by crystallization, depending on the type and fraction of crystalline phases formed. Jantzen and Bickford (1985) investigated the effect of crystallization on the durability of Savannah River defense waste glasses. The crystalline phases precipitated from the glasses after simulated canister centerline cooling were spinel, acmite, and nepheline. The results from the MCC–1 durability tests showed that the noncrystallized glass samples gave reproducible leach rates, but the crystallized samples did not. Variations of up to two times were observed for the leach rates of crystallized samples. Waste glasses that contained crystalline phases had leach rates one to three times greater than the noncrystallized glasses of the same composition.

Jain et al. (1993) reported the influence of heat treatment on the glass durability of the target Reference 6 composition produced at the WVDP. Spinel phases were identified as the major crystalline

phases in the glass after isothermal heat treatments at temperatures of 500 to 900 °C for periods of 1 to 96 hr. The PCT results indicated that, in all cases, the boron leach rate of the heat-treated glass increased. For samples heat-treated at 600 and 700 °C, boron release increased with heat treatment time because of the increase of the volume fraction of spinel phases.

Glass durability as a function of crystallization was studied for Hanford HLW glasses subjected to the canister centerline cooling heat treatment (Hrma et al., 1994). The crystalline phases occurring most frequently were spinel, Li_2SiO_3, and clinopyroxene, followed by olivine, SiO_2, hematite, zircon, orthopyroxene, and nepheline. Crystallization of nepheline and SiO_2 significantly decreased glass durability, and crystallization of clinopyroxene and zircon showed almost no effect on glass durability.

13.5 TANK WASTE REMEDIATION SYSTEM CONCERNS

The phase stability of HLW glasses is sensitive to the overall glass composition and the thermal history of the system. Both liquid-liquid phase separation and crystallization have detrimental effects on the glass durability. Liquid-liquid phase separation can be suppressed by controlling the polarizing power of various additive oxides, and the heat treatment conditions for crystallization can be specifically determined through the development of a TTT diagram. A design of the target glass composition and a heat-treatment process of the waste glass that prevents significant phase changes to ensure glass durability is desirable to meet the requirements of the WAPS.

13.6 SUMMARY

Phase stability in glass can be affected by either liquid-liquid phase separation or crystallization on cooling from melt. For the glass waste form, both the phase separation and crystallization processes can result in inhomogeneous microstructure in glass that may affect the reliability of the waste glass process and product performance. The phase stability requirements that include the development of a TTT diagram for each projected waste type have been outlined in the WAPS. Liquid-liquid phase separation can be confined within an immiscibility boundary, which can be experimentally determined using the opalescence method. Various sodium borosilicate submixture systems have been successfully used to predict phase separation in Hanford HLW glasses. In an attempt to improve the predictability of the glass durability model, a composition-dependent phase separation discriminator has been mathematically derived and used to distinguish the phase-separated glasses from the homogeneous glasses. Crystallization can occur in nuclear waste glasses during continuous cooling of pour canisters and annealing of quenched glasses. The TTT diagram is a useful tool for scoping the heat treatment conditions for crystallization. TTT diagrams for each of the major HLW glasses have been developed. Experimental results indicate that both liquid-liquid phase separation and crystallization have a detrimental effect on the glass durability of nuclear waste glasses. Controlling the glass compositions and defining the heat treatment conditions that avoid phase separation and crystallization are keys to achieving waste glass durability control during processing.

13.7 REFERENCES

Bickford, D.F., and C.M. Jantzen. Devitrification of defense nuclear waste glasses: Role of melt insolubles. *Journal of Non-Crystalline Solids* 84: 299–307. 1986.

Casler, D.G., and P.R. Hrma. Nonisothermal kinetics of spinel crystallization in HLW glass. *Proceedings of the Materials Research Society Symposium.* Symposium Proceedings 556. Pittsburgh, PA: Materials Research Society: 255–262. 1999.

Cicero, C.A., S.L. Marra, and M.K. Andrews. *Phase Stability Determinations of DWPF Waste Glasses (U).* WSRC–TR–93–227. Revision 0. Aiken, SC: Westinghouse Savannah River Company. 1993.

Hrma, P.R., G.F. Piepel, M.J. Schweiger, D.E. Smith, D.-S. Kim, P.E. Redgate, J.D. Vienna, C.A. LoPresti, D.B. Simpson, D.K. Peeler, and M.H. Langowski. *Property/Composition Relationships for Hanford High-Level Waste Glasses Melting at 1150 °C.* Volume 2. PNL–10359. Ceramic Transactions Richland, WA: Pacific Northwest National Laboratory. 1994.

Jain, V., S.M. Barnes, I. Joseph, L.D. Pye, I.L. Pegg, and P.B. Macedo. Impact of heat-treatment on the chemical stability of nuclear waste glasses produced at the West Valley Demonstration Project (WVDP). *Proceedings of the Glass and Optical Materials Division Meeting of the American Ceramic Society, Stone Mountain, Georgia.* Ceramic Transactions Volume 30. M.C. Weinberg, ed. Westerville, OH: American Ceramic Society: 367–370. 1993.

Jantzen, C.M., K.G. Brown, and T.B. Edwards. Predicting phase separation in nuclear waste glasses. *Proceedings of the Environmental Issues and Waste Management Technologies in the Ceramic and Nuclear Industries V, Indianapolis, Indiana, April 25–28, 1999.* Ceramic Transactions Volume 107. G. Chandler and X. Feng, eds. Westerville, OH: American Ceramic Society. 2000.

Jantzen, C.M., and D.S. Bickford. Leaching of devitrified glass containing simulated SRP nuclear waste. *Proceedings of the Materials Research Society Symposium.* Symposium Proceedings 44. Pittsburgh, PA: Materials Research Society: 135–146. 1985.

Joseph, I., A. Mathur, C. Capozzi, J. Sehgal, D. Butts, D. McPherson, and L.D. Pye. *The Crystallization Behavior of the West Valley Reference Borosilicate Glass.* DOE–NE–44139–44.West Valley, NY: West Valley Nuclear Services Company, Inc. 1988.

Kawamoto, Y., and M. Tomozawa. Prediction of immiscibility boundaries of ternary silicate glasses. *Physics Chemistry Glasses* 22: 11–16. 1981.

Reynolds, J.G., and P.R. Hrma. The kinetics of spinel crystallization from a high-level waste glass. *Proceedings of the Materials Research Society Conference.* Symposium Proceedings 465. Pittsburgh, PA: Materials Research Society: 65–69. 1997.

Simpson, J.C., D. Oksoy, T.C. Cleveland, L.D. Pye, and V. Jain. The statistics of the time-temperature-transformation diagram for oxidized and reduced West Valley reference 6 glass. *Proceedings of the Environmental and Waste Management Issues in the Ceramic Industry II Symposium. 96th Annual Meeting of the American Ceramic Society, Indianapolis, Indiana, April 25–27, 1994.* Ceramic Transactions Volume 45. D. Bickford, S. Bates, V. Jain, and G. Smith, eds. Westerville, OH: American Ceramic Society: 377–387. 1994.

Taylor, P. *A Review of Phase Separation in Borosilicate Glasses, With Reference to Nuclear Waste Immobilization.* AECL–10173. Pinawa Manitoba, Canada: Whiteshell Nuclear Research Establishment. 1990.

Tomozawa, M. Phase Separation in glass. *In Treatise on Materials Science and Technology.* Ceramic Transactions Volume 17. M. Tomozawa and R.H. Doremus eds., New York: Academic Press, Inc.: 71–113. 1979.

Tovena, I., T. Advocat, D. Ghaleb, E. Vernaz, and F. Larche. Thermodynamic and structural models compared with the initial dissolution rates on "SON" glass melts. *Proceedings of the Materials Research Society Conference.* Symposium Proceedings 333. Pittsburgh, PA: Materials Research Society: 595–602. 1994.

14 SUMMARY

The review of the history of waste form development and the information (data and models) on glass melt properties for various type of commercial and waste glass compositions indicate that the behavior of glasses is complex and cannot be expressed in simple terms for all wastes. The glass composition needs to be designed uniquely for each waste type. The lessons learned or the existing database of HLW glasses can be used as a guideline to narrow the scope of development research needed to meet the requirements.

This report has been written to assist the NRC in

- Determining if sufficient information exists to assess safety considerations regarding vitrification of the Hanford wastes
- Determining if current regulatory guidelines are adequate for controlling implementation of vitrification process to immobilize HLW at Hanford
- Identifying the existence of technical uncertainties
- Assessing where future guidance may be warranted.